

Table of Contents

Preface .....	1
Personnel aboard R/V METEOR during cruise M52/1 .....	3
Participating institutions .....	3
1 Introduction .....	5
2 Cruise narrative .....	9
3 Weather report .....	17
4 Multibeam swathmapping .....	18

# RV METEOR CRUISE REPORT M52/1 MARGASCH

MARINE GAS HYDRATES OF THE BLACK SEA

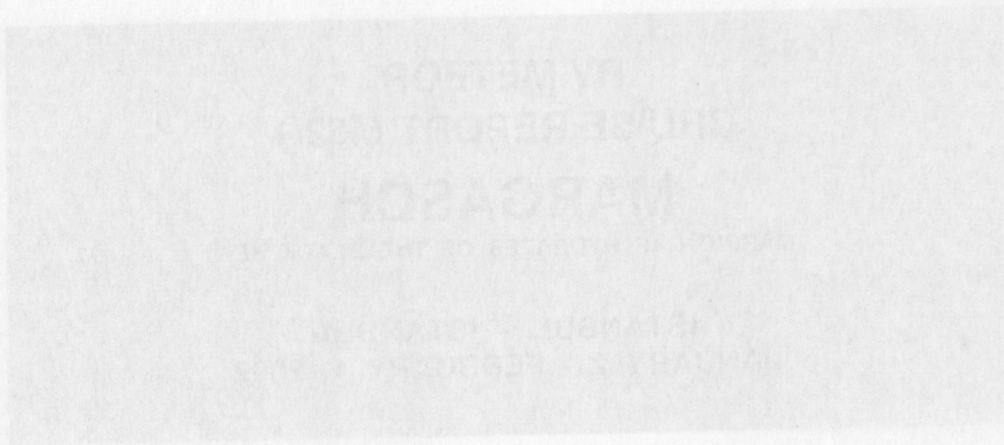
ISTANBUL - ISTANBUL  
JANUARY 2 - FEBRUARY 1, 2002

Edited by  
Gerhard Bohrmann and Silke Schenck  
with contributions of cruise participants

**GEOMAR**  
Forschungszentrum  
für marine Geowissenschaften  
der Christian-Albrechts-Universität  
zu Kiel

**KIEL 2002**  
**GEOMAR REPORT 108**

**GEOMAR**  
Research Center  
for Marine Geosciences  
Christian Albrecht University  
in Kiel



Edited by  
Gerhard Bohrmann and Silke Schenck  
with contributions of cruise participants

Redaktion dieses Reports: Gerhard Bohrmann und  
Silke Schenck

Editor of this issue: Gerhard Bohrmann and Silke  
Schenck

GEOMAR REPORT  
ISSN

GEOMAR REPORT  
ISSN

**GEOMAR**  
Forschungszentrum  
für marine Geowissenschaften  
der Christian-Albrechts-Universität  
zu Kiel  
D-24148 Kiel  
Tel. (0431) 600-2555, 600-2505

**GEOMAR**  
Research Center  
for Marine Geosciences  
Christian Albrecht University  
in Kiel  
D-24148 Kiel  
Tel. (49) 431/ 600-2555, 600-2505



## RV METEOR, Cruise Report M52/1

MARGASCH: Istanbul – Sevastopol – Istanbul (January 2 – February 1, 2002)

### Table of Contents

	<i>Preface</i> .....	1
	<i>Personnel aboard R/V METEOR during cruise M52/1</i> .....	3
	<i>Participating institutions</i> .....	3
1	<i>Introduction</i> .....	5
2	<i>Cruise narrative</i> .....	9
3	<i>Weather report</i> .....	17
4	<i>Multibeam swathmapping</i> .....	18
5	<i>Sidescan sonar mapping</i> .....	26
6	<i>PARASOUND</i> .....	38
7	<i>High-resolution multichannel reflection seismics</i> .....	50
8	<i>Refraction seismic work</i> .....	64
9	<i>Visual seafloor observation</i> .....	84
10	<i>Geological sampling and results</i> .....	99
11	<i>Temperature measurements</i> .....	132
12	<i>Water column</i> .....	136
13	<i>Biology</i> .....	144
14	<i>References</i> .....	149

### Appendix

Edited by  
Gerhard Bohrmann and Silke Schenck  
with contributions of cruise participants



## PREFACE

G. Bohrmann

The study of gas hydrates has been attracting much attention in the recent years, because methane hydrate exists in large reservoirs in permafrost soils and deep marine sediments. Its influence on and interaction with the environment is manifold and may have been underestimated in the past.

R/V METEOR cruise M52/1 MARGASCH focussed on the investigation of environmental conditions for the formation of gas hydrate in the central Black Sea and in the Sorokin Trough southeast of the Crimea peninsula. It was a highly interdisciplinary approach which brought together an international group of scientists from institutions in Germany, Ukraine, Russia and France. Our research included high-resolution geoacoustical investigations of the seafloor and the subbottom using a wide range of frequencies and techniques, video mapping of the seafloor, investigations of the water column, and sampling of gas hydrates, in order to determine the detailed distribution and the amount of gas hydrate in a selected area (Sevastopol mud volcano). An additional objective was the relationship of gas hydrate to fluid migration through the sediments and to gas venting.

The Black Sea is an appropriate area for gas hydrate research because gas hydrate in near-surface sediments has been documented by Russian scientists on many cruises in the past 30 years. Gas plumes in the water column have also been recorded at around 5000 locations. Based on the stability field and the regional PT conditions gas hydrate can be expected in the Black Sea in areas with water depths of more than 700 m. Such gas hydrate deposits represent highly reactive methane reservoirs with strongly variable material

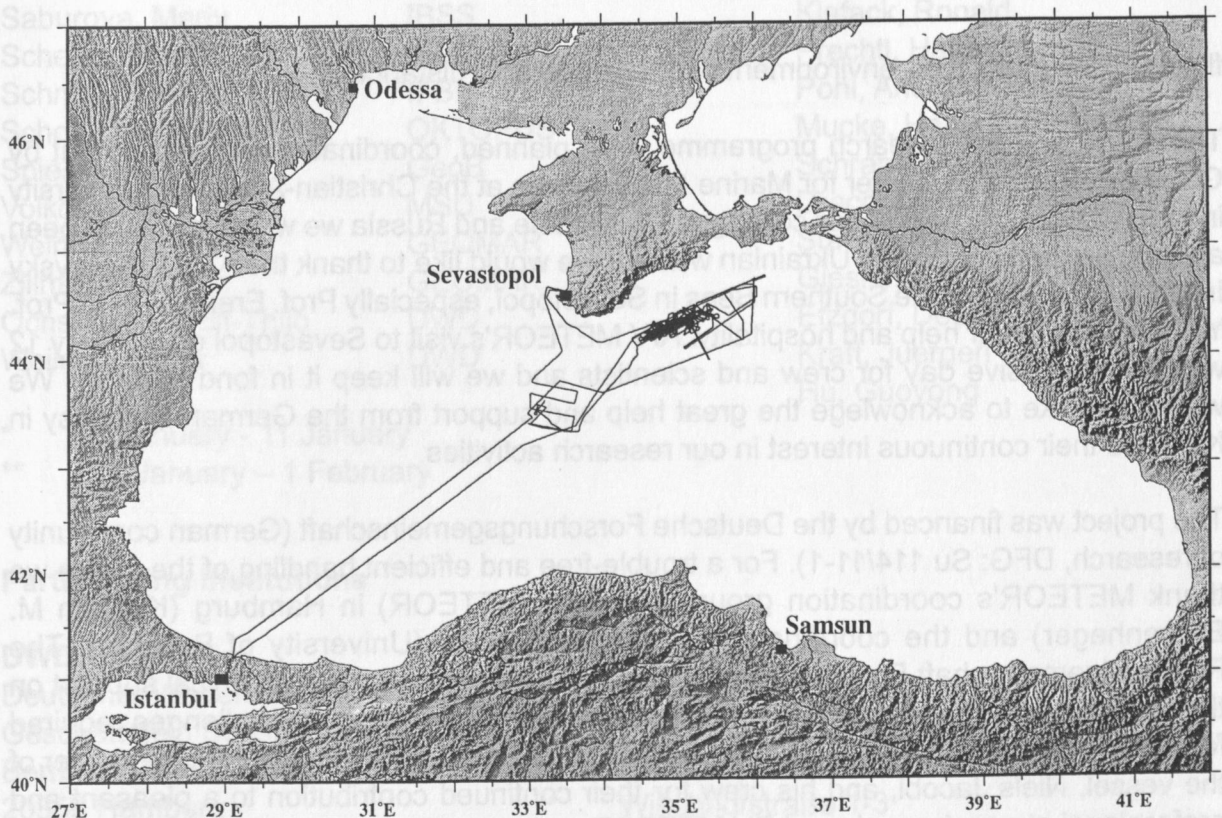


Fig. 1: Cruise track of R/V METEOR cruise M52/1 (MARGASCH).





Fig. 2: R/V METEOR in the harbour of Istanbul (Turkey).

fluxes. They affect their environment over considerable distances.

The cruise and the research programme were planned, coordinated and carried out by GEOMAR Research Center for Marine Geosciences at the Christian-Albrechts University in Kiel. Without the help of our colleagues in Ukraine and Russia we would not have been able to realize the cruise in Ukrainian waters. We would like to thank the A.O. Kovalevsky Institute of Biology of the Southern Seas in Sevastopol, especially Prof. Ereemeev and Prof. Y. Tokarev, for their help and hospitality. R/V METEOR's visit to Sevastopol on January 12 was an impressive day for crew and scientists and we will keep it in fond memory. We would also like to acknowledge the great help and support from the German Embassy in Kiev and their continuous interest in our research activities.

The project was financed by the Deutsche Forschungsgemeinschaft (German community of research, DFG; Su 114/11-1). For a trouble-free and efficient handling of the cruise we thank METEOR's coordination group (Leitstelle METEOR) in Hamburg (Kapitän M. Berkenheger) and the coordinator Dr. Jürgen Pätzold (University of Bremen). The Reedereigemeinschaft Forschungsschiffahrt (RF Bremen) provided technical support on the vessel in order to accommodate the large variety of technological challenges required for complex sea-going operations. We would like to especially acknowledge the master of the vessel, Niels Jacobi, and his crew for their continued contribution to a pleasant and professional atmosphere aboard RV METEOR.

**Personnel aboard R/V METEOR during cruise M52/1****Scientific Crew**

Bohrmann, Gerhard	GEOMAR
Abegg, Friedrich	GEOMAR
Aloisi, Giovanni	GEOMAR
Artemov, Yuriy G.	IBSS
Bannert, Bernhard	OKTOPUS
Bialas, Jörg	GEOMAR
Broser, Anne	GEOMAR
Domeyer, Bettina	GEOMAR
Drews, Manuela	GEOMAR
Foucher, Jean-Paul	IFREMER
Greinert, Jens	GEOMAR
Heidersdorf, Felix	GeoB
Ivanov, Michael*	MSU
Blinova, Valentina**	MSU
Klaucke, Ingo	GEOMAR
Krastel, Sebastian	GeoB
Leder, Thomas	GeoB
Naß, Kristin	GEOMAR
Naupold, Peer	GeoB
Petersen, Asmus	KUM
Polikarpov, Igor G.	IBSS
Saburova, Mariy	IBSS
Schellig, Frank	IFBM
Schmale, Oliver	IFBM
Schott, Thorsten	OKTOPUS
Spieß, Volkhard	GeoB
Volkonskaya, Anna	MSU
Weinrebe, Wilhelm	GEOMAR
Zillmer, Matthias	GEOMAR
Ochsenhirt, Wolf-Thilo	DWD
Weiland, Hans	DWD

\* 2 January - 11 January

\*\* 11 January – 1 February

**Crew members**

Jakobi, Niels
Meyer, Oliver
Mallon, Lutz
Aden, Nils-Arne
Koethe, Wolfgang
Schlenker, Wilhelm
Schueler, Achim
Schmiedeskamp, Jan
Beyer, Helge
Bekaan, Steffen
Heygen, Ronald
Stammer, Kurt
Voss, Martin
Stenzler, Joachim
Teichert, Klaus
Prinz, Udo
Isbrecht, Frank
Zeitz, Holger
Wieden, Wilhelm
Ernst, Arnold
Horzella, Ernst
Klafack, Ronald
Prechtel, Hans-Juergen
Pohl, Andreas
Mucke, Hans-Peter
Schrapel, Andreas
Dracopoulos, Eugenios
Staengl, Guenter
Gieske, Ralf
Etzdorf, Detlef
Kraft, Juergen
Hu, Guoyong

**Participating Institutions****DWD**

Deutscher Wetterdienst  
Geschäftsfeld Seeschifffahrt  
Bernhard-Nocht-Str. 76  
20359 Hamburg  
GERMANY

**GEOMAR**

GEOMAR Forschungszentrum für  
Marine Geowissenschaften der  
Christian-Albrechts-Universität  
Wischhofstraße 1-3  
24148 Kiel  
GERMANY



**GeoB**

Fachbereich 5 – Geowissenschaften  
Universität Bremen  
Klagenfurterstraße  
28359 Bremen  
GERMANY

**IBSS**

A.O. Kovalevsky Institute of Biology  
of the Southern Seas, National  
Academy of Science of the Ukraine  
Prospekt Nakhimova 2  
99011 Sevastopol  
UKRAINE

**IFBM**

Institut für Biogeochemie und  
Meereschemie  
Universität Hamburg  
Bundesstraße 55  
20146 Hamburg  
GERMANY

**IFREMER**

Institut Français de la Recherche  
pour l'exploitation de la Mer  
BP 70  
29280 Plouzané  
FRANCE

**KUM**

Umwelt-und Meerestechnik Kiel GmbH  
Wischhofstraße 1-3, Geb. D5  
24148 Kiel  
GERMANY

**MSU**

UNESCO-MSU Center for Marine  
Geosciences, Faculty of Geology  
Moscow State University  
Vorobjevi Gory  
119899 Moscow  
RUSSIA

**OKTOPUS**

Oktopus GmbH  
Kieler Str. 51  
24594 Hohenweststedt  
GERMANY



Fig. 3: Cruise participants of R/V METEOR Cruise M52/1.



## 1. INTRODUCTION

M. Ivanov

### 1.1. Regional Geology of the Central Black Sea

The Central Black Sea is the deepest part of the Black Sea (>2000 m). It joins the Andrusov Ridge separating the eastern and western part of the Black Sea. This part of the basin shows a generally flat seafloor topography with water depths of 2100-2200 m, except the relief of the mud volcanoes of up to 150 m above the seafloor. Mud volcanism occurs in the northern part of this area within a region which differs structurally from the rest of the West Black Sea Basin by the presence of small folds, flexures and faults (Ivanov et al. 1989). Nine mud volcanoes were described in this area (Fig. 4), and seven of them had been surveyed on previous TTR cruises (Ivanov et al., 1992, Limonov et al., 1994, Woodside et al., 1997).

The Cenozoic sediment thickness in this part of the basin is about 12 km. It consists of the Paleocene-Eocene sequence of about 4 km, the Maikopian formation (Oligocene-Lower Miocene) also about 4 km thick and upper Miocene-Pliocene sediments of 1.8 km. This sequence is overlain by Quaternary deposits of about 1.8 km (Tugolesov et al., 1995).

The upper part of the geological section shows numerous fractures and small faults related to low amplitude anticlines. This is an unusual structure for the West Black Sea Basin. Mud volcanoes have not been observed in the part of the basin where such features are absent. The mud volcanoes show well-expressed reliefs on the seafloor, as mounds of up to 20 to 150 meters. They consist of extruded mud breccia with large mudflows on their slopes.

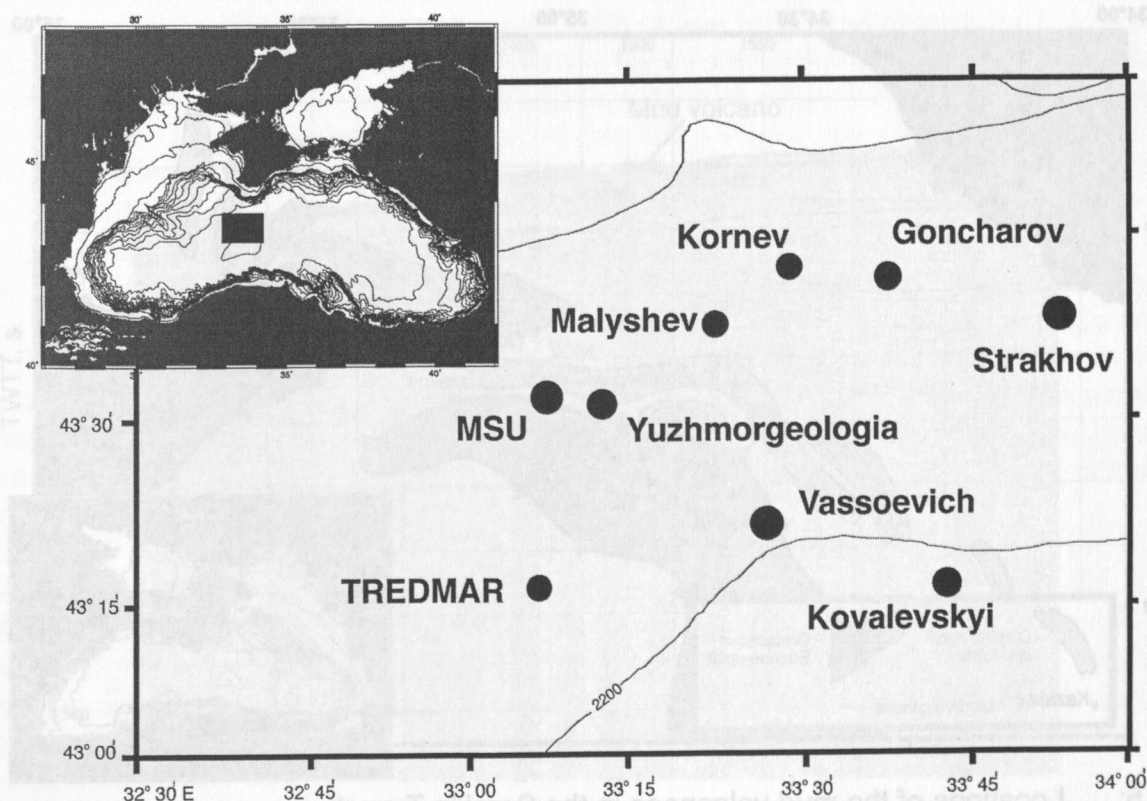


Fig. 4: Locations of the mud volcanoes in the central part of the Black Sea.

Evidence of mud volcanism can be found up to 7 km below the seafloor, such as feeder channels and gas presence in sediments shown by bright spots. Some buried ancient mud volcanoes can be recognized as well. The reflectors around the feeder channels are usually bent down due to the velocity anomaly in gas saturated sediments, but also by collapsing of walls of the channels. The roots of mud volcanoes are located most probably in the thick Maikopian clay formation, but on some multichannel seismic records they can be traced to the Cretaceous rocks. Unfortunately there are no paleontological data age of the rock clasts in mud volcanic breccia (Ivanov et al., 1992).

In this area there are clear signs of fluid flows, which are expressed as transparent vertical columns in the seismic facies, usually accompanied by bright spots above or adjacent to the mud volcanoes (Bouriak, 1994, 1995). Many samples of gas hydrates, carbonate crusts and bacterial mats were recovered from mud volcanoes of this area.

## 1.2 Regional Geology of the Sorokin Trough

The Sorokin Trough is one of the large depressions distinguished in the deep part of the Black Sea. It lies along the southeastern margin of the Crimean Peninsula and has a length of 150 km and a width of 45-50 km (Tugolesov, 1985). From the southeast the Sorokin Trough is bounded by the Cretaceous-Eocene Shatskiy and Tetyaev Rises recognised by seismic investigations. The trough is considered to be a foredeep of the Crimean Mountains and its formation began in the Oligocene (Andreev, 1976). The inner structure of the Sorokin Trough was produced by lateral compression in a SE-NW direction, created by movement of the Shatskiy and Tetyaev Rises. Overpressured fluids have created some specific features of the inner structure, such as mud volcanoes (Fig. 5).

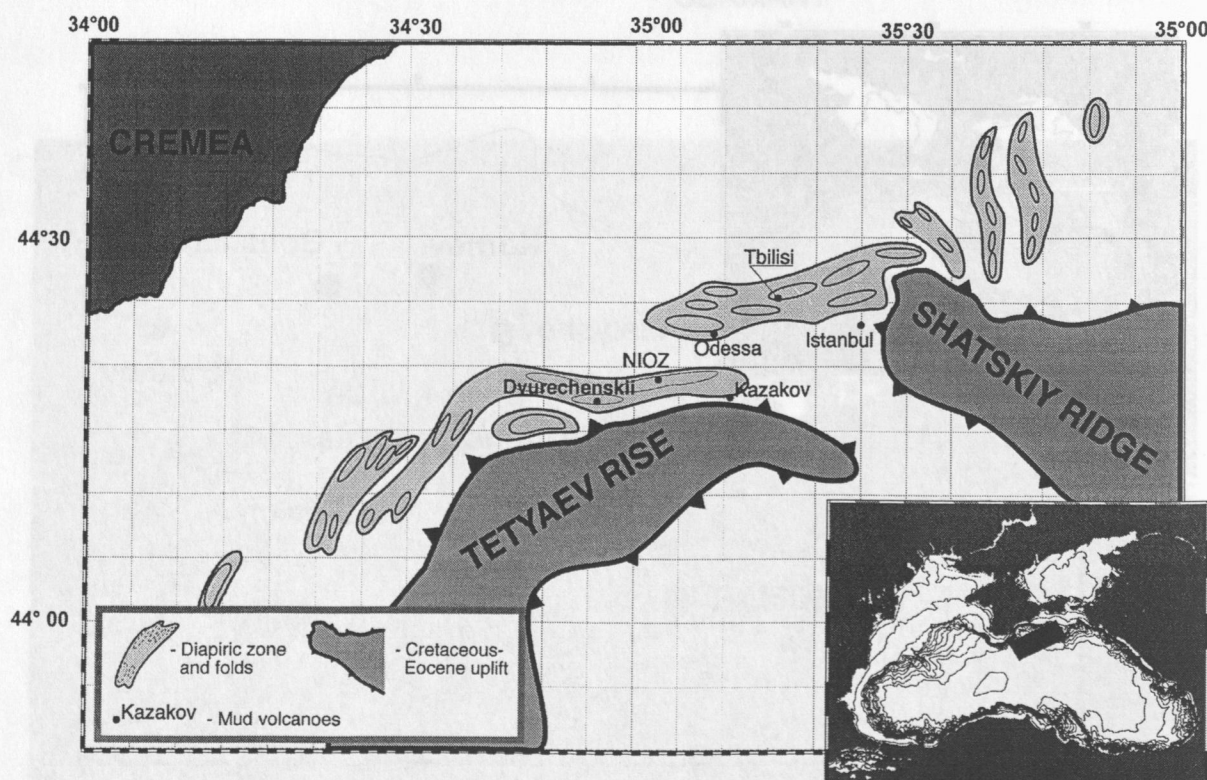


Fig. 5: Locations of the mud volcanoes in the Sorokin Trough.



According to seismic profiling performed during the TTR-6 and TTR-11 cruises, two main units are recognized in the sedimentary cover of the trough (Woodside et al., 1997). The lower one is likely to represent an upper part of the Maikopian Formation (Oligocene-Lower Miocene) and Pliocene deposits and is intensively folded and disturbed by numerous faults which can also be traced into the upper unit (Limonov et al., 1997). The thickness of the units varies from 5 to 6 km. The Quaternary deposits representing the upper unit are characterized by subparallel bedding and form a blanket pattern relative to the lower unit. It can largely be subdivided into fan deposits of the palaeo-Don and palaeo-Kuban Rivers and basinal deposits consisting of hemipelagic sediments and turbidites originating from the Crimean Mountains. The thickness of the unit is largely controlled by the underlying diapirs but generally increases toward the northeast (Limonov et. al., 1997). These diapiric folds are of particular interest since they originated due to the protrusion of plastic, water-saturated clays of the Maikopian Formation. Previous works established an elongated pattern of the diapirs coaxial to the general trend of the Sorokin Trough (Tugolesov, 1985). In the western part of the area (around 34°30'E), the folds trend N25°-30°, but to the east, between 34°40'E and 35°30'E, they are characterized by a sublatitudinal areujw (Fig. 5). These easterly folds have curved shapes in a plan view, following the slopes of the buried Tetyaev Rise and Shatskiy Ridge. From longitude 35°30'E to the east, the strike direction of the fold axis gradually changes, first to NW-SE, then longitudinal, and finally to a N10° trend.

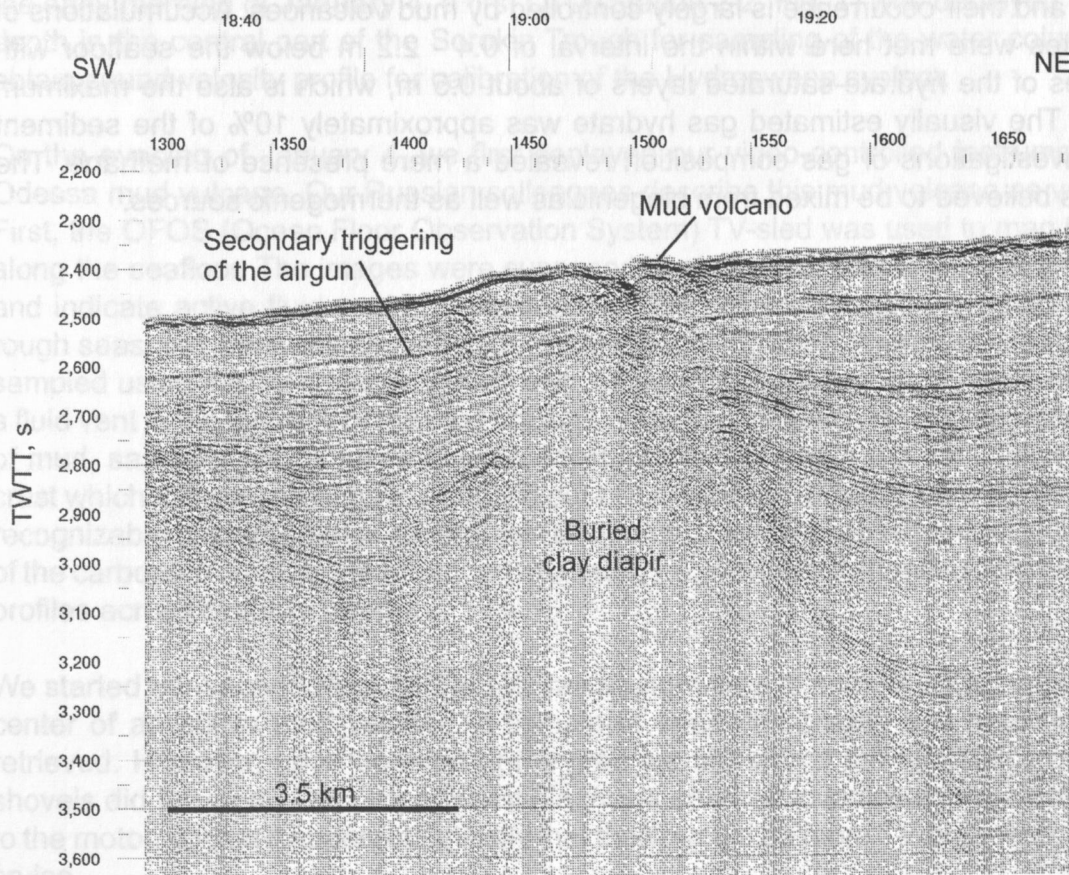


Fig. 6: Mud volcano on the top of a buried clay diapir.



The observed trends of the clay diapirs are evidence of approximately south-north lateral tectonic compression. The rigid blocks of the Tetiaev Rise and the Shatskiy Ridge, moving northwards make an impact on the northerly structures. The ledges of rises are considered as stamps stressing the Maikopian clays and causing the diapirs to grow (Limonov et al. 1997).

The mud volcanoes mentioned above were discovered in the study area in the late 1980s and since then have been the focus of scientific interest for numerous expeditions. They have developed on the large diapiric bodies as well as on the secondary diapirs (Fig. 6). Most of these occur on the slopes of the larger structures, probably because upward fluid migration is most active between the diapiric walls and surrounding sediments. When the parent diapirs are deeply buried, the associated mud volcanoes are seen as narrow columnar disturbances on seismic sections. The morphology of the mud volcanoes is highly variable and both depressed and dome-shaped structures are observed (Limonov et al., 1997). Their activity is usually accompanied by eruptions of mud breccia onto the seafloor. From acoustic data, there is also much evidence for gas saturation of the surrounding subbottom sediments. Another remarkable feature of the mud volcanoes of the Sorokin Trough is that mud breccia sometimes contain gas hydrates.

Ginzburg (Ginzburg et al. 1990), who specially investigated the Sorokin Trough for gas hydrate occurrences in 1989, believed them to have formed as a result of gas and fluid filtration through the zone with appropriate thermobaric conditions on their way upward in the sedimentary pile. The gas hydrates were recovered in the area at the top of the diapiric structures and their occurrence is largely controlled by mud volcanoes. Accumulations of gas hydrates were met here within the interval of 0.4 - 2.2 m below the seafloor with thicknesses of the hydrate-saturated layers of about 0.5 m, which is also the maximum thickness. The visually estimated gas hydrate was approximately 10% of the sediment volume. Investigations of gas composition revealed a mere presence of methane. The methane is believed to be mixed from biogenic as well as thermogenic sources.

## 2. CRUISE NARRATIVE

G. Bohrmann

R/V METEOR left Istanbul on **January 2** around noon, and we enjoyed a last glance on the picturesque sight of the snow-covered city, situated between the Golden Horn, the Marmara Sea and the Bosphorus. The last day of the old year and the first day of the new year had been dedicated to equipment mobilization in the harbour, which had been quite extensive due to the large number of systems, containers and working groups involved. By the evening of **January 1**, all scientists had arrived on board. The scientific party consisted of geophysicists, geologists, geochemists, biologists, oceanographers and meteorologists from Germany, France, Ukraine and Russia.

We reached the Black Sea after a three-hour transit through the Bosphorus. The steeply rising coastline of the Bosphorus, forming the border between Europe and Asia, with palaces, ruined castles and villages, has preserved its charming landscape in spite of a lot of modern construction that has been going on recently. Although air temperatures were around zero °C, we enjoyed our three-hour passage under a bright blue sky. Entering the Black Sea gave some of us a hard time as seas got rougher. The situation improved, though, after a few hours. The remaining transit to our working area at the Sorokin Trough, southeast of the Crimean Peninsula, was used for further preparation of the laboratories and the working deck, as well as for getting introduced to the ship by the crew. We also ran first tests of the reflection and refraction seismic systems. On the afternoon of **January 3**, the snow-covered high plateaus of the impressive steep coast of Crimea came into sight. On the early morning of **January 4**, a first CTD (Station 2-2, Fig. 7) was deployed to 2000 m depth in the central part of the Sorokin Trough for sampling of the water column and to obtain sound velocity profile for calibration of the Hydrosweep system.

On the evening of January 4, we first deployed our video-controlled instruments at the Odessa mud volcano. Our Russian colleagues describe this mud volcano as very active. First, the OFOS (Ocean Floor Observation System) TV-sled was used to map three lines along the seafloor. The images were supposed to give us an overall view of the structure and indicate active fluid vents on the seafloor. We obtained excellent results in spite of rough seas and were able to find quite suitable sampling sites. A subrecent mud flow was sampled using the TV-controlled multicorer, followed by very precise TV-grab sampling of a fluid vent in the top area of the mud volcano. The grab yielded a highly interesting mixture of mud, sapropel and other lithologies. Most interesting was a 2-3 cm - thick carbonate crust which the grab must have punched out of the seafloor. Directly beneath was a clearly recognizable bacterial mat of several mm thickness. It must be closely linked to the genesis of the carbonate crust. In the afternoon of **January 5**, we started shooting seismic reflection profiles across Sorokin Trough.

We started our second week with a TV-grab at night-time to sample a fluid vent site in the center of an active mud volcano. A sample of seep carbonates and mud breccia was retrieved. However, upon opening of the grab we found that the hydraulics of the large shovels did not work. Our properly first diagnosis seemed to indicate irreparable damage to the motor, so that it appeared unlikely that there would be more TV-grab work during this cruise.

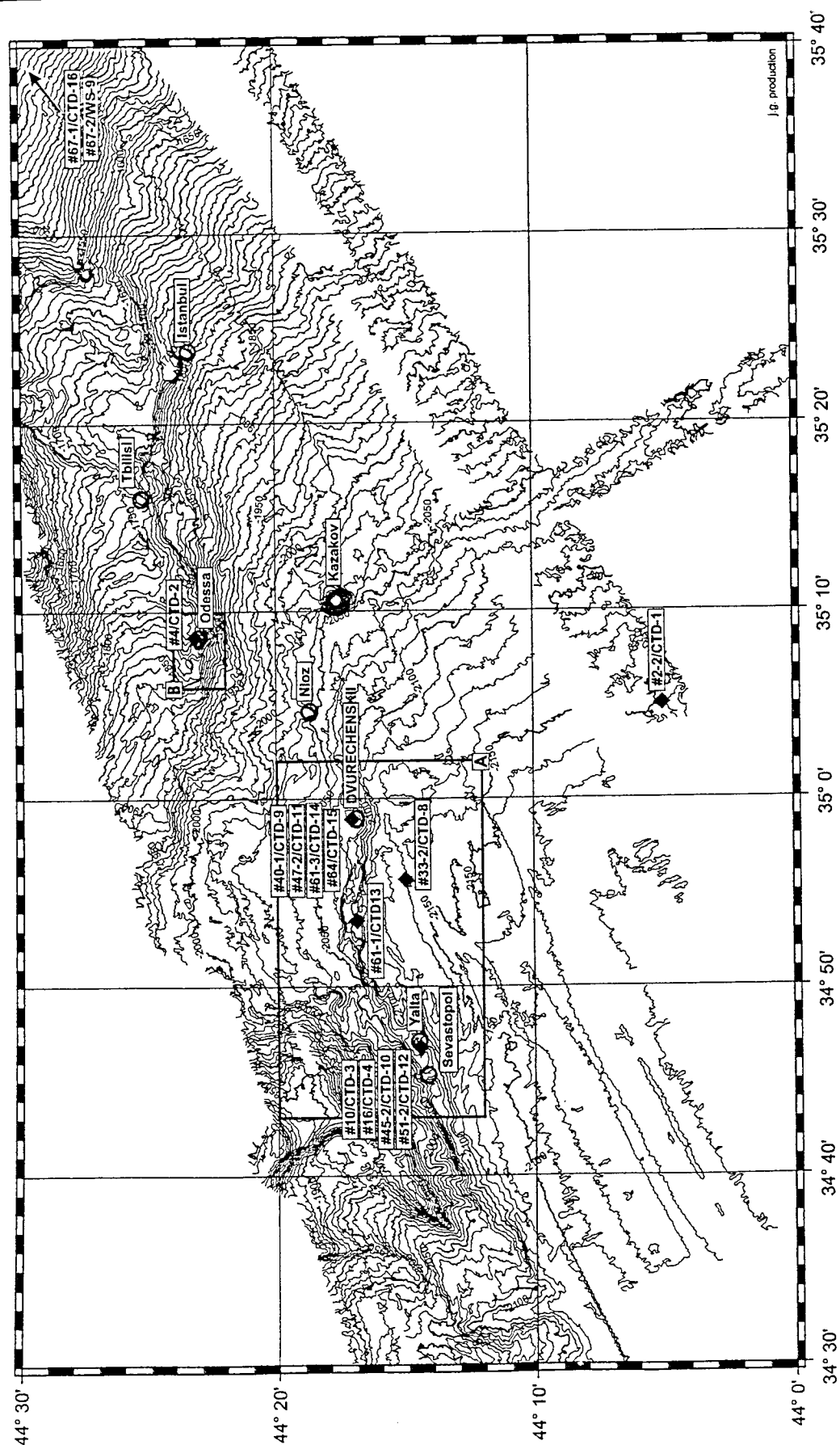


Fig. 7: Major working area in the Sorokin Trough showing location sites.



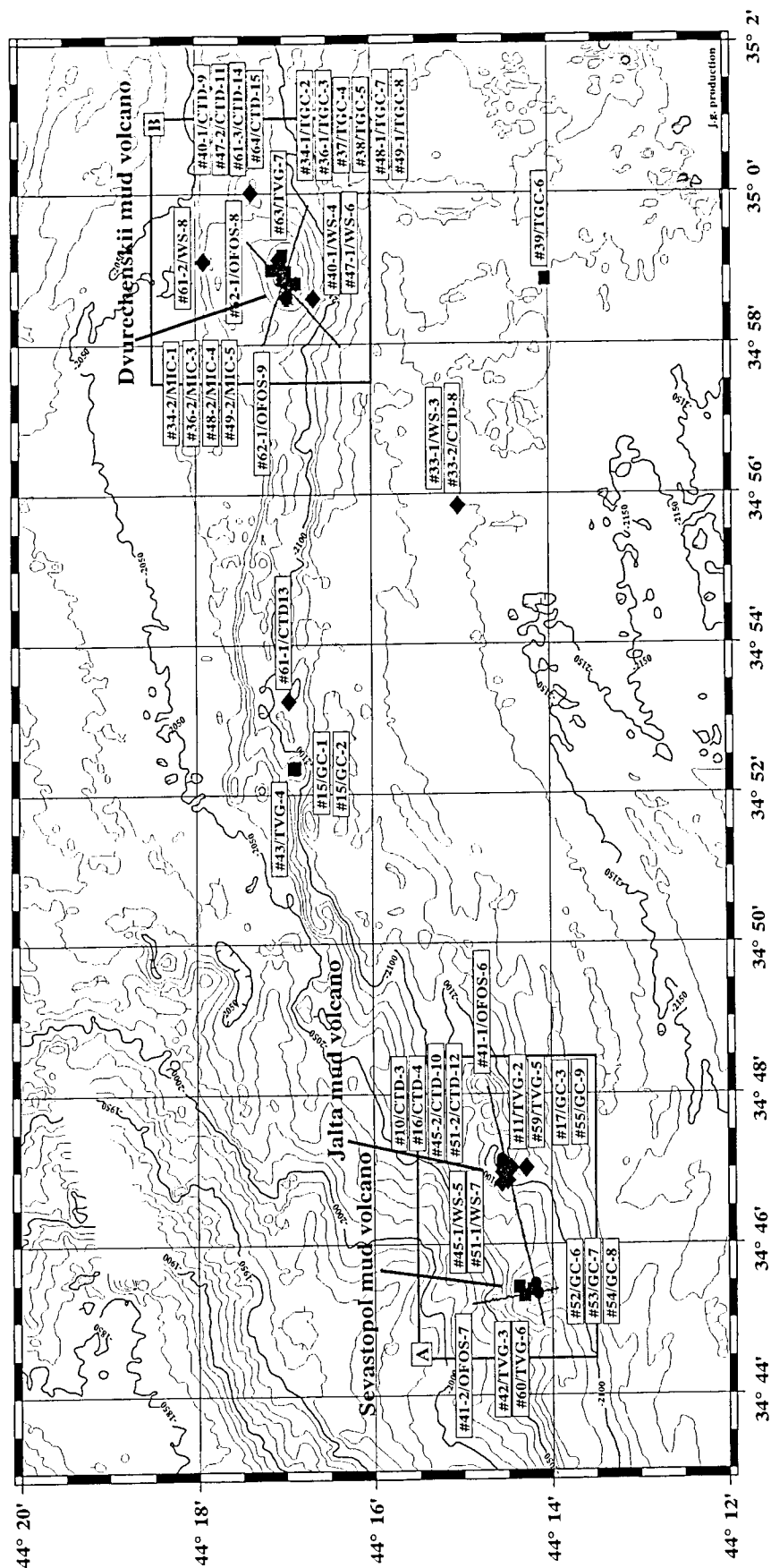


Fig. 8: Locations in the area of Dvurechenskii and Sevastopol mud volcanoes.

Next on our agenda was refraction seismic mapping. Ten ocean bottom seismometers (OBS) and five ocean bottom hydrophones (OBH) were deployed in a cross pattern with the centre focusing on the Kazakov mud volcano and the Odessa mud volcano being covered at the cross margin (Fig. 7). Morphologically, Kazakov mud volcano is cone-shaped with approximately 2.5 km in diameter, rising 120 m above the 2000-m-deep abyssal plain. The Odessa mud volcano is much smaller with a relief height of 30 m and a diameter of 0.5 km. Corresponding to the deployment pattern, two orthogonal lines were covered by RV METEOR with two large-volume airguns of 32 l generating signals of around 8 Hz. For about 2/3 of the profiles, additional signals could be generated using a 1.7 l GI gun. However, the GI gun had to be recovered when the seas became too rough. Bad weather also kept us from deploying a streamer parallel to the large airguns. We expect seismic recordings to allow imaging of the deeper structure of the mud volcanoes in order to learn more about the sources and depths of mud expulsion.

The subsequent recovery of the OBS/OBH was hampered by a wind strong of force 7. With an air temperature of -8°C, splash water quickly froze on the working deck. When the wind increased even more, to Beaufort 8 and sometimes even 9, we had to stop working for a few hours.

On the following morning, the bad weather had gone and we were able to take gravity cores from two mud volcanoes (Stations 15 and 17, Fig. 8). The data supplied by our Russian colleagues helped us to choose our sampling locations very precisely. The first two cores, each about 1 m long, were taken directly from active venting fields. They contained massive up to 5 cm thick gas hydrate layers just a few cm to mm below the seafloor. The third location was at a relatively fresh mud flow. For the first time, several thermometers were mounted to the outer tube of the 6-m-long gravity corer, so that we were able to determine a temperature gradient of 6 millidegrees per m of sediment depth. We also retrieved a 4.10 m long sediment core, that was apart from its upper section of about 50 cm, completely interspersed with thin, white gas hydrate layers. The gas hydrate layers apparently already began to dissociate during recovery when reaching water depths of less than 700 m. When the core was opened on deck, the material sampled at 2000 m water depth was exposed to further decompression and warming and gas hydrate dissociation increased further. Gas bubbled from the sediments everywhere. The core appeared to be fizzing. A detailed pore water profile will be worked out to gain more information on the chemistry and the complicated diagenetic reactions of sediments containing gas hydrate.

The rest of that very successful day in gas hydrate sampling was dedicated to further reflection seismic surveying, which took until noon of the next day and was followed by the first deployment of the sidescan sonar. We soon noticed that small alterations would be necessary to render the system fully functional. The following hours, and especially the transit to Sevastopol, were used for further reflection seismic surveying.

R/V METEOR entered the bay of Sevastopol, which is protected by two flanking jetties, on **January 11**. The city of Sevastopol is situated in the south-west of the Crimean coastal range and has over 25 bays, offering an abundance of natural harbours. It was the main base of the former Soviet fleet in the Black Sea. During the approach, we gained a first impression of the city's architecture. Many of us were later able to see more on a tour of the

city, which had kindly been organized by our partners from A.O. Kovalevsky Institute of Biology of the Southern Seas. Meanwhile, on R/V METEOR there was a tightly packed schedule, the highlights being a press conference for a large number of interested journalists and a reception for invited guests. The ship did very well performing its difficult and strenuous diplomatic duties. The German ambassador had come from Kiev. His presence and interventions have forwarded future scientific cooperation between Ukraine and Germany.

We left Sevastopol in the morning of **January 12**. In the afternoon, we arrived at our second working area in the central Black Sea and started a 24-hour seismic reflection survey along several east-west profiles in order to image larger tectonic structures around mud volcanoes. Afterwards, MSU mud volcano was examined more closely (Fig. 9). After having taken samples from the water column above the mud volcano, we started doing some OFOS profiles in the evening of **January 13**.

**January 14** was dedicated to work in the central Black Sea. This area is characterised by several mud volcanoes that rise up to 150 m above the basin floor of the 2100 - 2200 m - deep Western Basin of the Black Sea. The objective of the investigations, especially of the reflection seismic survey, was to evaluate whether one of the mud volcanoes would be suitable for high-resolution 3-D seismic mapping. Although some of the structures appeared suitable, we decided to concentrate the high-resolution survey on our first working area the Sorokin Trough, which had shown a much larger variety of mud volcanoes of different sizes. Work in the central area was completed by a deployment of the new digitally recording high-resolution side-scan sonar. The system is towed at a depth of about 100 m above the

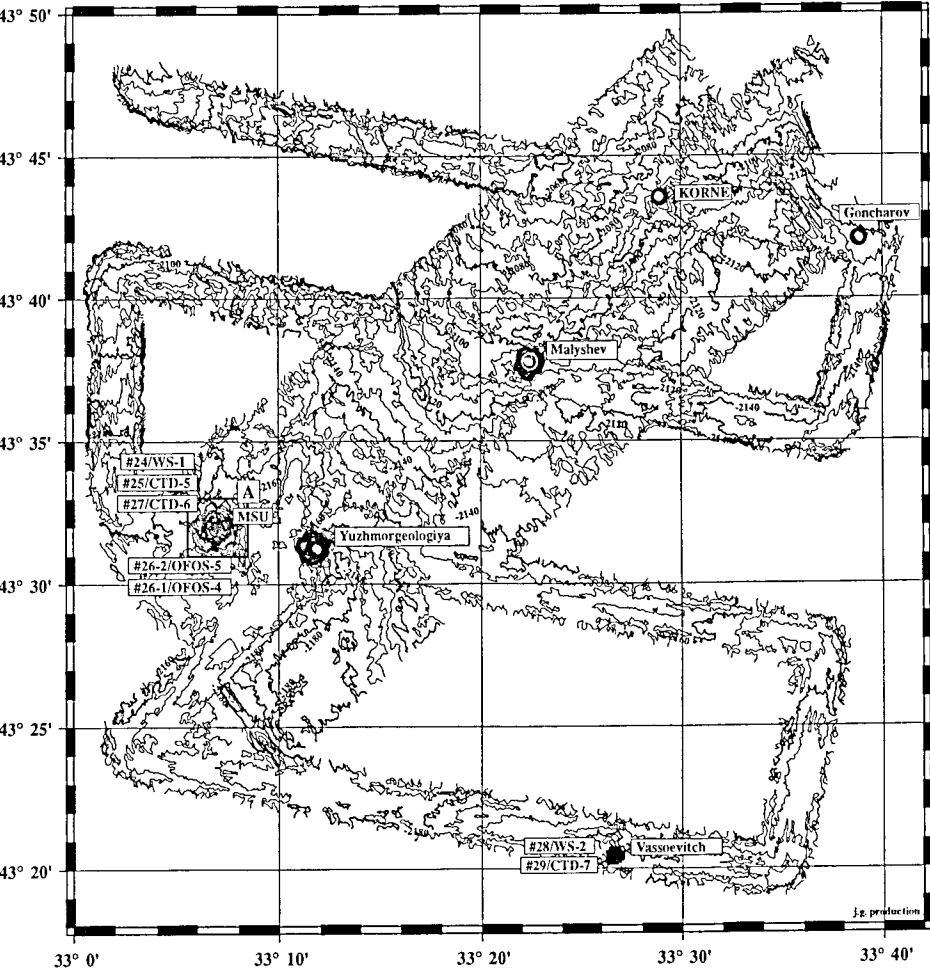


Fig. 9:  
Location map of  
the central Black  
Sea area.

seafloor and maps an up to 1.5 km-wide swath profile, providing detailed images of morphological and lithological changes of the seafloor. There is still some fine-tuning to be done concerning the analogue representation of the data. However, we were quite satisfied with the first results.

In the night of **January 14** we went back to our former study area the Sorokin Trough, which belongs to the Eastern Basin of the Black Sea. The Eastern Basin and the Western Basin are separated by the Andrusov Ridge. Preliminary processing of the seismic reflection data from our previous surveys had raised some questions concerning the Sorokin Trough. In order to answer the question, we obtained another 20 hours of seismic profiling and especially of Parasound mapping, the latter providing data of excellent quality. Afterwards, side-scan sonar mapping was carried out in several areas dominated by mud volcanoes, including Dvurechenskii mud volcano. Dvurechenskii has a different structure than other mud volcanoes. It is not cone-shaped but flat-topped resembling a volcanic crater lake of about 1 km diameter that is filled to its edge.

An extensive sampling programme including gravity corer, mini corer and detailed sampling of the water column was run on **January 17 and 18** (Fig. 8). The gravity corer was equipped with thermistor thermometers. For the first time, information could be obtained on the in situ temperature of the sediment within Dvurechenskii mud volcano. We were quite surprised by the results. While water temperatures are about 9°C at the seafloor, the upper sediment in the central part of the mud volcano showed temperatures of up to 16°C in depths of up to 6 m. These high temperatures suggest a currently active rise of mud in Dvurechenskii mud volcano. In spite of the high temperature, the pressure is high enough in 2000 m water depth to allow the formation of gas hydrate. All four sedimentary cores from the mud volcano contain plenty of finely dispersed gas hydrate which dissociates fast when exposed on board. Gas hydrate dissociation is a strongly endothermic reaction. It uses heat from its surroundings and causes a marked decrease of temperature. The temperature taken with a thermometer on board, shortly after the cores had been opened, showed that the sediment had cooled to only 3°C. Such a marked cooling from the 16°C measured at the seafloor can only be explained by an extensive and very effective dissociation of gas hydrate that cannot be limited to what we saw on board but must already have started when the cores were moving upwards in the water column.

Almost all of the pore water samples from Dvurechenskii mud volcano show a high salt content, indicating a content of chloride up to 2.5 times higher than that of seawater. Such a high chloride content can only be explained by a salt source below the seafloor or by the highly effective process of salt enrichment as an effect of gas hydrate formation. This topic will be investigated in shore-based laboratories by measuring several geochemical trace elements and by specific isotope analyses. Above the mud volcano, our two colleagues from Hamburg have detected for the first time an increased concentration of hydrocarbons in the water column, indicating that the mud releases an increased amount of these substances into the water column. Based on images from another OFOS deployment indicating promising sampling site, we decided on two more sites for the TV-grab. The grab had been repaired due to strong efforts of our technicians with great support by the ship's crew. Precise handling of the instrument yielded two very interesting samples. The time of another 48-hour side-scan sonar survey was used for preliminary evaluation of some of the collected data and to discuss the seismic data obtained so far in order to prepare next week's 3-D survey.

At the beginning of our fourth week we completed the side scan sonar survey that had been started on the weekend. We had been mapping for two days, covering an area of about 200 km<sup>2</sup> that contains several mud volcanoes and that is particularly interesting with respect to our gas hydrate studies. The system was equipped with a deep-towed sediment echosounder, the recordings of which turned out to be of exceptional quality. Its high vertical resolution allowed imaging of some small mudflows in the vicinity of mud volcanoes. A very strong reflector appeared over much of the survey area at a depth of a few meters within the sediments. It may represent the transition from marine sediments of the Black Sea to the lake sediments below. More than 9,000 years ago, the Black Sea was a freshwater lake. When the sea level rose after the last glacial period, it quickly filled with sea water that entered through the Bosphorus from the Marmara Sea until the Black Sea was finally connected to the Mediterranean Sea.

On **January 21** we ran a long sampling programme including gravity corer and mini corer. Another set of gravity cores was taken from Dvurechenskii mud volcano, again with thermistor thermometers mounted to the outer tube (Fig. 8). There was an increased temperature flow in the western and southern areas of the mud volcano, however, it was far less pronounced than in the centre of the mud rise. A second set of water sampling and CTD above the active mud volcano showed a markedly increased concentration of methane near the seafloor, which is evidence for a current gas venting activity. Further gravity cores were taken from two adjacent mud volcanoes, each of them about 1 km in diameter. None of them had a name, and as they turned out to be quite important for our present work, we chose to call them „Sevastopol“ and „Yalta“ mud volcanoes. Almost 5 days were subsequently spent on seismic work focussing on Sevastopol mud volcano. An area of 7 x 2.5 km was covered by seismic 3-D mapping in order to obtain detailed images of the pathways that gases and fluids take when moving upwards from deeper sediment layers. Seismic signals from an airgun and a watergun were recorded parallelly by a high-resolution streamer system at the surface and by 14 ocean bottom hydrophones and seismometers at the seafloor. Apart from providing information about sedimentary layering and tectonic processes, the combined data will help quantifying volume characteristics in order to find out the locations and the quantities of gas hydrate enclosed in the sediment. The distribution of gas hydrates will therefore be worked out in connection with pathways of gas and fluid venting and to the presence of near- surface mud volcanoes. The seismic work ended after a successful recovery of all ocean bottom units on Saturday night (**January 26**), and we returned with our bags full of valuable seismic data.

The weekend preceding our fifth week in the Black Sea was dedicated to TV grab sampling at the Sevastopol and Yalta mud volcanoes. One of the deployments was hampered by battery failure, so that the grab had to be recovered before a sample had been taken. On the second deployment, however, we were able to retrieve a highly interesting 7 cm - thick bacterial mat on a carbonate crust. In the night of **January 27**, the TV sled was run along two profiles across the Dvurechenskii mud volcano. At the edge of the mud volcano, we identified a relatively large area covered by a white bacterial mat. In the centre of the volcano we observed numerous active vent sites in the form of small holes with elevated rims, sticking out from an otherwise very homogeneous seafloor. A further TV grab sample from one of the vents consists of sediment that carries a lot of water. When the finely dispersed gas hydrate dissociated, the sediment liquefied. Within this sample, there are a few single rocks, the largest of them the size of a fist. They are identified as exotic clasts



originating from the Maikopian Formation. The Maikopian Formation is a sediment sequence that is about 20-30 my old. Situated at a depth of about 6 km under the seafloor, it is generally seen as the source area of the mud volcanoes. A CTD towed on our TV-sled showed a clear increase of temperature in the water column above the mud volcano. The maximum temperature correlates well with the centre of the mud volcano.

On **January 28**, we took samples of the water column and made another deployment of the side-scan sonar, using the 410 kHz resolution signal directly above the flat top of the mud volcano. At a distance of only 10 m from the seafloor, the swath profile is only 100 m wide, but the resolution is much higher, so that objects on the seafloor can be imaged down to a centimeter scale. On the evening of **January 29**, we went to the eastern edge of our working area in order to sample known gas vents at shallow depths. We could indeed confirm the occurrence of three gas vents at water depths of 300 - 700 m. The vents are marked by acoustic plumes in the water column above the seafloor and can be detected by the 18 kHz Parasound signal. A set of CTD and water sampling was run on one of these plumes, complemented by plankton netting. Some additional Hydrosweep and Parasound mapping was run until the evening of **January 30**, when the station work of METEOR cruise M52/1 - MARGASCH officially closed.

During the cruise, the different working groups presented their preliminary results during scientific meetings which took place every two days in METEOR's conference room. The quality as well as the amount and variety of interesting results show that M52/1 was an unusually successful cruise. We would therefore like to thank all the persons and institutions who have contributed to this success.

### 3. WEATHER

H. Weiland

The weather situation in the first week of the cruise was dominated by a stationary high over Central Europe with a ridge extending to Russia. From time to time, lows moved southeastward from Scandinavia at the eastern flank of the high. Wind from the northeast prevailed with forces between Bft 5 and 7, at temperatures between  $-3$  and  $-5^{\circ}\text{C}$ . Only during the passage of the lows the wind turned to southwest and the temperatures rose to about  $+4^{\circ}\text{C}$ . In the northeastern part of the Black Sea the northeasterly wind showed to be quite steady because of a low over the southeastern part of the Black Sea, which often develops above the warm water there. It will then sit in the lee of the Caucasian mountains. The pressure-gradient opposite to the Russian ridge will then be strengthened, an example of which was observed on January 8 in the evening, when the northeastern winds increased to Bft 8 and the temperature fell to minus  $9^{\circ}\text{C}$ . Very cold air from southern Russia flowed into the Black Sea between the Caucasus and the Crimea across the icy Sea of Asov due to a strengthened ridge over Ukraine. On January 9 the situation changed. The ridge of high pressure moved south and at the northern flank of the European high pressure area mild air masses floated into Russia. The wind was calm, the temperatures above zero and the sky cloudy. This situation remained unchanged for ten days.

On 20 January the fronts of Atlantic lows reached the Black Sea. In the next days strong storm-depressions moved from England to Scandinavia, thus the Black Sea area was situated in a flow of mild air from southwesterly directions with forces between Bft 3 and 6. The cloud cover was variable and the temperatures remained near  $8^{\circ}\text{C}$ . In general, during most of this cruise the conditions of the wind-forces did not correspond to the mean climatic values for January in this area. At an average of nearly 15 knots, January is the month with the highest wind force. While the wind comes from the northeast on about 30 per cent of days, forces will be above Bft 8 on an average of 25 per cent. Fortunately, on this cruise the wind force was significantly lower most of the time.

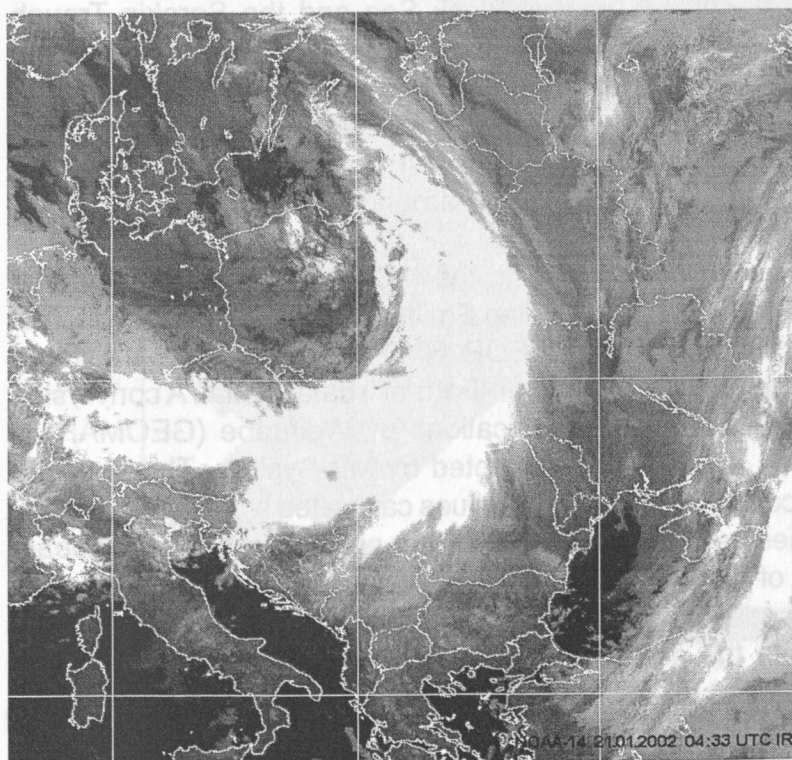


Fig. 10:  
Weather chart of January 21,  
showing the Black Sea in a  
calm situation.



### 3. MULTIBEAM SWATHMAPPING

(W. Weinrebe, I. Klaucke, and watchkeepers)

Onboard R/V METEOR, the HYDROSWEEP DS2 multibeam system by ATLAS-ELEKTRONIK is available for continuous bathymetric profiling. Using a frequency of 15.5 kHz and 59 beams in a swath of 90° the system can map the seafloor with a scanline width of up to twice the water depth. The range of the central beam is up to 10,000 m with an error of about 1%. The range of the outer beams is up to 7,000 m with a precision of about 1% if the ship's roll is less than 10° and pitch less than 5°. Corrections for the ship's attitude (roll, pitch, heave) are applied automatically. Due to the fixed beam angle of 2.3°, the resolution depends on the water depth and the slant angle and varies from about 80 m to 200 m in water depths of 2,000 m to 2,500 m.

To calculate depths from the echo time delays, information is required on the velocity of sound in the different water layers. HYDROSWEEP applies a special calibration scheme by interchanging transmitting and receiving transducers and thus sounding along the track to determine an average water sound velocity (Schreiber and Schencke, 1990). Yet in certain areas this algorithm fails (Flueh and von Huene, 1994). Direct measurement of sound speed at different depths using a CTD yields better results.

Postprocessing of HYDROSWEEP data comprises merging navigational data, calculating depths and positions of the footprints of the beams, removing artifacts and erroneous datapoints, and generating a digital terrain model (DTM). The ATLAS HYDROMAP software is available on board for that purpose. However, for several reasons outlined in Flueh and von Huene (1994) and Weinrebe (1997), the academic software MB-System (Caress and Chayes, 1996) from Lamont-Doherty Earth Observatory is preferred for HYDROSWEEP data processing.

HYDROSWEEP multibeam data were continuously recorded as long as RV METEOR operated in the two research areas in the central Black Sea and the Sorokin Trough respectively. A total of 207,970 pings were recorded during 560 h along a track of around 4,500 km, yielding 12,270,230 data values. However, as the position of the transducer on the hull of RV METEOR is not optimal, the performance of the system is strongly dependent on wind, wave, swell, and current conditions. Eventually, just 124,418 pings and 577,267 beams (depth values) were usable, resulting in a rate of around 50%.

HYDROSWEEP data were processed onboard using the MB-System software (Caress and Chayes, 1996) and the GMT software (Wessel and Smith, 1991) as well as a bunch of inhouse programmes and scripts. Onboard RV METEOR, HYDROSWEEP data are stored in the ATLAS SURF („Sensor-Unabhängiges Rohdaten-Format“) data format. A conversion programme written by von Lom (GeoB) with modifications by Weinrebe (GEOMAR) is applied to the data for conversion into a format accepted by MB-System. The software does not convert travel time data correctly, so the depth values calculated by HYDROSWEEP based on average sound velocities have to be used for further processing. The multibeam sweeps, including all 59 beams of a swath, were cleaned and edited to eliminate erratic points. Edited sweeps were then assembled, gridded, and contoured with GMT Software. No filters were applied to smooth the data. Grid cell size was chosen to gain highest resolution, but avoiding aliasing, with typical values of 100 m.

**Bathymetry data of TTR6-cruise**

In addition to the HYDROSWEEEP data, multibeam data recorded with a Simrad EM-12S system onboard RV GELENDZHIK during the TTR6-cruise (Woodside et al., 1997) were available in digital form and could be merged with the HYDROSWEEEP data. The Simrad EM-12S is a newer generation multibeam system applying a swath of 120° and recording 150 beams. The EM-12S had been installed onboard RV GELENDZHIK just prior to the TTR6-cruise, and did not operate with optimal performance during that cruise. The data (Fig. 13a) show several problems with improper attitude correction and erroneous water sound velocity treatment. Even after a thorough reprocessing a misfit between different tracks is visible (Fig. 13a). However, this dataset in combination with HYDROSWEEEP data of the M52/1 cruise (Fig. 13b) comprise a valuable basis to image the seafloor morphology in the research areas.

**Central Black Sea area**

The area in the central Black Sea south of the Crimean Peninsula mapped during the TTR6 and M52/1 cruises is shown in Fig. 11. The larger southwest - northeast trending block was mapped with the Simrad EM12-S multibeam system during the TTR6 cruise, whereas the lawn-mower pattern represents tracks surveyed with D during M52/1. The overall bathymetry of the area is essentially flat with a slight dip towards the south, with water depths increasing from 2,000 m to about 2,200 m. Dominant features in the area are six mud volcanoes: MSU, Yuzhmorgeologiya, Malyshev, Kornev, Goncharov, and Vassoevitch, rising up to 120 m above the adjacent ocean floor. The mud volcanoes show quite different shapes. A typical distinct steep cone structure is found at Yuzhmorgeologiya,

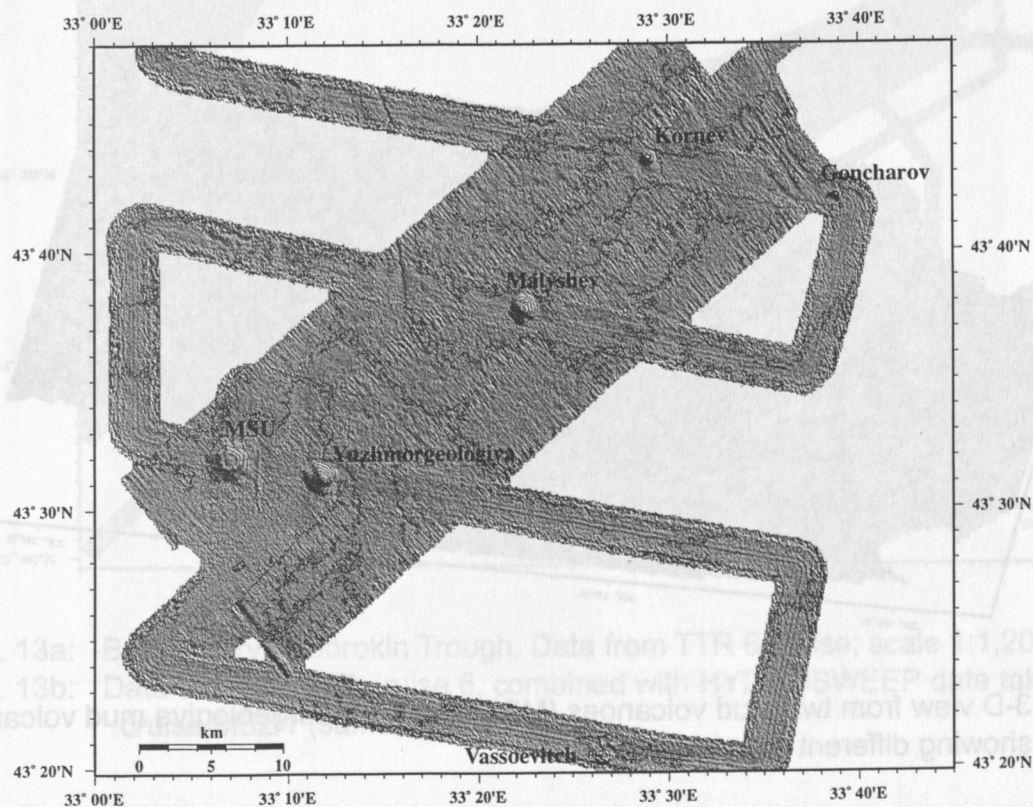


Fig. 11: Bathymetry of the area of investigation in the central Black Sea.



Malyshev, Kornev, and Goncharov, sometimes accompanied by a circular surrounding depression (Fig. 12), whereas MSU has a flattened top with an elevated rim. Vassoevitch is just an irregularly shaped depression, possibly with a central pipe.

### Sorokin Trough

The main working area was inside the northeastern box (Fig. 5) permitted for research around the Sorokin Trough. A large part of this area had already been mapped with a Simrad EM12S multibeam system during the TTR6 cruise (Fig. 13a; Ivanov et al., 1996). However, with the HYDROSWEEP data acquired during cruise M52/1, this area was considerably extended (Fig. 13b). The general morphology in the Sorokin Trough area is quite smooth with water depths around 2,000 m, decreasing towards the coast with increasing relief (Fig. 13a). Figures 14, 15, and 17a show different parts of the area at a larger scale in shaded relief bathymetric images. Though processing artifacts and erroneous data are visible, fine details of the morphology are clearly detectable. As in the central Black Sea area (Fig. 11), several distinct mud volcanoes can be detected. Fig. 15 shows the main mud volcanoes in the annotated area. The variability of morphological expressions of different mud volcanoes is quite obvious, ranging from distinct steep cone-shaped mounts (Kazakov, NIOZ, Istanbul) to shallow depressions with a small central uplift (Dvurenchenskii). This is even more obvious in the perspective images of the area (Fig. 16a, view from southwest; Fig. 16b, view from northeast, and Fig. 17b, showing the most northeasterly part in a view from southwest). A general downslope sediment transport is visible in abundant concave sediment waves in most parts of the area.

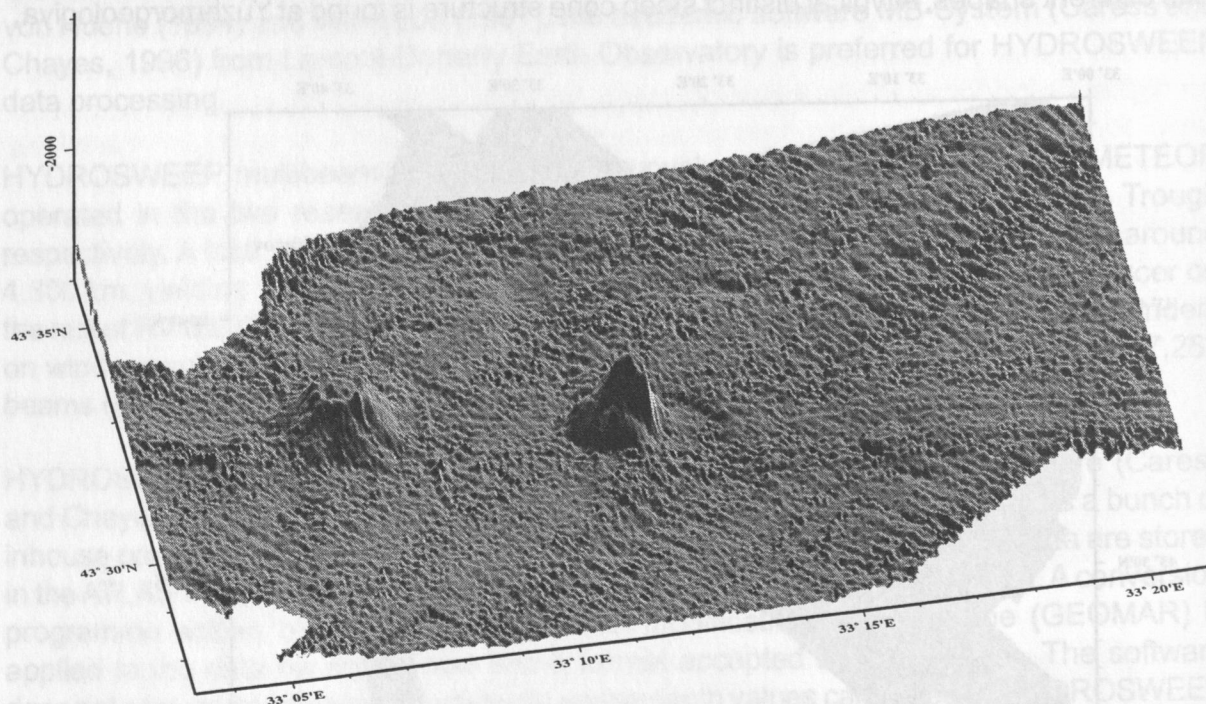


Fig. 12: 3-D view from two mud volcanoes (MSU and Yuzhmorgeologiya mud volcano) showing different morphology.

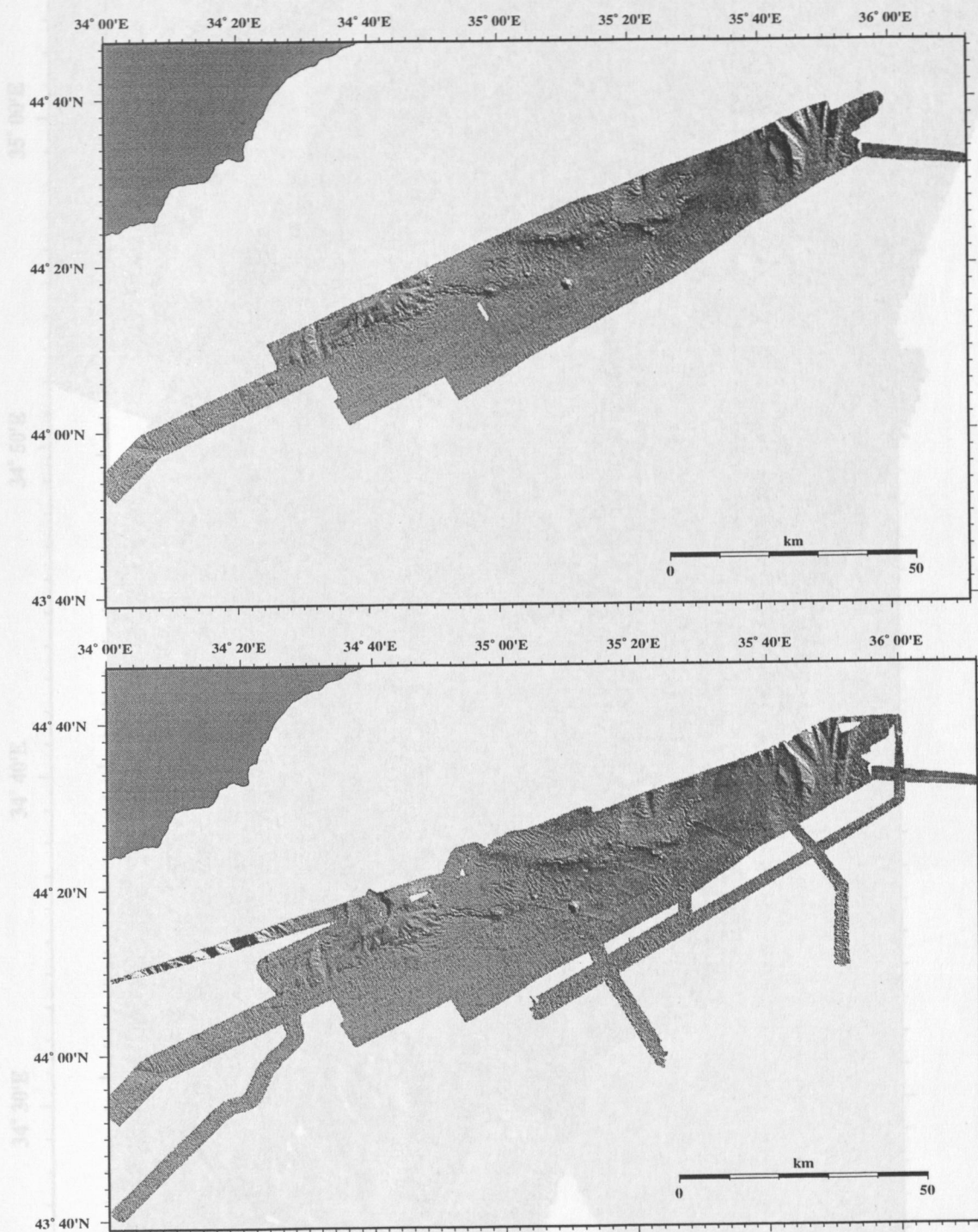


Fig. 13a: Bathymetry of Sorokin Trough. Data from TTR 6 cruise; scale 1:1,200,000.

Fig. 13b: Data set from TTR cruise 6, combined with HYDROSWEEEP data taken during cruise M52/1 (same scale).

Fig. 15: Detailed bathymetry of the Sorokin Trough in the area of the Sevastopol and Yalta mud volcanoes, scale 1:350,000, illumination 40°.



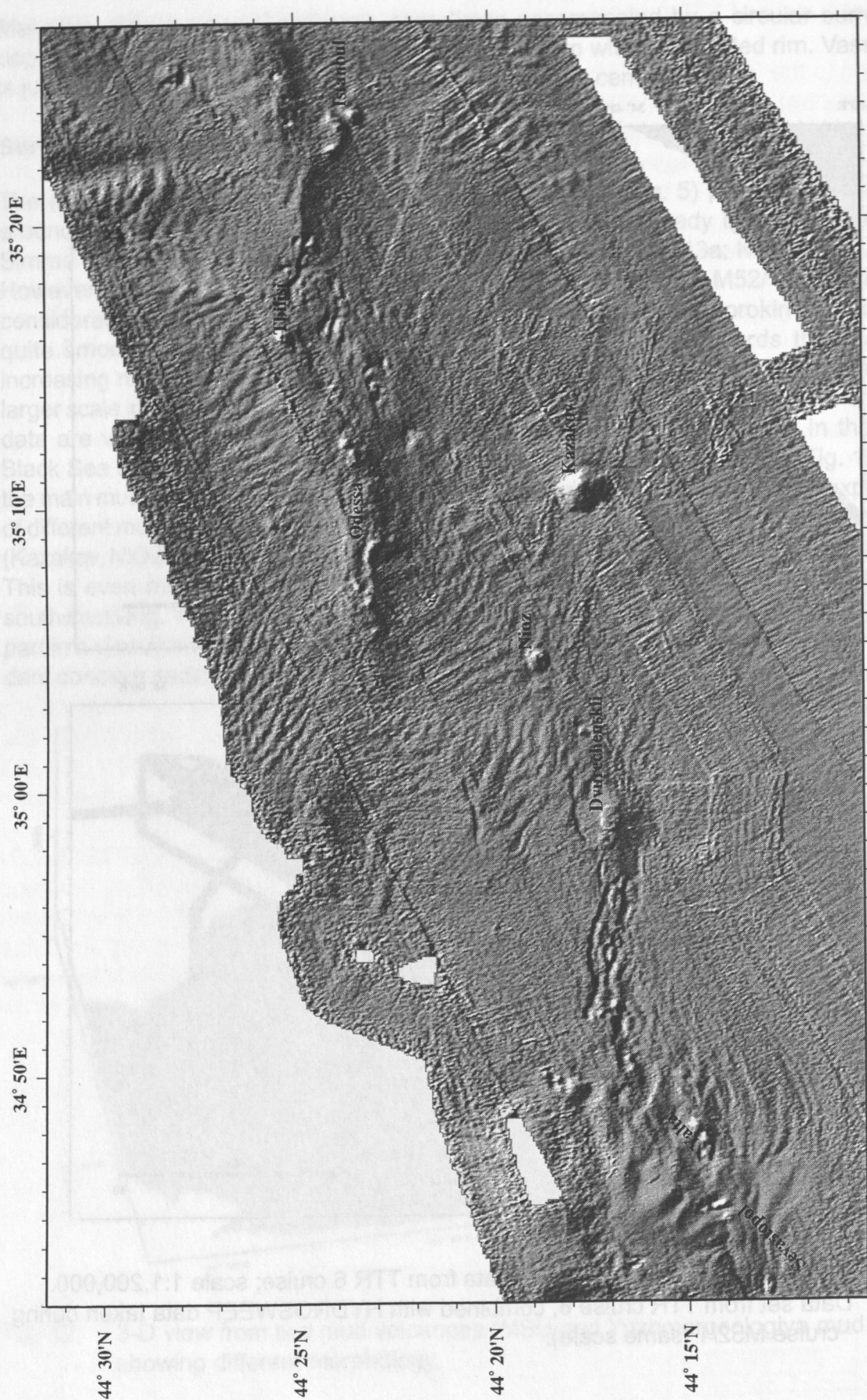


Fig. 14: Bathymetry of the central Sorokin Trough; scale 1:350,000.



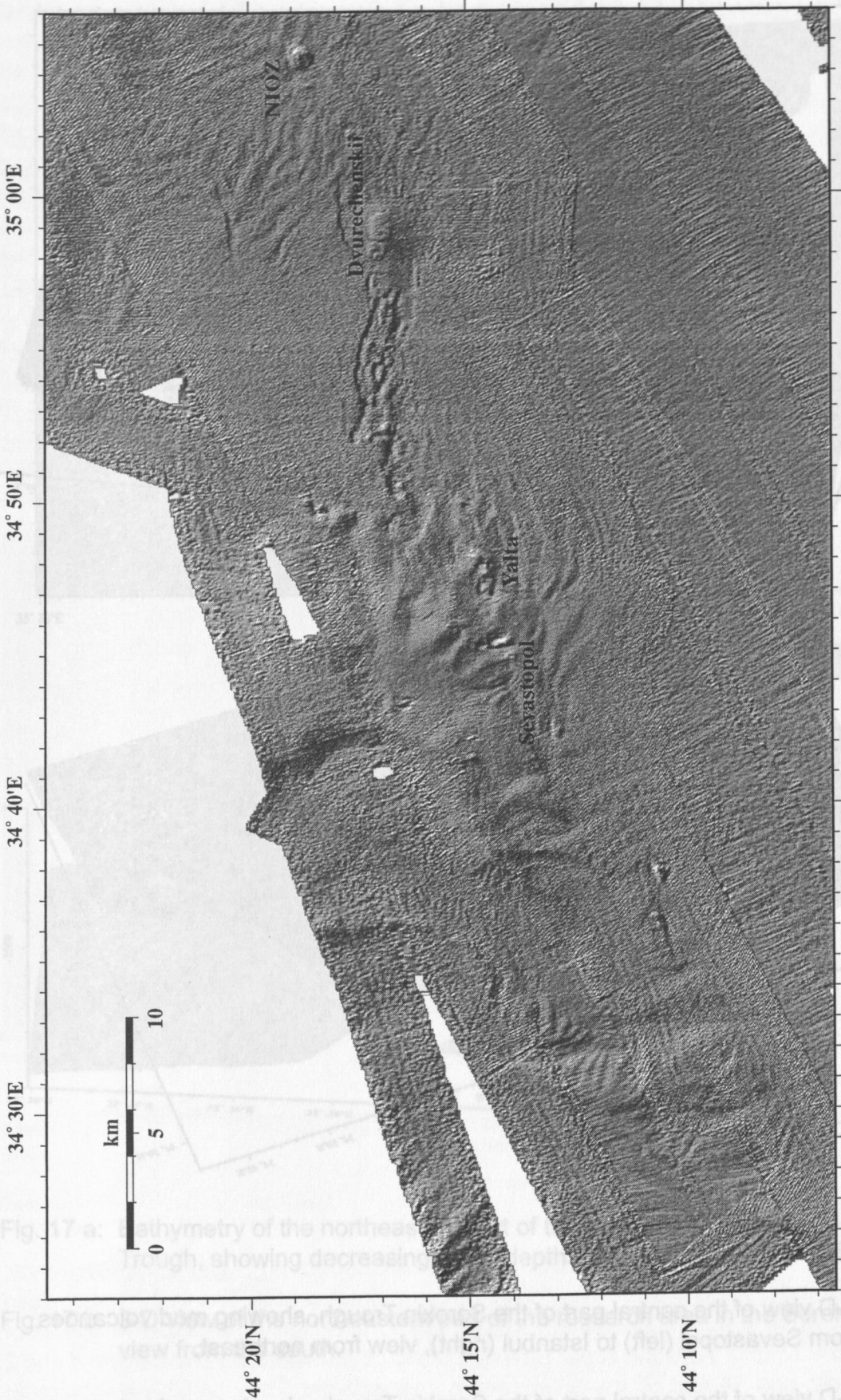


Fig. 15: Detailed bathymetry of the Sorokin Trough in the area of the Sevastopol and Yalta mud volcanoes; scale 1:350,000; illumination 40.

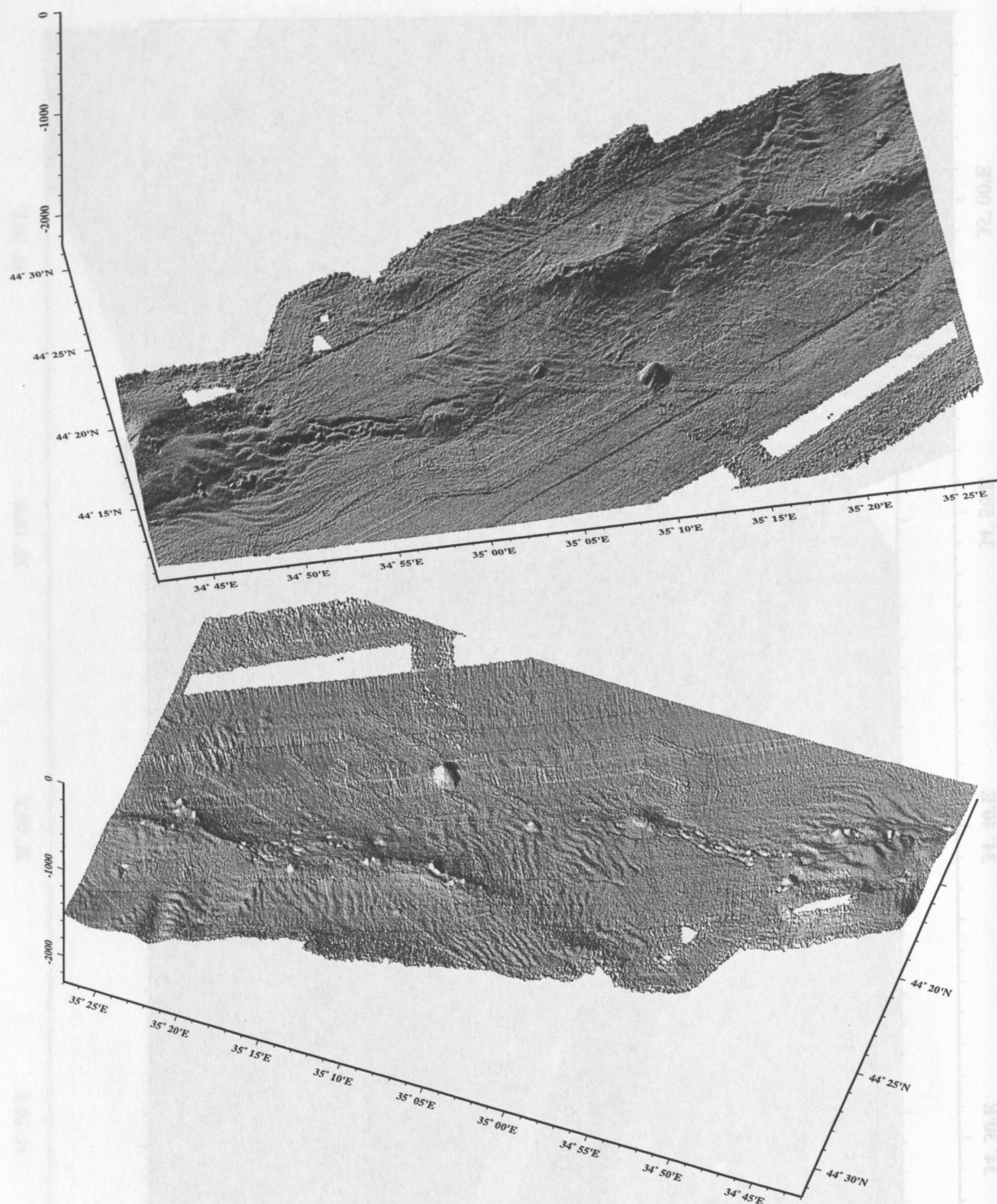


Fig. 16 a: 3-D view of the central part of the Sorokin Trough, showing mud volcanoes from Sevastopol (left) to Istanbul (right), view from northeast.

Fig. 16 b: 3-D view of the central part of the Sorokin Trough, showing mud volcanoes from Istanbul (left) to Sevastopol (right), view from northeast.



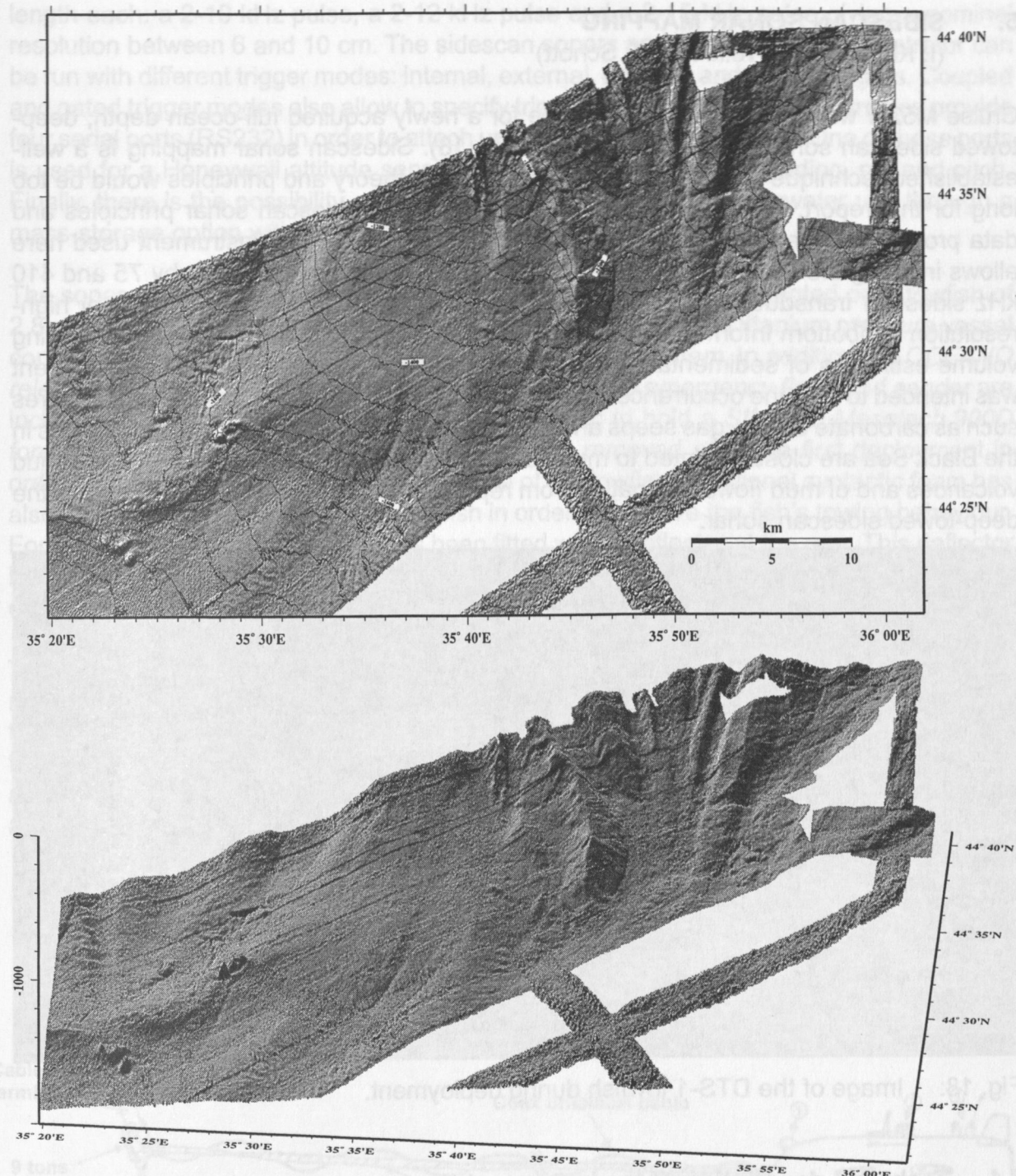


Fig. 17 a: Bathymetry of the northeastern part of the research area in the Sorokin Trough, showing decreasing water depths and higher relief towards the coast.

Fig. 17 b: 3-D view of the northeastern part of the research area in the Sorokin Trough, view from the south.



## 5. SIDESCAN SONAR MAPPING

(I. Klaucke, W. Weinrebe, T. Schott)

Cruise M52/1 was the first scientific cruise for a newly acquired full-ocean depth, deep-towed sidescan sonar system, the DTS-1 (Fig. 18). Sidescan sonar mapping is a well-established technique and a thorough summary of its theory and principles would be too long for this report. For more detailed information about sidescan sonar principles and data processing, please refer to Blondel and Murton (1998). The instrument used here allows imaging the backscatter intensity of the seafloor at high resolution by 75 and 410 kHz sidescan transducers. This surface information can be integrated with very high-resolution subbottom information of the uppermost sedimentary layer, therefore allowing volume estimates of sedimentary units at the seafloor. For cruise M52/1 the instrument was intended to map the occurrences of near-surface gas hydrates and associated features such as carbonate crusts, gas seeps and pockmarks. As these gas hydrate occurrences in the Black Sea are closely related to mud volcanism, the surface expression of these mud volcanoes and of mud flows originating from represented another target for the use of the deep-towed sidescan sonar.

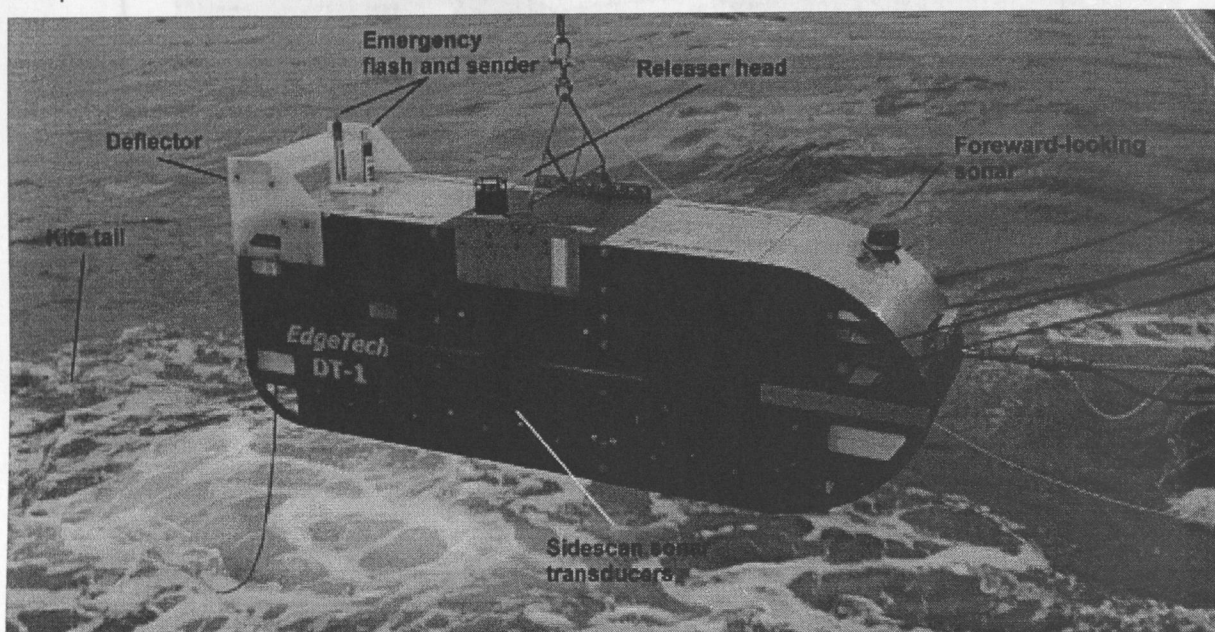


Fig. 18: Image of the DTS-1 towfish during deployment.

### 5.1 Technical description of the instrument

#### 5.1.1 Underwater set-up

The DTS-1 sidescan sonar (Fig. 18) is a *EdgeTech Full-Spectrum (FS-DW)* dual-frequency, chirp sidescan sonar working with 75 and 410 kHz centre frequencies. The 410 kHz sidescan sonar emits a pulse of 40 kHz bandwidth and 2.4 ms duration (giving a range resolution of 1.8 cm) and the 75 kHz sidescan sonar provides a choice between two pulses of 7.5 and 2 kHz band width and 14 and 50 ms pulse length, respectively. They provide a maximum resolution of 10 cm. In addition to the sidescan sonar sensors, the DTS-1 contains a 2-16 kHz, chirp subbottom penetrator providing a choice of three different pulses of 20 ms pulse

length each: a 2-10 kHz pulse, a 2-12 kHz pulse and a 2-15 kHz pulse giving a nominal resolution between 6 and 10 cm. The sidescan sonars and the subbottom penetrator can be run with different trigger modes: internal, external, coupled and gated triggers. Coupled and gated trigger modes also allow to specify trigger delays. The sonar electronics provide four serial ports (RS232) in order to attach up to four additional sensors. One of these ports is used for a Honeywell attitude sensor providing information on heading, roll and pitch. Finally, there is the possibility of recording data directly in the underwater unit through a mass-storage option with a total storage capacity of 30 Gbyte.

The sonar electronics are housed in a titanium pressure vessel mounted on a towfish of 2.8 m x 0.8 m x 0.9 m in dimension. The towfish houses a second titanium pressure vessel containing the wet-end of the *SEND DSC-Link telemetry system*. In addition, an *OCEANO releaser* with separate receiver head and a *NOVATECH emergency flash and sender* are included in the towfish. The towfish is also designed to hold a *SIMRAD Mesotech 900D foreward-looking sonar*, but this sensor has been removed after the first deployment in order to gain additional buoyancy at the nose of the towfish. Additional syntactic foam has also been placed in the front of the towfish in order to improve the fish's towing behaviour. For the same reason, the towfish has been fitted with a deflector at the rear. This deflector has five positions from 0 to -5 and is designed to reduce the pitch of the towfish. During cruise M52/1, -3 proved to be the most useful setting.

The towfish is connected to the sea cable via the depressor (2 tons weight) through a 40 m long coax umbilical cable. The umbilical cable is tied to a buoyant rope that takes up the actual towing forces. Another rope has been taped to the buoyant rope and serves for pulling in the instrument in case of an emergency recovery during bad weather. An additional knotted, buoyant rope of 20 m is attached to the tail of the fish and serves as a kite tail for stabilisation of the towfish.

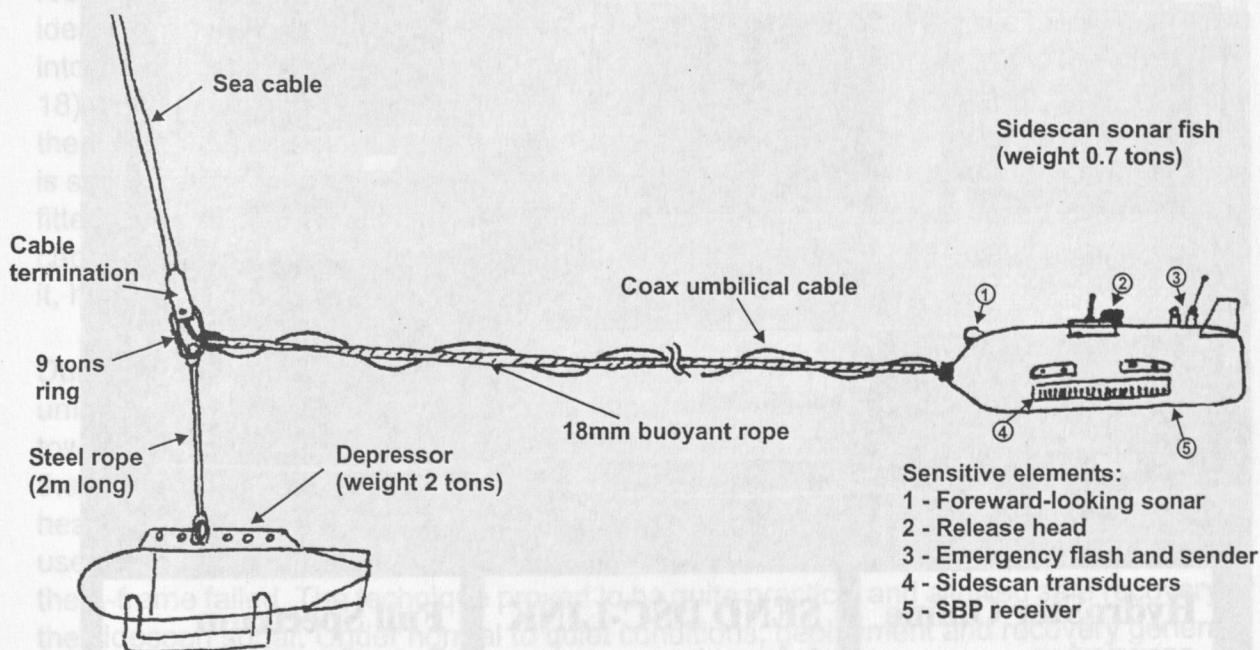


Fig. 19: The DTS-1 towing configuration.



### 5.1.2 Laboratory set-up

The laboratory set-up consists of three elements: the dry-end of the *SEND DSC-Link* telemetry, the *Edgetech* surface interface unit *FS-IU* and the topside unit running *ELAC HydroStar Online* software (Fig. 20, Fig. 21). *HydroStar Online* allows general running of the sidescan sonar and subbottom penetrator operations as well as onscreen display of a subset of the acquired data. Unfortunately some additional settings such as the trigger mode or data window size can only be changed by accessing the underwater electronics directly via the *FS-IU*. The *FS-IU* also runs *JStar*, a diagnostic software tool, that also allows running some basic data acquisition and data display functions.

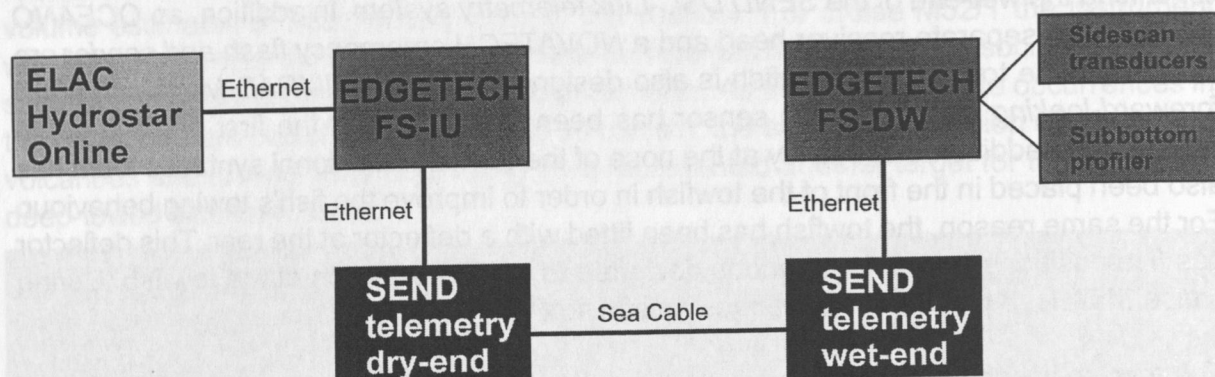


Fig. 20: The DTS-1 electronics configuration.

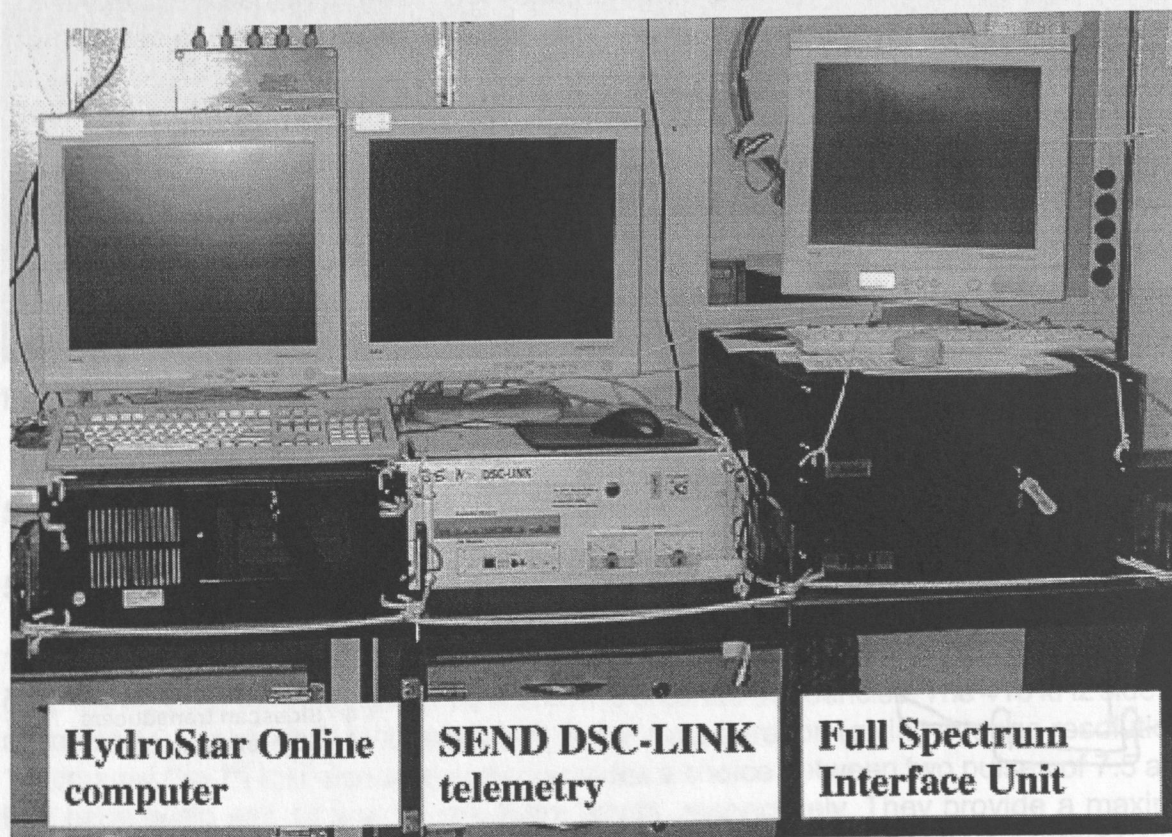


Fig. 21: The laboratory set-up.

### 5.1.3 Software

The main operations of the DTS-1 sidescan sonar are essentially run using *HydroStar Online*, a multibeam bathymetry software developed by *ELAC Nautik GmbH* and recently adapted to the acquisition of *EdgeTech* sidescan sonar data. This software package allows onscreen representation of the data, of the fish's attitude, and of the ship's navigation. It also allows setting some principle parameters of the sonar electronics, such as the selected pulse, the range, the power output, the gain and the ping rate. Unfortunately, the present version of *HydroStar Online* does not allow to set the range of registered data, nor the trigger mode or the master subsystem in coupled trigger mode. *HydroStar Online* also allows to start and stop data storage either in XSE-format on the *HydroStar Online* computer or in JSF-format on the *FS-DW*. Simultaneous storage in both XSE and JSF-formats is also possible. Both systems change files when a file size of approximately 10 Mb is reached. How fast this file size is reached depends on the amount of data generated, which in turn essentially depends on whether the high-frequency sidescan sonar is used or not. The amount of data generated is also a function of the sidescan sonar and subbottom pulses and of the data window that is specified in the sonar.ini file on the *FS-DW* (Appendix 2). The data window specifies the range over which data are sampled. Proper selection of this parameter strongly depends on the selected range of the sidescan sonar systems in order to avoid good data to be cut off, or to prevent too large amounts of unuseful data using up storage space.

### 5.2 Deployment and recovery procedures

The operations for deployment and recovery of the sidescan sonar are a bit demanding and require relatively calm sea for a handling that is safe for both crew and instrument. During cruise M52/1 three seamen, the boatswain, the sidescan sonar technician and the responsible scientist were on deck for the operations. The sidescan sonar instrument should ideally be towed via the A-frame. With no speed made by the ship the kite tail is first thrown into the water and left to drift away. Then the sidescan towfish is heaved into the water (Fig. 18) and released with a special hook allowing to detach the crane cable. The sidescan fish then also drifts astern with minimal speed made by the ship. Meanwhile, the buoyant rope is secured. Then the depressor is put in place below the A-frame, the buoyant towing rope fitted to the end termination of the sea cable, and the umbilical cable connected to the sea cable. Any loose ends are securely tied up and the depressor, with the towfish attached to it, heaved into the water (Fig. 22).

During recovery, first the depressor is pulled in and the umbilical cable is detached. The umbilical cable and towing rope are secured while the depressor is put away. Then the towfish is manually pulled near the stern of the ship and one man tries to attach the hook of the crane to the towfish. If this operation should fail in bad weather, the towfish could be heaved in with the additional rope taped to the umbilical cable. Fortunately, we only had to use this technique during the last recovery of the sidescan sonar when the hydraulics of the A-frame failed. The technique proved to be quite practical and allowed safe recovery of the sidescan sonar. Under normal to quiet conditions, deployment and recovery generally took 30-45 minutes. The total time for deployment and recovery in 2000 m water depth was approximately 3 hours each with a maximum winch speed of 0.7 m/s.



### 5.3 Settings used during the cruise

The DTS-1 sidescan sonar was deployed five times during cruise M52/1 with deployment times ranging from 10 to 52 hours. During these deployments a total of 530 km<sup>2</sup> of low-frequency sidescan sonar, 0.4 km<sup>2</sup> of high-frequency sidescan sonar and 410 line km of subbottom profiler data have been collected. Deployment of the sidescan sonar and its operation over a long cable required much flexibility in navigation. Without USBL navigation, the correct position of the towfish was not known. In any case, precise waypoints cannot be given, as the position of the towfish with respect to the ship depends on many factors including ship's speed, surface and bottom currents, and cable length. Therefore, profile start and end points as given in the list of stations (see Appendix 1) refer to the position of the ship and do not imply that sidescan sonar data coverage corresponds to these start and end points.

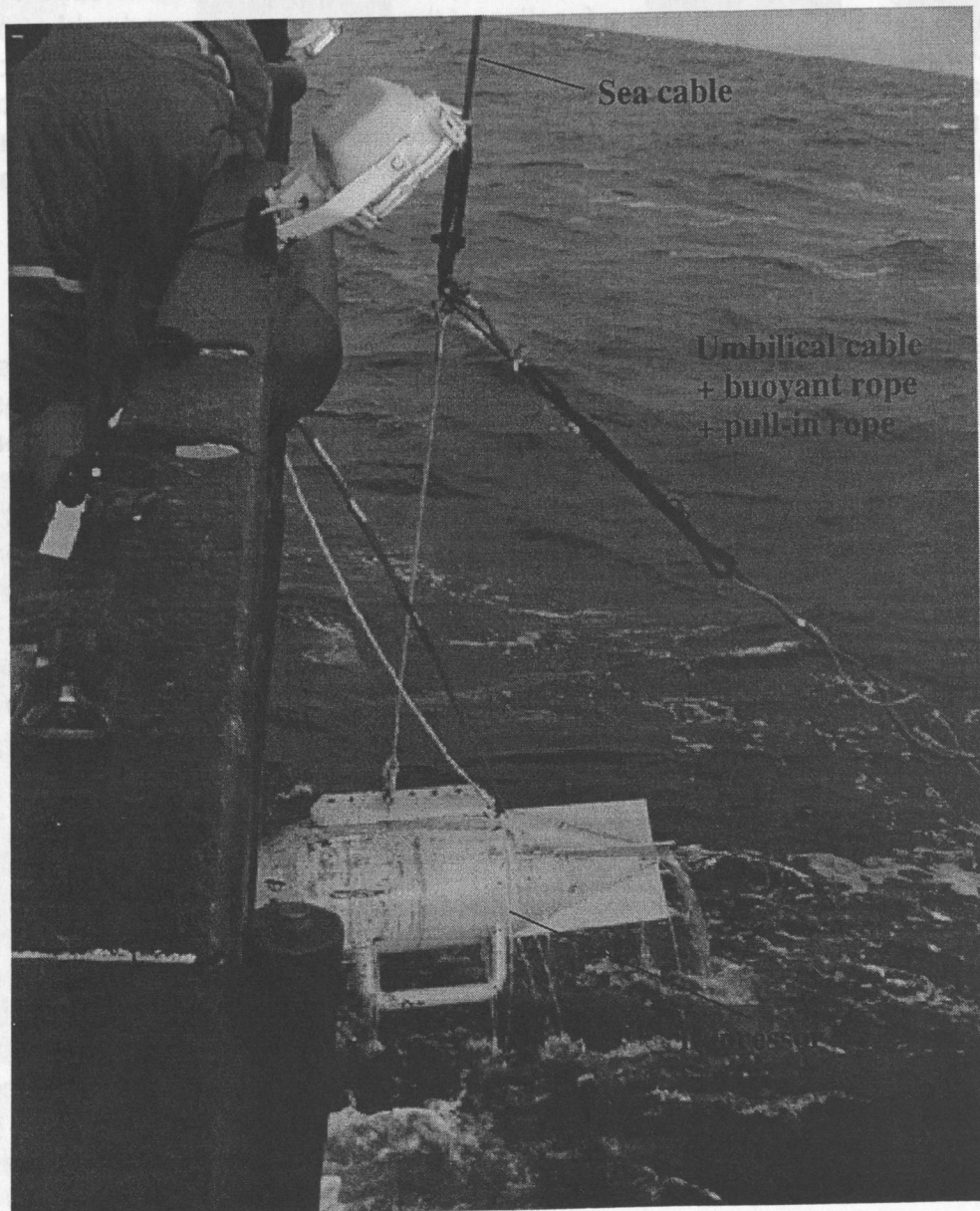


Fig. 22: Deployment of the depressor.

### 5.3.1 Deployment 1

The first deployment of the DTS-1 lasted for 7 hours on 10-01-02 from 14:12 to 21:13. It was also the first deployment of the DTS-1 in deep water and was designed to cover the same track as our Russian colleagues had covered with the MAK-1 30 kHz sidescan sonar (Fig. 23). This track was to cover the NIOZ and Kasakov mud volcanoes. This deployment was also intended as a test for different settings of the sidescan sonar and to test possible interferences by the HYDROSWEEP and PARASOUND acoustic sources. Prior to deployment all scientists involved agreed that the heavy depressor (2 tons) compared to the usual 0.7-1.0 ton depressor weights should keep cable length to a minimum. Not knowing the fish's depth, the sidescan and subbottom profiler records were to be used for detecting the seafloor. However, having no experience with the representation of the sidescan images onscreen without certainty about proper functioning of the acquisition software, we stopped the experiment and decided that depth information for the towfish is necessary for safe use of the instrument. Among the useful information we gained from this deployment are data concerning the trimming of the towfish. The attitude sensor indicated pitch and roll values of the towfish (nose and starboard down) that were too strong for proper functioning of the subbottom penetrator. The subbottom penetrator requires pitch and roll values of no more than  $\pm 6^\circ$ . Pitch values decreased with higher survey speed of 3 knots through the water underlining the effect of the deflector mounted to the towfish.

### 5.3.2 Deployment 2

Deployment 2, lasting for 11 hours between 14-01-02, 13:25 and 15-01-02, 00:45 was carried out in the Central Black Sea. Here one 35 km long track covered mostly flat-lying deposits with a small mud volcano towards the end (Fig. 24). 22.5 km<sup>2</sup> of low-frequency sidescan sonar have been collected during this deployment together with 35 line km of subbottom profiler data. Between deployments 1 and 2 the forward-looking sonar was removed from the set-up and an additional 13.5 kg of syntactic foam could be placed at the front of the towfish. This turned out to reduce previously observed high pitch and roll values. During this deployment a 12 kHz pinger was attached to the sea cable 30 m above the depressor providing the much needed depth information. It turned out that more than double the water depth was required as cable out before the seafloor came in sight. This strongly contradicted initial assumptions about the required cable length (see deployment 1). All possible output signals were tested during this deployment. The 14 ms pulse for the 75 kHz sidescan sonar at 1500m range (0.49 Hz ping rate) and the 2-10 kHz subbottom profiler pulse (1 Hz ping rate) gave the most satisfying results. However, there was always strong interference on both records. These interferences were generated by the sidescan sonar for the subbottom profiler, and vice versa. According to the manufacturer the interferences might be reduced by coupling the trigger of the two sensors. The test with a 'quiet' ship in order to determine possible interferences by other acoustic sources onboard was hindered by these strong interferences, but subsequent tests have shown that *Hydrosweep* and *Parasound* are not a major problem, if ever. During deployment 2 data were recorded in .xse format on the *HydroStar Online* computer only.

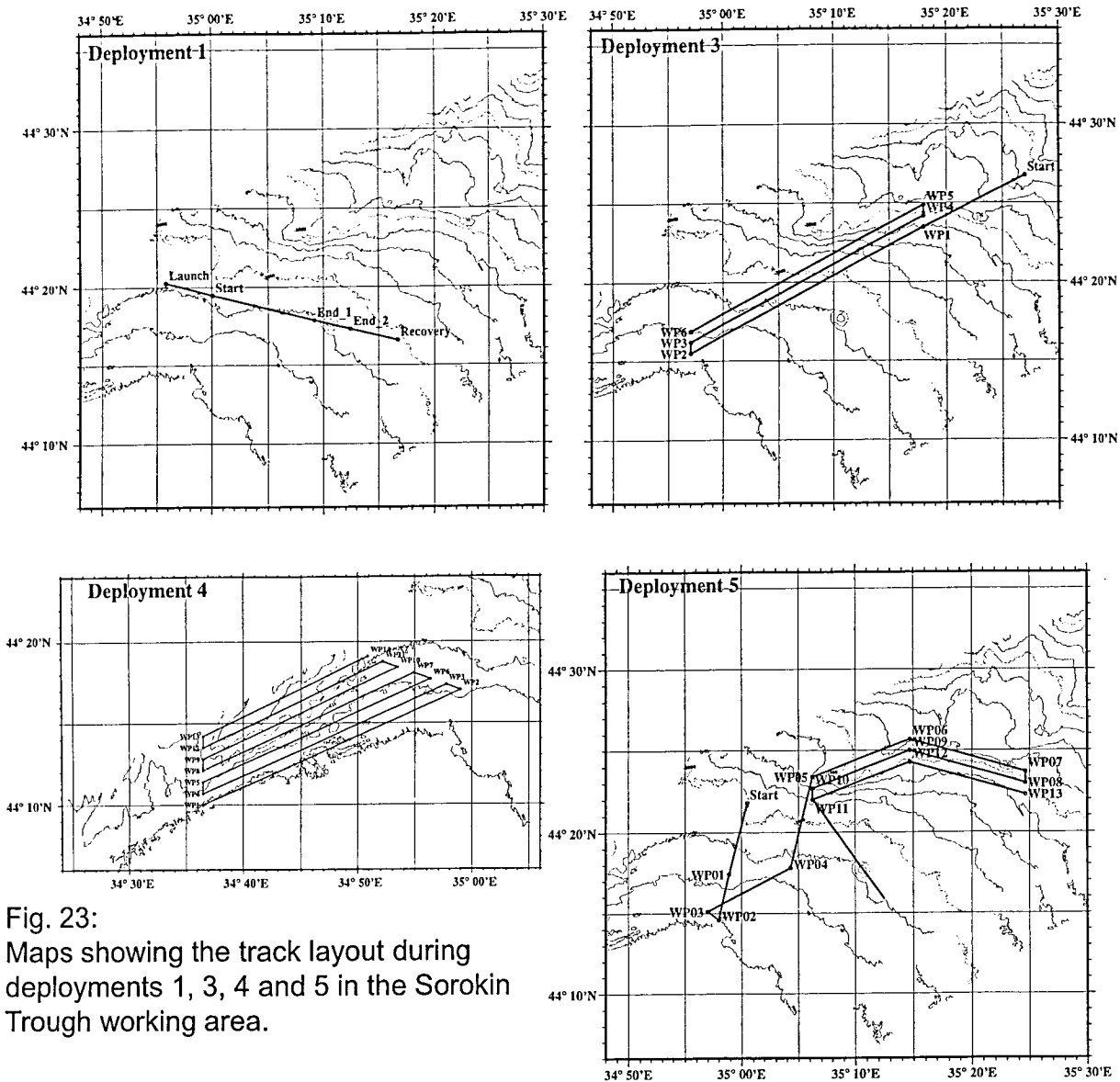


Fig. 23:  
Maps showing the track layout during  
deployments 1, 3, 4 and 5 in the Sorokin  
Trough working area.

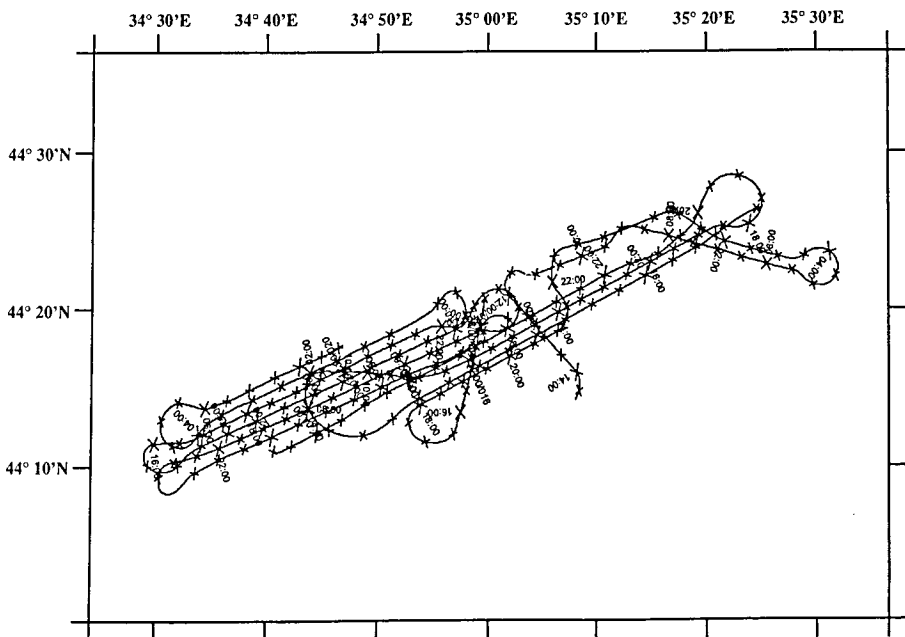


Fig. 24:  
Map showing the  
ship's track during the  
sidescan sonar  
deployments in the  
Black Sea.



### 5.3.3 Deployment 3

The 21-hour deployment 3 between 16-01-01, 22:54 and 17-01-02, 04:58 was again situated in the Sorokin Trough southeast of Crimea and consisted of three parallel tracks of 31 km each. In addition to 95 line km of subbottom profiler, 70 km<sup>2</sup> of low frequency sidescan sonar data have been collected during this deployment. The three tracks are 1,200 m apart and covered the NIOZ and Dvurechenskii mud volcanoes in the southwest (Fig. 23). During the deployment strong surface currents of about 1 kn were flowing in a southwesterly direction. This strongly influenced the necessary length of the cable. While sailing with the current, cable length was up to 30% above that required when sailing against the current.

Deployment 3 was also the first possibility to practise turns with the instrument in deep water. Turning while staying in recording range of the seafloor was very time-consuming and took as long as 5 hours. The quickest way to turn around was pulling in enough cable to stay in safe distance from the seafloor (about 1.5 times water depth) and then turn as tight as safe navigation permits. In this case, turning in 3 hours or slightly less is possible at 2000 m water depth.

### 5.3.4 Deployment 4

The fourth deployment of the sidescan sonar during cruise M52/1 (19-01-02, 08:02 to 21-01-02, 09:30) concentrated on the SE Crimean continental slope between 34°37'E and 35°E. It consisted of 7 parallel, SW-NE trending tracks with a track-spacing of 1,200 m. Again, only the 75 kHz sidescan sonar (14 ms pulse) and the subbottom penetrator (2-10 kHz, 20 ms pulse) were enabled. A total of 200 line km of subbottom profiler data and 300 km<sup>2</sup> of low-frequency sidescan sonar data were recorded. Modifications of the trigger between the two systems did not work, despite setting the TRIGGER MODE to the correct value in the sonar.ini file. It turned out after further enquiry from *EdgeTech* that the TRIGGER SYSTEM parameter also has to be changed and added to the sonar.ini file. During deployment 4 the range of the data window was set to 13000 allowing for sampling over a total range of 1500 m. A setting of 1500 m for the range in *HydroStar Online* allowed for a ping rate of 0.49 Hz while the subbottom penetrator continued to trigger at 1 Hz.

Some profiles of this deployment were run with the current and others against the current resulting in great differences in cable length. In addition, a strong bottom current appeared towards the end of the survey. When surveying with this bottom current cable length came to a minimum and a good operating depth was reached with only slightly more cable length than water depth. While this is good news for the navigation of the towfish, it turned out to be very negative for data quality. Following the last turn, data quality decreased markedly to a point where only very weak echoes returned to the subbottom penetrator while the sidescan sonar did no longer show identifiable structures. With weather conditions at the surface turning bad, we decide to stop the last profile and recover the instrument prematurely. All system checks, performed after the instrument had been recovered, did not indicate any failure or problem with the electronics and we decided that the current conditions at depth must have been responsible for poor data quality.

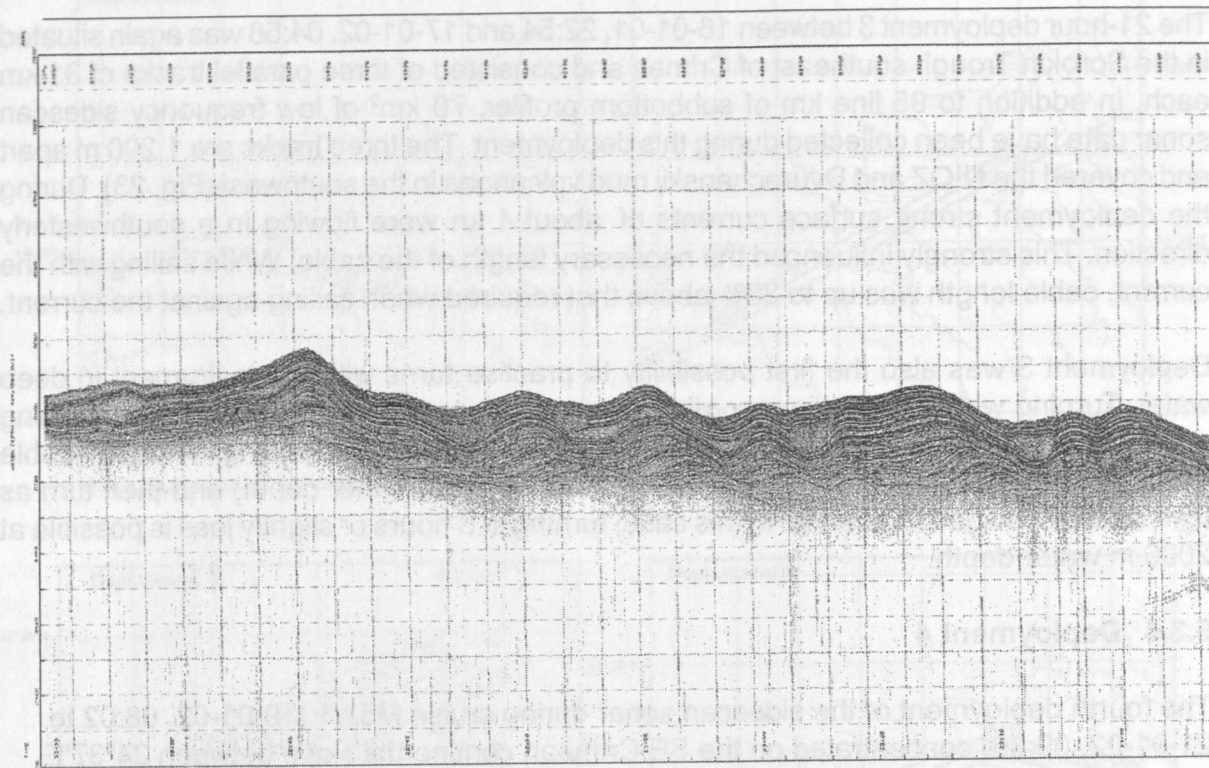


Fig. 25: Example of subbottom profiler data from deployment 3.

The data of deployment 4 were recorded as .xse files on the *HydroStar Online* computer and as .jsf files on the *FS-DW*. These .jsf files were subsequently uploaded without going through *HydroStar Online*.

### Deployment 5

The fifth and last deployment of the sidescan sonar lasted from 28-01-02, 13:17 until 29-01-02, 15:49. It consisted of 8 profiles with a total length of 90 km that yielded 140 km<sup>2</sup> of low-frequency sidescan sonar data from Dvurechenskii, NIOZ, Odessa, Tiblissi and Istanbul mud volcanoes. The first profile of the deployment crossing Dvurechenski mud volcano was designed to gain data with the very-high-resolution sidescan sonar (0.4 km<sup>2</sup> of data) that could be compared with a previously run OFOS track along the same line. During this first line all three sensors were running, although running the 75 kHz sidescan sonar at 15-20 m altitude above the seafloor does not provide a good range. The data window size for the high-frequency sidescan sonar was set to 4,000 samples per side allowing for approximately 105 m total range. This setting proved to be insufficient. Many good backscatter returns were truncated and the possible range of the 410 kHz sidescan sonar is probably closer to 200 m than 100 m. Unfortunately, the range setting in *HydroStar Online* that determines the ping rate remained at 10.0 m range resulting in too high a ping rate for the selected data window. The subbottom profiler (2-10 kHz, 20 ms pulse) and low-frequency sidescan sonar finally pinged in coupled mode, where the low frequency sidescan sonar acted as the master trigger. Unfortunately, here again, the range setting in *HydroStar*

*Online* remained at the default value resulting in a ping frequency of 0.98 Hz. Running the system in this mode resulted in data transmission rates (up to 260 kB/s) between the *FS-DW* and the *FS-IU* that reached the capacity of the Coax cable. A slight overflow (data loss) occurred at two occasions, but these data were still recorded in the towfish.

During the turn between WP2 and WP3 the high-frequency sonar was turned off and for the remainder of the profile only 75 kHz sidescan sonar and 2-10 kHz subbottom profiler data were collected. The profiles were intended to cross NIOZ mud volcano between WP4 and WP5. However, it proved extremely difficult to steer the ship in a way to keep the towfish close to the track line. In the case of this mud volcano, we missed it by more than 750 m (the range of the transducer per side) on either the port or the starboard side. After WP10, the track layout had to be changed because of time constraints and instead of continuing the turn to WP11, a new track over NIOZ mud volcano was designed. This time the mud volcano was crossed by the towfish 2.5 miles behind the ship (water depth = 2,100 m, cable length = 4,300 m, speed over ground = 3.5 kn indicating an almost straight cable).

### 5.3 Initial results

Due to problems in the data flow from the acquisition software to the processing software, an initial interpretation of the data is not possible. Thanks to the help of V. Spiess we are, however, capable of assessing the data quality. As always with new systems, many problems turned up. Some could be solved on board by ourselves and in conjunction with the manufacturer, some others remain to be solved.

#### 5.3.1 Data quality

Once the initial problems in running the instrument had been solved and after slowly getting closer to ideal settings, the data obtained were of generally high quality. Subbottom profiler data easily reached 20 metres of penetration in fine-grained sediment and sometimes even more (Fig. 25). Resolution, at the same time, was very high with reflectors of about 20 centimetres apart being clearly resolved. The detail shown in the subbottom profiler was well above that of the *Parasound* data, as a first, quick comparison indicates.

The data of the high-frequency (410 kHz) sidescan sonar also exceeded our expectations (Fig. 26). With a total range of well above 100 m and probably close to 200 m, a relatively broad section of the seafloor can be imaged at high resolution. Nominal resolution for this sensor is 2.6 cm and as a rule of thumb, 4 times this value may be achieved by most sidescan sonar systems. Detailed comparison and calibration of the high frequency sidescan sonar with OFOS video observations will ultimately reveal the true performance of this sensor.

The data quality of the low-frequency sidescan sonar was more ambiguous. The resolution seemed to be very good, although we do not yet have any possibility to assess the resolution (Fig. 27). After processing the sidescan sonar data, a comparison with the MAK-1 30 kHz data of our Russian colleagues will help assessing data resolution. The range of the instrument, on the other hand, was disappointing. The manufacturer stated a total range of 1500m. Yet, this value was only achieved in few places with high backscatter reflectivity. We do not know yet if interesting data have been recorded in other places as well, as high-



frequency noise and interferences are a problem in the far range of the low-frequency sidescan sonar. Some of these interferences are related to the incorrect trigger modes set for the early deployments of the cruise. However, while the strongest interferences such as those seen in figure 28 have been removed, additional high-frequency noise remained. These problems will have to be discussed with the sidescan manufacturer after the cruise.

### 5.3.2 Preliminary observations and interpretations

At present it is not possible to draw any detailed conclusions about the features we have seen on both the sidescan sonar images and the subbottom profiler data. The subbottom profiler data are not yet normalised to the altitude of the towfish and do not represent true morphology. Sidescan sonar images are not processed and not georeferenced.

A few features, however, are noticeable. The areas around mud volcanoes show widespread signs for mud flow activity, both at the surface and at depth. Many of these mud flows are interbedded with hemipelagic sediments indicating intermittent flow activity. Further away from mud volcanoes and fields of mud volcanoes, the seafloor appears to be relatively featureless. In the western part of this 'normal' seafloor area, a particular phenomenon could be observed on the subbottom profiler. Here, the strongest echo is not the bottom echo but another reflector at depths of about 6 metres. It has been speculated on board if this reflector represents the boundary between freshwater lake deposits at depth and current anoxic seawater conditions.

Other observations could be made on Dvurechenskii mud volcano that shows a number of not yet clearly identified flow structures on its steeper southern flank. Towards the top of the volcano, sheet-like eroded crusts are well visible and may hold clues for the distribution of gas hydrates. At present it cannot be said if near-surface gas hydrates have been imaged, but the sidescan sonar data obtained during cruise M52/1 are very promising and will reveal interesting results about the recent evolution of the Black Sea.

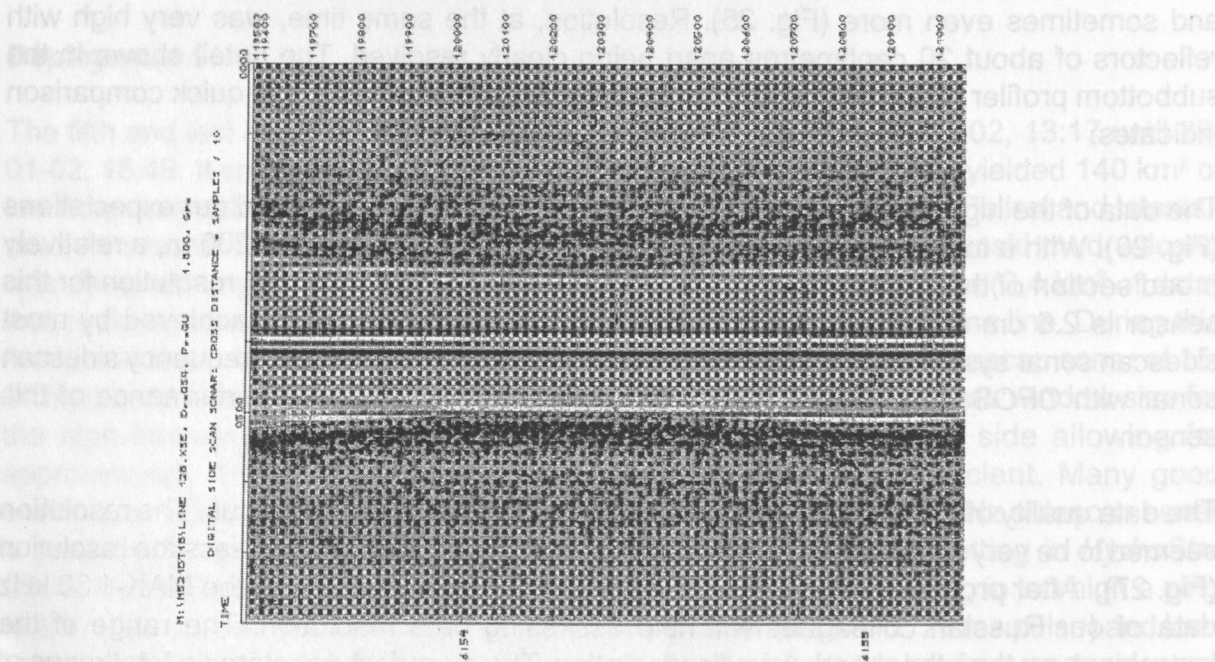


Fig. 26: Example of 410 kHz sidescan sonar data (range 100m) from Dvurechenskii mud volcano.

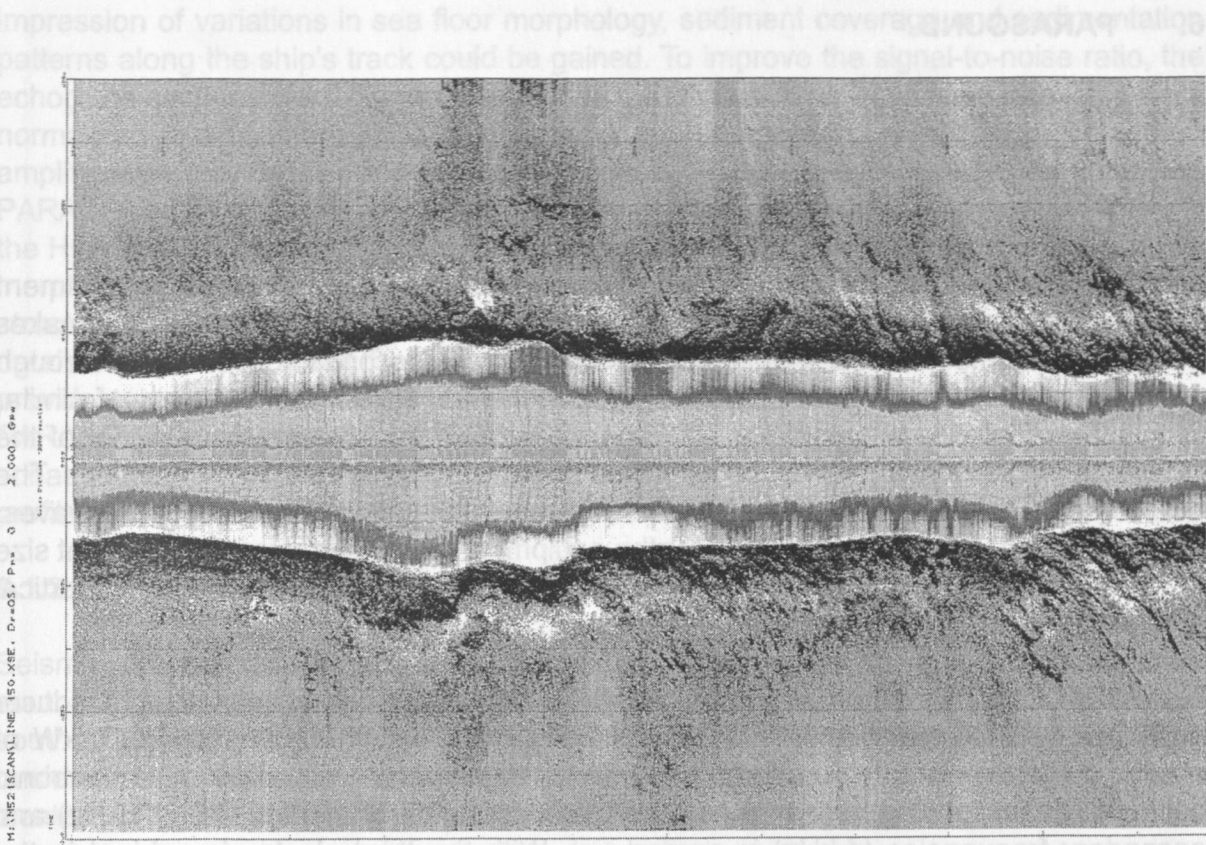


Fig. 27: Example of 75 kHz sidescan sonar data (range 720 m) from deployment 3.

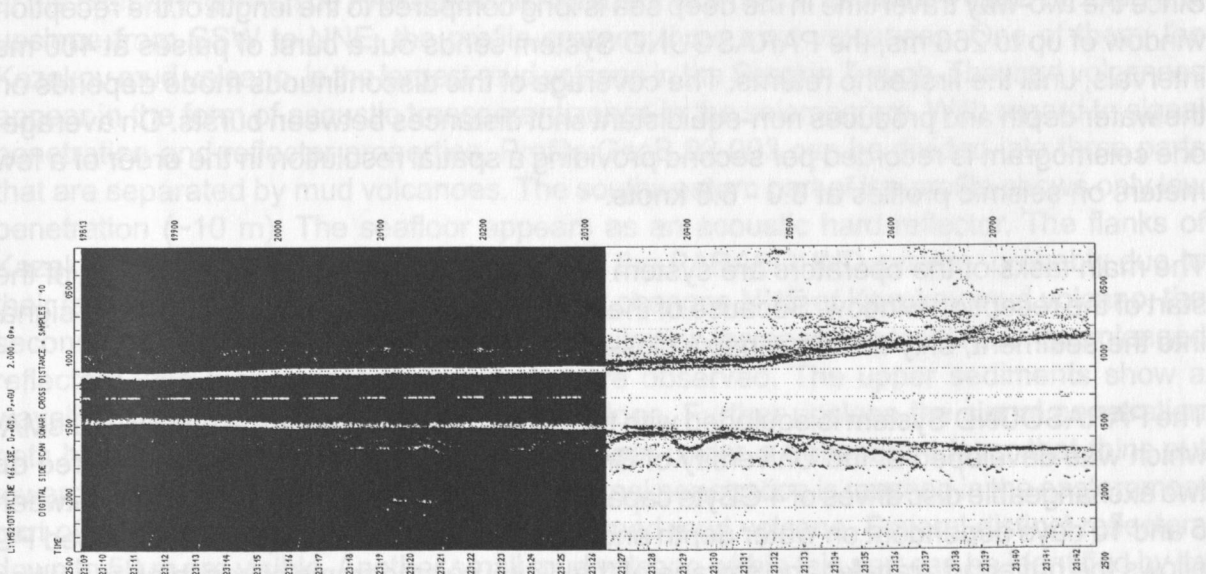


Fig. 28: Example of 75 kHz sidescan sonar data (range 1,500 m) from deployment 4.

## 6. PARASOUND

### 6.1 General

F. Heidersdorf, V. Spieß, S. Krastel, T. Leder, P. Naupold

#### 6.1.1 Parameters and Preliminary Data Processing

The PARASOUND system works as both a low-frequency narrow-beam sediment echosounder and a high-frequency echosounder to determine the water depth. It makes use of the parametric effect, which produces waves with secondary frequencies through nonlinear acoustic interaction of finite amplitude waves. If two sound waves of similar frequencies (here 18 kHz and e.g. 22 kHz) are emitted simultaneously, a signal of the difference frequency (e.g. 4 kHz) is generated for sufficiently high primary amplitudes. The new component is travelling within the emission cone of the original high frequency waves, which is limited to an angle of only 4° for the equipment used. Therefore, the footprint size of 7% of the water depth is much smaller than for conventional systems and both vertical and lateral resolution are significantly improved.

The PARASOUND system is permanently installed on the ship. The hull-mounted transducer array has 128 elements on an area of approximately 1 m<sup>2</sup>. It requires up to 70 kW of electric power due to the low degree of efficiency of the parametric effect. In 2 electronic cabinets, beam forming, signal generation and separation of primary (18, 22 kHz) and secondary frequencies (4 kHz) is carried out. With the third electronic cabinet in the echosounder control room, the system is operated on a 24 hour watch schedule.

Since the two-way travel time in the deep sea is long compared to the length of the reception window of up to 266 ms, the PARASOUND System sends out a burst of pulses at 400 ms intervals, until the first echo returns. The coverage of this discontinuous mode depends on the water depth and produces non-equidistant shot distances between bursts. On average, one seismogram is recorded per second providing a spatial resolution in the order of a few meters on seismic profiles at 6.0 - 6.5 knots.

The main tasks of the operators are system and quality control and the adjustment of the start of the reception window. Because of the limited penetration of the echosounder signal into the sediment, only a short window close to the sea floor is recorded.

The PARASOUND System is equipped with the digital data acquisition system PARADiGMA, which was developed at the University of Bremen (Spieß, 1993). The data are stored on two exchangeable disc drives of 4 GByte capacity, allowing continuous recording for between 5 and 10 days dependent on water depth and shot rate. The Pentium-processor based PC allows the buffering, transfer and storage of the digital seismograms at very high repetition rates. From the emitted series of pulses usually every second pulse is digitized and stored, resulting in recording intervals of 800 ms within a pulse sequence. The seismograms were sampled at a frequency of 40 kHz, with a typical registration length of 266 ms for a depth window of about 200 m. The source signal was a band limited, 2 - 6 kHz sinusoidal wavelet of 4 kHz dominant frequency with a duration of 2 periods (~500 µs total length).

Already during the acquisition of the data an online processing was carried out. For all profiles, PARASOUND sections were plotted with a vertical scale of several hundred meters. Most of the changes in window depth could thereby be eliminated. From these plots, a first



impression of variations in sea floor morphology, sediment coverage and sedimentation patterns along the ship's track could be gained. To improve the signal-to-noise ratio, the echogram sections were filtered with a wide band pass filter. In addition, the data were normalized to a constant value much smaller than the average maximum amplitude, to amplify especially deeper and weaker reflections. During the entire cruise, the combined PARASOUND/PARADIGMA system worked without significant problems. In combination with the Hydrosweep system, Parasound serves as an efficient tool to determine the seafloor morphology, to characterize and analyze sediment deposition processes and sediment structures. PARASOUND measurements along the multichannel seismic lines reveal detailed information about the uppermost sediment layers. In addition PARASOUND also provides precious information for suitable coring sites and in situ measurements. PARASOUND data were collected during the entire cruise, i.e. parallel with seismic, sidescan sonar, and OFOS measurements as well as on transits between stations. Some additional profiles were chosen to fill gaps in the previously collected data.

### 6.1.2 Shipboard Results

Seismic and geological investigations during Cruise M52-1 were concentrated on two areas south of the Crimea peninsula (Fig. 29). The central Black Sea working area is located south of Sevastopol and includes the Parasound profiles shown in Figure 31 and 32. A busier investigation area (Profiles shown in Figures 30, 33, 34) was the Sorokin Trough located southeast of the Crimea peninsula.

Profile GeoB 02-003 is one of the seismic overview profiles measured right at the beginning of the cruise (Fig 44). The PARASOUND data of this profile is shown in Figure 30. Running upslope from SSW to NNE, the profile crosses three mud volcanoes. One of them, the Kazakov mud volcano, is the largest mud volcano in the Sorokin Trough. The mud volcanoes appear in the form of acoustic transparent zones in the seismogram. With regard to signal penetration and reflector properties, Profile GeoB 02-003 can be divided into three parts that are separated by mud volcanoes. The southwestern part of the profile shows only low penetration (~10 m). The seafloor appears as an acoustic hard reflector. The flanks of Kazakov mud volcano cannot be imaged by the PARASOUND system, probably due to their large slope angle. The reflection pattern changes NNE of Kazakov mud volcano, the second part of this profile. Here the signal penetration increases up to 30 m. Only prolonged reflectors with high reflection amplitudes are observed. The upper sediments show a wavelike structure indicating sliding on the slope. Further upslope the signal penetration gets higher and single deeper reflectors appear under a transparent layer that thins out towards another mud volcano. The highest signal penetration is reached in the easternmost part of the profile that starts NNE of an unnamed mud volcano. Several distinct reflectors down to 50 m are visible. Another small mud volcano within this part can be identified by its acoustic transparency.

Profile GeoB 02-030 is a nearly eastward directed profile in the central Black Sea working area (Fig. 31). It crosses two mud volcanoes named Moscow State University (MSU) and Yuzhmorgeologiya. The maximum signal penetration in this seismogram is about 30 m. East and west of both volcanoes mainly prolonged reflectors can be observed, whereas distinct reflectors occur between them. A fault coming close to the sediment surface can be seen between the two mud volcanoes. Within the MSU and Yuzhmorgeologiya mud volcanoes no acoustic reflectors are visible.

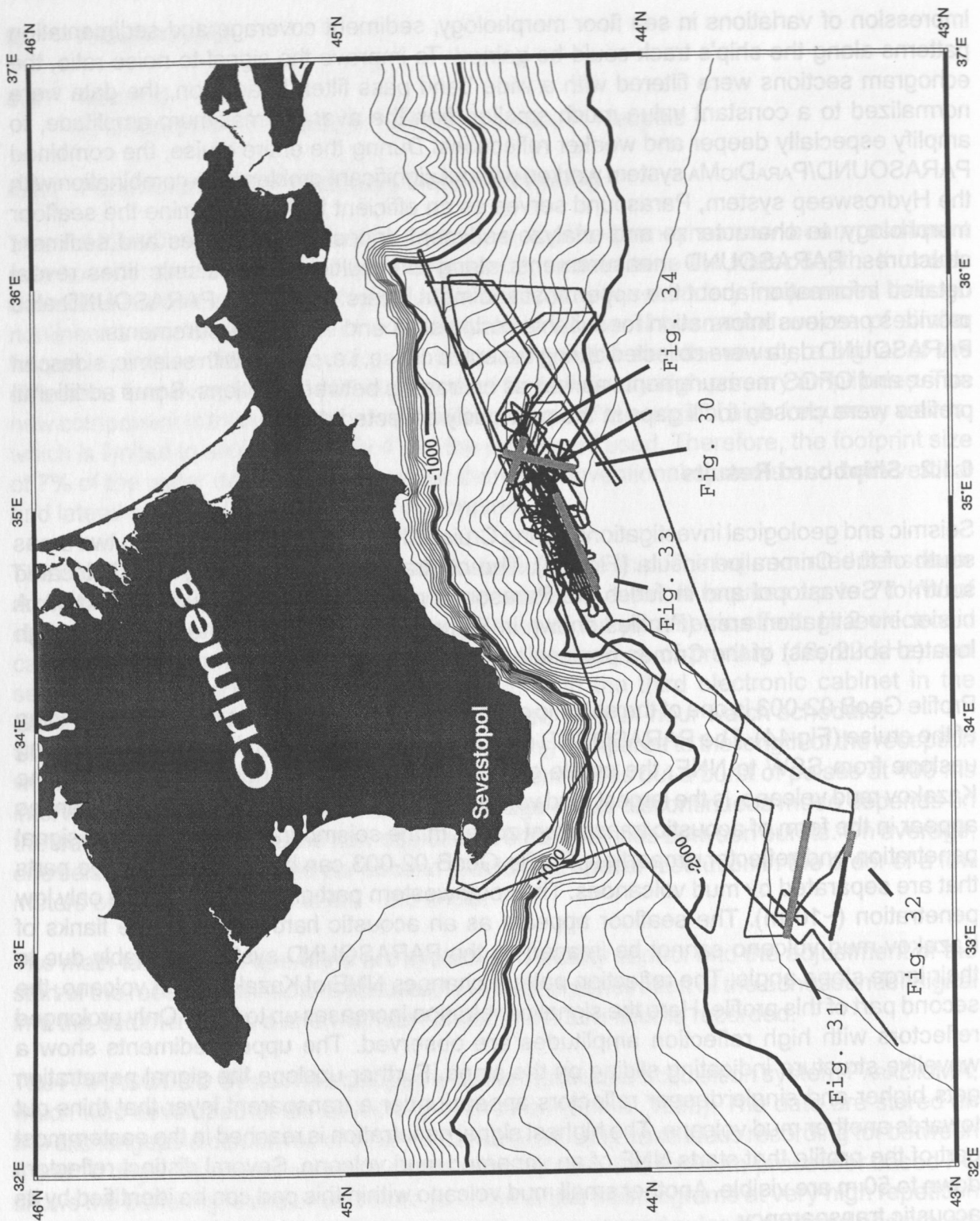


Fig. 29: Track of R/V METEOR during cruise M52/1. Locations of presented PARASOUND profiles and figure numbers are indicated.

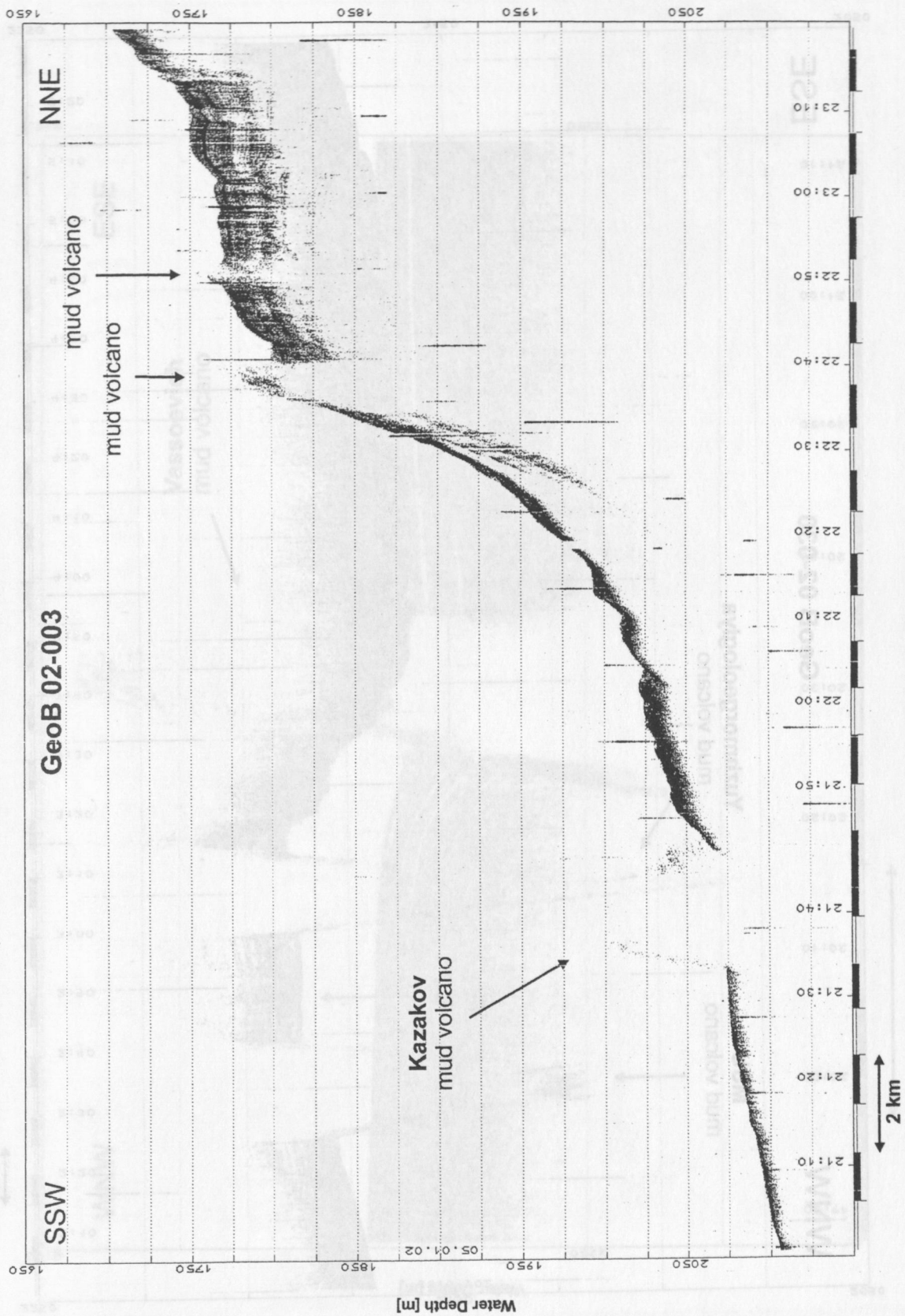


Fig. 30: PARASOUND section on the southern slope of the Crimea peninsula. Data were collected on the seismic profile GeoB 02-003. The profile crosses several mud volcanoes at a water depth between 1,700 and 2,100 m. For location see Fig. 29.



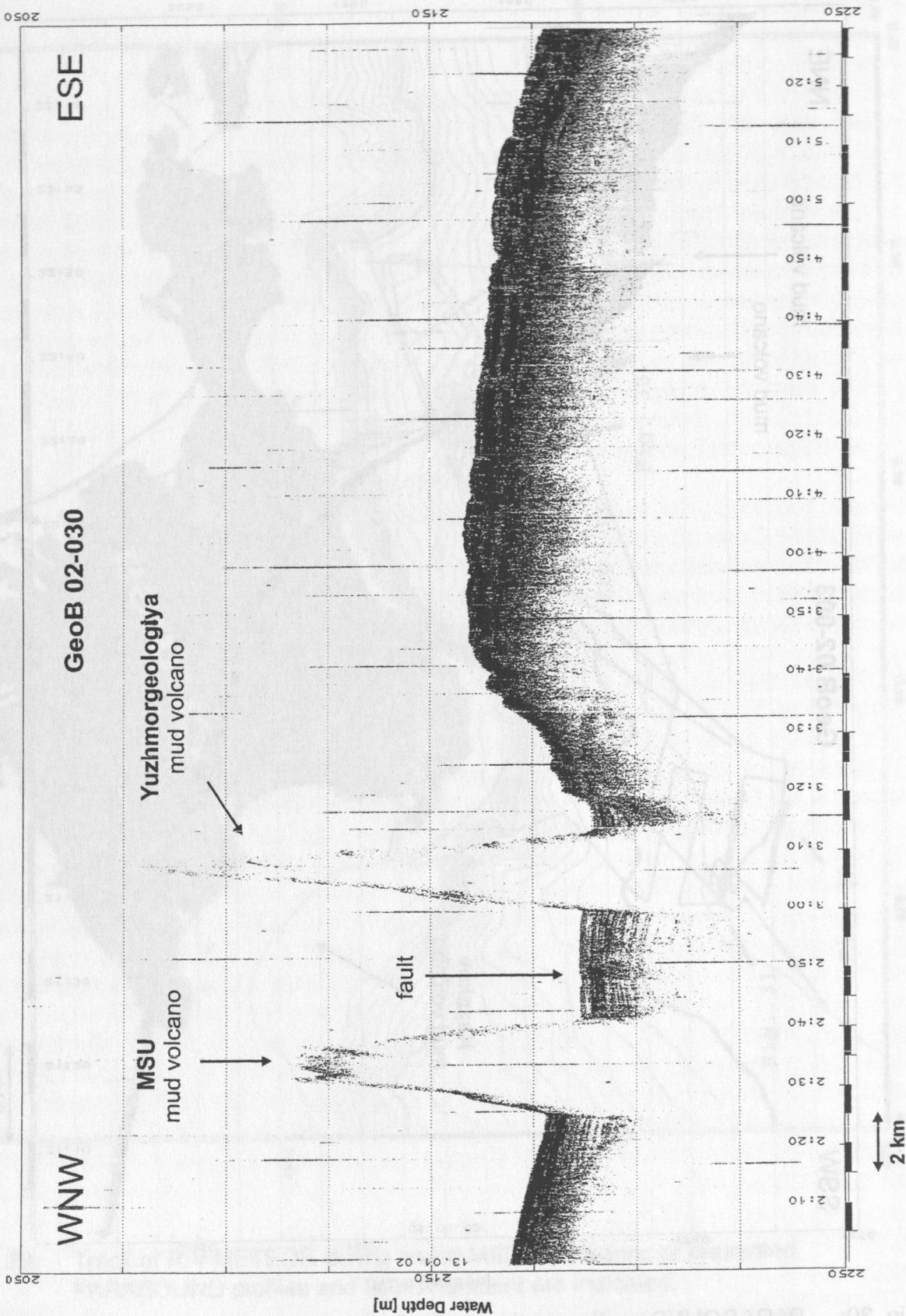


Fig. 31: PARASOUND profile in the central Black Sea working area. The section was recorded on the seismic Profile GeoB02-030. For location see Fig. 29.

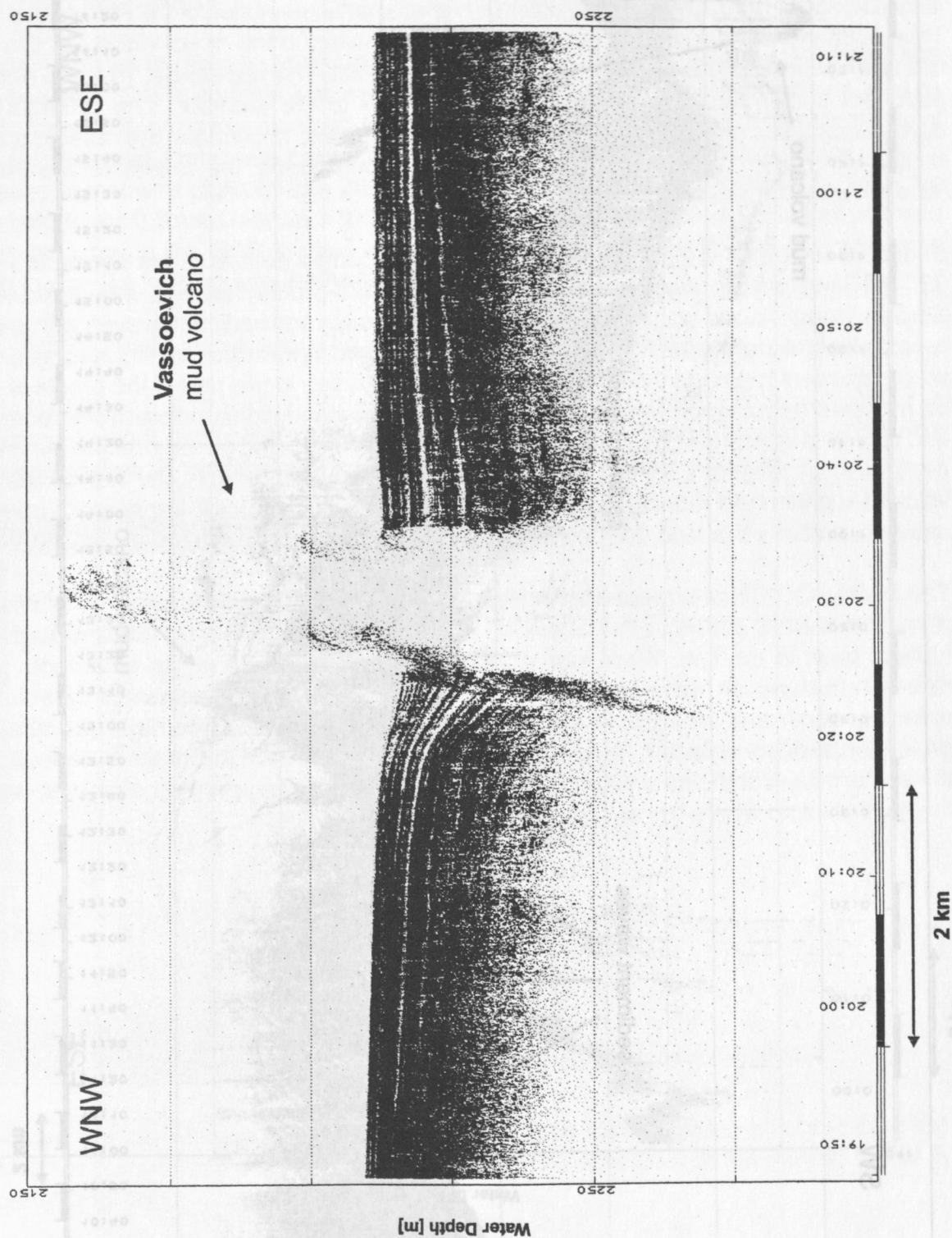


Fig. 32: PARASOUND section recorded on a DTS profile in the basin south of the Crimea peninsula. The seismogram shows sediment structures in the direct vicinity of the Vassoievich mud volcano. For location see Fig. 29.

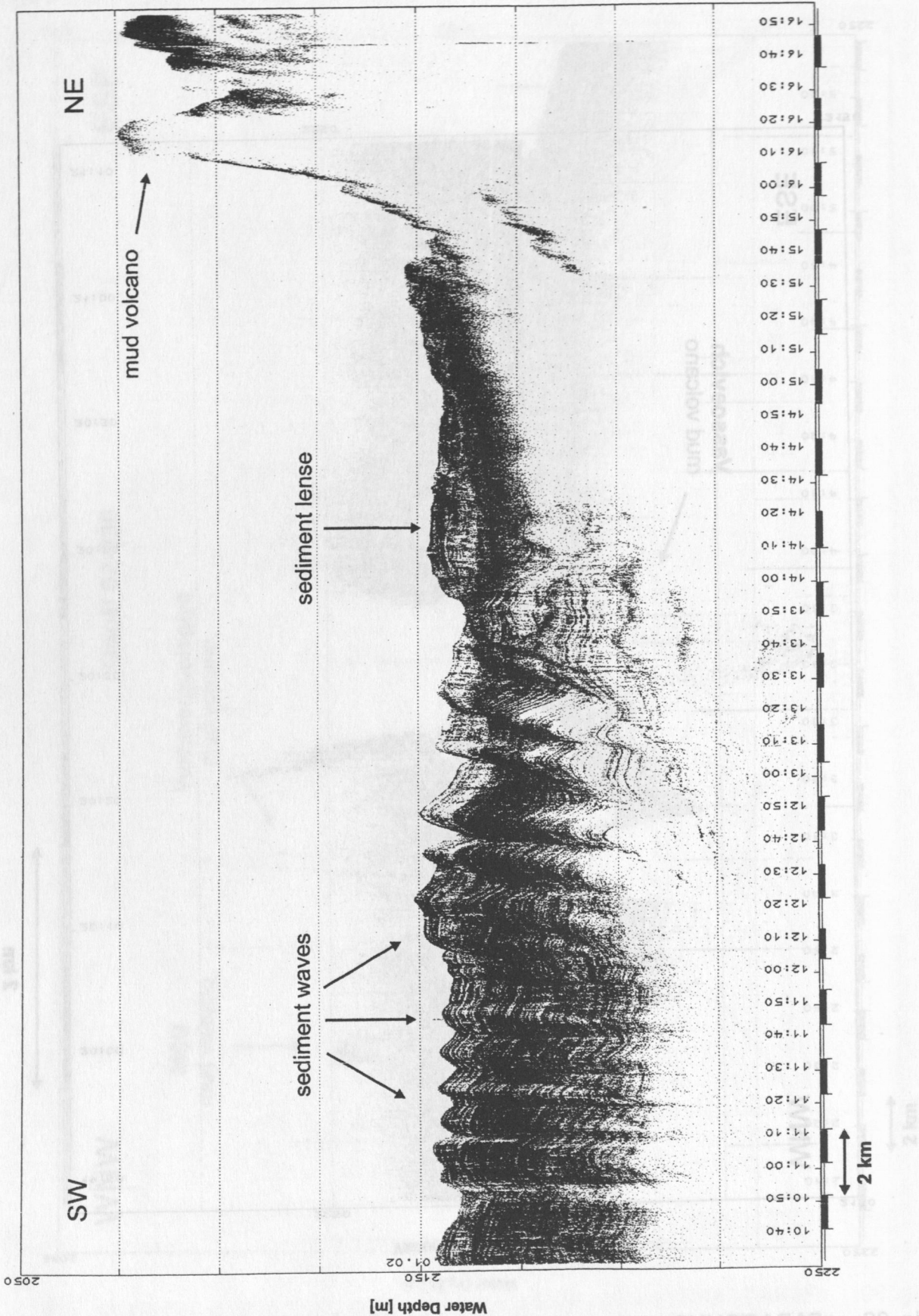


Fig. 33: Sediment waves close to a mud volcano. The PARASOUND data correspond to a DTS profile measured at the deeper slope south of the Crimea peninsula. For location see Fig. 29.



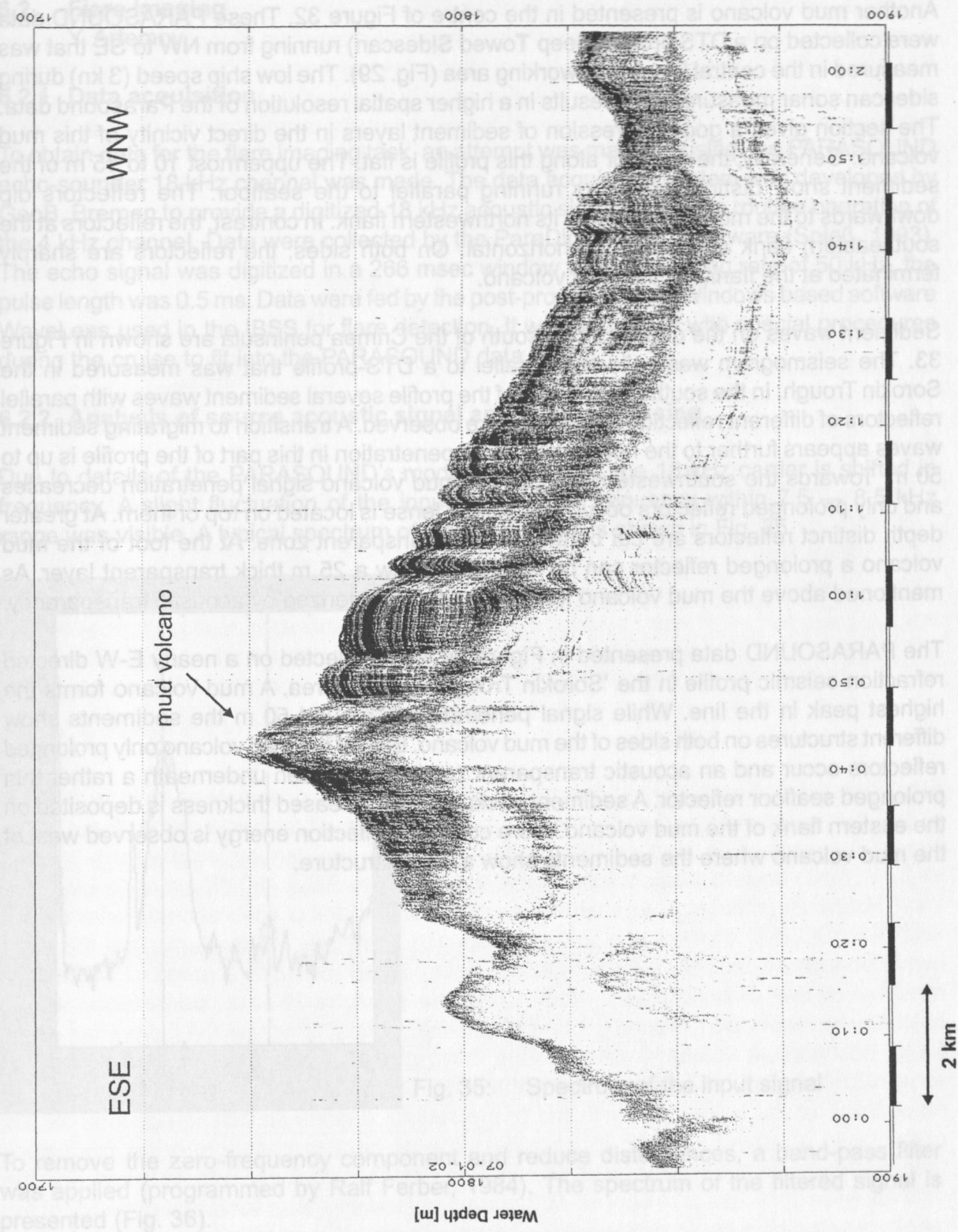


Fig. 34: PARASOUND data recorded on an E-W oriented profile in the Sorokin Trough working area. The seismogram shows different sediment structures on both sides of a mud volcano. For location see Fig. 29.

Another mud volcano is presented in the centre of Figure 32. These PARASOUND data were collected on a DTS profile (**D**ee**P** **T**owed **S**idescan) running from NW to SE that was measured in the central Black Sea working area (Fig. 29). The low ship speed (3 kn) during sidescan sonar measurements results in a higher spatial resolution of the Parasound data. The section gives a good impression of sediment layers in the direct vicinity of this mud volcano. Generally, the seafloor along this profile is flat. The uppermost 10 to 15 m of the sediment show distinct reflectors running parallel to the seafloor. The reflectors dip downwards to the mud volcano near its northwestern flank. In contrast, the reflectors at the southeastern flank appear nearly horizontal. On both sides, the reflectors are sharply terminated at the flanks of the mud volcano.

Sediment waves on the deeper slope south of the Crimea peninsula are shown in Figure 33. The seismogram was collected parallel to a DTS-profile that was measured in the Sorokin Trough. In the southwestern part of the profile several sediment waves with parallel reflectors of different reflection amplitudes are observed. A transition to migrating sediment waves appears further to the northeast. Signal penetration in this part of the profile is up to 50 m. Towards the southwestern flank of the mud volcano signal penetration decreases and only prolonged reflectors occur. A sediment lense is located on top of them. At greater depth distinct reflectors are cut by an acoustic transparent zone. At the foot of the mud volcano a prolonged reflector can be identified below a 25 m thick transparent layer. As mentioned above the mud volcano itself is again characterized by acoustic transparency.

The PARASOUND data presented in Figure 34 were collected on a nearly E-W directed refraction seismic profile in the 'Sorokin Trough' working area. A mud volcano forms the highest peak in the line. While signal penetration is around 50 m the sediments show different structures on both sides of the mud volcano. East of the mud volcano only prolonged reflectors occur and an acoustic transparent zone can be seen underneath a rather thin prolonged seafloor reflector. A sediment package with increased thickness is deposited on the eastern flank of the mud volcano. More coherent reflection energy is observed west of the mud volcano where the sediments show a wavy structure.

## 6.2 Flare Imaging

Y. Artemov

### 6.2.1 Data acquisition

To obtain data for the flare imaging task, an attempt was made by using the PARASOUND echo-sounder 18 kHz channel was made. The data acquisition system was developed by GeoB, Bremen to provide a digitized 18 kHz acoustic signal parallel to routine operation of the 4 kHz channel. Data were collected by the ParaDigMa (4.10) software (Spieß, 1993). The echo signal was digitized in a 266 msec window with a sampling rate of 50 kHz, the pulse length was 0.5 ms. Data were fed by the post-processing MS Windows based software WaveLens used in the IBSS for flare detection. It was appended with special procedures during the cruise to fit into the PARASOUND data format.

### 6.2.2 Analysis of source acoustic signal and data processing

Due to details of the PARASOUND's mode of operation, the 18 kHz carrier is shifted in frequency. A slight fluctuation of the input echo-signal frequency within 7.5 — 8.5 kHz range was visible. A typical spectrum of the input signal is shown in Fig. 35.

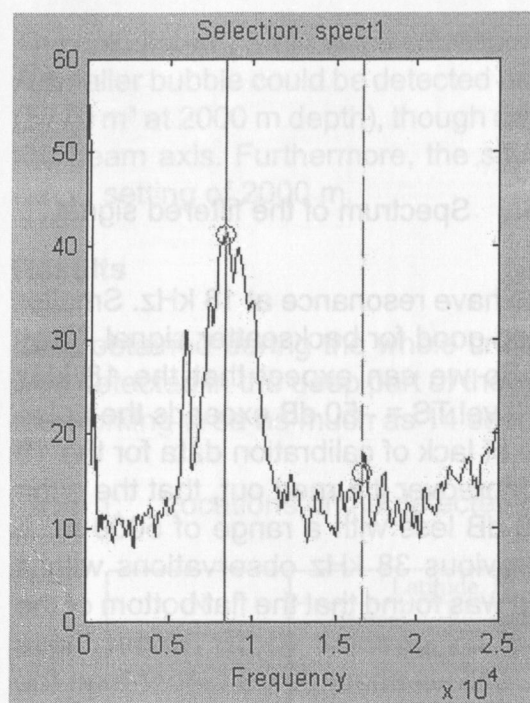


Fig. 35: Spectrum of the input signal

To remove the zero-frequency component and reduce disturbances, a band-pass filter was applied (programmed by Ralf Ferber, 1984). The spectrum of the filtered signal is presented (Fig. 36).

Under the assumption that backscatters in the water column are distinguished by the echo energy, the input signal was squared and passed logarithmic transformation. To reduce processing time we did not extract the envelope. Nevertheless good quality echograms were derived by using the Wave Lens imaging tool. A typical 18 kHz PARASOUND echogram is shown in Fig. 37.



First of all, we tried to clarify to what extent the PARASOUND system could detect single or bunched methane bubbles. This depends on acoustic properties of methane bubbles and PARASOUND parameters. For bubbles we used a resonant model (Clay C.S., and Medwin, H., 1977), assuming that methane bubbles contain the ideal gas with the ratio of specific heat capacities  $\gamma = 1.28$ . Dependence of methane bubble target strength (TS) at 2000 m depth on bubble size for 18 kHz was estimated (Fig. 38).

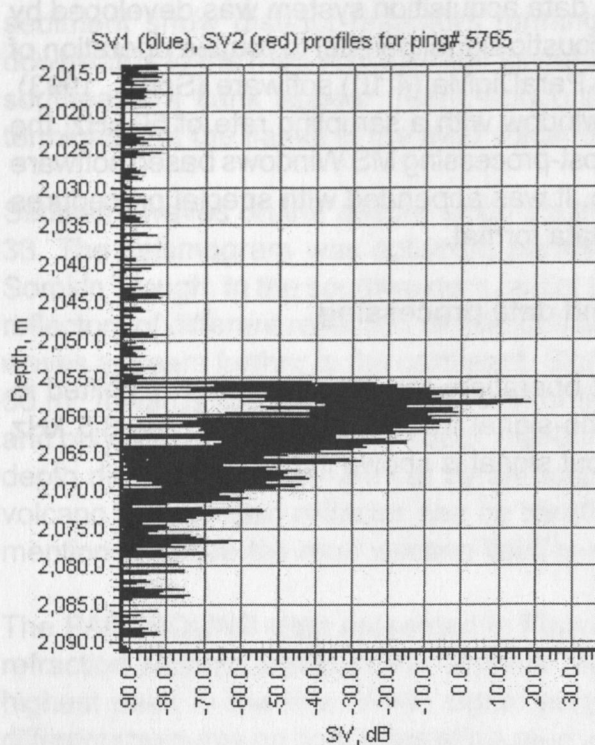


Fig. 36: Spectrum of the filtered signal

Fig. 38 shows that methane bubbles of 2.5 mm radius have resonance at 18 kHz. Smaller (e.g. 2 mm radius) as well as larger bubbles are also good for backscatter signal. They have TS values of as high as  $-50$  dB and more. So we can expect that the 18 kHz PARASOUND could detect such bubbles if the echo level  $TS = -50$  dB exceeds the noise level. Examining this issue we met troubles because of lack of calibration data for the 18 kHz PARASOUND channel, e.g. voltage response. Moreover it turned out, that the echo level depends on the range switch setting, being 30 dB less with a range of 5000 m. A tentative coarse estimation was made using our previous 38 kHz observations with a calibrated scientific echo-sounder SIMRAD EK-500. It was found that the flat bottom of the Black Sea gives a volume backscattering echo level SV of about  $-5$  dB. Under those circumstances the bottom echo level of the PARASOUND is about 80 dB higher than the noise level for the worst case with the range setting. It gives an estimated value for the noise level of about  $-85$  dB in consideration of bottom backscattering frequency independence. Assuming that a 18 kHz PARASOUND transducer with  $4^\circ$  angle has the equivalent beam angle  $\psi$  of about 0.003 steradian, an estimation for target strength of the weakest detectable backscatterer at the beam axis could be as follows:

$$TS_{min} = SV_{min} + 20 \log(R) + 10 \log(\psi) + 10 \log(c \cdot \tau / 2)$$

$$TS_{min} = -85 + 20 \log(2000) + 10 \log(0.003) + 10 \log(1500 \cdot 0.0005 / 2) = -48.5 \text{ (dB)}$$

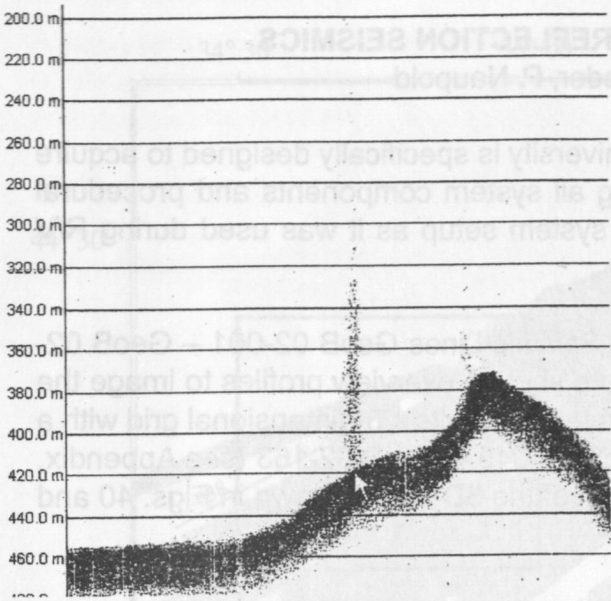


Fig. 37:  
18 kHz PARASOUND echogram  
showing two distinct bubble plumes.

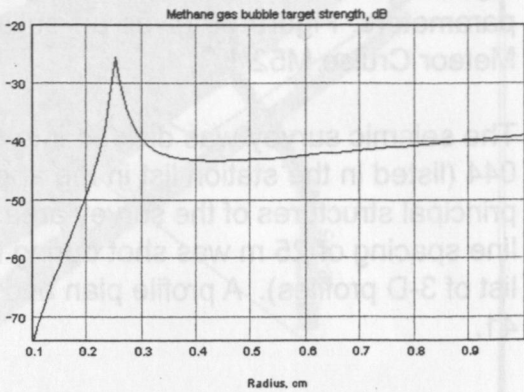


Fig. 38:  
Target strength of various size methane  
gas bubbles at 18 kHz for 2000 m depth.

The calculated TSmin value corresponds approximately to a 2 mm radius methane bubble. A smaller bubble could be detected as well if several bubbles occur in the insonified volume (5770 m<sup>3</sup> at 2000 m depth), though depending on their quantity and position with respect to the beam axis. Furthermore, the situation was much better with a PARASOUND depth range setting of 2000 m.

Results

Data obtained during the whole cruise were examined. No methane gas bubble stream was detected in the deep part of the working area. During the survey in the shallow part of the working area as much as 14 seep sites were detected (Table 1).

Table 1: Locations of the detected gas bubble streams

N	Latitude, N		Longitude, E		Water depth, m
	degrees	minutes	degrees	minutes	
1	44	41,492	35	56,288	763,4
2	44	42,122	35	58,588	560,2
3	44	42,462	35	59,818	517,4
4	44	42,521	36	0,043	507,7
5	44	42,772	36	3,772	308,5
6	44	41,797	36	0,422	655,9
7	44	42,752	35	59,862	447,3
8	44	42,793	35	59,832	435,0
9	44	42,815	35	59,788	430,0
10	44	42,805	35	59,680	447,9
11	44	42,788	35	59,862	440,6
12	44	42,881	35	59,798	418,3
13	44	43,123	35	59,845	377,7
14	44	42,245	35	59,943	582,1

## 7. HIGH-RESOLUTION MULTICHANNEL REFLECTION SEISMICS

S. Krastel, V. Spieß, F. Heidersdorf, T. Leder, P. Naupold

The multichannel seismic system of Bremen University is specifically designed to acquire high resolution seismic data through optimizing all system components and procedural parameters. Figure 39 gives an outline of the system setup as it was used during R/V Meteor Cruise M52/1.

The seismic survey was divided into two parts. Seismic Lines GeoB 02-001 – GeoB 02-044 (listed in the station list in the appendix) were shot as overview profiles to image the principal structures of the survey area. Based on these results a 3-dimensional grid with a line spacing of 25 m was shot during Lines GeoB 02-045 – GeoB 02-163 (see Appendix, list of 3-D profiles). A profile plan and the location of the 3D box is shown in Figs. 40 and 41.

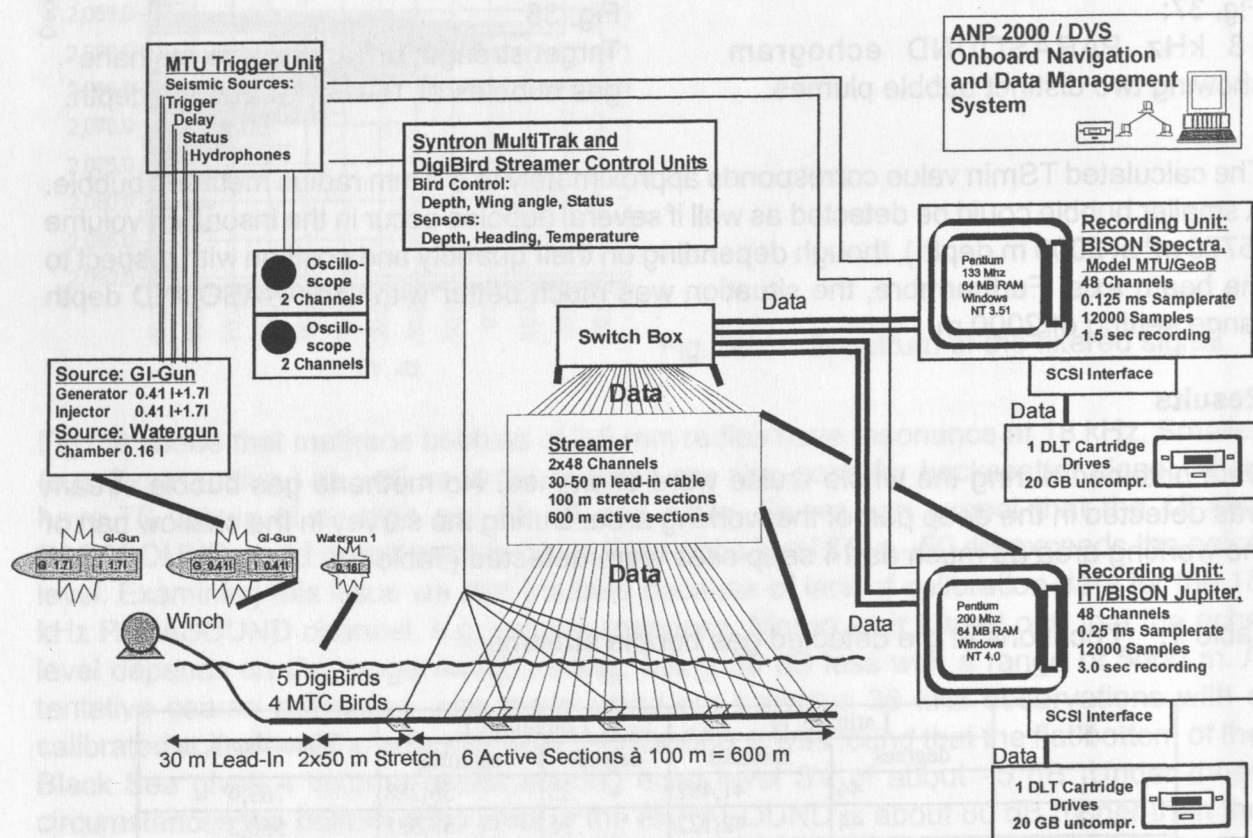


Fig. 39: Outline of the Bremen high resolution reflection seismic system.



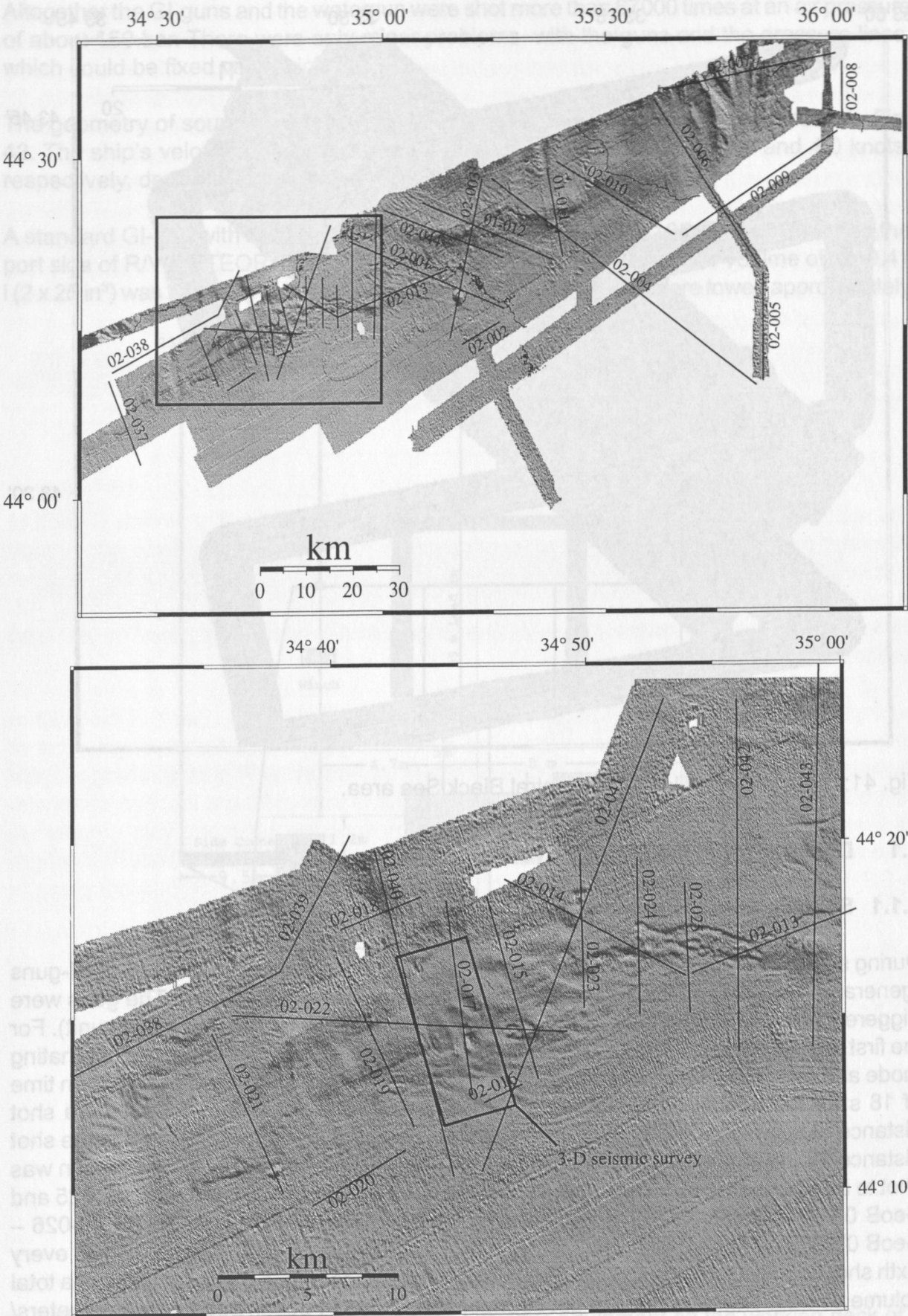


Fig. 40: Seismic lines in the Sorokin Trough area (above). Survey box is enlarged below indicating the area of 3-D seismic survey..

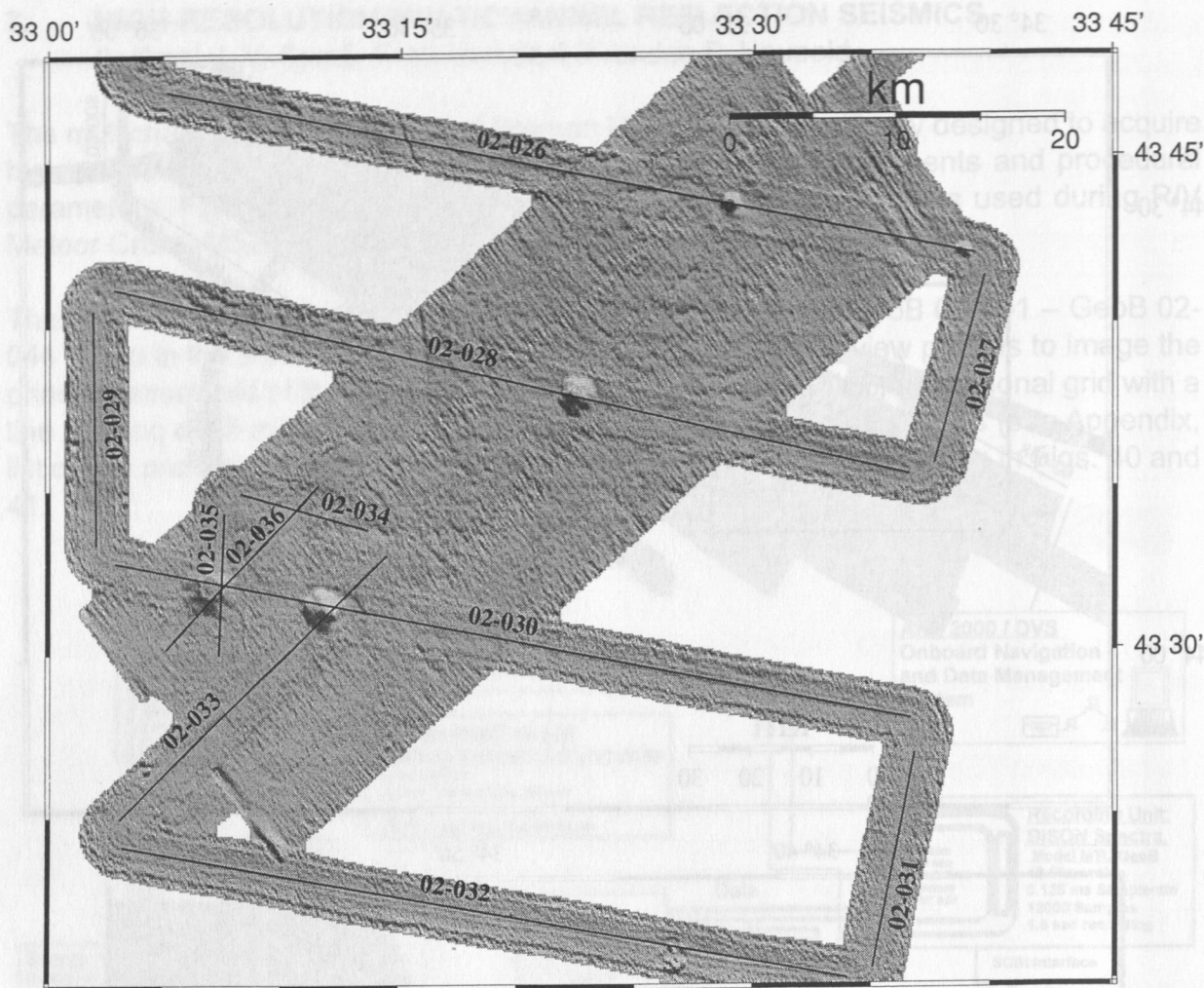


Fig. 41: Seismic profiles in the central Black Sea area.

## 7.1 Description of the seismic system

### 7.1.1 Seismic sources and compressor

During seismic surveying, three different seismic sources were used, two types of GI-guns (generator-injector gun, 2 x 1.7 l and 2 x 0.4 l) and one water gun (0.16 l). The guns were triggered in a quasi-simultaneous mode at a time interval of 9 s (see also trigger unit). For the first profiles (GeoB 02-001 – GeoB 02-012) the GI-guns were operated in an alternating mode and only one GI-gun was shot at each time interval, resulting in a shot repetition time of 18 s for the different GI-guns. Owing to an average ship speed of 6.5 knots, a shot distance of approximately 30 m to 35 m was thus obtained for the watergun while the shot distance for the single GI-guns is 60 m to 70 m. For all other profiles only one GI-gun was shot to achieve better coverage of the subsurface. Lines GeoB02-013 – GeoB 02-025 and GeoB 02-037- GeoB 02-163 were shot with the 0.4 l GI-gun while lines GeoB 02-026 – GeoB 02-036 were shot with the 1.7 L gun. For lines GeoB 02-045 – GeoB 02-163 every sixth shot was fired simultaneously with both GI-guns in the airgun mode resulting in a total volume of 4.2 l. This was done to get stronger signals for 14 ocean bottom seismometers/ ocean bottom hydrophones which were deployed on the seafloor for this part of seismic recording (see chapter 8).



Altogether the GI-guns and the watergun were shot more than 67000 times at an air pressure of about 150 bar. There were only minor problems with the guns and the pressure lines, which could be fixed very quickly.

The geometry of source and receiver systems during the measurements is shown in Fig. 42. The ship's velocity during deployment and retrieval was between 3.0 and 4.0 knots, respectively, depending on weather conditions and surface currents.

A standard GI-gun with normal chamber volume of  $2 \times 1.7 \text{ L}$  ( $2 \times 105 \text{ in}^3$ ) was towed on the port side of R/V METEOR, the second GI-gun with a reduced chamber volume of  $2 \times 0.41 \text{ L}$  ( $2 \times 25 \text{ in}^3$ ) was towed by a crane on the starboard side. The guns were towed approximately

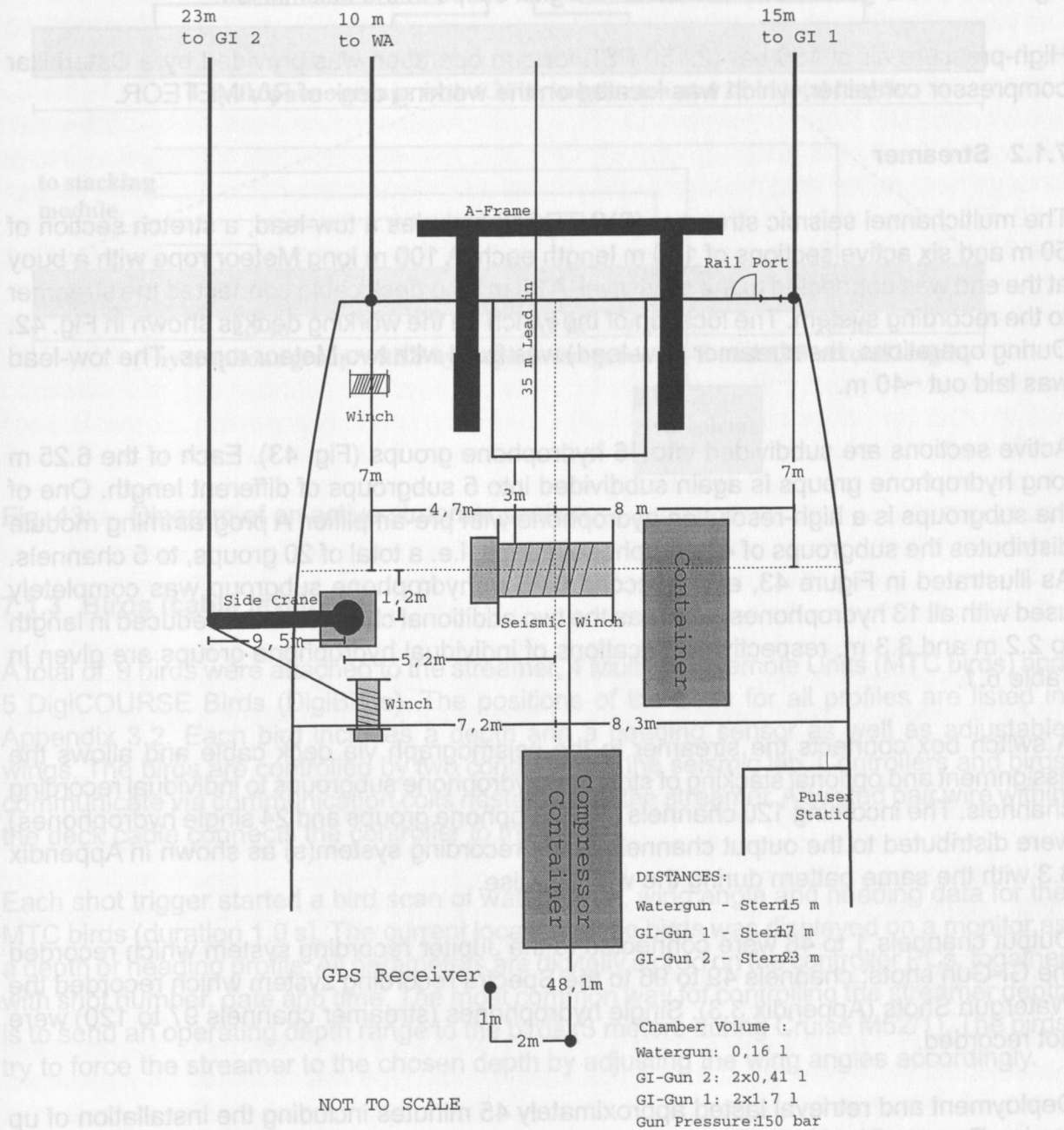


Fig. 42: Schematic drawing showing major seismic equipment on the working deck of R/V METEOR.



17 and 15 m, respectively, behind the ship's stern. The towing wires were connected to a bow with the single GI-guns hanging on two chains 40 cm beneath. An elongated buoy, which stabilized the gun in a horizontal position at a water depth of ~1.4 m, was connected to the bow by two rope loops. The injector was triggered with a delay of 30 ms for the GI gun with reduced chamber volume and 50 ms for the gun with normal chamber volume with respect to the generator signal, which basically eliminated the bubble signal. The other source was a S15 water gun (Sodera) with a volume of 0.16 l (10 in<sup>3</sup>). The water gun was towed between the GI-guns approximately 15 m behind the ship's stern. The umbilicals were secured by strong ropes to avoid damage to the pressure lines and electric cables due to rubbing or bending. A steel frame held the watergun in a tight position parallel to the elongated buoy in a depth of approximately 0.5 m. During operations, the near field source signature of the guns was checked on a digital scope in the seismic lab.

High-pressure air of 150 bar (2,150 PSI) for gun operation was provided by a Caterpillar compressor container, which was located on the working deck of R/V METEOR.

### 7.1.2 Streamer

The multichannel seismic streamer (SYNTRON) includes a tow-lead, a stretch section of 50 m and six active sections of 100 m length each. A 100 m long Meteor rope with a buoy at the end was connected to the tail swivel. A 30 m long deck cable connected the streamer to the recording system. The location of the winch on the working deck is shown in Fig. 42. During operations, the streamer (tow-lead) was fixed with two Meteor ropes. The tow-lead was laid out ~40 m.

Active sections are subdivided into 16 hydrophone groups (Fig. 43). Each of the 6.25 m long hydrophone groups is again subdivided into 5 subgroups of different length. One of the subgroups is a high-resolution hydrophone with pre-amplifier. A programming module distributes the subgroups of 4 hydrophone groups, i.e. a total of 20 groups, to 5 channels. As illustrated in Figure 43, every second 6.25 m hydrophone subgroup was completely used with all 13 hydrophones, whereas the two additional channels were reduced in length to 2.2 m and 3.3 m, respectively. Locations of individual hydrophone groups are given in Table 6.1.

A switch box connects the streamer to the seismograph via deck cable and allows the assignment and optional stacking of streamer hydrophone subgroups to individual recording channels. The incoming 120 channels (96 hydrophone groups and 24 single hydrophones) were distributed to the output channels of the recording system(s) as shown in Appendix 3.3 with the same pattern during the whole cruise.

Output channels 1 to 48 were connected to the Jupiter recording system which recorded the GI-Gun shots; channels 49 to 96 to the Spectra recording system which recorded the Watergun Shots (Appendix 3.3). Single hydrophones (streamer channels 97 to 120) were not recorded.

Deployment and retrieval lasted approximately 45 minutes including the installation of up to nine Remote Bird Units (RUs; see below).

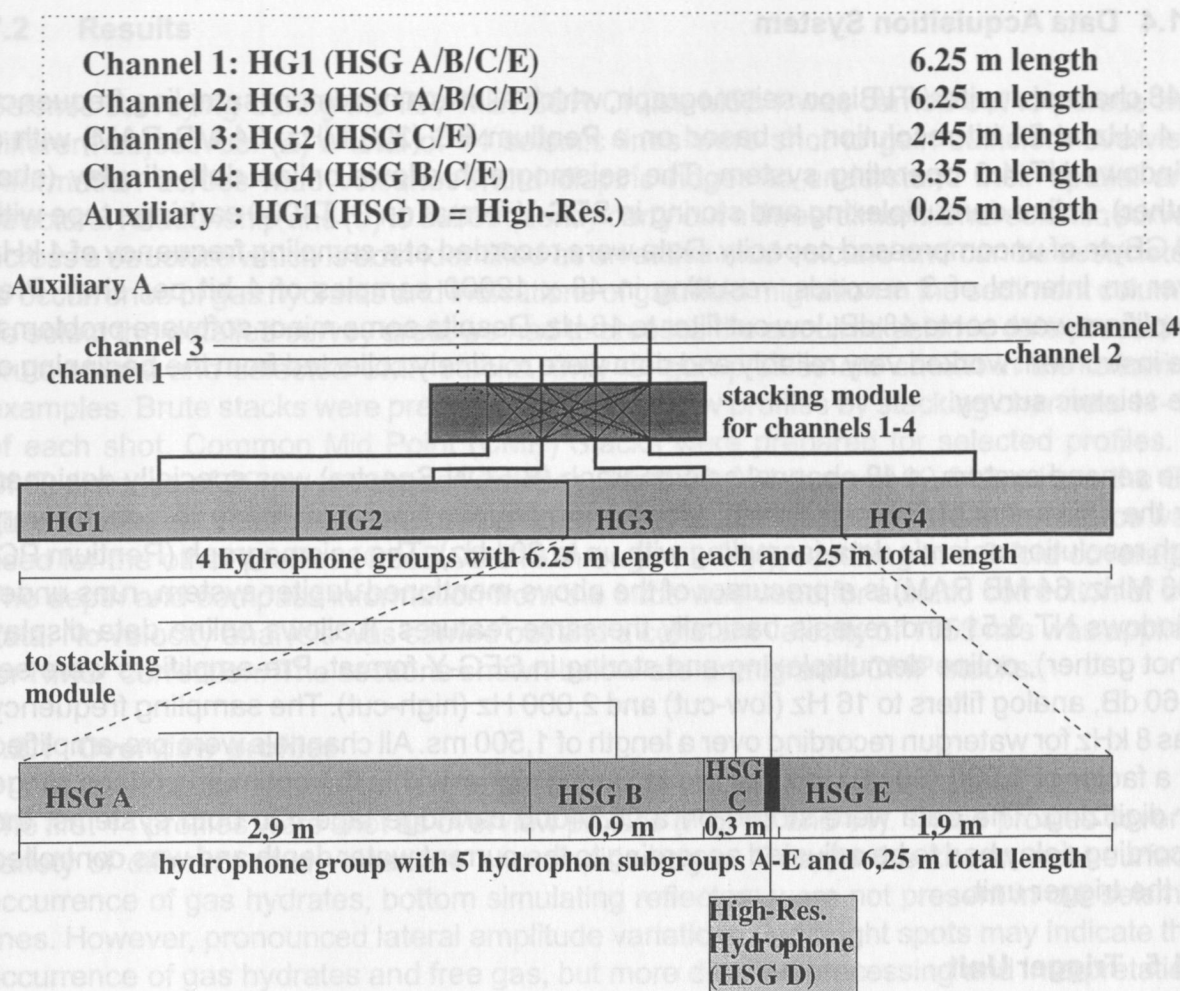


Fig. 43: Diagram of an active streamer section.

### 7.1.3 Birds (cable levelers)

A total of 9 birds were attached to the streamer, 4 MultiTrak Remote Units (MTC birds) and 5 DigiCOURSE Birds (DigiBirds). The positions of the birds for all profiles are listed in Appendix 3.2. Each bird includes a depth and a heading sensor as well as adjustable wings. The birds are controlled by two controllers in the seismic lab. Controllers and birds communicate via communication coils nested within the streamer. A twisted pair wire within the deck cable connects the controller to the coils.

Each shot trigger started a bird scan of water depth, wing angle and heading data for the MTC birds (duration 1.0 s). The current location of the birds was displayed on a monitor as a depth or heading profile. All parameters are digitally stored on the controller PCs, together with shot number, date and time. The most common way for controlling the streamer depth is to send an operating depth range to the birds (3 meters during Cruise M52/1). The birds try to force the streamer to the chosen depth by adjusting the wing angles accordingly.



#### 7.1.4 Data Acquisition System

A 48 channel Jupiter/ITI/Bison seismograph, which allows a maximum sampling frequency of 4 kHz at 24 bit resolution, is based on a Pentium PC (200 MHz; 64 MB RAM) with a Windows NT 4.0 operating system. The seismograph allows online data display (shot gather), online demultiplexing and storing in SEG-Y format on DLT4000 cartridge tape with 20 GByte of uncompressed capacity. Data were recorded at a sampling frequency of 4 kHz over an interval of 3 seconds, resulting in 48 x 12000 samples of 4 bit per shot. Pre-amplifiers were set to 48 dB, low cut filter to 16 Hz. Despite some minor software problems, the instrument worked very reliably and data were routinely collected from the beginning of the seismic survey.

The second system, a 48 channel seismograph (BISON Spectra) was specially designed for the University of Bremen, which allows a continuous operation mode to acquire very high resolution seismic data (sampling with up to 20 kHz). The seismograph (Pentium PC; 133 MHz; 64 MB RAM) is a precursor of the above mentioned Jupiter system, runs under Windows NT 3.51 and reveals basically the same features. It allows online data display (shot gather), online demultiplexing and storing in SEG-Y format. Pre-amplifiers were set to 60 dB, analog filters to 16 Hz (low-cut) and 2,000 Hz (high-cut). The sampling frequency was 8 kHz for watergun recording over a length of 1,500 ms. All channels were pre-amplified by a factor of 1,000 (60 dB) to keep the incoming signal within the optimum voltage range for digitizing. The data were stored on a DLT4000 cartridge tape. On both systems, the recording delay had to be adjusted according to the current water depth and was controlled by the trigger unit.

#### 7.1.5 Trigger Unit

The custom trigger unit controls seismic sources, seismographs, the MTC bird controller and the online plotter with separate filters and digital scopes (near-field hydrophones). The unit is set up on an IBM compatible PC with a Windows NT 4.0 operating system and includes a real-time controller interface card (SORCUS) with 16 I/O channels, synchronized by an internal clock. The unit is connected to an amplifier unit and a gun amplifier unit. The PC runs a custom software, which allows defining arbitrary combinations of trigger signals. It was used to optimize the available recording time for the three seismic sources and to reduce the shot distance.

Trigger times can be changed any time during the survey. Through this feature, the recording delay can be adjusted to water depth without an interruption of data acquisition. The amplifier unit converts the controller output to positive or negative TTL levels. The gun amplifier unit, which generates a 60V/8 Amp. trigger level, controls the magnetic valves of the individual seismic sources. It was placed in the pulser station close to the gun pressure controls for immediate shutdown of gun operation.

Appendix 3.4 shows the trigger schemes which were used during the survey for two recording systems and three different source types. Each source type was recorded on a separate tape, one at the Bison Spectra for the water gun source and one on the Bison Jupiter for the GI-gun sources. Recording and data storage took place parallelly on both systems. In this mode, an additional processing step of splitting records of the different GI-guns is required for the profiles shot with both GI-guns prior to standard seismic data processing.



## 7.2 Results

Seismic surveying during the R/V METEOR Cruise M52/1 was carried out to pursue two different objectives: (a) a total of 44 seismic lines were shot to gain sufficient overview information across mud volcanoes and diapiric ridges to understand their spatial and structural relationship and (b) to subsequently carry out a three-dimensional seismic survey across a structure which is both identified as an active mud volcano and can be associated to occurrence of gas hydrates and indications of gas/fluid migration in the sediment column. To select the detailed survey area, we had to process the acquired seismic data producing brute stacks and selected CMP stacks. Only GI-gun profiles are shown in the following examples. Brute stacks were prepared for all overview profiles by stacking channels 11-16 of each shot. Common Mid Point (CMP) Stacks were prepared for selected profiles. A CMP distance of 20 m was chosen for lines GeoB 02-001 through 02-012, where the GI-guns of different volume were shot in an alternating mode, while a 10 m CMP distance was used for the other profiles (GeoB 02-013 through 02-044), resulting in a 9-fold coverage. The depth and compass information from the birds was used for a static correction of the data. No velocity analysis was carried out and a constant velocity of 1550 m/s was applied for NMO correction. The sections shown below are unmigrated CMP stacks.

### 7.2.1 Overview profiles

The first 44 profiles were shot as overview profiles (Fig. 40 and 41). These profiles cover a variety of different mud volcanoes and diapiric ridges. Despite the known near-surface occurrence of gas hydrates, bottom simulating reflectors were not present in our seismic lines. However, pronounced lateral amplitude variations and bright spots may indicate the occurrence of gas hydrates and free gas, but more detailed processing and interpretation of the seismic profiles is necessary to identify and quantify gas hydrates and free gas. Most seismic profiles were shot in the Sorokin Trough (Fig. 40), an area with abundant mud volcanoes. A typical example crossing different types of mud volcanoes is shown on line GeoB 02-003 (Fig. 44) oriented in a SSW-NNE direction. The larger mud volcano at the southwestern end of the profile is the Kazakov mud volcano. Kazakov mud volcano is cone-shaped with a diameter of ~ 2.5 km and a height of ~ 120 m above the surrounding seafloor. The area beneath Kazakov mud volcano is characterized by a transparent zone with a width similar to the diameter of the mud volcano probably serving as the main feeder channel. This zone can be vertically traced to more than 1.5 s TWT which is the maximum seismic penetration of our system. The root of this mud volcano is therefore not visible, but the depth of the roots may exceed 7–9 km (Limonov et al., 1994).

The upper 700 ms of the sediments around Kazakov mud volcano are characterized by relatively thick (< 100 ms) transparent units which are separated by strong reflectors. Reflectors beneath this unit are closely spaced and show a good continuity. Whether Kazakov mud volcano is located on a fault zone is not clearly imaged by the seismic data, but reflectors, which could be identified in the upper part of the section, do not show a major offset.

Another type of mud volcano is located between CMPs 850 and 1100 on profile GeoB 02-003 (Fig. 44). Such mud volcanoes, located close to Istanbul mud volcano, belong to a belt of mud volcanoes associated with a morphological step. The diameters of the mud volcanoes

## GeoB 02-003 GI-Gun (0.4 I)

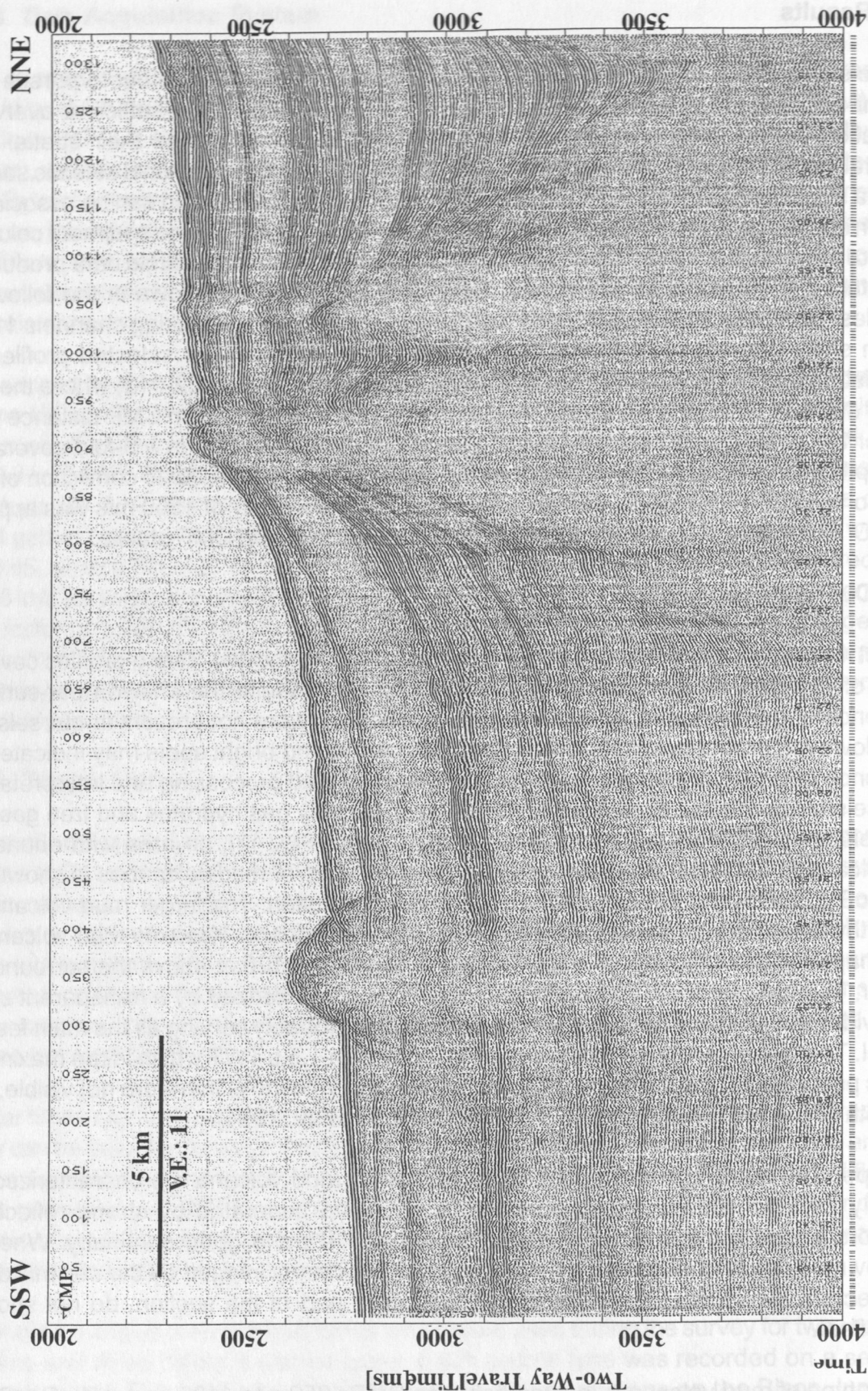


Fig. 44: CMP stack of seismic line GeoB 02-003 crossing Kazakov mud volcano and a group of unnamed mud volcanoes close to Istanbul mud volcano. CMP distance = 20 m.



imaged on line GeoB 02-003 are ~ 1 km for the mud volcano located around CMP 900 and 500 m for the mud volcano at CMP 1050; the heights are 45 m and 15 m, respectively. The feeder channel in the upper 300 – 400 ms TWT reveals about the same diameter as the mud volcano itself. Diapirs are clearly imaged beneath. These structures are interpreted as mud diapirs originating from the Maikopian formation, which is characterized by low-density clays and plastic behavior. The diapirs beneath the mud volcanoes are separated by narrow sedimentary basins. At a depth of about 3.3 s TWT the diapirs seem to be connected to a larger structure over an extent of more than 8 km. The flanks of the mud diapirs are overlapped by well stratified sediments. These sediments are typically bent upwards near the diapirs but around the upper part of the feeder channels the reflectors are slightly bent downwards. This may indicate a collapse of the sedimentary layers subsequent to eruption activity, but may also result from a velocity anomaly, which may be caused by relatively low velocity water- and gas- saturated sediments within the feeder channel (Limonov et al., 1994). At the northeastern end of the profile sedimentary basins are visible. Well stratified sediments are clearly imaged down to a sub-bottom depth of > 1.5 s TWT beneath the seafloor. Such basins are often found in close vicinity to the mud diapirs. While uplift was associated with the growth of the mud diapirs subsidence might have occurred at other places leading to the formation of the sedimentary basins. Such structures are very comparable to salt diapirism.

The western part of seismic line GeoB02-013, oriented from east to west, crosses Dvurechenskii mud volcano (Fig. 45). This flat-topped mud volcano was studied intensely during Cruise M52-1. OFOS tracks, sediment sampling, and heat flow measurements revealed that Dvurechenskii mud volcano is presently active. The seismic data show a very limited penetration of ~500 ms adjacent to the mud volcano. The upper sediments are dominated by thick transparent units separated by bands of high amplitude reflections. No coherent reflectors were found beneath the mud volcano itself, but numerous diffraction hyperbolae. Dvurechenskii mud volcano is underlain by a broad mud diapir and only the western limit of the diapir can be seen at the very end of the seismic section. Though Dvurechenskii mud volcano was most active we did not consider it as a target for the detailed 3-dimensional seismic survey as it is too large to be surveyed within our limited time and because it does not show great structural variability.

Seismic line GeoB 02-030 (Fig. 46), oriented from west to east, is an example of the second main working area, the central Black Sea (Fig. 41). The sedimentary section is clearly divided into two units. The upper unit is about 300 ms TWT thick. It is generally characterized by horizontally layered, strong continuous parallel reflectors. Some small zones with chaotic reflections are visible in the eastern part of this profile. The lower boundary of this unit is a ~20 ms thick transparent zone. The amplitudes of the lower unit are slightly weaker and the numerous reflectors are interrupted by faults at several locations. A major fault is clearly visible between the two mud volcanoes at CMP 880. The offset of the fault increases with increasing depth and the fault does not penetrate in the sediments of the upper seismic unit. This fault is probably related to the development of the two nearby mud volcanoes but it does not seem to be a major pathway for fluids itself. The two mud volcanoes on profile GeoB 02-030 are the Moscow State University mud volcano in the west and the Yuzhmorgeologiya mud volcano in the east. These mud volcanoes are by far the largest in the central Black Sea with diameters at the seabed from 2 – 2.3 km and elevations above the surrounding seafloor of 80 m- 120 m. These mud volcanoes were also studied during



GeoB 02-013 GI-Gun (0.4 1)

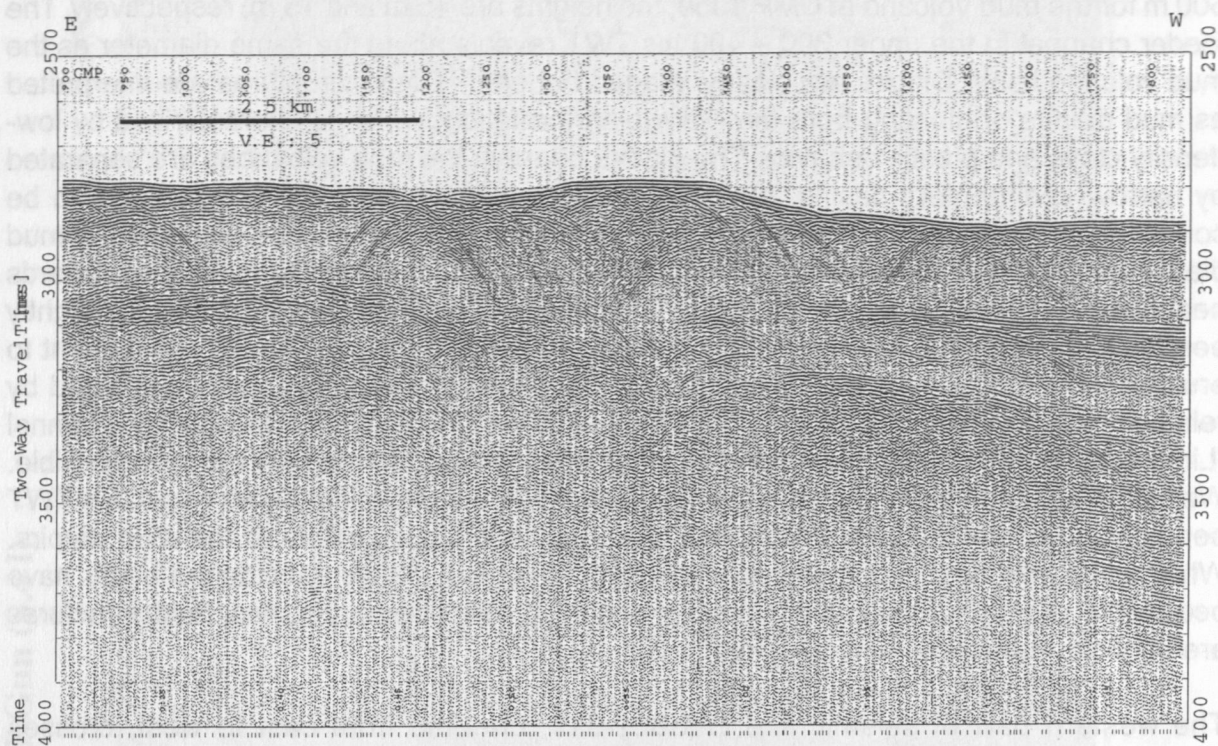


Fig. 45: CMP stack of a section of seismic line GeoB 02-013 crossing Dvurechenskii mud volcano. CMP distance = 10 m.

the third UNESCO-ESF "Training-through-Research" Cruise of RV Gelendzhik in 1993 with an OKEAN sidescan sonar (Limonov et al., 1994). Moscow State University mud volcano has a complex shape with a crater-like structure and a well defined rim, while Yuzhmorgeologiya mud volcano is cone-shaped with an almost circular basis. The mud volcanoes have been built up over long time periods, most possibly as a result of successive, massive mud flows that spread from eruptive centers in the crater over the rim and across the flanks (Limonov et al., 1994).

The feeder channels of both mud volcanoes are narrow within the upper sedimentary unit (~ 1 km) though their width is difficult to determine in an unmigrated section. They slightly widen with increasing depth. The feeder channels are mostly transparent and no coherent reflectors are visible. An interesting anomaly is visible near both feeder channels at a depth between 3.3 and 3.4 s TWT. Diffractions and/or reflections occur within the feeder channels and a reflector with a strong amplitude and an irregular reflection pattern can be traced into the surrounding sediments. This pattern may be caused by abundant mud flows which would indicate a period of strong activity of both mud volcanoes but the reflection pattern can also be related to the occurrence of gas.

### 7.2.2 3D-Multichannel Seismic and Tomographic Survey near Yalta/Sevastopol mud volcanoes

The main goal of the 3D-survey was to image lateral variations in structure and amplitude in an area which could be related to gas hydrate occurrences and fluid/gas migration. Therefore the overview profiles were used to identify such an area. The western profiles in

GeoB 02-030 GI-Gun (0.4 l)

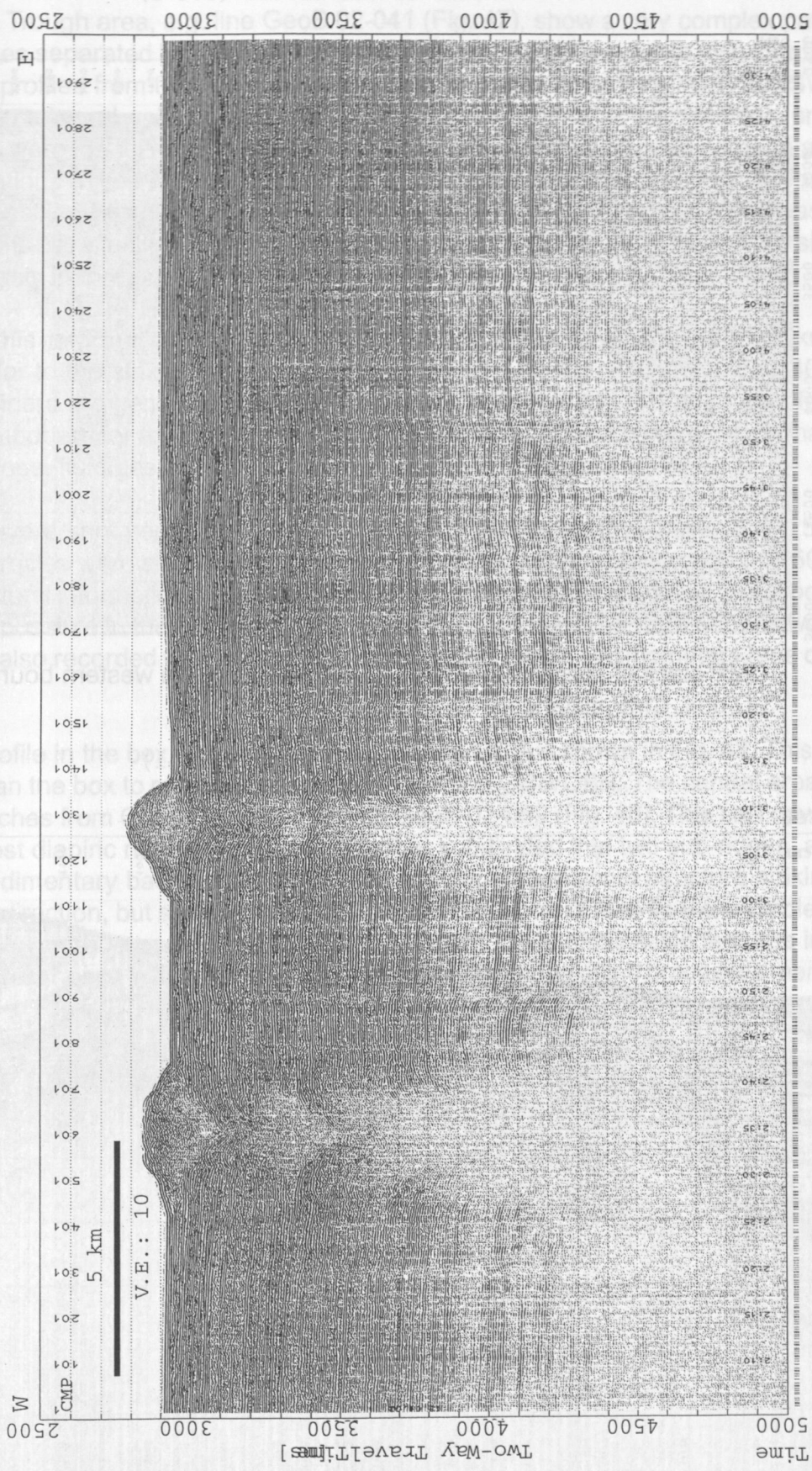


Fig. 46: CMP stack of seismic line GeoB 02-030 crossing Moscow State University and Yuzhmorgeologiya mud volcano. CMP distance = 10 m.



GeoB 02-041 GI-Gun (0.4 l)

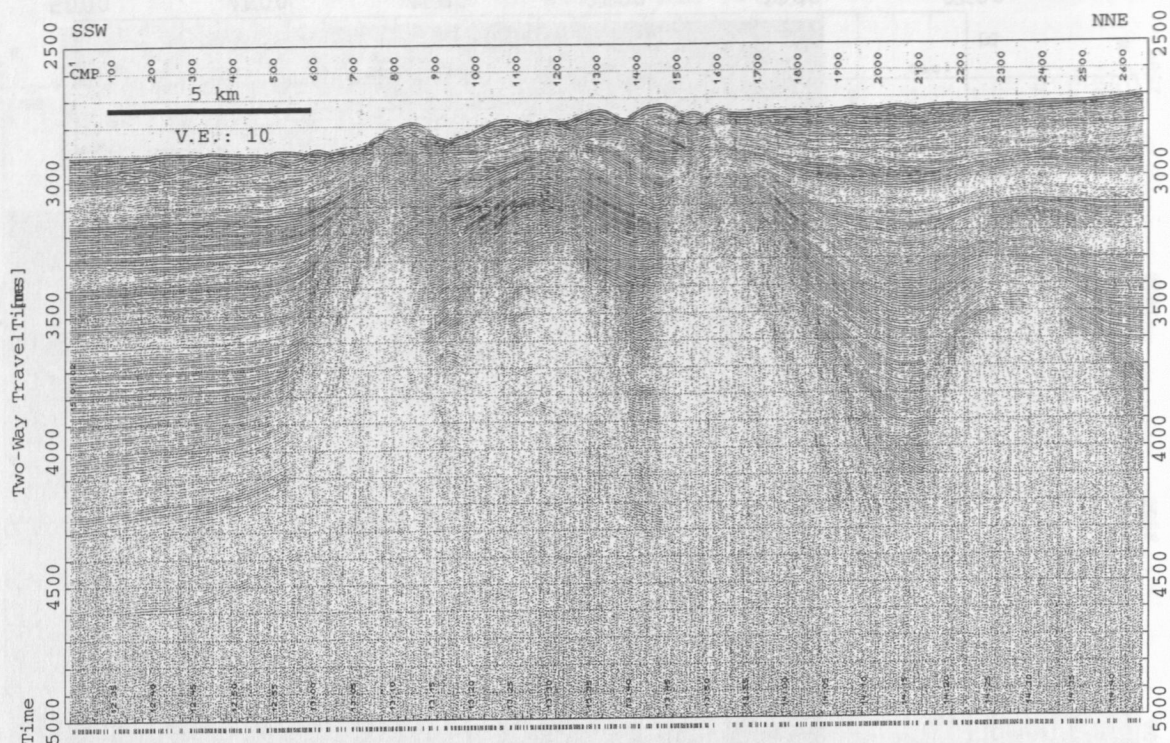


Fig. 47: CMP stack of seismic line GeoB 02-041 crossing the western boundary of the 3-D box. CMP distance = 10 m.

GeoB 02-059 GI-Gun (0.4 l)

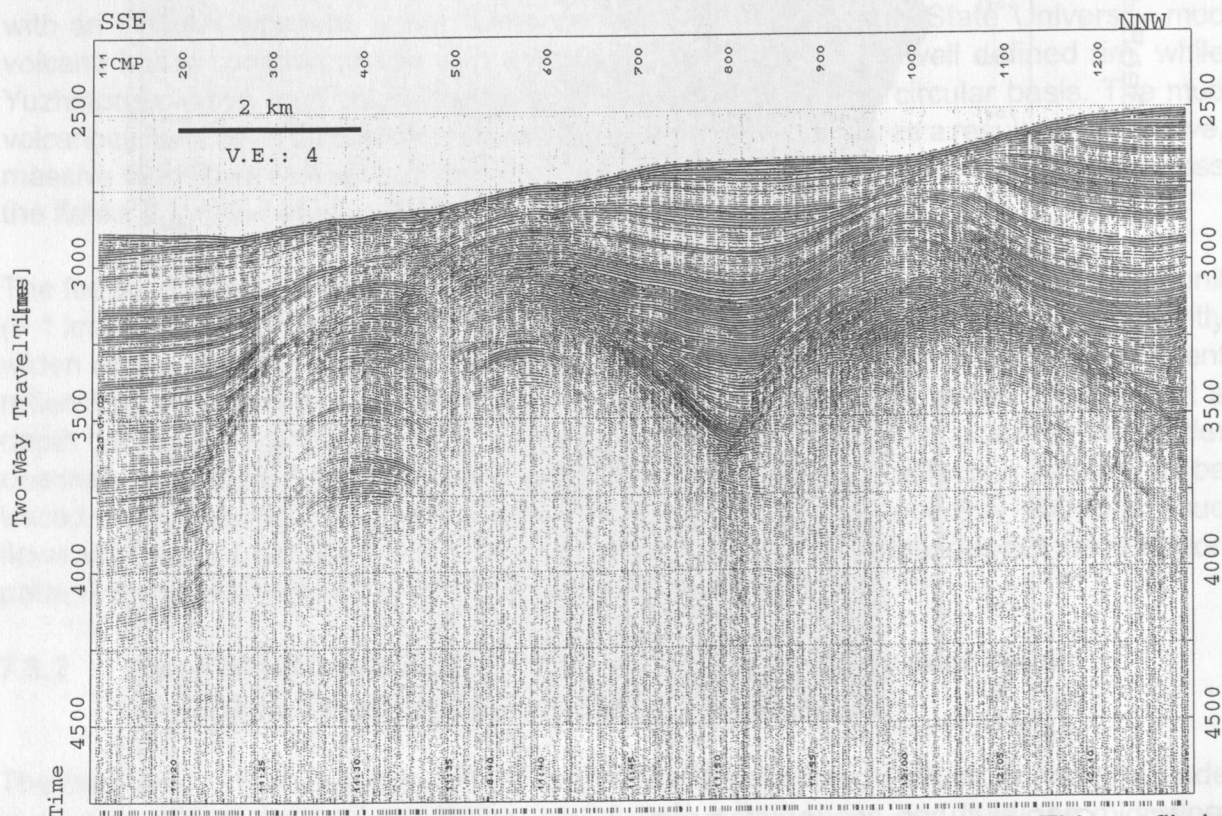


Fig. 48: CMP stack of seismic line GeoB 02-059. CMP distance = 10 m. This profile is part of the 3-D survey. 4 OBH/ OBS were located on this line.



the Sorokin Trough area, e.g. line GeoB 02-041 (Fig. 47), show a very complex pattern of diapiric ridges separated by sedimentary basins. Similar structures were also identified on most other profiles from this area, indicating diapiric ridges to be striking in a WSW-ENE direction. Small mud volcanoes, but also small depressions in the seafloor, probably pockmarks, were identified particularly on the edge of the southernmost ridge. In addition lateral variations in the reflection amplitude make this area most interesting. The ridge itself is basically a two-dimensional structure but several smaller features such as faults and variations in reflection pattern and amplitude are visible on a smaller scale showing great variability in three dimensions.

Based on this information we chose a box, 2.5 km wide parallel to and 7.5 km long perpendicular to the strike direction of the diapiric ridge for the 3D-survey (Fig. 40). This layout considers the general structures in this area but allows to image smaller features which are important for an understanding of the evolution of this area, e.g. the formation of mud volcanoes, fluid/gas migration, and the occurrence of gas hydrate.

81 Profiles were shot perpendicular to the strike of the diapirs at a distance of 25 m. 24 additional profiles were shot on the sides of the box with a line spacing of 50 m – 500 m to gather structural information at the edges of the box up to a width of 5 km but 3-D processing will only be possible in the central part of the box. 11 cross profiles were shot as well. The shots were also recorded with 14 ocean bottom hydrophones/ seismometers (see chapter 8).

A central profile in the box crossing 4 of the 14 OBH/OBS is shown in Fig. 48. This profile is longer than the box to record refracted energy at the OBS/OBH. The central area of the 3D-Box reaches from CMP 170 to 920 on line GeoB 02-059 (Fig. 48). This part covers the southernmost diapiric ridge, which can be further subdivided into two sub-ridges, and the adjacent sedimentary basins. The ridge itself is a two-dimensional structure striking in a WSW-ENE direction, but several small faults and indications of fluid flow are visible in this profile. The fully processed data set will allow to trace these small scale features in three dimensions and hence will significantly improve our knowledge of the processes mentioned above.

## 8. REFRACTION SEISMIC WORK

J. Bialas, A. Broser, A. Volkonskaya, M. Zillmer, A. Petersen

### 8.1 The GEOMAR Ocean Bottom Hydrophone / Seismometer (OBH/S)

The first GEOMAR Ocean Bottom Hydrophone was built in 1991 and tested at sea in January 1992. Since then more than 1700 successful dives have been completed. For M52/1 a total of 5 OBH and 10 OBS instruments were available and deployed at 29 sites.

#### The Ocean Bottom Hydrophone

The principle design of the instrument is shown in Fig. 49a. The system components are mounted on a steel pipe which holds the buoyancy body on its top. The buoyancy is made of syntactic foam and is rated, as are all other components of the system, for a water depth of 6,000 m. Attached to the buoyant body are a radio beacon, a flash light, a flag and a swimming line for retrieving from aboard the vessel. The hydrophone for the acoustic release is also mounted here. The release transponder is a model *RT661* made by *OCEANO Technology*. In order to avoid corrosion of the two pressure cases while keeping them as light in weight as possible the latest generation has been made of titanium. Communication with the instrument is possible through the ship's transducer system, and even at maximum speed and ranges of 4 to 5 miles release and range commands are successful. For anchors, we use pieces of railway tracks weighing about 40 kg each. The anchors are suspended 2 to 3 m below the instrument. The sensor is an *E-2PD* hydrophone from *OAS Inc.*, and the recording device is a *MBS recorder of SEND GmbH*, which is contained in its own pressure tube and mounted below the buoyant body opposite the release transponder (Flüh and Bialas, 1996).

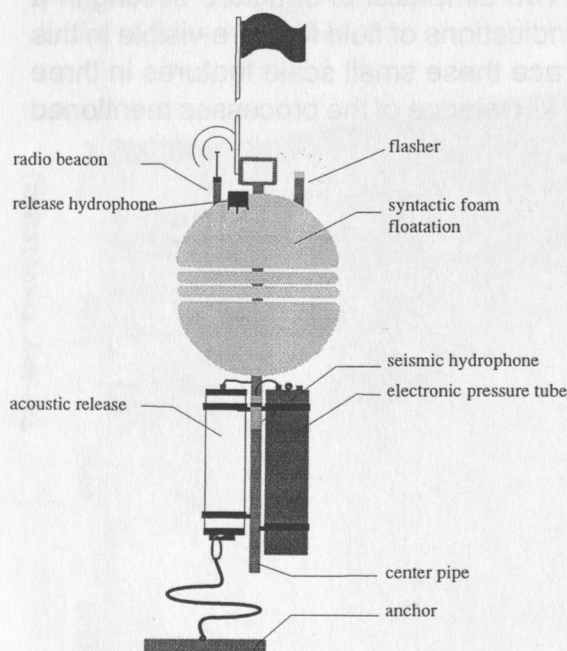


Fig. 49 a: Principle design of the GEOMAR OBH (Flüh and Bialas, 1996)

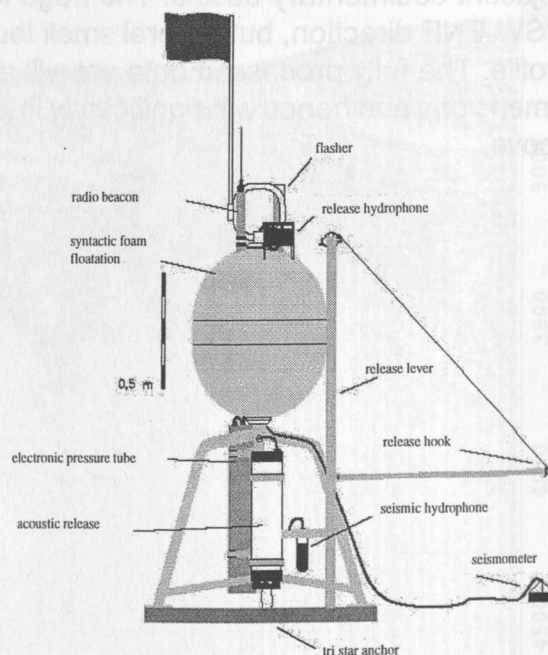


Fig. 49 b: Principle design of the GEOMAR OBS (Bialas and Flüh, 1999).



## The Ocean Bottom Seismometer

The Ocean Bottom Seismometer (OBS) construction (Bialas and Flueh, 1999; Fig. 49b) is based on the experiences with the GEOMAR OBH. For system compatibility the acoustic release, pressure tubes, and the hydrophone are identical to those used for the OBH. Syntactic foam was used as floatation as well but of larger diameter due to the increased payload. In contrast to the OBH, the OBS has three legs around a center post to which the anchor weight is attached. Little plates at the end of the anchor legs increase the size of the foot rest at the ground while their size and possible holes will prevent gliding during descent. While the OBH floats about 1 m above the sea bottom, the OBS is positioned at the sea bottom to avoid collisions between the seismometer cable and the anchor. The sensitive seismometer is deployed about 1 m to the side of the system once the OBS reaches the sea floor. During descent to the ocean bottom, the footplate of the seismometer release lever is about one meter below the base of the anchor and therefore hits the seafloor first. At touch down the baseplate forces an upward movement of the lever which lays out the seismometer hook until the seismometer anchor is about 0.5 m above the seafloor. At about 45 degrees to the vertical the seismometer is released from its hook and falls to the sea floor from about 1 m height, ensuring coupling between the seismometer and the sea floor. At this time the only connection from the seismometer to the instrument is a cable and an attached wire which retracts the seismometer during ascent to the sea surface. A possible vibration of the system carrier will therefore not be transmitted mechanically to the seismometer. All three channels are recorded by the standard MBS recorder as used in the OBH units. Parallel to these three channels the standard hydrophone is recorded on the fourth channel.

## Marine Broadband Seismic Recorder (MBS)

The so-called *Marine Broadband Seismic recorder (MBS)* (Bialas and Flueh, 1999), manufactured by *SEND GmbH* avoids mechanically driven recording media, and the PCMCIA technology allows for static flash memory cards to be used as unpowered storage media. Nevertheless, advanced technology has led to the availability of PCMCIA standardized micro drives certified for temperatures as low as +2°C. Providing 1 GB data capacity they still have the advantage of extremely reduced power consumption and do not influence the electronics by their spinning disc. A data compression algorithm is implemented to increase data capacity. The *MBS* system requires a low power consumption of 1.5 W. Depending on the sampling rate, data output could be in 16 to 18 bit signed data. Based on digital decimation filtering, the system was developed to fulfill a variety of seismic recording requirements. Therefore, the band width reaches from 0.1 Hz for seismological observations to the 50 Hz range for refraction seismic experiments and up to 10 kHz for high resolution seismic surveys. The basic system is adapted to the required frequency range by setting up the appropriate analogue front module. Alternatively, 1, 2, 3 or 4 analogue input channels may be processed. The time base is based on a DTCXO with a 0.05 ppm accuracy over temperature. Setting and synchronizing the time as well as monitoring the drift is carried out automatically by synchronization signals (DCF77 format) from a GPS-based coded time signal generator. Clock synchronization and drift are checked after recovery and compared with the original GPS units. After software preamplification the signals are low-pass filtered using a 5-pole Bessel filter with a -3 dB corner frequency of 10 kHz. Then each channel is digitized using a sigma-delta A/D converter at a resolution



of 22 bits producing 32 bit signed digital data. After delta modulation and Huffman coding the samples are saved on PCMCIA storage cards together with timing information. Up to 4 storage cards can be used. Currently, up to 1 GB per card are available. Data compression allows more than 6 GB of data capacity. Recently, the technical specifications of flash disks (disk drives of PCMCIA technology) have been modified to operate below 10 °C. After recording the data is copied from flashcards to a PC workstation. The data is decompressed and data files from a maximum of four flash cards are combined into one data set and formatted according to the PASSCAL data scheme using a 16 or 32 bit data format.

## 8.2 Seismic Sources

For the reconnaissance survey seismic signals were generated by two Model PAR 800 CT BOLT airguns (Fig. 50). Each gun has a volume of 32 liters (2,000 inch<sup>3</sup>), and generates a signal with a main frequency centered around 6 to 8 Hz including higher harmonics. The guns were towed attached to blocks on the outer side of the A-frame, with two pier winches controlling the towing. Each gun was suspended on two floats with an additional float attached to the supply lines to prevent contact between the gun and the towing wire. The guns were towed 60 m behind the vessel and operated at 150 bar in 7 to 8 m depth. Helped by newly welded bold eyes on the guns to support crew handling with securing ropes, the guns could be handled smoothly all of the time. Due to the large distance needed between the guns and the rear of the vessel for safety reasons, the guns tend to drifting to the center, leaving no space to deploy the streamer in between. Nevertheless an additional GI gun could be deployed on the port side for the first line. Due to heavy weather conditions the gun need to be recovered on the second profile.

During cruise M52/1, the guns were used along two seismic reconnaissance profiles. After the first deployment the supply line of the starboard gun was cut and needed to be repaired. The total operation time was close to 21 hours, with more than 1,100 shots fired, always at a 60 s shot interval. The additional GI-gun was shot intermediately with 20 sec intervals. This was well within the capability of the compressor system, which worked smoothly and caused no delays or interruptions. The trigger signal was supplied by the reflection seismic group (see chapter 7)

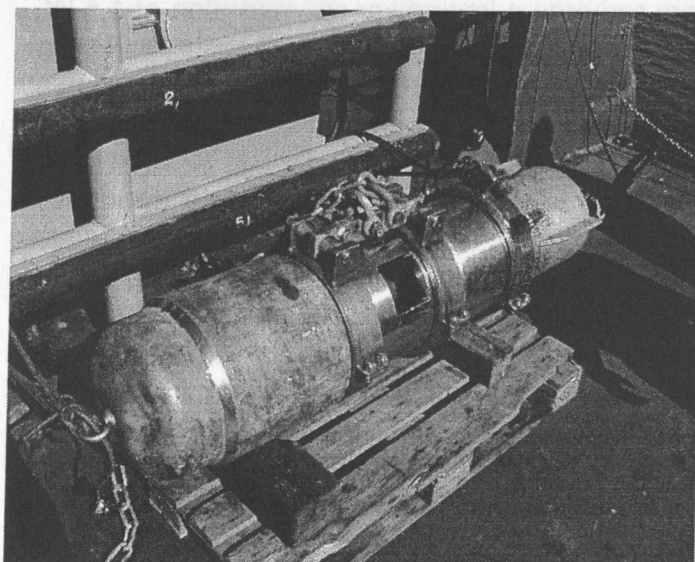


Fig. 50: 32 I Bolt PAR 800 CT airgun.

### 8.3 OBH/S wide angle seismic data processing

#### 8.3.1 Data Processing

The OBH/S data recorded on the MBS have to be converted into standard SEG-Y format for further processing. The necessary program structure was partly taken from the existing REFTEK routines and modified for the OBH requirements and GEOMAR's hardware platforms. Because the GEOMAR OBH/S works in a continuous mode, most of the modifications to the existing program package had to be done on the parts of the program which handle continuous data streams. A flow chart shown in Fig. 51 illustrates the processing scheme applied to the raw data. A detailed description of the main programs follows below.

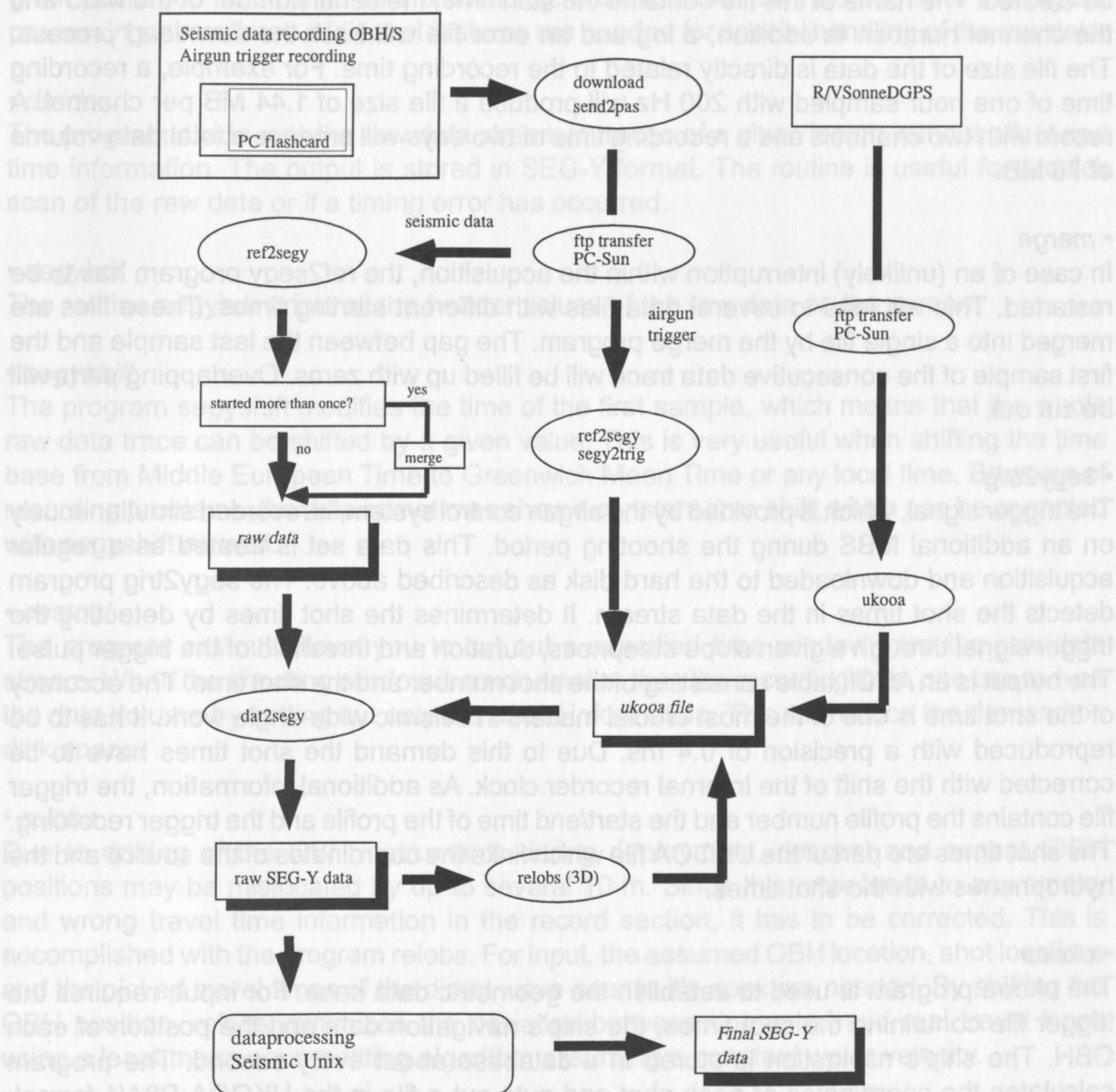


Fig. 51: Processing flow of OBH/S data from raw data to SEG-Y records.



- *send2pass*

For the PC cards used with the MBS recorder, data expansion and format conversion into PASSCAL data format is performed using a DOS based PC. The program *send2pass* reads the data from the set of up to four flashcards used during recording. Decompressed data are written onto the PC's hard disk using the PASSCAL data format. Either 16 or 32 bit storage is available in order to adopt the resolution during the acquisition. After ftp transmission to a SUN workstation, *ref2segy* and all other software can be used to handle and process the data files and store them as SEG-Y traces.

- *ref2segy*

This program will produce a pseudo SEG-Y trace consisting of one header and a continuous data trace containing all samples. For each channel (different amplifications) one file will be created. The name of this file contains the start time, the serial number of the MBS and the channel number. In addition, a log and an error file will track the download process. The file size of the data is directly related to the recording time. For example, a recording time of one hour sampled with 200 Hz will produce a file size of 1.44 MB per channel. A record with two channels and a recording time of two days will produce a total data volume of 70 MB.

- *merge*

In case of an (unlikely) interruption within the acquisition, the *ref2segy* program has to be restarted. This will lead to several data files with different starting times. These files are merged into a single file by the *merge* program. The gap between the last sample and the first sample of the consecutive data trace will be filled up with zeros. Overlapping parts will be cut out.

- *segy2trig*

The trigger signal, which is provided by the airgun control system, is recorded simultaneously on an additional MBS during the shooting period. This data set is treated as a regular acquisition and downloaded to the hard disk as described above. The *segy2trig* program detects the shot times in the data stream. It determines the shot times by detecting the trigger signal through a given slope steepness, duration and threshold of the trigger pulse. The output is an ASCII table consisting of the shot number and the shot time. The accuracy of the shot time is one of the most crucial matters in seismic wide-angle work. It has to be reproduced with a precision of 0.4 ms. Due to this demand the shot times have to be corrected with the shift of the internal recorder clock. As additional information, the trigger file contains the profile number and the start/end time of the profile and the trigger recording. The shot times are part of the UKOOA file which links the coordinates of the source and the hydrophones with the shot times.

- *ukooa*

The *ukooa* program is used to establish the geometric data base. For input, requires the trigger file containing the shot times, the ship's navigation data and the position of each OBH. The ship's navigation is stored in a database about every second. The program calculates the coordinates of each shot and puts out a file in the UKOOA-P84/1 format. Corrections for offsets between antenna and airguns as well as consistency checks are included. This file will be used when creating a SEG-Y section via the *dat2segy* program.



- *dat2segy*

The *dat2segy* program produces standard SEG-Y records either in a 16 or 32 bit integer format by cutting the single SEG-Y trace (from the merged *ref2segy* file) into traces with a certain time length. It reads both the *ukooa* file with the geometry information and the downloaded raw data as produced with the *ref2segy* program. In addition, the user can use several parameters for controlling the output. These parameters are information about the profile and the receiver station, number of shots to be used, trace length, time offset of the trace and reduction velocity (to determine the time of the first sample within a record). The clock drift of the recorder is also taken into account and corrected for. The final SEG-Y format consists of the file header followed by the traces. Each trace consists of a trace header followed by the data samples. The output of the *dat2segy* program can be used as input for further processing with Seismic Unix (SU) and other commercially available program packages for seismic data processing. Beside these main programs for the regular processing, sometimes additional features are needed for special handling of the raw data:

- *divide*

The program *divide* cuts the raw data stream in traces of a given length without offset and time information. The output is stored in SEG-Y format. The routine is useful for a quick scan of the raw data or if a timing error has occurred.

- *segyhdr*

The routine *segyhdr* prints all the header values of the raw data on the screen.

- *segyshift*

The program *segyshift* modifies the time of the first sample, which means that the whole raw data trace can be shifted by a given value. This is very useful when shifting the time base from Middle European Time to Greenwich Mean Time or any local time. Because of recording problems, the data sometimes show a constant time shift, which can be corrected with *segyshift* as well.

- *castout*

The program *castout* allows you to cut out a specified time window from the raw data stream. When the shooting window is much smaller than the recording time, one can reduce the data volume by cutting out only the useful information. This will reduce the demand on disk space.

- *relobs*

Due to drifting of the OBH instruments during deployment, descent and ascent, OBH positions may be mislocated by up to several 10 m. Since this error leads to asymmetry and wrong travel time information in the record section, it has to be corrected. This is accomplished with the program *relobs*. For input, the assumed OBH location, shot locations and the picked travel times of the direct wave near to it's apex are needed. By shifting the OBH position, *relobs* minimizes the deviation between computed and real travel times using a least mean square fitting algorithm assuming a constant water velocity.

### 8.3.2 OBH/OBS-data analysis and processing with source signals of 32 liter Bolt airguns

*Raw data:* As an example, the hydrophone component of OBS record section 09 for refraction profile 02 is shown in Fig. 52.

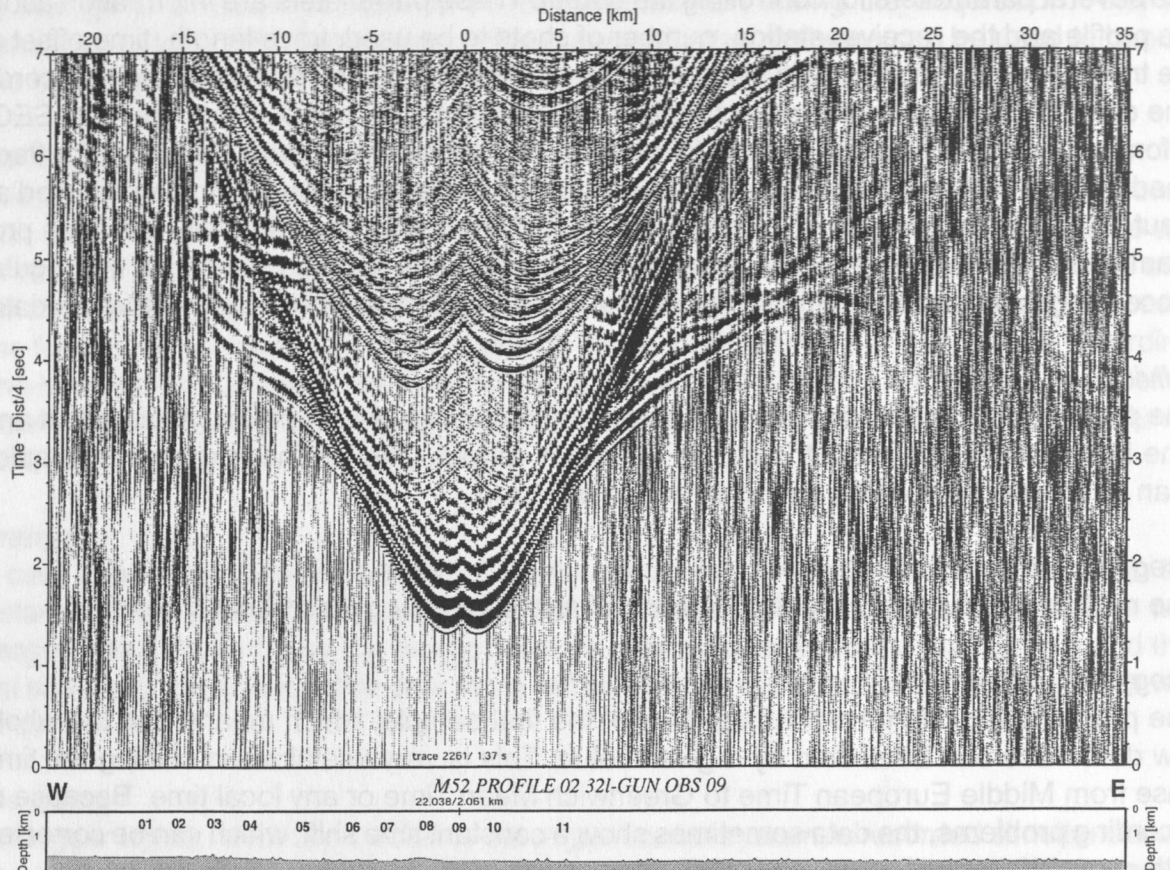


Fig. 52: Record section from OBS 09 hydrophone, profile 02.

*Frequency filter analysis:* To determine the frequencies of the seismic energy, filter panels with narrow frequency band passes were tested (Fig. 53). The butterworth bandpass filter applied with minimum delay characteristics is described by four corner frequencies: lower stop/pass band boundary and upper pass/stop band boundary. The frequencies on the filter panels correspond to the lower and upper pass frequencies. The main energy for the refraction waves is between 5-20 Hz. The main energy of the wide angle phase between 3.5 and 5 s in the offset range from 20-35 km is between 5-10 Hz. As there is still an energy content for the refracted events in the 20-30 Hz panel the final filter was chosen from 2/4-35/70 Hz which can be seen in Fig. 54 (compare with Fig. 52).

*Deconvolution analysis:* The raw seismic section is dominated by the ringing effects of the airgun bubble. To improve the temporal resolution of the seismic data a deconvolution is applied to compress the basic seismic wavelet. The recorded wavelet has many components, including the source signature, recording filter, and hydrophone/geophone response. Ideally, deconvolution should compress the wavelet components and leave only the earth's reflectivity in the seismic trace. The deconvolution algorithm which was applied is the Wiener predictive deconvolution in a moving operator window, based on the following assumptions:



1. The earth's reflectivity is 'white'.
2. The wavelet shows the minimum-delay phase behavior.

Input for the test of the deconvolution operator are the raw data of OBS 08 from refraction profile 01 shown in Fig. 55 (here already bandpass filtered for display purposes). The final deconvolution operator results for this seismic section are shown in Fig. 56. Fig. 57 shows the autocorrelation function of the raw data and after predictive deconvolution. On the undeconvolved data in Fig. 55 the strong bubble pulse with 200ms wavelength can be seen up to the 7th order. The seismic signal is shortened to a spike after predictive deconvolution and the bubble pulse is suppressed, which can be seen in the autocorrelation of the deconvolved data. The best resolution is obtained for a predictive length of 40 ms and an operator length of 400 ms, but with a reduction of signal-to-noise ratio especially on the near offset traces.

After deconvolution, the butterworth bandpass filter with minimum delay characteristic is applied as described above. In addition, a distance dependent amplitude weighting is applied as well as an offset dependent amplitude scaling.

*Processed data:* A comparison of the preprocessed data in Fig. 56 to the unprocessed (bandpass frequency filtered) data in Fig. 55 shows a clear reduction of the low and mono-frequency noise in the near and far offset traces and moderate compression of the wavelet signal. At the near offset traces reflections can be identified between the direct wave and multiple of the direct wave due to suppression of the bubble pulse. For the picking of events and model building by ray tracing the processed sections were used.

*Final processing sequence:*

- Input: SEG-Y-data, 0.4 ms sampling rate with complete geometry information.
- Wiener predictive deconvolution: operator length 400 ms, prediction interval 40 ms.
- Butterworth bandpass frequency filter.
- Offset dependent amplitude weighting.
- Offset dependent amplitude scaling.

### 8.3.3 OBH/OBS-data analysis and processing with source signals of 1.7 liter G1 gun

*Raw data:* As an example, OBH record section 14 of refraction profile 01 is shown in Fig. 58.

*Frequency analysis:* To determine the frequencies of the seismic energy, filter panels with narrow frequency pass bands for OBH 14 are shown in Fig. 59. The butterworth filter applied with minimum delay characteristics is described by four corner frequencies: lower stop/pass band boundary and upper pass/stop band boundary. The frequencies on the filter panels correspond to the lower and upper pass frequencies. The main energy for the refracted phases can only be seen in the panel of 5-100 Hz. Shallow reflection phases can be identified up to frequencies between 100-200 Hz and the direct wave up to 300-400 Hz. There is a very low frequency content in the acoustic signal as well, which can be seen in the autocorrelation function in Fig. 61. To retain even the higher frequency content of the near offset reflections and to get rid of the low frequency content a bandpass filter was



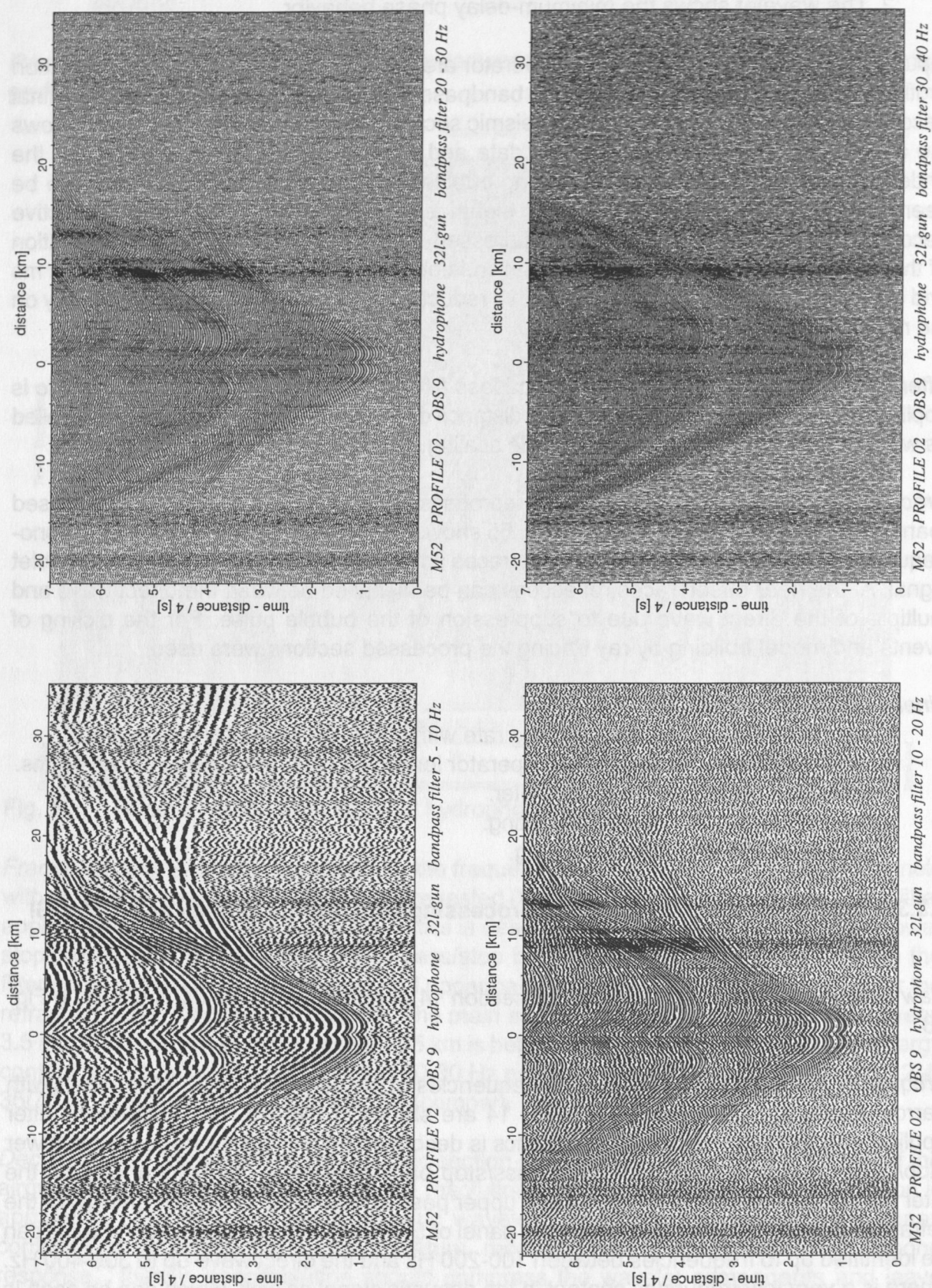


Fig. 53: Bandpass frequency test panels for the 32 l airgun.

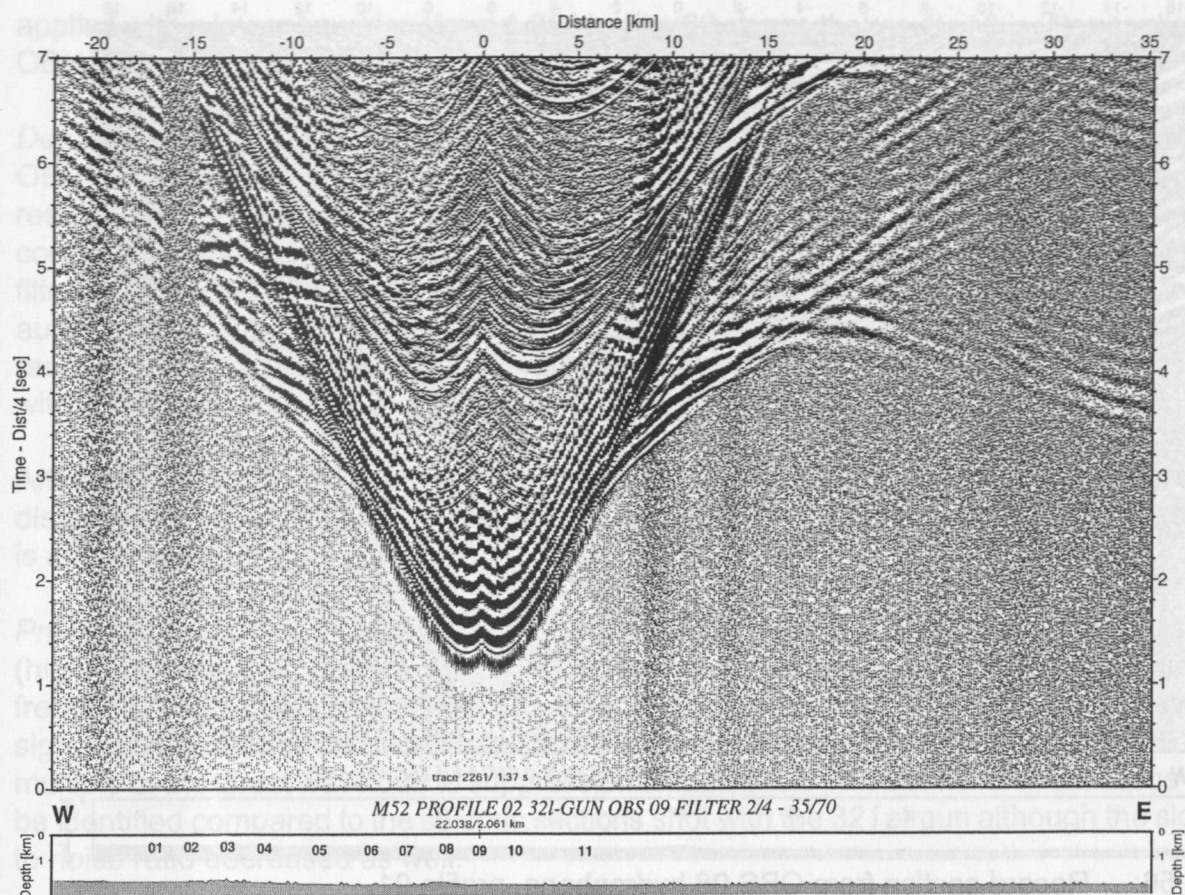


Fig. 54: Record section from OBS 09 hydrophone, profile 02.

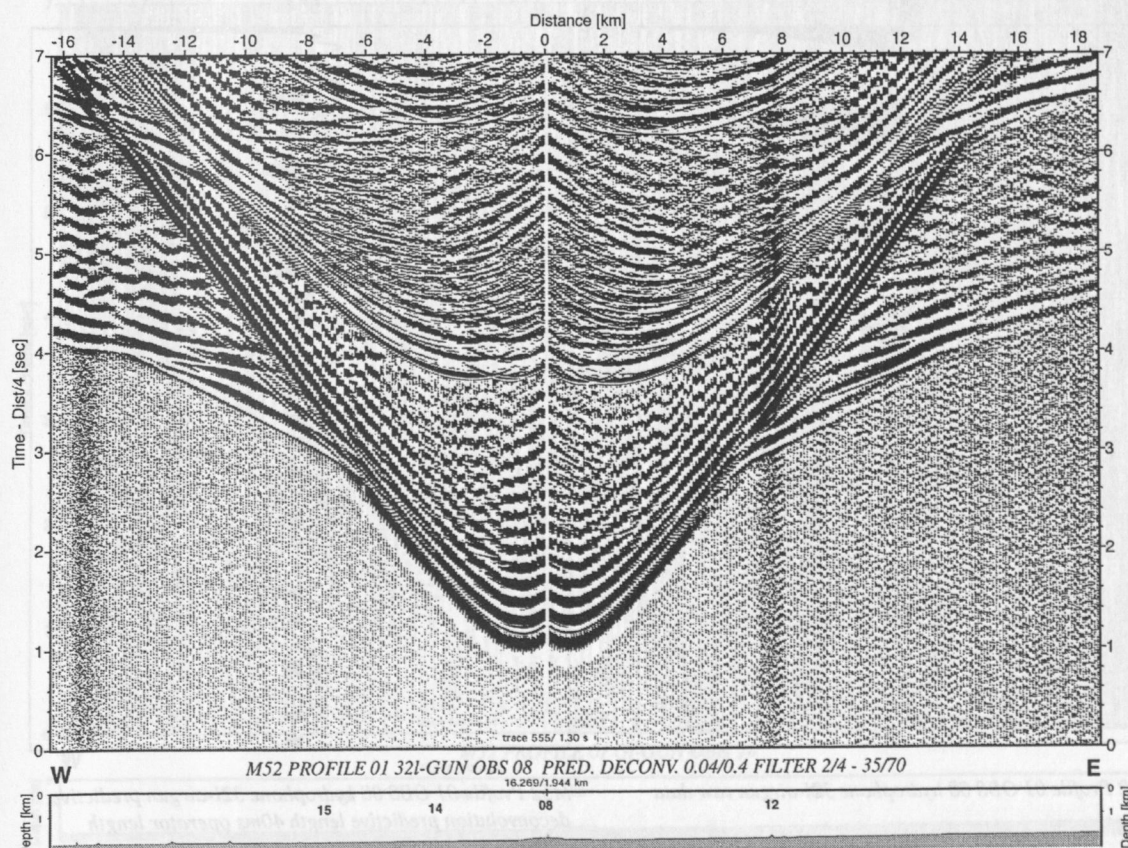


Fig. 55: Record section from OBS 08 hydrophone, profile 01.



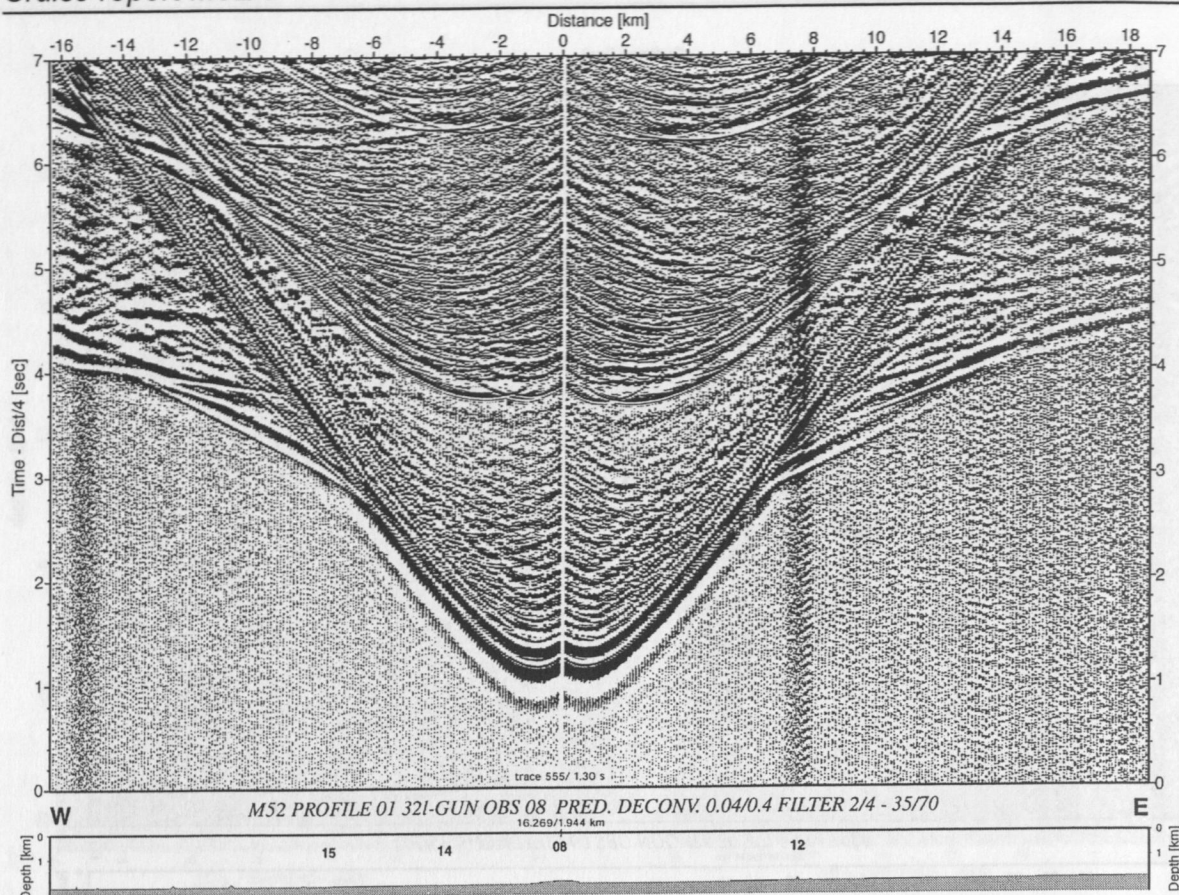
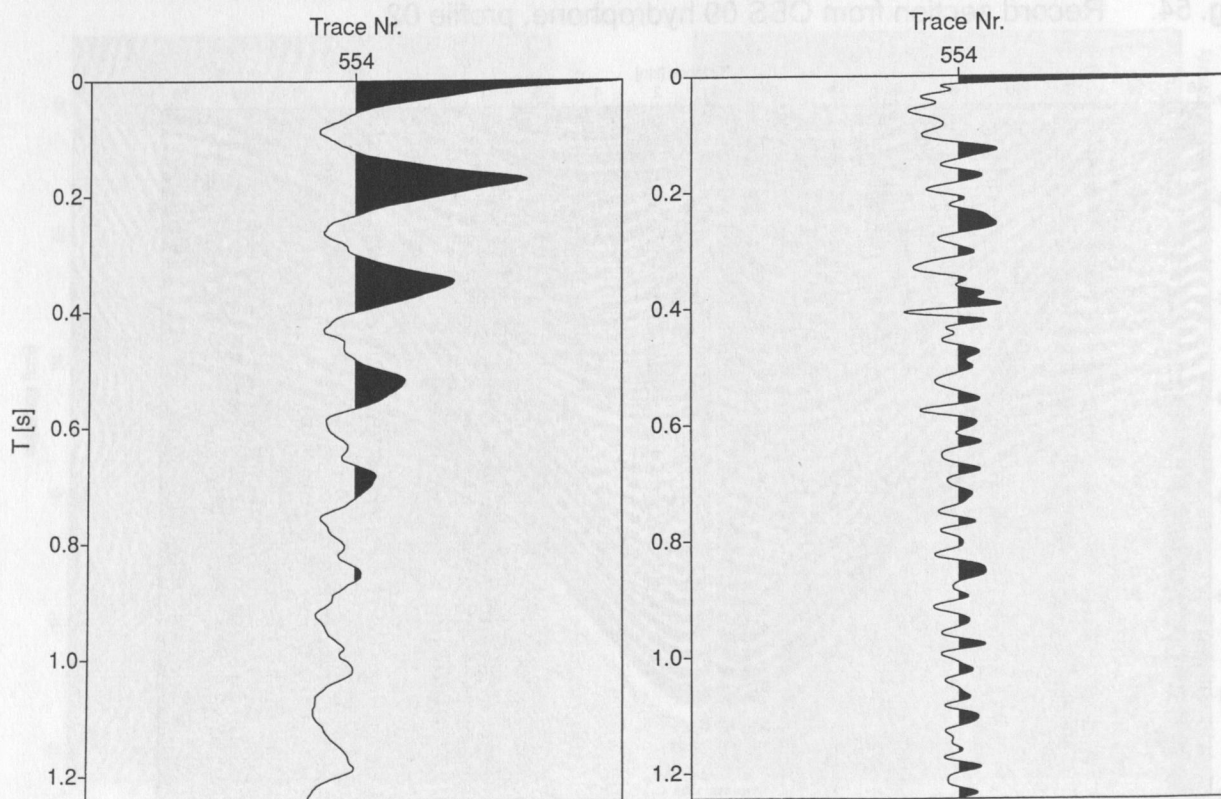


Fig. 56: Record section from OBS 08 hydrophone, profile 01.



M52 Profile 01 OBS 08 hydrophone 321-airgun raw data

M52 Profile 01 OBS 08 hydrophone 321-airgun predictive deconvolution predictive length 40ms operator length 400ms

Fig. 57: Autocorrelation from OBS 08 of raw hydrophone component data (left) and of processed trace after predictive deconvolution (right).



applied with a lower boundary from 4-20 Hz. Fig. 60 shows the result of this filter applied at OBH 14 from profile 01.

*Deconvolution analysis:* Input for the test of the deconvolution operator are the raw data of OBH 14 from refraction profile 01 shown in Fig. 58. The final deconvolution operator results for this seismic section are shown in Fig. 62. Due to the strong low frequency content that is visible in the autocorrelation function in Fig. 61, the highpass frequency filter was applied before predictive deconvolution to shorten the signal. Fig. 61 shows the autocorrelation function of the raw data as well as after predictive deconvolution. The best resolution is obtained for a predictive length of 8 ms and an operator length of 200 ms but with a reduction of signal-to-noise ratio especially on the far offset traces.

After deconvolution the highpass filter is applied again as described above. In addition a distance dependent amplitude weighting as well as an offset dependent amplitude scaling is applied.

*Processed data:* A comparison of the preprocessed data in Fig. 59 to the unprocessed (highpass frequency filtered) data in Fig. 61 shows a clear reduction of the low and mono-frequency noise in the near and far offset traces and moderate compression of the wavelet signal. At the near offset traces reflections can be identified between the direct wave and multiple of the direct wave due to suppression of the bubble pulse and more reflections can be identified compared to the seismic sections shot with the 32 l airgun although the signal to noise ratio decreased as well.

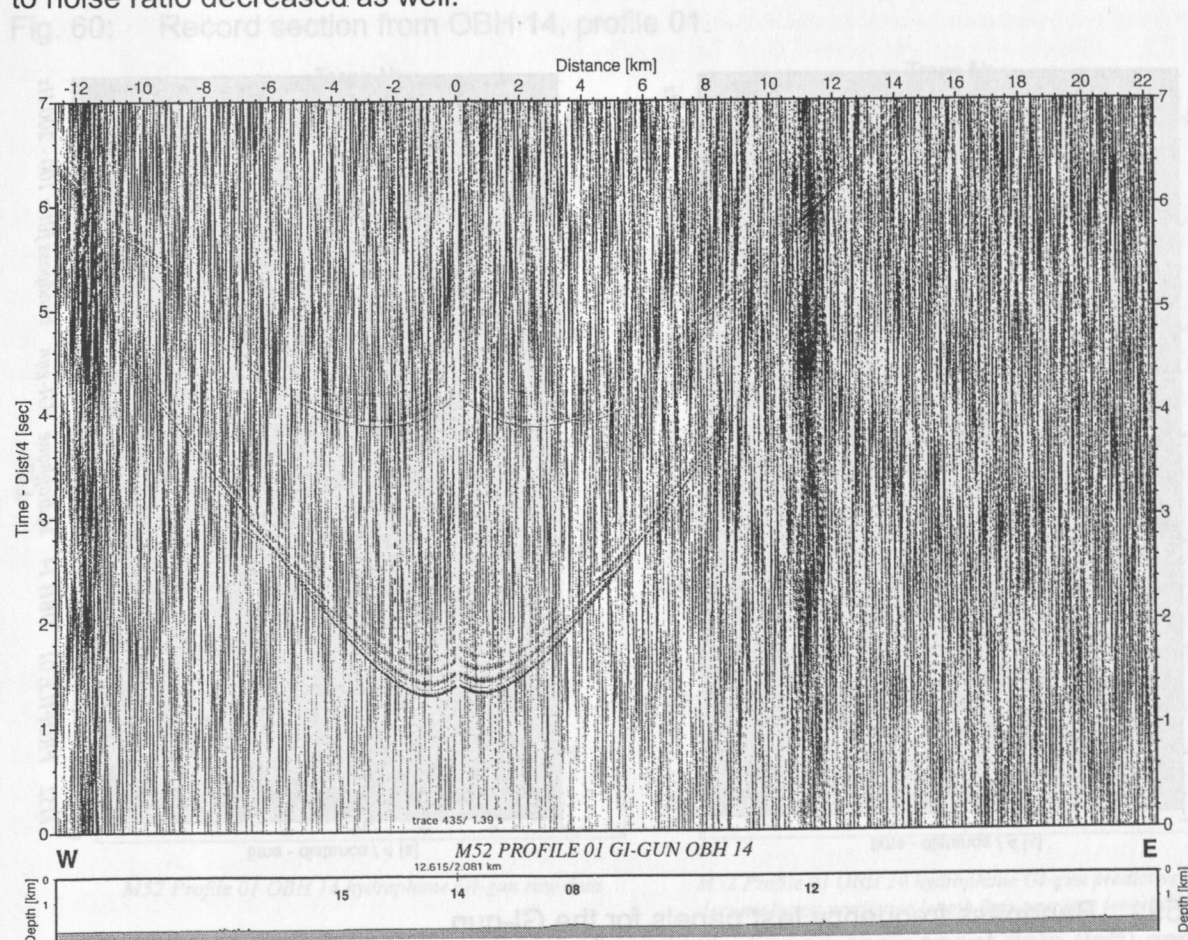


Fig. 58: Record section from OBH 14, profile 01.

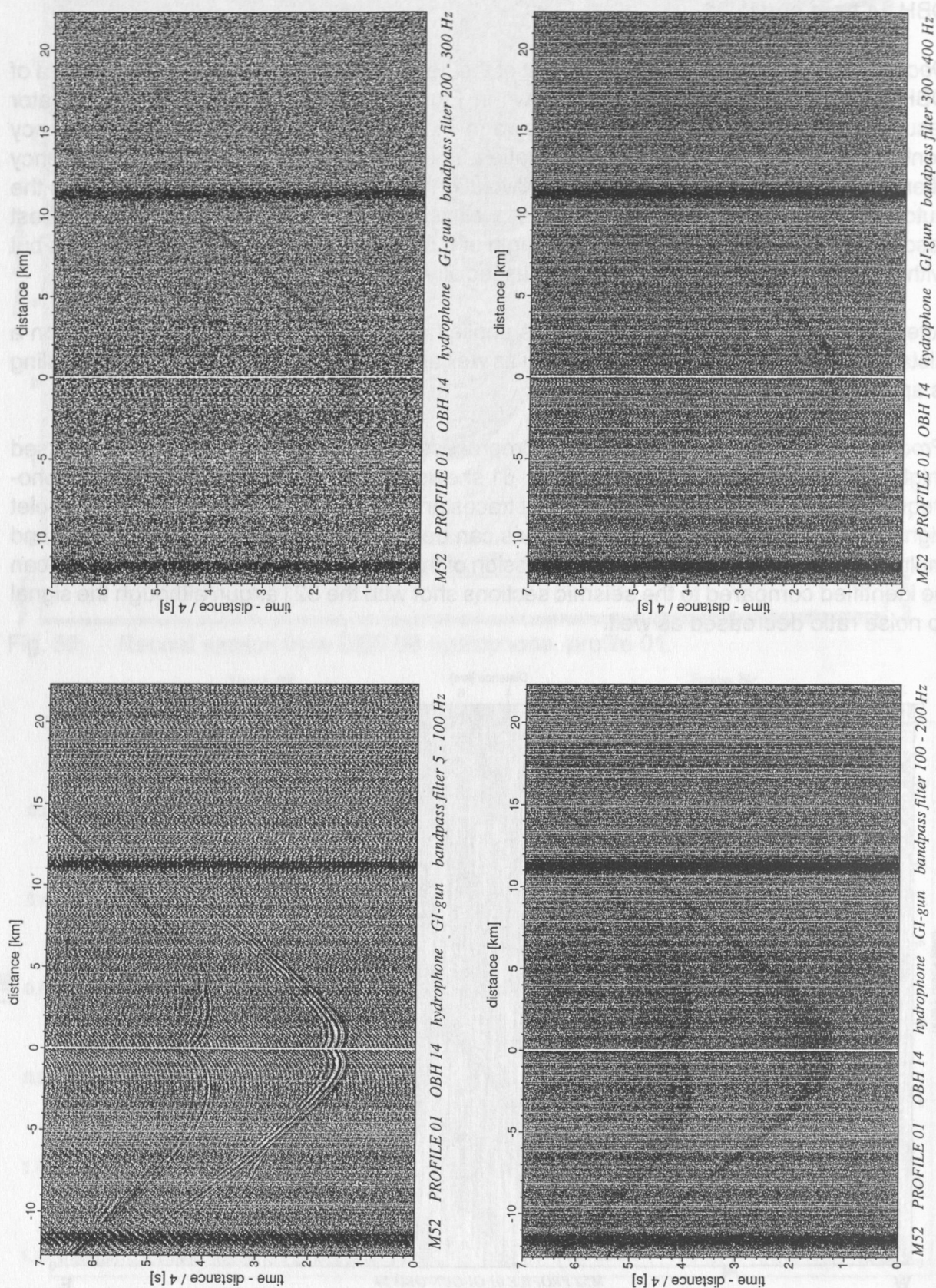


Fig. 59: Bandpass frequency test panels for the GI-gun.



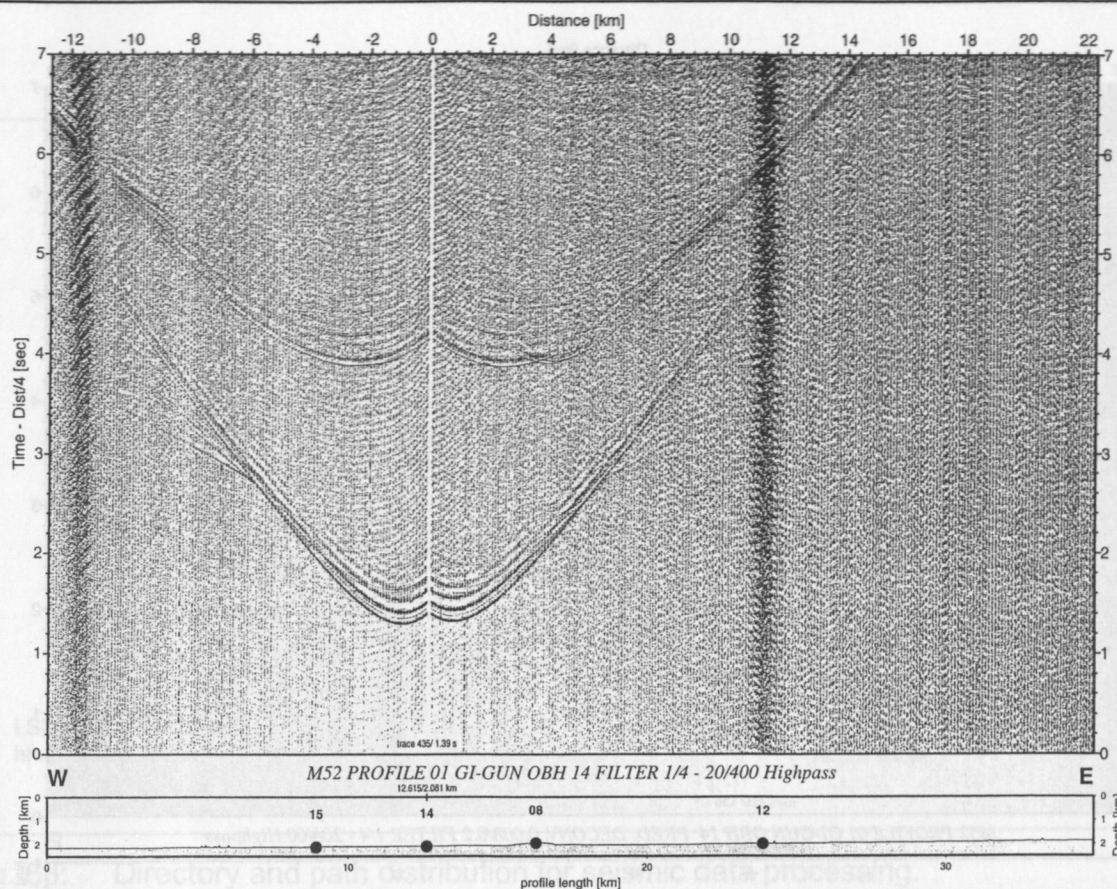
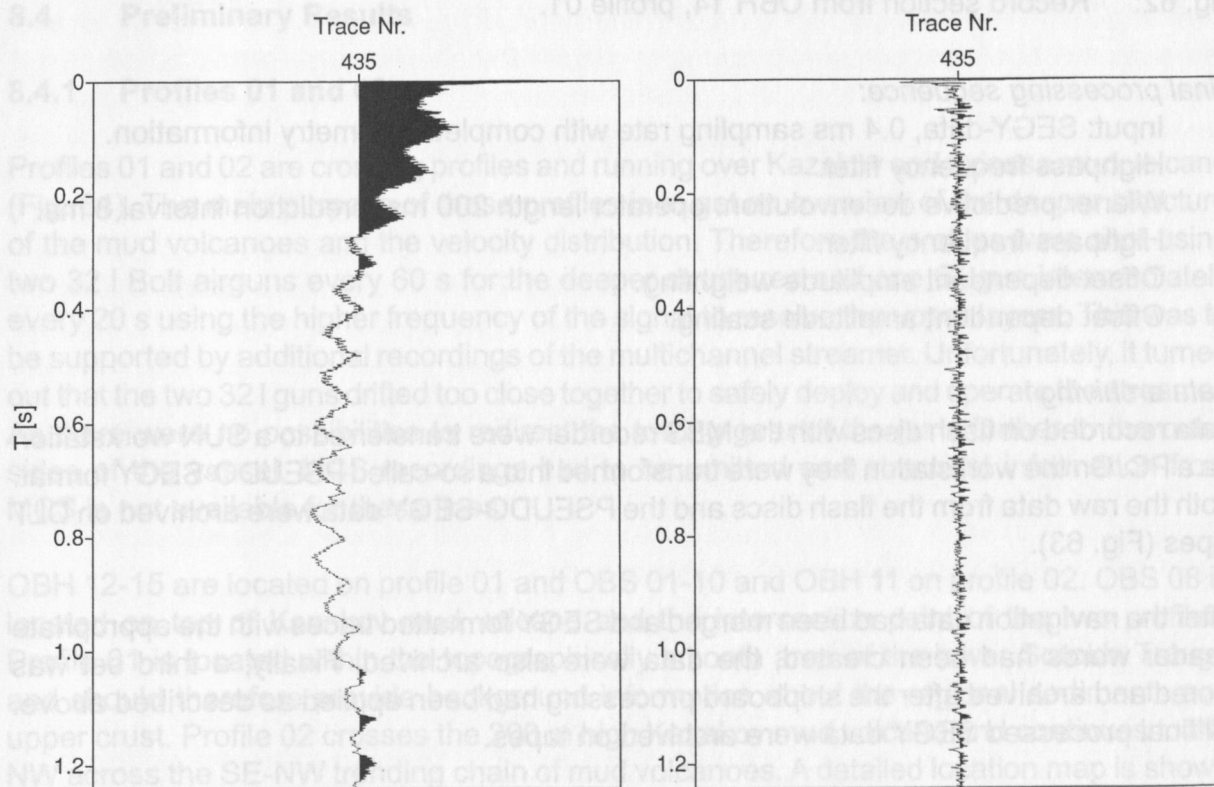


Fig. 60: Record section from OBH 14, profile 01.



M52 Profile 01 OBH 14 hydrophone GI-gun raw data

M52 Profile 01 OBH 14 hydrophone GI-gun predictive deconvolution predictive length 8ms operator length 200ms

Fig. 61: Autocorrelation from OBH 14 of raw hydrophone component data (left) and of processed trace after predictive deconvolution (right).



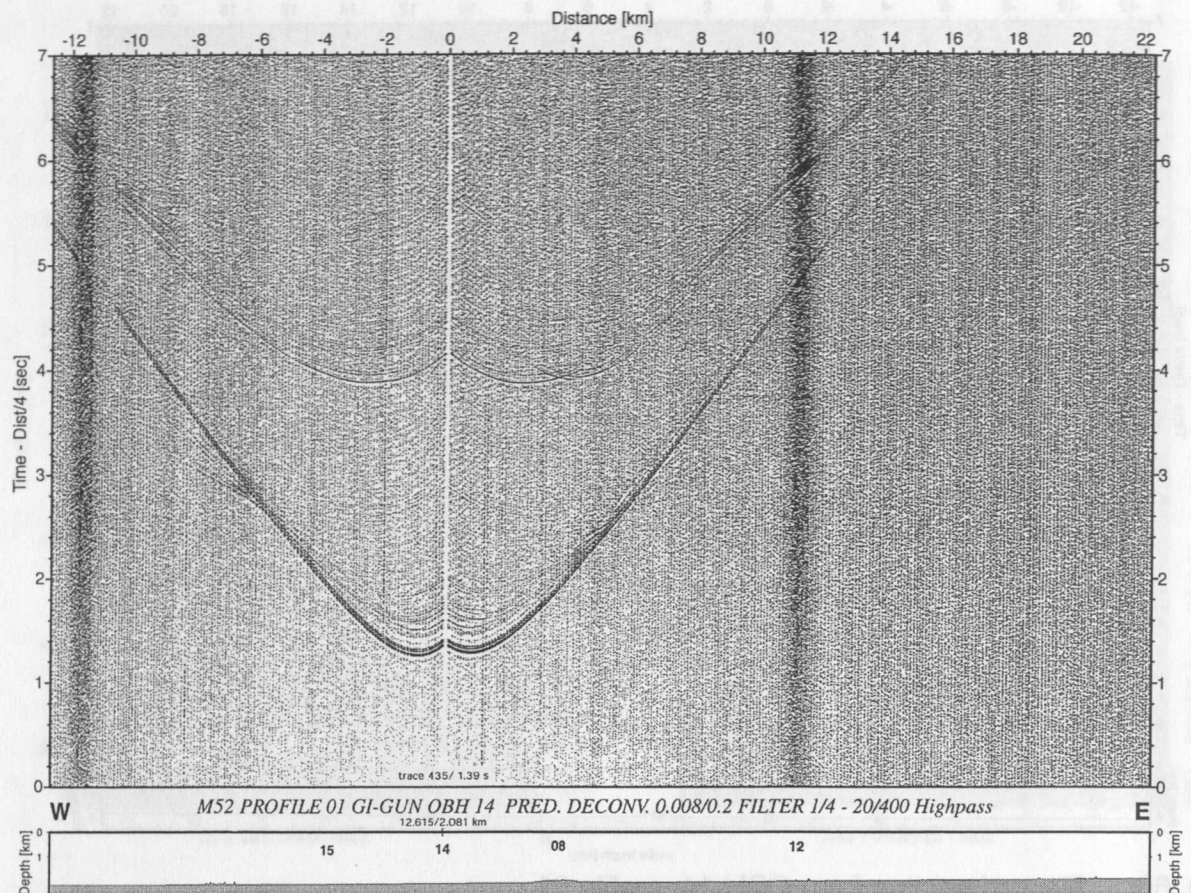


Fig. 62: Record section from OBH 14, profile 01.

*Final processing sequence:*

- Input: SEGY-data, 0.4 ms sampling rate with complete geometry information.
- Highpass frequency filter.
- Wiener predictive deconvolution: operator length 200 ms, prediction interval 8 ms.
- Highpass frequency filter.
- Offset dependent amplitude weighting.
- Offset dependent amplitude scaling.

*Data archiving*

Data recorded on flash discs with the MBS recorder were transferred to a SUN workstation via a PC. On the workstation they were transformed into a so-called PSEUDO-SEGY format. Both the raw data from the flash discs and the PSEUDO-SEGY data were archived on DLT tapes (Fig. 63).

After the navigation data had been merged and SEGY formatted traces with the appropriate header words had been created, the data were also archived. Finally, a third set was stored and archived after the shipboard processing had been applied as described above. All final processed SEGY data were archived on tapes.

The preprocessed seismic sections (hydrophone or vertical component) are shown in Appendix 4.

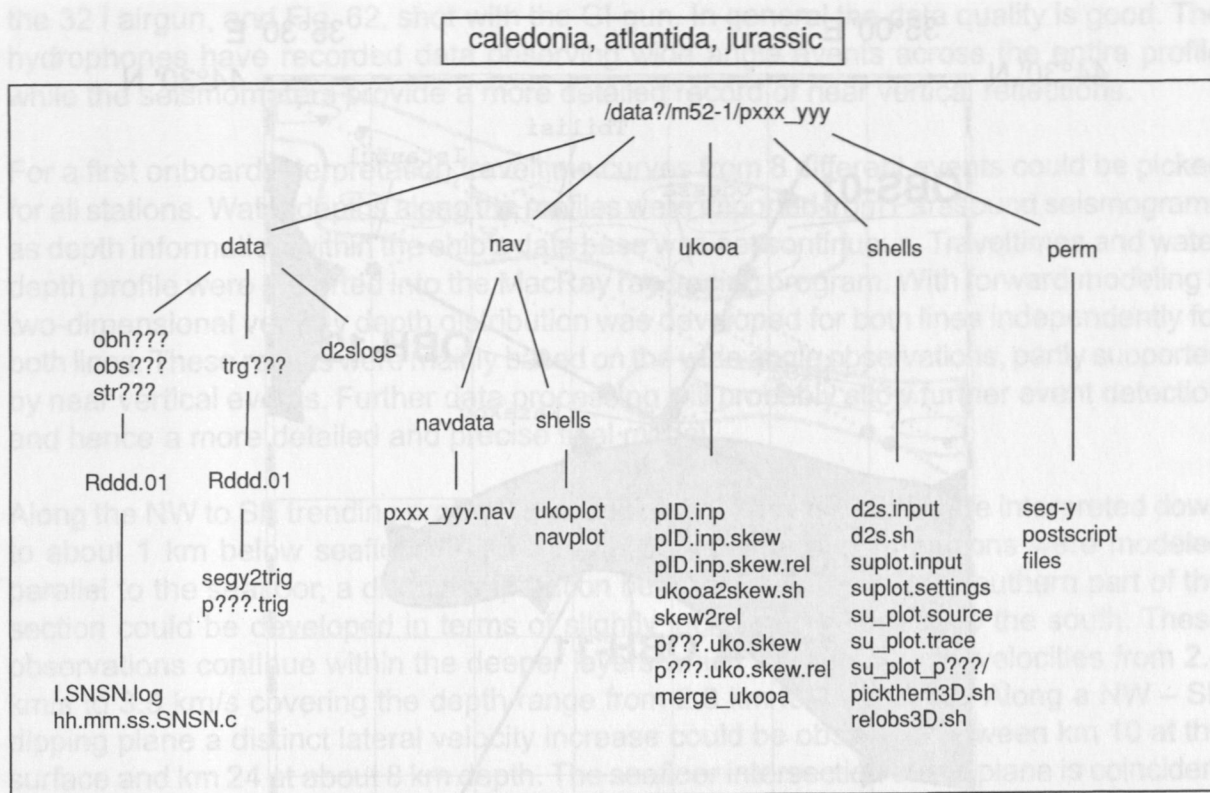


Fig. 63: Directory and path distribution for seismic data processing.

## 8.4 Preliminary Results

### 8.4.1 Profiles 01 and 02

Profiles 01 and 02 are crossing profiles and running over Kazakov and Odessa mud volcano (Fig. 64). The main purpose of these profiles is to get an overview of the deeper structure of the mud volcanoes and the velocity distribution. Therefore the profiles were shot using two 32 I Bolt airguns every 60 s for the deeper structures and one GI gun intermediately every 20 s using the higher frequency of the signal to resolve the upper layers. This was to be supported by additional recordings of the multichannel streamer. Unfortunately, it turned out that the two 32 I guns drifted too close together to safely deploy and operate the streamer. As there were no possibilities to redirect the towing gear of the guns further to the outer sides of the vessel, MCS recordings had to be omitted and structural information from MCS is not available for these lines.

OBH 12-15 are located on profile 01 and OBS 01-10 and OBH 11 on profile 02. OBS 08 is located on top of Kazakov mud volcano and the intersection point of the two profiles. Profile 01 is located within the topographically smooth area of the lower Sorokin Trough and should therefore provide background information about the regional sediments and upper crust. Profile 02 crosses the 200 m high Kazakov mud volcano and continues to the NW across the SE-NW trending chain of mud volcanoes. A detailed location map is shown in Fig. 64. All 15 instruments were deployed with variable spacing from 1 NM up to 2 NM. The total length of profile 01 is 35 km and of profile 02 about 60 km.



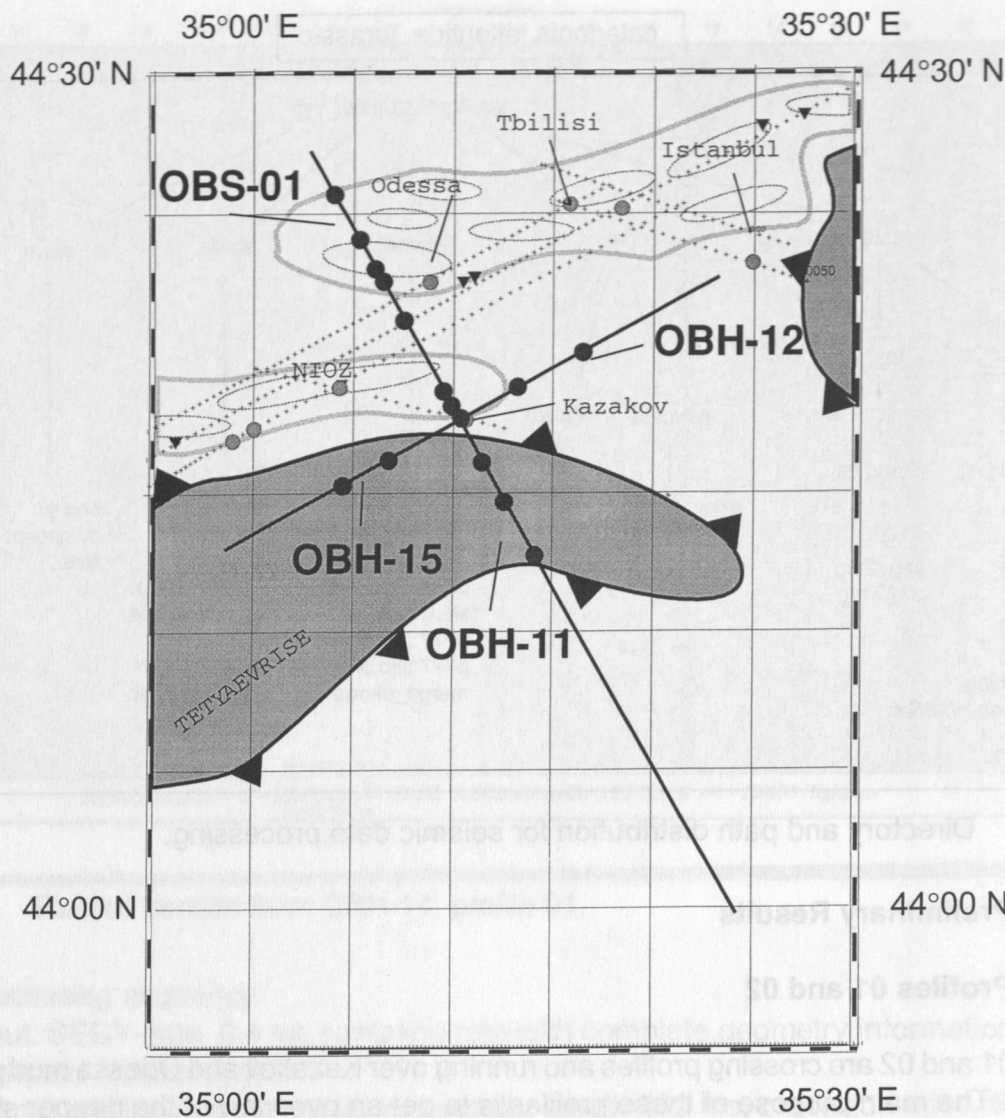


Fig. 64: Location of the OBH/S deployment lines #1 and #2 (modified according to Woodside et al., 1997).

Immediately after shooting, OBS 01 to OBS 11 were recovered safely. The recovery had to be interrupted because of bad weather. Later, some gravity coring and CTD stations were done before OBH 12 to OBH 15 were recovered. The recorder and data of OBH 13 were damaged due to water that had leaked into the pressure cylinder. Detailed information about instruments and shots are given in Appendices I and II.

### Modeling and interpretation

All OBS and OBH data were processed using standard processing on board. A detailed description of data processing is given in chapter 8.3. Unfortunately, the hydrophone component of OBS 04 and 07 did not record any data, but the vertical component of those seismometer stations can be used for modeling instead.

Examples of the record sections along the profile are shown in Fig. 55 and 56, shot with



the 32 l airgun, and Fig. 62, shot with the GI-gun. In general the data quality is good. The hydrophones have recorded data observing wide angle events across the entire profile while the seismometers provide a more detailed record of near vertical reflections.

For a first onboard interpretation traveltimes curves from 8 different events could be picked for all stations. Water depths along the profiles were imported from Parasound seismograms as depth information within the ship's data base was not continuous. Traveltimes and water depth profile were imported into the MacRay ray tracing program. With forward modeling a two-dimensional velocity depth distribution was developed for both lines independently for both lines. These results were mainly based on the wide angle observations, partly supported by near vertical events. Further data processing will probably allow further event detection and hence a more detailed and precise final model.

Along the NW to SE trending profile 02, velocities from 1.5 to 2 km/s were interpreted down to about 1 km below seafloor (Fig. 65). Although the refraction horizons were modeled parallel to the seafloor, a distinct separation between a northern and southern part of the section could be developed in terms of slightly increasing velocities to the south. These observations continue within the deeper layers which were formed by velocities from 2.4 km/s to 3.5 km/s covering the depth range from 2.8 km to 7 km depth. Along a NW – SE dipping plane a distinct lateral velocity increase could be observed between km 10 at the surface and km 24 at about 8 km depth. The seafloor intersection of this plane is coincident with the Southern rim of the Odessa – Tbilisi mud volcano region mapped by Woodside et al. (1997; Fig. 64) Further down, the velocity distribution is homogeneous throughout the profile. Values increase from 4.1 km/s at 7.5 km depth to 5.8 km/s at 18 km depth. These deeper horizons show a slight uplift underneath Kazakov mud volcano while the uppermost layers do not show any correlation of velocity or structural changes related to an expected conduit underneath the volcano. A relation between the uplift of the deeper horizons and the proposed position of Tetyaev Rise could be assumed but needs further investigation.

The SW – NE trending cross profile 01 was located in the lower part of the Sorokin Trough was to serve as as background information. A first ray-tracing model (Fig. 66) identifies 6 refracting horizons which coincide with those from profile 02 with less than 100 m depth variation. The velocity distribution at the intersection of both lines is comparable for the uppermost 5 km depth. Below this depth there is a larger discrepancy between the two lines. Nevertheless an uplift of the interfaces underneath Kazakov mud volcano has been modeled on both profiles. In contrary to line 02 this uplift can be observed in the uppermost layers as well. To the SW and NE the velocity distribution is relatively homogeneous while the lowermost horizons show undulations of several 100 m depth change.

#### 8.4.2 3-D High Resolution Experiment

The major aim of the seismic experiments was a high resolution investigation across a mud volcano in order to resolve not only the trace of the conduit but also the physical parameters of the surrounding sediment. Therefore several structures were investigated with MCS profiles before this target was chosen. Several aspects needed to be matched by the structure of investigation. Due to limited time and the amount of 14 OBH/S instruments the main area of the mud volcano was not supposed to exceed 1 km in diameter. In addition clear events were to be detected during the overview measurements to the sides of the structure.

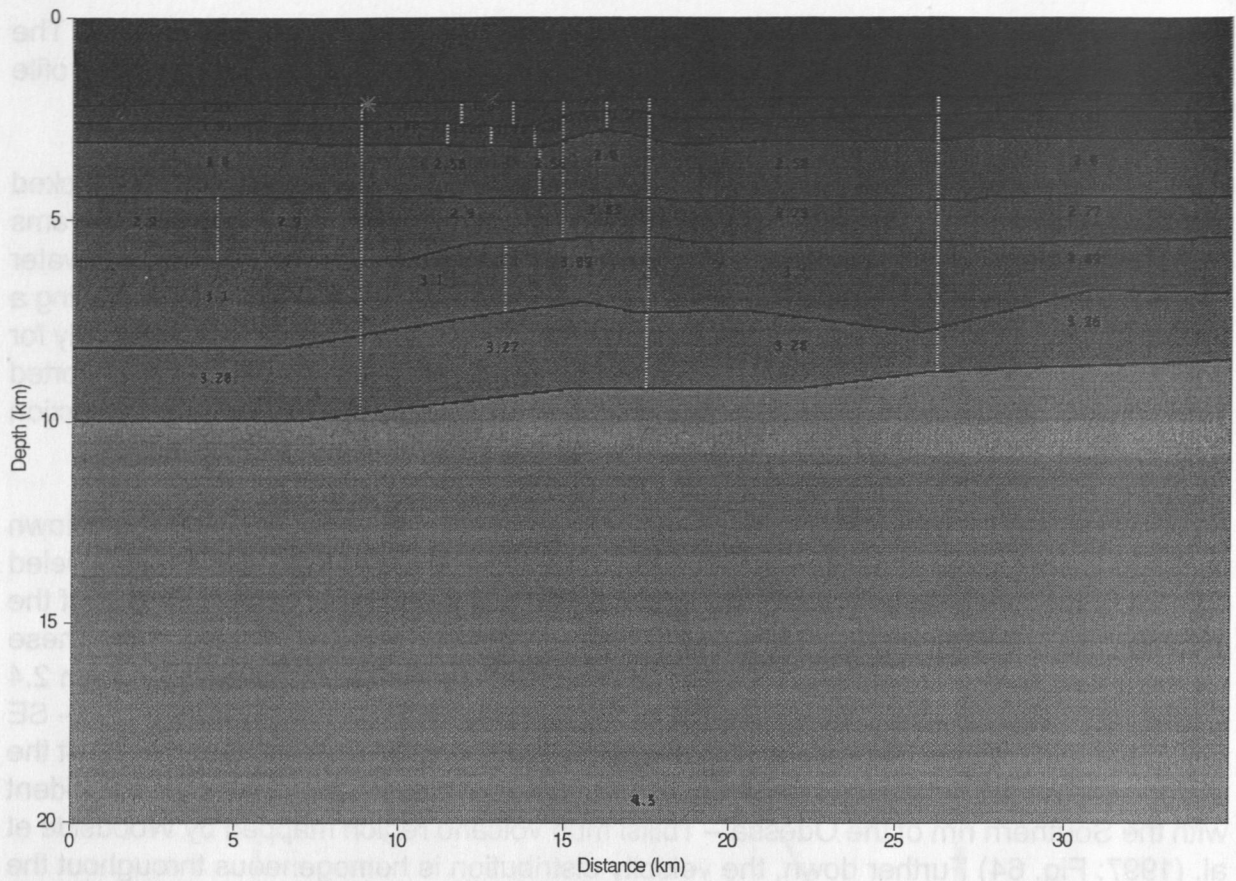


Fig. 65: Forward model of profile 01. Preliminary version without further comparison to MCS data.

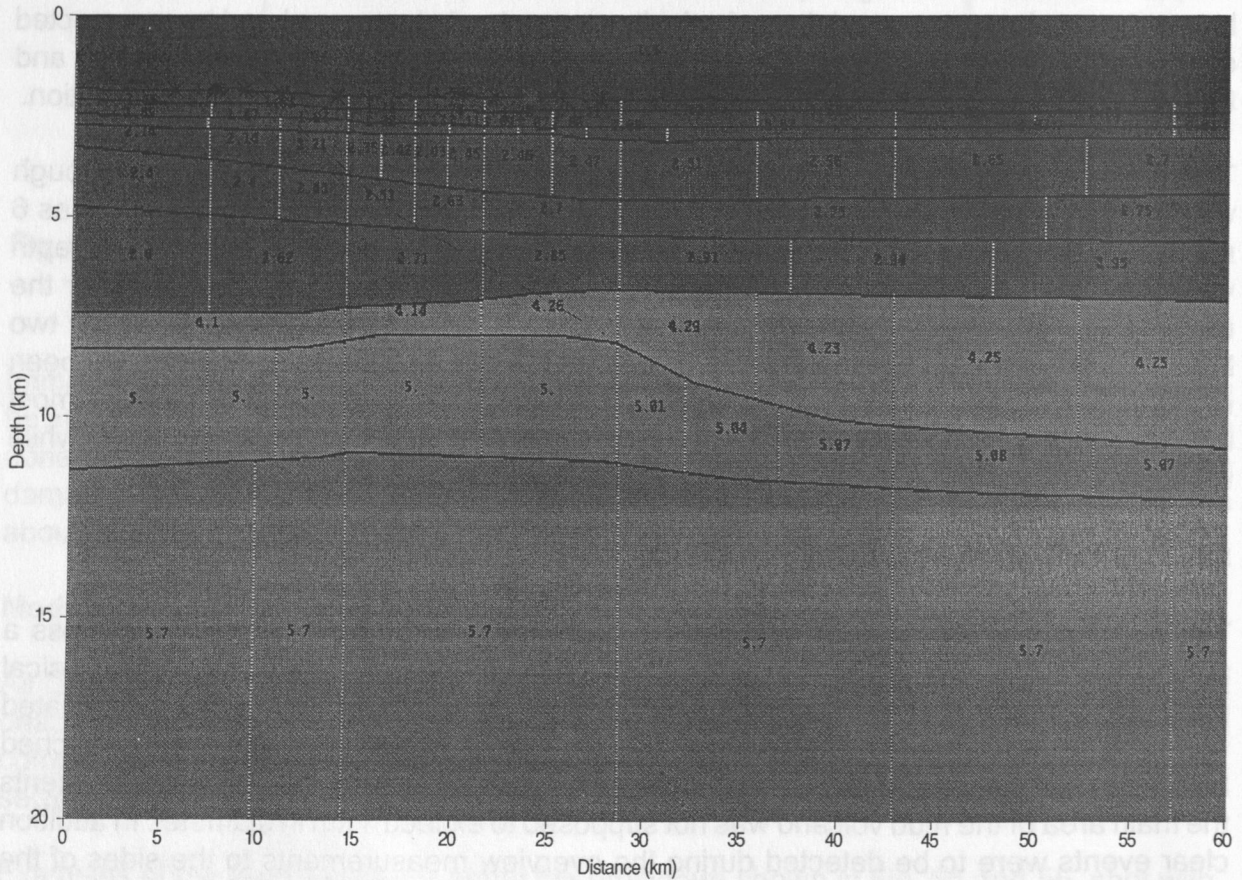


Fig. 66: Forward model of profile 02. Preliminary version without further comparison to MCS data.



After careful consideration and discussion with the geological groups onboard, a structure north of Sevastopol mud volcano was chosen for this experiment. Experience with the first two wide angle seismic lines showed that due to a low background noise level the compression algorithm within the MBS recording devices achieved good results which expanded the recording capacity from nominal 2.5 days to about 4 days. As the remaining time of the expedition did not allow a second deployment, a network of 163 profiles with varying offsets was scheduled. Within the center of this box 10 OBS and 4 OBH could be deployed at a nominal offset of 400 m between each instrument (Fig. 67). At first, elongated lines were shot across the OBH/S positions to enable three-dimensional relocation of the instrument positions. Then this central part of the 3-D area was covered by profiles which were positioned 25 m apart. To the outer borders of the area this offset was extended to 50 m and 100 m in order to achieve a complete coverage within the time of four days. Shots were fired every 10 sec from two GI-guns and one water gun. GI-gun shots were already recorded on the OBH/S instruments during the first wide-angle profile. As can be seen from the examples of chapter 8.3, the energy of the gun allowed detection of events of up to about 6 km offset. In order to enlarge the distance, the two GI-guns were fired simultaneously every minute, which was to produce more powerful shots that should be recorded by the OBH/S from larger distances.

After recovery, a first check indicated that the stations should indeed have recorded data over a time span of almost four days. An amount of as much as 45 Gigabyte of data had to be preprocessed on the playback PC before ftp transmission to the SUN computer network where data archiving on backup tapes could be performed. This procedure took three days of operation which in turn did not enable to process and display any of the data.

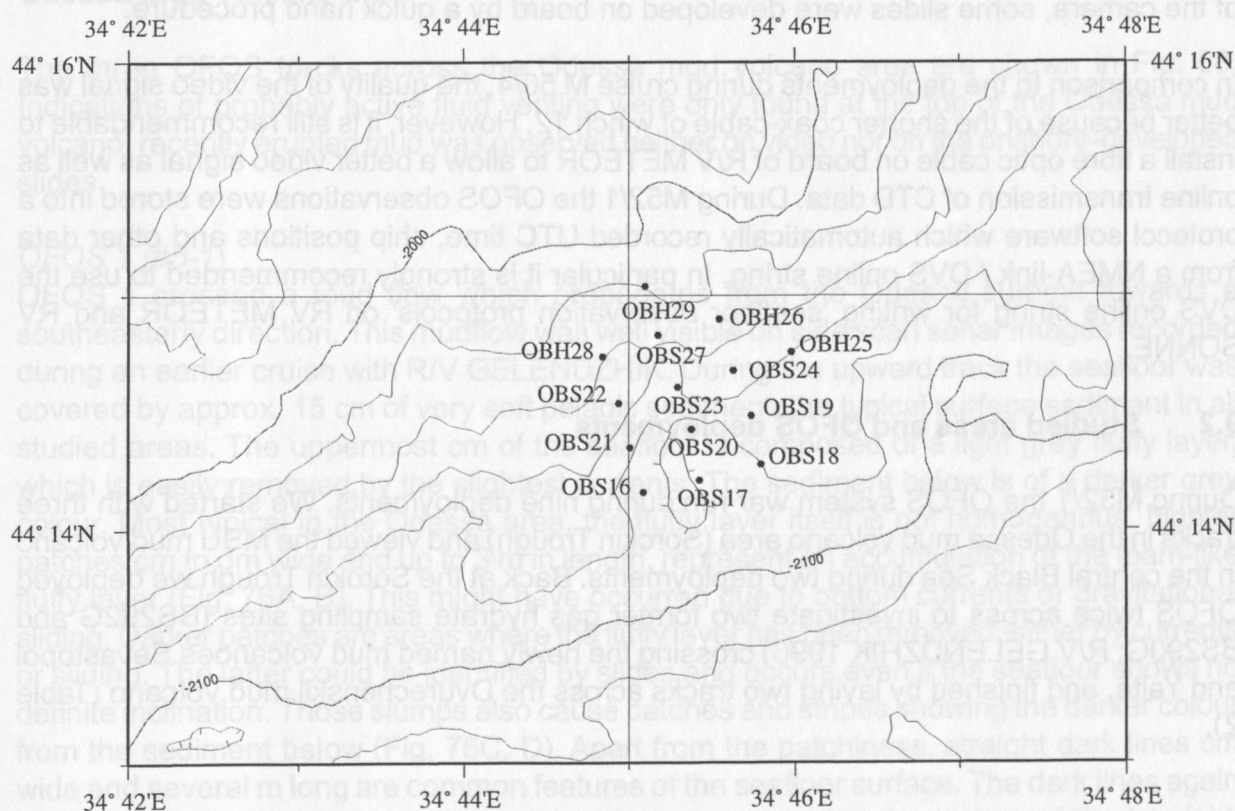


Fig. 67: Location map of the 3-D deployment. For profile coverage refer to chapter 6 reflection seismics.



## **9. VISUAL SEAFLOOR OBSERVATION**

J. Greinert, B. Bannert, G. Aloisi, F. Abegg, V. Blinova

The main task of the visual seafloor observation was locating active vent sites at mud volcanoes in the Sorokin Trough and the Central Black Sea area. The observation allows precise sediment sampling by coring and pre-investigation of the target area for later TV-MUC or TV-grab deployments. The investigation is also useful for the interpretation of sediment echo sounder investigations or sidescan sonar mapping, it can help to define the cause of strong or weak surface reflections and can be used for ground-truthing.

### **9.1 Equipment and observation procedure**

We used the Ocean Floor Observation System (OFOS), which is a TV-guided sled of 165 x 125 x 145 cm equipped with a BW video camera, two Xenon lamps (OKTOPUS), an underwater slide camera with flash (BENTHOS), three laser pointers (OKTOPUS) and a FSI memory CTD. The CTD was additionally equipped with a SeaPoint turbidity meter (optical back scatter : OBS); data were recorded every 2 seconds.

For the seafloor observation procedure, OFOS is towed by the ship with less than 1 kn along a pre-defined track with less than 1 kn; the distance to the bottom is manipulated by the winch. During M 52/1 the weight below the OFOS was 1.5 m away from the camera. Via the deck unit slides can be taken manually; the camera aperture was set to 5.6 and the focus range was set between 0.8 and 1.2 m. The video signal was permanently recorded on tapes. In order to check the quality of the slides, the flash illumination and the focusing of the camera, some slides were developed on board by a quick hand procedure.

In comparison to the deployments during cruise M 50/4, the quality of the video signal was better because of the shorter coax-cable of winch 12. However, it is still recommendable to install a fibre optic cable on board of R/V METEOR to allow a better video signal as well as online transmission of CTD data. During M52/1 the OFOS observations were stored into a protocol software which automatically recorded UTC time, ship positions and other data from a NMEA-link / DVS online string. In particular it is strongly recommended to use the DVS online string for writing 'seafloor observation protocols' on RV METEOR and RV SONNE.

### **9.2 Studied areas and OFOS deployments**

During M52/1 the OFOS system was run during nine deployments. We started with three tracks in the Odessa mud volcano area (Sorokin Trough) and viewed the MSU mud volcano in the central Black Sea during two deployments. Back at the Sorokin Trough we deployed OFOS twice across to investigate two former gas hydrate sampling sites (BS292G and BS290G; R/V GELENDZHIK 1996) crossing the newly named mud volcanoes Sevastopol and Yalta, and finished by laying two tracks across the Dvurechenskii mud volcano (Table 2).

Table 2: OFOS deployments of M52/1; date/ time and latitude/ longitude are ship positions when OFOS reached the bottom or was lifted off.

Station	Date / Time	Latitude / Longitude	Water depth	Target & Remarks
OFOS 1 / #5-1	04.01.02 / 18:41	44°22.461 / 35°08.614		Mudflow south east of Odessa mud volcano summit
	04.01.02 / 20:45	44°23.270 / 35°09.499		
OFOS 2 / #5-2	04.01.02 / 22:48	44°22.799 / 35°08.216		Odessa mud volcano
	05.01.02 / 00:27	44°23.276 / 35°08.903		
OFOS 3 / #5-3	05.01.02 / 02:14	44°23.010 / 35°06.220		Two mud volcanoes 1.25 Nm west of Odessa mud volcano
	05.01.02 / 04:21	44°23.642 / 35°07.494		
OFOS 4 / #26-1	13.01.02 / 19:57	43°32.337 / 33°07.444		MSU mud volcano; loop at the beginning in the north
	13.01.02 / 23:50	43°31.520 / 33°06.300		
OFOS 5 / #26-2	14.01.02 / 00:42	43°31.615 / 33°06.238		MSU mud volcano; tow tracks in E-W direction across the south edge of the summit; OFOS the whole time at the bottom
	14.01.02 / 04:04	43°31.636 / 33°06.488		
OFOS 6 / #41-1	18.01.02 / 09:16	44°14.099 / 34°44.098	2097 m	Crossing a previous gas hydrate sampling site (BS-292G) and gas sampling site (BS-291G); observation of the later 3D seismic area
	18.01.02 / 12:58	44°14.722 / 34°48.085	2074 m	
OFOS 7 / #41-2	18.01.02 / 14:46	44°14.897 / 34°45.201	2050 m	Collapsed mud volcano; perpendicular to 41-1, investigating a geophysically interesting area
	18.01.02 / 17:10	44°13.937 / 34°45.401	2114 m	
OFOS 8 / #62-1	27.01.2002 / 23:47	44°16.348 / 34°57.962	2147 m	Dvurechenskii mud volcano; also used for correlation with high resolution side scan sonar mapping; ACTIVE SEEPS!
	28.01.2002 / 02:10	44°17.405 / 34°59.396	2094 m	
OFOS 9 / #62-2	28.01.2002 / 03:55	44°17.240 / 34°57.988	2100 m	Dvurechenskii mud volcano; ACTIVE SEEPS!
	28.01.2002 / 06:07	44°16.701 / 34°59.846	2116 m	

## Odessa mud volcano area

The three OFOS tracks across the Odessa mud volcano area are shown in Fig. 68. Indications of probably active fluid venting were only found at the top of the Odessa mud volcano; recently erupted mud was observed neither on video nor on the onshore-developed slides.

### OFOS 1 (#5-1)

OFOS 1 crossed a mud flow which propagates from the Odessa summit towards a southeasterly direction. This mudflow was well visible on side scan sonar images recorded during an earlier cruise with R/V GELENDZHIK. During the upward track the seafloor was covered by approx. 15 cm of very soft pelagic sediment, the typical surface sediment in all studied areas. The uppermost cm of the seafloor is composed of a light grey fluffy layer, which is easily removed by the slightest currents. The sediment below is of a darker grey colour. Most typical in the Odessa area, the fluffy layer itself is not homogenous. Lighter patches cm to dm wide and up to 3 m in length, represent an accumulation of the foam-like fluffy layer (Fig. 76A, B). This might have occurred due to bottom currents or gravitational sliding. Darker patches are areas where the fluffy layer has been removed, either by currents or sliding. The latter could be identified by slides and occurs even if the seafloor shows no definite inclination. Those slumps also cause patches and stripes showing the darker colour from the sediment below (Fig. 76C, D). Apart from the patchiness, straight dark lines cm wide and several m long are common features of the seafloor surface. The dark lines again represent areas where the fluffy layer has been removed but the reason of the 'straight' removal could not be found out for sure. A possible reason for these sometimes even crisscrossing lines (Fig. 76E) might be a removal of the fluffy layer due to particles that

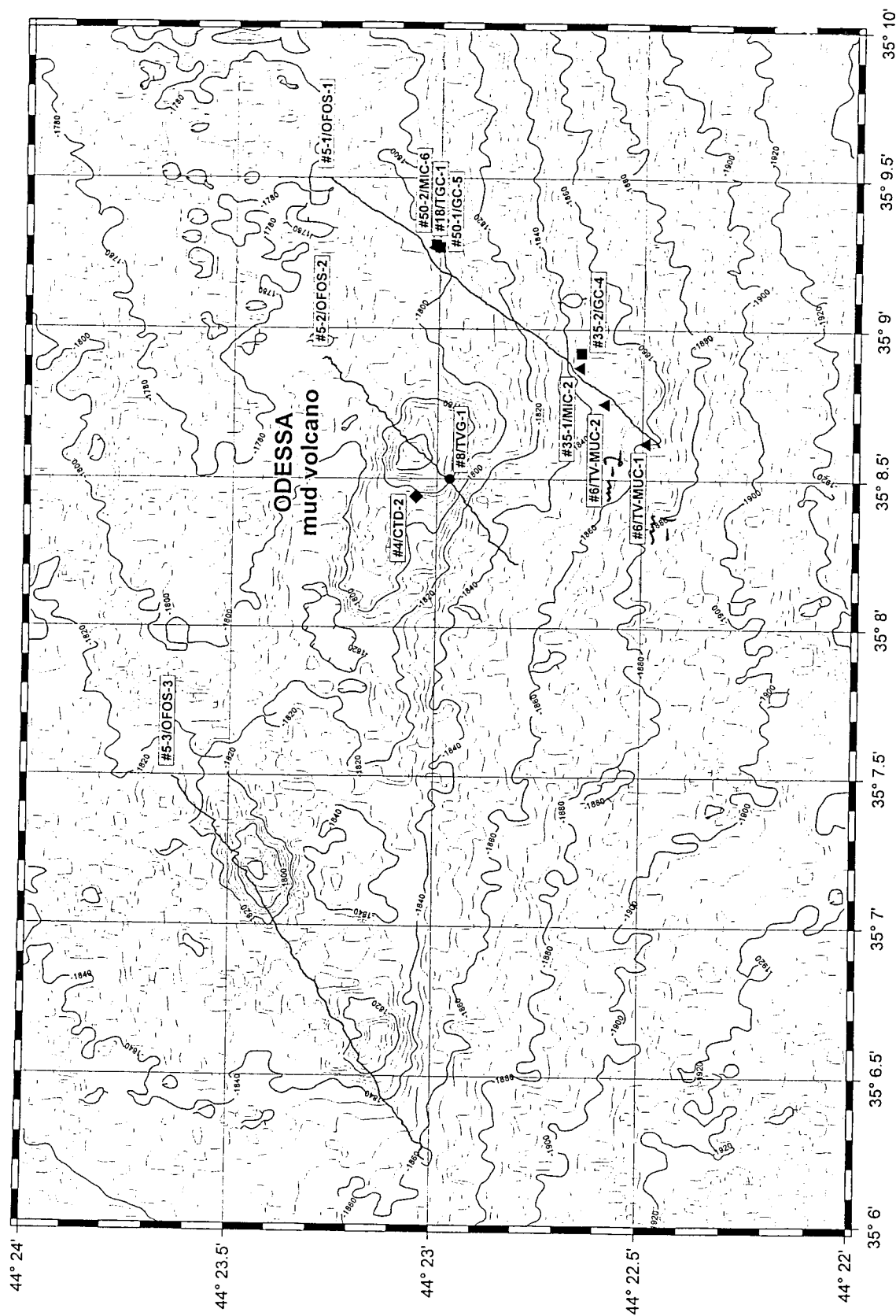


Fig. 68: Bathymetric map showing the three OFOS tracks and stations in the Odessa working area.



rolled over the seafloor. Some times the lines are very similar to bioturbation trails, although this is rather unlikely because of the anoxic environment of the Black Sea. Another typical feature for all OFOS tracks were bright white, elongated spots of 5 to 10 cm in length and 1-2 cm in width. These white spots could be identified as dead fish, most likely anchovy, arriving on the seafloor as detritus from the uppermost water column (Fig. 76G). Dead jelly fish (Fig 76H) and seldom larger fish (Fig. 76I) were observed as well during other OFOS tracks.

Wide parts of OFOS 1 only showed a soft sediment coverage without any signs of the suggested mud flow or signs of fluid venting. Structures similar to horizontal bedding plains, cm to dm in thickness (Fig. 77A) as well as few talus blocks of boulder size could be observed between 1,800 and 1,805 m water depth in an area characterized by a slightly rougher / wavier morphology (Fig. 69). Similar bedding structures were also observed close to the end of the track at 1,780 m water depth. In both areas the plains were covered by sediment and we assumed that these plains might be carbonate crusts. After careful

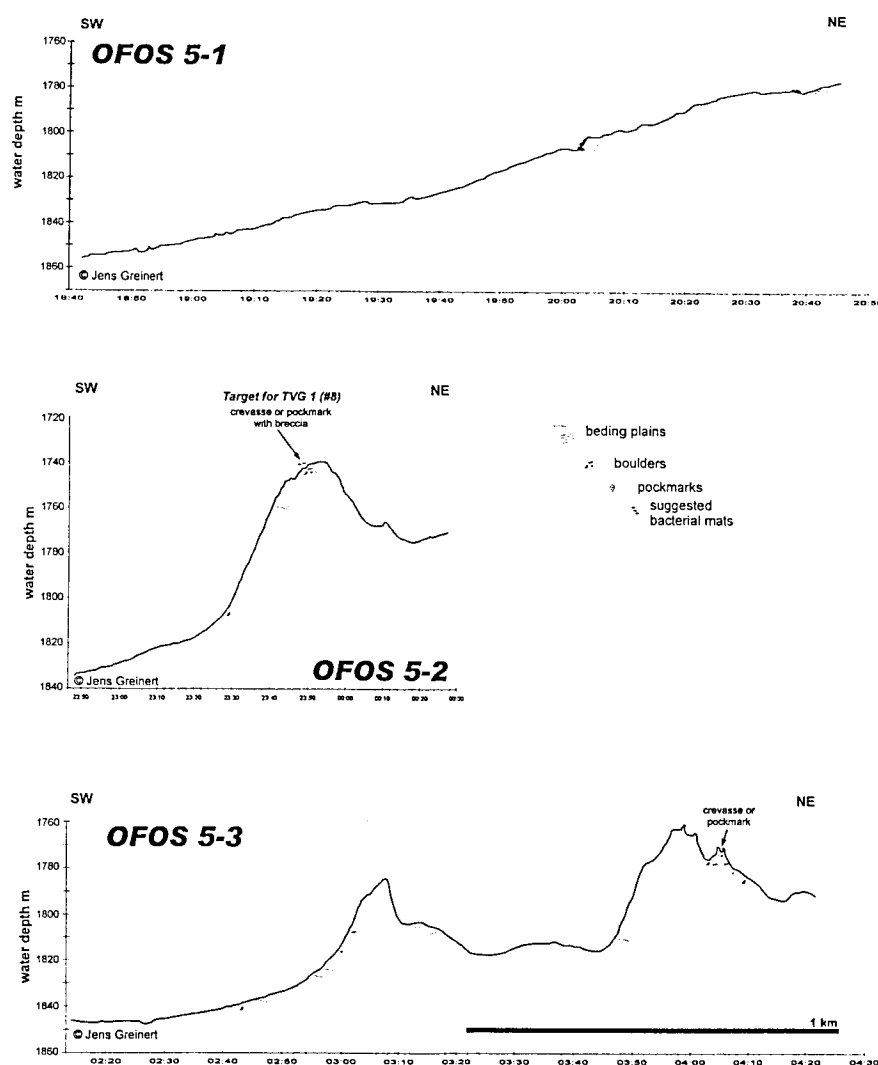


Fig. 69: Depth profiles of OFOS 1 to 3, observing a mud flow from Odessa mud volcano and two unnamed mud volcanoes west of Odessa. All track profiles are of the same horizontal and vertical scale.

investigation of the slides we suggest that these bedding plains constitute semi-consolidated sediment layers which crop out at small scarps showing a cross section of different mud-flows interlaced with breccia flows with coarser components of up to block size. In Figure 69 the depth profile of the track is shown, constructed from the recorded pressure of the OFOS CTD. Salinity, temperature and optical backscatter gave no further information with respect to fluid venting the OFOS tracks 1, 2 and 3. Their depth-related changes are coincident with the water column properties measured by the SeaBird 911 Plus CTD water sampling stations.

#### OFOS 2 (#5-2)

OFOS track 2 crossed the Odessa mud volcano and along most of the track showed a similar sediment coverage as OFOS track 1. The first bedding plains were observed at a water depth of 1760 m at the southern flank of Odessa. At the southern edge of the summit some smaller scarps cut through breccia, which build up the mud volcano; the observation showed blocks of different sizes as well as bedding plains (Fig. 69). Slightly south of the summit two steep steps of 1 to 2 m in height again showed the unsorted coarse breccia but also a white, mat-like coverage at blocks or other elevated edges and in the form of vein-like structures of dm in size on the sediment. Thorough investigation of the slides strengthens the assumption that these white mats are bacterial mats (Fig. 77B); during M52/1 TVG 1 (#8) was deployed to sample this area.

#### OFOS 3 (#5-3)

OFOS 3 crossed two unnamed mud volcanoes west of Odessa (Fig. 68). Starting at the south the sediment showed the typical soft composition and a coverage by a fluffy layer. At the lower part of the southern mud volcano flank some sediment-covered blocks were seen at 1830 m water depth. Bedding plains and blocks were crossed at the steepest part of the flank distributed over an area of some tens of meters. Following the downslope of the 20 m high summit, the bottom showed only a soft sediment coverage. Some bedding plains were observed at this northern flank and at the foot of the northern mud volcano (Fig. 69). The northern flank of this mound gave the best insight into the material that builds the mud volcanoes. Over a length of approx. 200 m a rough morphology of small hills, ridges and steeper steps (m high) showed irregularly occurring blocks, outcropping bedding plains and gravel patches of the breccia-composed mud volcano. Here, a crater-like depression (1 m in diameter and 50 to 70 cm deep) was observed, which might have been formed by an up-floating massive gas hydrate block as known from Hydrate Ridge (Oregon, USA; Suess et al., 2001) or might represent the centre of an eruptive mud outflow (similar to Fig. 77B).

### MSU mud volcano

Fig. 70a shows the tracks of both OFOS deployments at the MSU mud volcano. The MSU shows a rather flat top with a crater-like structure. No clear signs of active fluid expulsion were observed in any of the tracks.

#### OFOS 4 (#26-1)

The first part of OFOS 4 was planned to cross a high backscatter area of a suspected large field of massive blocks recognized during previous side scan sonar investigations (Fig. 70b). Unfortunately we already crossed this area while the OFOS went down to the seafloor. We made a second attempt to cross this area by sailing northward, but again we missed

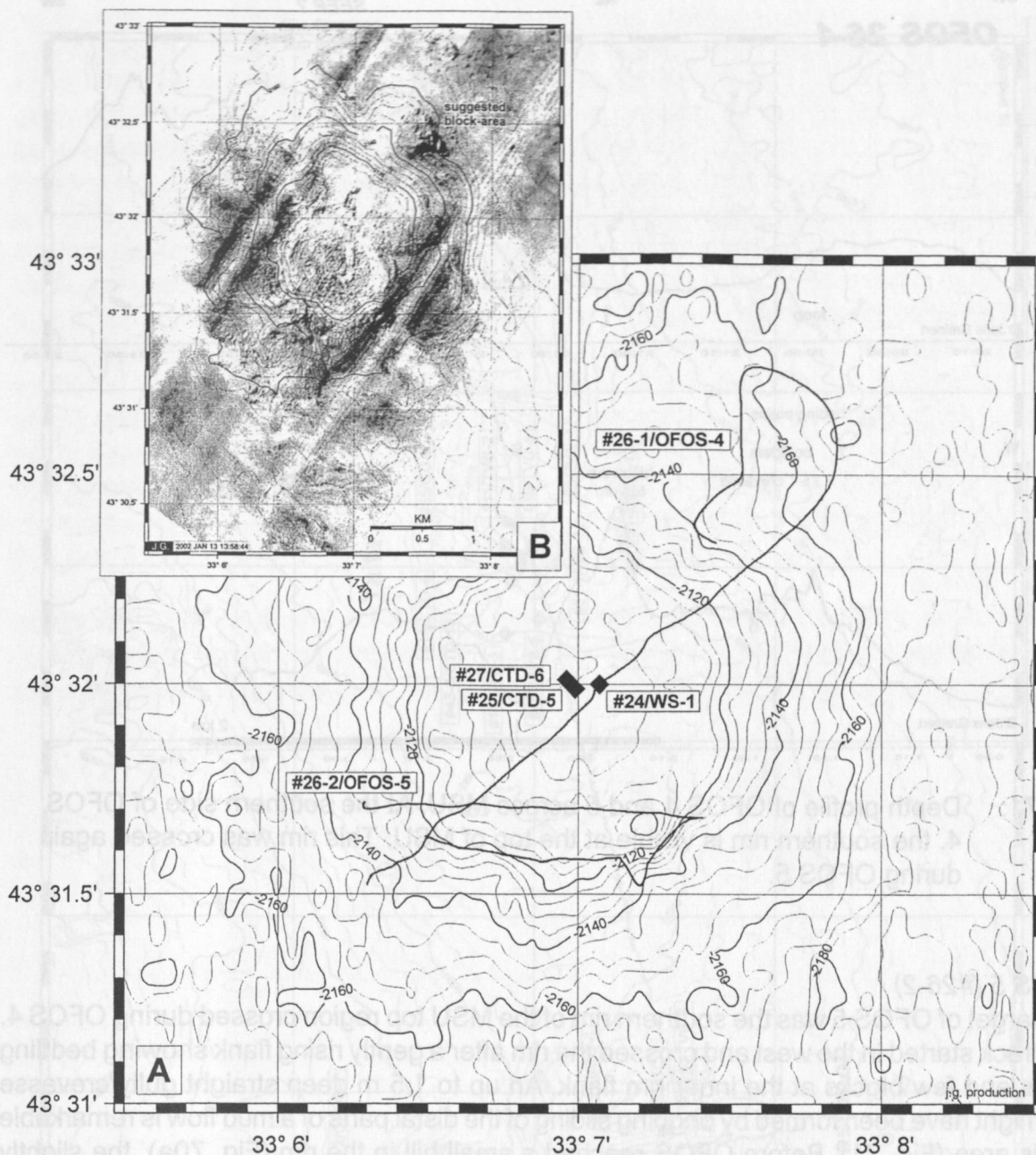


Fig. 70a: Bathymetric map of the MSU mud mound in the central working area with both OFOS tracks of station 26. A rim can be observed at the top region in SW direction with a separate mound at the eastern end.

Fig. 70b: Side scan image of the MSU from a previous TTR cruise.

the area, which lies in the loop of our track (Fig. 70a). Starting the planned track in SW direction, we found soft sediment with lighter and darker patches and lines (Fig. 76 B-D) that covered the seafloor in the loop and the way up to the summit of MSU. At the top we crossed a 10 m high rim that surrounds the top area. At the inner flank bedding plains that build small steps (Fig. 77 C, D) and a few boulders were observed (Fig. 71). Crossing the slightly elevated central area, we only once observed bedding plains and a few boulders in a generally more wavy area that is well visible by side scan sonar. More bedding plains were observed at the SW rim of the top building steps of several dm in height. Their density increased but was still below 15 % of the observed southern rim area.



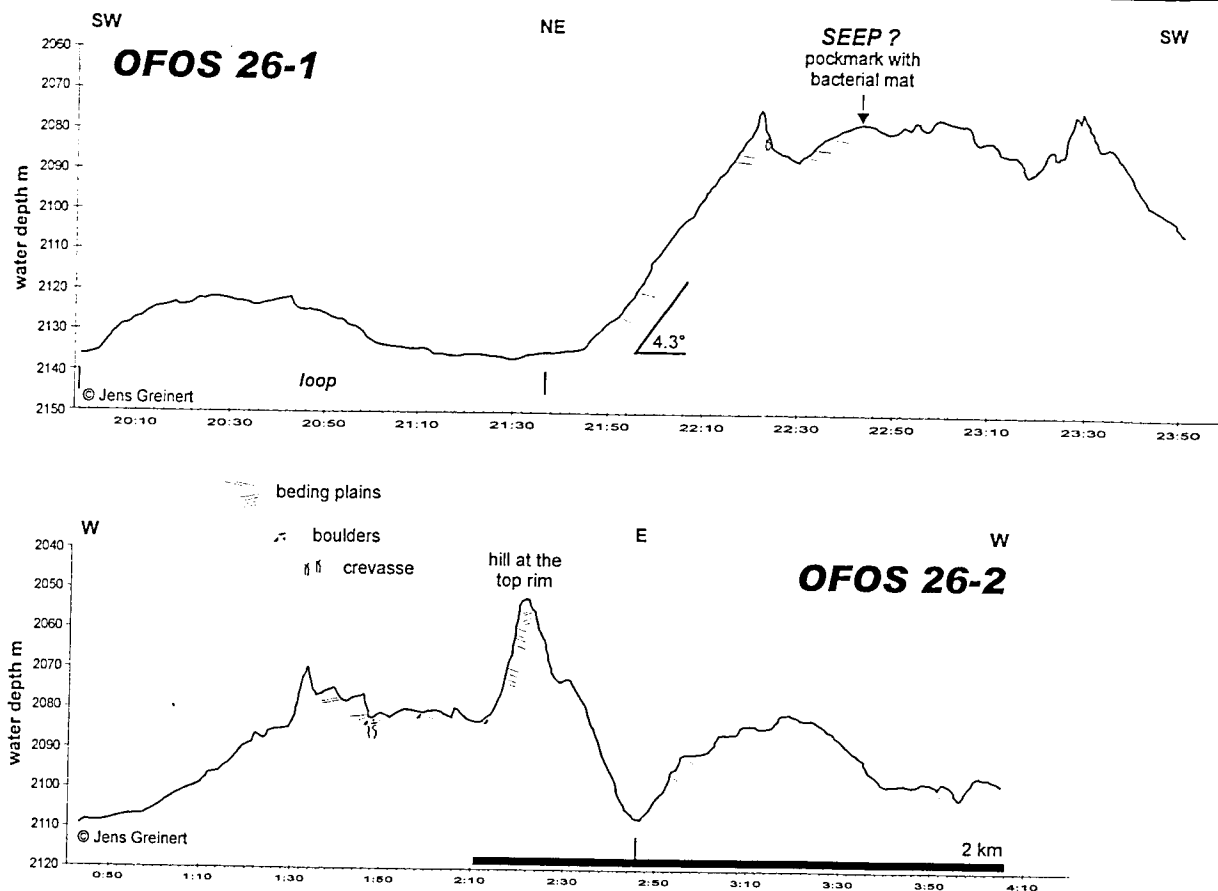


Fig. 71: Depth profile of OFOS 4 and 5 across MSU. At the southern side of OFOS 4, the southern rim is visible at the top of MSU. This rim was crossed again during OFOS 5.

#### OFOS 5 (#26-2)

The target of OFOS 5 was the southern rim of the MSU top region crossed during OFOS 4. The track started in the west and crossed the rim after a gently rising flank showing bedding plains and few blocks at the inner rim flank. An up to 1.5 m deep straight gully/crevasse that might have been formed by ongoing sliding of the distal parts of a mud flow is remarkable in this area (Fig. 71). Before OFOS reached a small hill in the rim (Fig. 70a), the slightly rough seafloor had shown a few randomly distributed bedding plains and scattered blocks. This changed during the upward track to the hill summit where outcropping bedding plains were quite common. Following the eastern flank downward we decided to view the rim structure again and retraced our way on a parallel course back, still with OFOS at the seafloor. Unfortunately we did not cross the rim again and bedding plains were observed only once.

#### Sevastopol and Yalta mud volcanoes

Fig. 72 shows the two OFOS tracks crossing the Sevastopol and Yalta mud volcanoes. No signs of active venting were recognized. However, the observation of assumed bacterial mats during OFOS 7 was followed up by sampling TVG station 42 and 60.

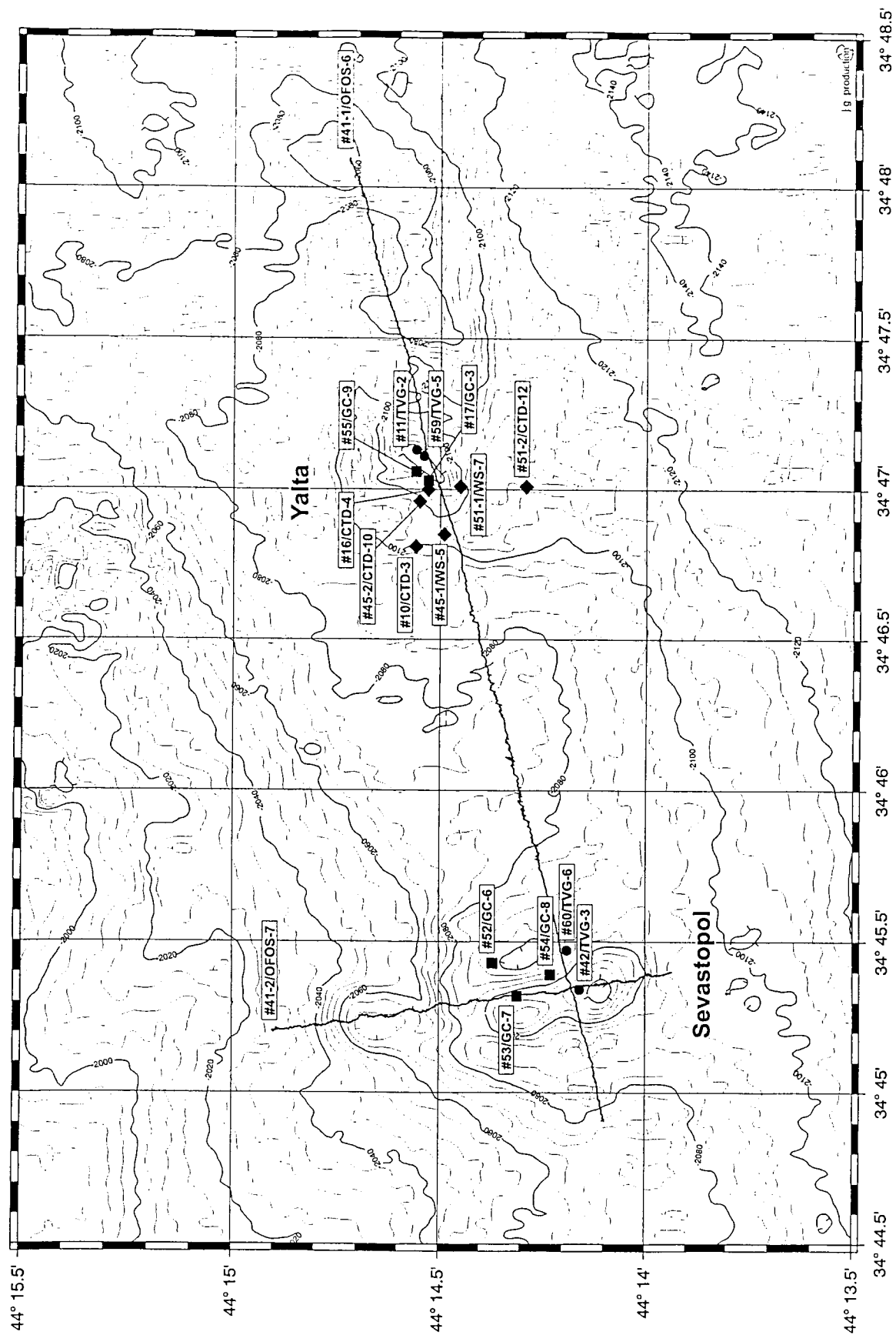


Fig. 72: Bathymetric map of the Sevastopol and Yalta mud volcano area with OFOS track 6 and 7.

**OFOS 6 (#41-1)**

OFOS 6 was planned to cross the gas hydrate sampling site BS-292G of the R/V GELENDZHIK cruise in 1996, which is located at Sevastopol mud volcano. The track was planned to cross the Yalta mud volcano only 1.5 miles east as well. Starting in the west, OFOS 6 went down the western flank of the collapsed central part of the Sevastopol mud volcano and crossed the southern summit of the central uplift. Up to this point, the seafloor was composed of soft sediment covered by the common fluffy layer (Fig. 76C, F-I). Bedding plains and a pockmark-like depression were observed at the eastern side of the summit before OFOS crossed a smooth and only sediment-covered, dome-like area (Fig. 77E) between Sevastopol and Yalta (Fig. 73). Up to the foot of the central uplift of the Yalta mud volcano the seafloor was only covered by soft sediment. This changed at the point where OFOS crossed the central uplift. Here, boulders of several dm to m in size lay randomly distributed on the seafloor and were covered by pelagic sediment. Some bedding plains were observed forming small steps of several dm in height. Their density increased at the foot of the eastern flank of the central uplift, before OFOS went up another hill, which might still be a part of the Yalta mud volcano (Fig. 72).

**OFOS 7 (#41-2)**

Because of the planned 3-D seismic survey in this area, OFOS 7 was run in N-S direction through a canyon north of the central uplift of Sevastopol and across the central uplift (Fig. 73). At the foot of the canyon some blocks were observed. After a second depression that

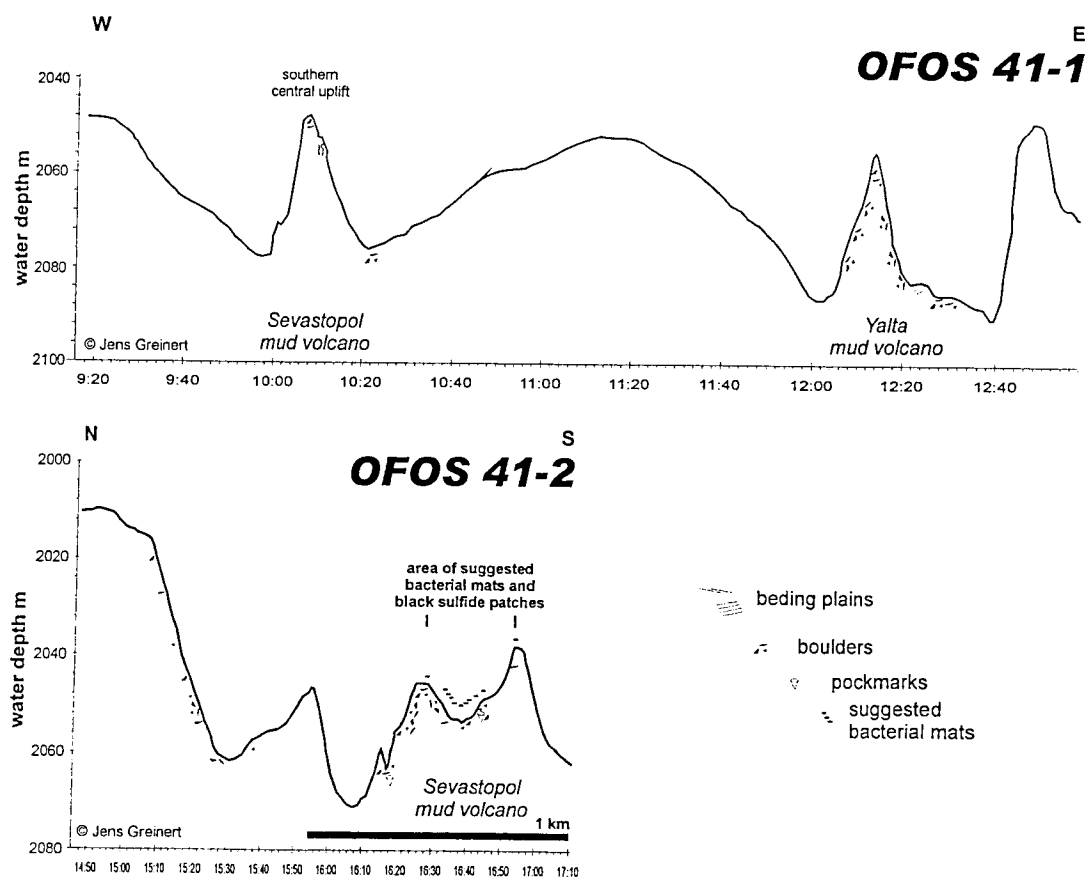


Fig. 73: Depth profile of OFOS 6 and 7 crossing the central uplifts of Sevastopol and Yalta. At the saddle between the two summits of the central uplift of Sevastopol many more boulders were observed as well as some light patches assumed to be bacteria mats.



represents the edge of the collapse structure of Sevastopol, both hills of the central uplift were crossed. A pockmark-like depression or gully of about 10 m width with more boulders was crossed at the foot of the northern uplift (Fig. 77F, G). We also recognized light patches, which were first interpreted as bacterial mats, but this was not confirmed by the slides. More boulders occurred up to the saddle between both summits. Here, lighter patches seen on the video were assumed to be bacteria mats during the cruise and led to sediment sampling in this area. Unfortunately the occurrence of bacteria mats could not be confirmed by the slides, but unique black patches (Fig. 77H) that were also seen on video point to iron-sulphides and possible mark the area of higher venting activity.

### Dvurechenskii mud volcano

Figure 74 shows the flat structure of the Dvurechenskii mud volcano that was crossed twice during Station 62. Compared to the previous tracks, we found definite signs of active fluid venting at the western edge and at the centre of the top during both tracks. Because of a thinner sediment coverage, higher heat flow and elevated bottom water temperatures, Dvurechenskii is the most recently active mud volcano investigated during M52/1.

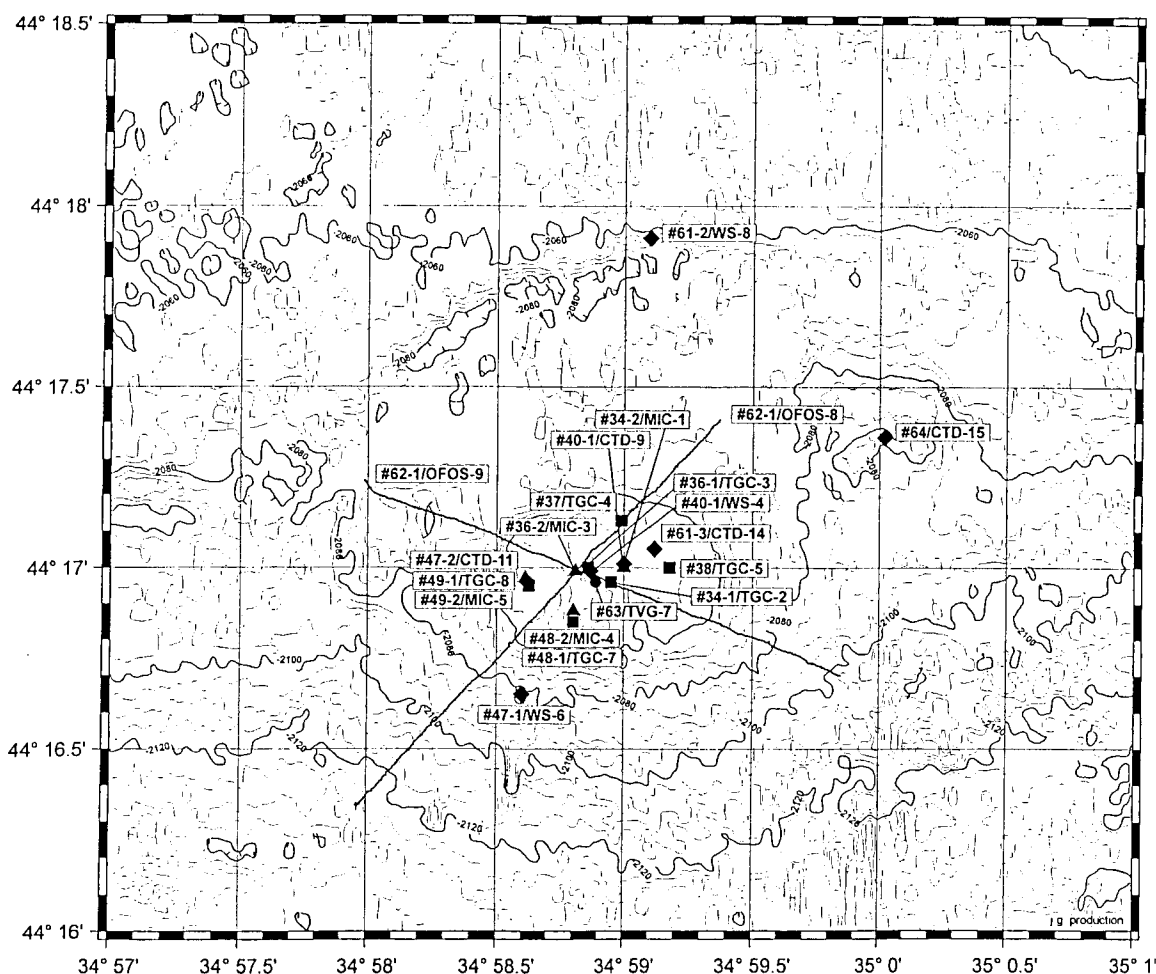


Fig. 74: Bathymetric map of the Dvurechenskii mud volcano with both OFOS tracks of station 62. At the centre of the very flat mud volcano, active seepage was visible through cm - to dm - sized light patches scattered over an area of approx. 20 - 30 m.

**OFOS 8 (#62-1)**

Starting SW of the Dvurechenskii mud volcano, OFOS 8 track went in NE direction following a line that was later examined more closely by side scan sonar during Station 65-1 (DTS-13). Along the gentle upslope we observed some areas where there were a few boulders and steps of bedding plains (Fig. 75). In the middle of the slope a gully/crevasse of some dm in depth possibly marks an area of disruptive cracks formed by the ongoing movement of mud breccia further downslope. More boulders and step-forming bedding plains of several cm to dm in height occurred at the steeper, 14 m high edge of the central Dvurechenskii summit. At the slightly wavy and rougher top, boulders, steps with outcropping bedding plains and crevasses were more common (Fig. 78A-C). This rougher surface is probably

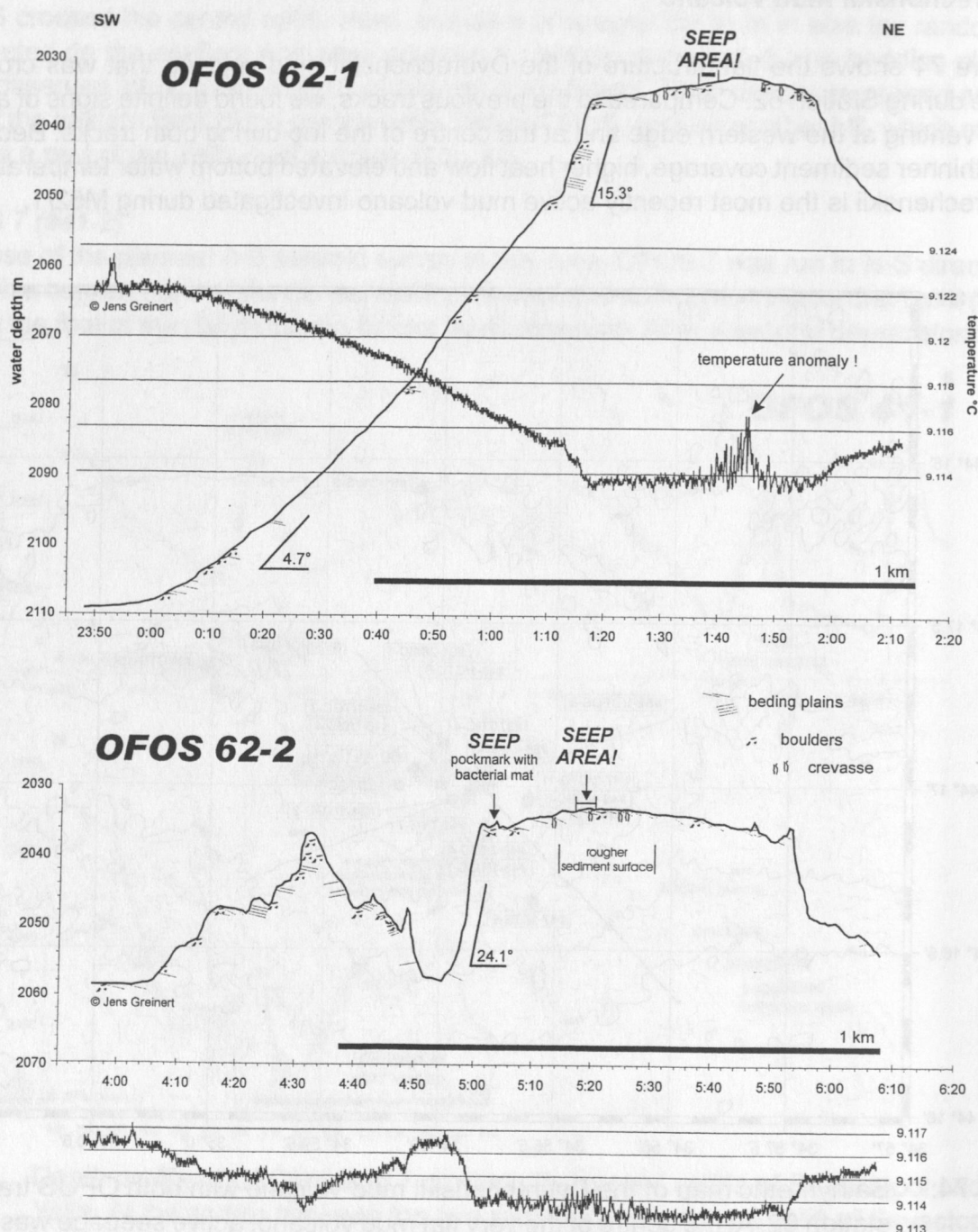


Fig. 75: Depth profile of OFOS 8 and 9 across the Dvurechenskii mud volcano.

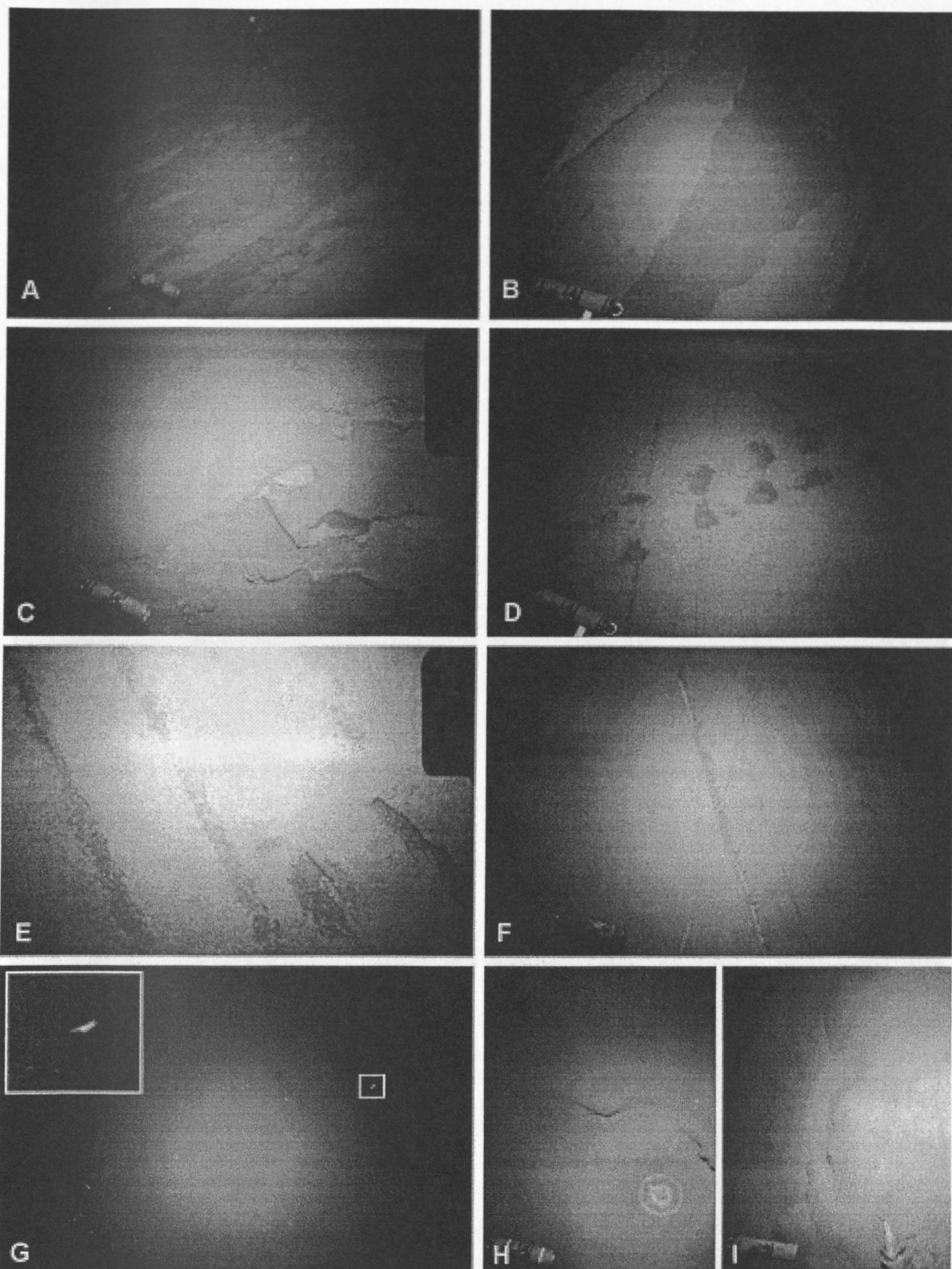


Fig. 76: Seafloor images from the Sorokin Trough and central Black Sea. A shows the typical 'patchy' light to dark grey colours induced by a fluffy layer of varying thickness. B shows a small-scale mud flow. The darker colour of the sediment below the fluffy layer is shown in C. The reason for the linear and regular removal of the fluffy layer in the images C-E could not be ascertained for sure. G to I show dead anchovies (G), jelly fish (H) and another fish species (I) lying on the seafloor as detritus from the uppermost layer.



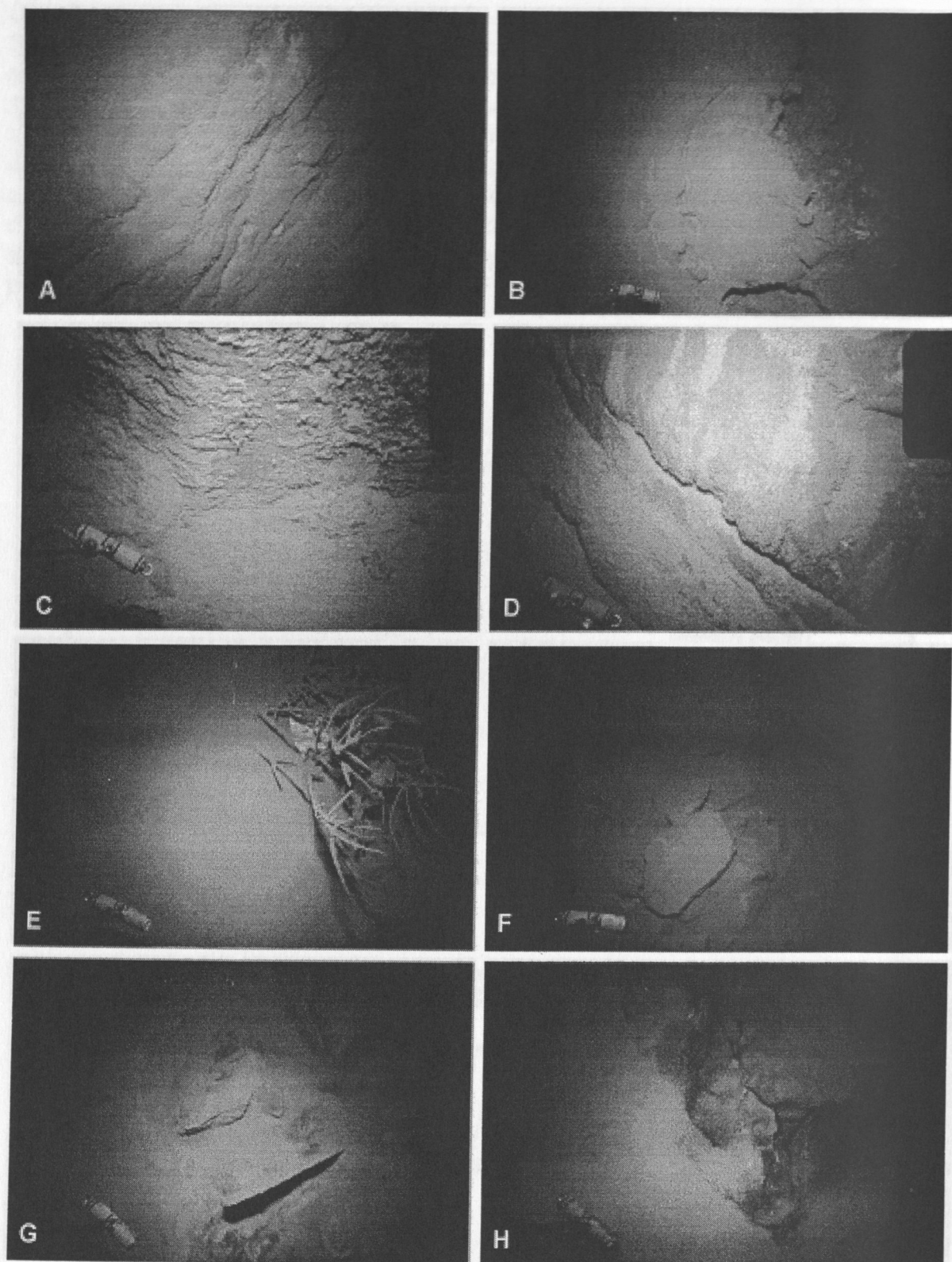


Fig. 77: Image A and B are from OFOS 5-2 and show bedding plains and the target area of TVG 1 (#8) at the top of Odessa. C and D are from OFOS 26 at the MSU showing a scarp and typical bedding plains. E-H are from OFOS 41; E shows the seafloor with a branch of a tree at the dome-like area between Sevastopol and Yaltamud volcano. Boulders and blocks between the two summits at the central uplift of Sevastopol are seen in F and G. Patches of dark material, probably sulphides, are shown in G and H and may point to active fluid venting.

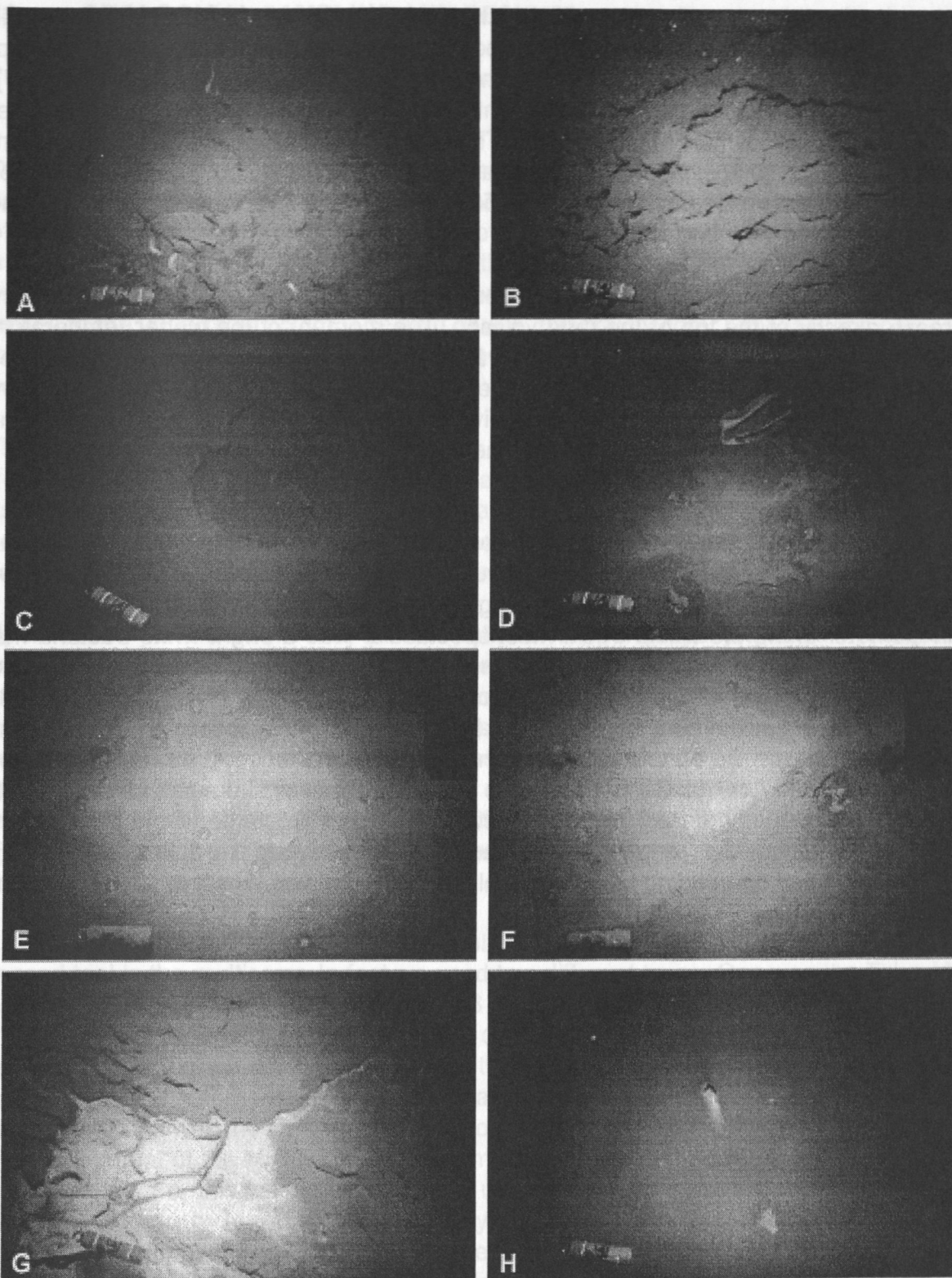


Fig. 78: Images from OFOS 62-1 and -2. Uneven morphology with light spots of possible bacteria mats and outcropping bedding plains at the top area of Dvurechenskii in A and B. C shows pockmark-like craters 1 m in diameter. D-F gives an impression of the main seepage area with several small lighter spots that are assumed to be fluid expulsion sites. In D, waste can be seen at the top. G shows the largest observed bacteria mat at the western edge of the top area of Dvurechenskii mud volcano (OFOS 62-2). H shows bright bacteria around two vent sites in the sediment.



the result of a thinner sediment coverage, which points to a sediment eruption that is younger than those of the other mud volcanoes observed. Almost at the centre of the top, an approx. 30 m wide area showed first definite signs of active fluid venting (Fig. 78D-F). Round spots of 1 to 3 dm in diameter and lighter grey to white in colour with a darker inner spot indicate bacterial mats at small seeps. These spots were randomly scattered in a dm to less than 2 m distance. Northeast of this area only blocks and some gullies/crevasses were observed before the track ended at 2,050 m water depth after we had gone down the sediment-covered northern edge.

During this OFOS track the temperature sensor of the CTD recognized a temperature increase directly at the top of the mud volcano. The moment of the higher temperature registration does not coincide with the observation of the scattered seeps and but occurred as we crossed the highest point of Dvurechenskii mud volcano. Even if the temperature change is only  $0.003^{\circ}\text{C}$ , it is a definite positive temperature anomaly that fits in with the higher temperature gradients observed by the heat flow sensors (chapter 11).

#### OFOS 9 (#62-2)

The last OFOS track during M52/1 started west of Dvurechenskii and crossed a small, but rough hill before it entered the top area of Dvurechenskii. In contrast to all other tracks we observed a lot of boulders, steps with bedding plains, crevasses and small pockmarks of 1 m in diameter along the whole track. Most spectacular was a bright white bacteria mat within one of those pockmarks just at the western edge of the top area of Dvurechenskii (Fig. 78G). Some tens of meters later we saw pure white bacteria mats that surrounded two circular holes in the bottom (Fig. 78H). Fortunately, OFOS crossed the area of the scattered small seeps from track 8 again and the correct position of this area was determined to be  $44^{\circ} 17.00' \text{ N} / 34^{\circ} 58.80' \text{ E}$ . Two more seep sites with similar small bacteria spots were observed during the track in ESE direction. During OFOS 8 the whole flat top area showed scattered boulders, one more pockmark and steps with bedding plains. The western flank itself showed no bedding plains and only two of them were observed shortly before OFOS left the bottom.



## 10. GEOLOGICAL SAMPLING AND RESULTS

### 10.1 Performance of sampling equipment; sampling

F. Abegg, A. Petersen, B. Bannert

During cruise M52/1, three different tools were used for seafloor sampling. Bulk sediment samples were taken with a large TV-grab. The advantage of this device is the large volume of recovered sediment. A disadvantage is the disturbance of the sample and in most cases a loss of the sediment surface. This on the other hand is the advantage of the multicorer. It provides an undisturbed core with a well preserved sediment surface, but its length is limited to the uppermost 55 cm. The third device, the gravity corer provides long cores (up to 600 cm). Its disadvantage is however that the soft surface of the sediment column may be damaged by the core catcher.

The first device to be described in detail is the TV-guided grab sampler. On R/V METEOR it is operated using winch no. 12 with a coaxial cable. The cable is used for the video uplink as well as for controlling the lights and the grab operation. The lights and the hydraulics are powered by two deep sea batteries. The device is equipped with an OSPRAY underwater camera and four lights of 150 W each. The sample volume is estimated to be 0.7 m<sup>3</sup>.

Upon recovery at site 11 (TVG-2) the TV-grab did not open properly. Intense investigation, during which the device was taken apart more or less completely, revealed a serious defect of the collector within the hydraulic pump motor. There was not much hope to get it fixed, but thanks to outstanding efforts of the ship's crew and the technicians the problem could be solved and further operation became possible. One permanent problem was the video quality. Due to scratches in the glass of the camera the interpretation of the video signal was difficult. Most of the grab deployments yielded a complete filling. One grab (59, TVG-5) recovered a piece of carbonate with bacterial mats. Upon sampling site 60 (TVG-6) the grab did not close due to low battery power.

A total of seven TV-guided grab samples could be retrieved which are listed in Table 3. The second tool is the multicorer. In fact we used two different types. One was the TV-guided large multicorer (TV-MUC) which allowed for 8 cores to be taken. The TV-MUC was equipped with two cameras, one looking into the drift direction and one towards the tubes. For the deployment, again we used winch 12 and the coaxial cable. The cable was used as a power cord for the cameras and both lights as well as for the video uplink.

The second one was the smaller mini-multicorer (MIC) with a capacity of 4 cores. After the first deployment of the MIC, with all tubes empty, the bottom indicator of the Seabird CTD was mounted. For this reason, winch 2 was used. The bottom contact was indicated by a W-meter and later by an indicator provided by the ship. Both multicorers use the same type of tubes. Its length is 61 cm, the outer diameter is 11cm and the inner diameter is 10 cm. TV-MUC and MIC stations are listed in Table 3. See the appendix for a complete station list.

In order to sample longer cores, a gravity corer with a weight of 1.2 t was used. It proved to be a multi-purpose tool. Three different barrels were used. The first one had a length of 300 cm. Its life ended during the second operation. The second barrel had a length of 370 cm. Both the deployments with the short barrel and with the 370 cm barrel are listed as 'GC' in all protocols. The third barrel had a length of 600 cm. It was equipped with temperature

Table 3: Sample list of TV-guided grab samples; pwc = pore water chemistry; mb = microbiology; cth = ct of gas hydrates.

Station	Date/ Time (UTC)	Lat. / Long.	Depth (m)	Recovery	Samples	Analyses
8 TVG-1	05/01/02 14:09	44° 22.97 35° 08.50	1784	full	carbonates bacteria	pwc mb
11 TVG-2	07/01/2002 02:51	44° 14.56 34° 47.13	2124	full	carbonates mud breccia	pwc mb
42 TVG-3	18/01/02 20:15	44° 14.16 34° 45.34	2089	full	non	pwc
43 TVG-4	18/01/02 23:36	44° 16.89 34° 52.34	2081	full	mud breccia	pwc
59 TVG-5	27/01/02 13:13	44° 14.54 34° 47.11	2124	approx. 1.5 l	carbonates + bacteria	mb
60 TVG-6	27/01/02 18:17	44° 14.19 34° 45.47	2108	empty		
63 TVG-7	28/01/02 08:51	44° 16.96 34° 58.89	2075	full	mud, gas hydrates	cth

Table 4: List of TV-MUC and MIC stations; pwc = pore water chemistry; ch4w = methane content of bottom water, mb = microbiology.

Station	Date / Time (UTC)	Lat. / Long. (N / E)	Depth (m)	Cores	Analyses
6 TV-MUC-1	05/01/2002 06:59:00	44° 22.49 35° 08.62	1889	A	empty
				B	pwc / ch4w, archive
				E	mb
				F	Vanni
				G	pwc / ch4w
6 TV-MUC-2	05/01/2002 09:42	44° 22.59 35° 08.62	1877	B	pwc
				D	mb
				F	archiv
34 MIC-1	17/01/02 11:38	44° 17.00 34° 59.00	2070	empty	
35 MIC-2	17/01/02 14:19	44° 22.65 35° 08.87	1870	A	pwc
36 MIC-3	17/01/02 20:00	44° 16.99 34° 58.81	2070	A	pwc, mb
48 MIC-4	21/01/02 16:24	44° 16.88 34° 58.80	2085	A	pwc
49 MIC-5	21/01/02 20:06	44° 16.97 34° 58.61	2089	A	pwc / ch4w
				B	mb
50 MIC-6	21/01/02 20:06	44° 16.97 34° 58.61	1834	A	pwc
				B	mb

sensors and a tiltmeter. More information regarding the temperature measurements will be given in chapter 11. Holding fixtures for the temperature sensors were welded to the barrel. Samples taken with this system are indicated as TGC (Thermistor Gravity corer). The outer diameter of the barrel is 14 cm, the inner diameter is 13.2 cm.

For most of the deployments, we used liners made of polythene sheeting instead of the normal PVC liners. It has the advantage of allowing fast access to the sample, which is important when recovering gas hydrates. After pulling the core out of the barrel it is simply cut open and sampling can start immediately.

PVC liners were used twice for special usage. The liners were pre-cut, consisting of six segments of a length of 55 cm and one segment of 40 cm. These segments were taped together. The intention was to freeze the whole core containing gas hydrates. Therefore a rapid cut of the core was necessary. This technique has proved to be reliable and very fast. More details will be given in chapter 10.3. On R/V METEOR, this work was done on winch No. 11 with a wire. All gravity cores are listed in Table 5.

Table 5: List of gravity corer stations. pwc = pore water chemistry (GEOMAR); gag = analysis of gas (MSU), gah = gas analysis of hydrates (MSU), gci = gas composition and isotopy (GEOMAR), cth = ct of gas hydrates (GEOMAR).

Station	Date / Time (UTC)	Lat. / Long. (N / E)	Depth (m)	Recovery (cm)	Samples	Analyses
15 GC-1	09/01/02 09:49	44° 16.89 34° 52.35	2081	90	cth	
15 GC-2	09/01/02 11:32	44° 16.87 34° 52.36	2060	87	cth	pwc gci
17 GC-3	09/01/02 14:06	44° 14.53 34° 47.03	2124	80	cth	
18 TGC-1	09/01/02 17:09	44° 23.01 35° 09.28	1836	410	cth	pwc
34 TGC-2	17/01/02 09:18	44° 16.96 34° 58.95	2074	365		pwc gag / gah
35 GC-4	17/01/02 15:58	44° 22.65 35° 08.92	1870	370	no gh, disposed	
36 TGC-3	17/01/02 18:06	44° 17.00 34° 58.86	2071	280		pwc
37 TGC-4	17/01/02 21:42	44° 17.13 34° 58.99	2073	580		pwc gag / gah
38 TGC-5	18/01/02 00:17	44° 17.00 34° 59.18	2075	390		pwc gag / gah
39 TGC-6	18/01/02 02:39	44° 14.03 34° 58.85	2161	310		pwc gag
48 TGC-7	21/01/02 14:45	44° 16.85 34° 58.80	2087	500		
49 TGC-8	21/01/02 18:17	44° 16.95 34° 58.63	2087	480	cth	gag / gah
50 GC-5	21/01/02 22:48	44° 23.00 35° 09.27	1835	165	whole core frozen, cth	
52 GC-6	22/01/02 05:27	44° 14.37 34° 45.43	2130	300		
53 GC-7	22/01/02 07:06	44° 14.31 34° 45.32	2128	320		gag
54 GC-8	22/01/02 08:36	44° 14.23 34° 45.39	2129	402		gag
55 GC-9	22/01/02 10:19	44° 14.56 34° 47.56	2127	165		gag



## 10.2 Seafloor sampling results

G. Aloisi, F. Abegg, V. Blinova, M. Drews, J. Greinert, M. Ivanov and G. Bohrmann

All coring stations are located in the Sorokin Trough area (Figs. 8, 68, 72 and 74; Table 6). Schematic core logs are presented in Figures 79 to 81. The sediment temperature was measured on board soon after the cores were opened. Sediment subsamples taken for sedimentological, organic geochemical and microbiological analysis are listed in Table 7. Reference to Woodside et al. (1997) is made for sampling locations based of previous geophysical and coring surveys conducted during the 6th Training Trough Research (TTR-6) cruise.

### Station 6-1 (TV-MUC-1)

This multicorer sample was taken on a mud flow extending south of the Odessa mud volcano (Fig. 68) where mud breccia with gas hydrates had been sampled during the TTR-6 cruise. It is located along OFOS line 1 in an area where the seafloor shows alternations of dark and white patches. No video image was available during this coring operation and detailed positioning of the multicorer with respect to seafloor features was not possible. This coring station was aimed at obtaining detailed pore-water profiles in mud breccia sediments possibly influenced by the presence of gas hydrates. All cores recovered over 40 cm of sediment. The cores were not opened on board so the lithological description is restricted to observations possible from the top of the core and through the transparent liner. In the top of the core there is one cm of very soupy sediment composed of dark brown – black flakes with a high water content. Very fine alternations of light grey, yellowish and black layers form the top 10 cm of the core. This is most probably recent pelagic sediment rich in organic matter which possibly covers large extensions of seafloor seen on OFOS line 1. Between roughly 10 and 30 cm a dark layer is present in an otherwise grey sediment core. These preliminary observations are consistent with the description of sediments recovered during the TTR-6 cruise from this area which show that the mud flow is covered by 30 cm of pelagic sediment including a sapropel layer. One core was stored at –20°C for further sedimentological analysis.

### Station 6-2 (TV-MUC-2)

This core aimed at recovering sediment from white patches to test the hypothesis, based on OFOS observations during line 1, that the white patches are areas where the uppermost organic-rich, black, pelagic sediment has been removed. The TV image was available but it is not clear if the corer was positioned on a white patch of seafloor. The cores were not opened on board. Reference is made to the preliminary core description to station 6-2 TV-MUC-1. One core was stored at –20°C for further sedimentological analysis.

### Station 8 (TVG-1)

This TV-grab sample was taken on the south-western flank of the Odessa mud volcano (Fig. 68) along OFOS line 2 where crusts were seen outcropping from an otherwise flat muddy seafloor. The grab was full and recovered dark grey hemipelagic mud, which gave off a strong H<sub>2</sub>S smell, and plenty carbonate crusts. The crusts, which seem to occur under about 10 cm of hemipelagic mud, are of 2 types (Fig. 80):

Crusts of the first type are well lithified, 2 – 3 cm thick, light grey smooth slabs. No particular textures are present apart from the finely grained calcareous cement. This is the most common type of crust which derives from the lithification of the hemipelagic mud which comprises the rest of the grabbed sedimentary material. Bacterial mats are commonly attached under these crusts and, in certain instances, they traverse the crusts from side to side. These mats, which have a mucus-like consistency, come in two colours: white and greenish. Bacterial colonies are also present in submillimetric pores on the superior surface of the crusts. These are reddish-yellowish in colour and have a variable consistency, from mucus-like to hardened (wax-like). Also present are brownish – black fibrous organic filaments of unknown origin. The second type of crusts are dark-grey, friable, up to 7 – 10 cm thick and have a layered, shale-like, fabric. No bacterial colonies are associated to these crusts. The pelagic section recovered in this grab attests for the inactivity in terms of mud emission of this flank of the Odessa mud volcano. The recovered hemipelagic mud section, however, is clearly influenced by the seepage of methane.

### **Station 11 (TVG-2)**

This TV-grab sample was taken from the 20 m high mound crossed by OFOS line 6, at the centre of the Yalta collapsed mud volcano (Fig. 72). The grab was full and recovered grey, sticky, matrix-supported mud breccia which gave off a strong H<sub>2</sub>S smell. Clasts are rare. Soft, subangular to sub-rounded laminated mudstones represent the most common lithology. Well-lithified calcareous clasts are also present and can have sizes of up to 40 cm across. The upper part of the grab is covered by a layer of carbonate crusts about 10 cm thick. These are derived from a limited lithification of mud breccia and frequently contain portions of unlithified mud breccia surrounded by cemented portions of mud breccia. When these are washed out, the cement geometry can be seen. It consists of well-defined, flat surfaces which isolate the unlithified mud mud breccia. Subcentimetric bivalve shells are present on the surface of some crusts.

### **Station 15-1 (GC-1)**

This gravity core was taken on a secondary mound in a bathymetrically negative structure interpreted as a collapsed mud volcano during the TTR-6 cruise (Fig. 8) and was aimed at recovering gas hydrates. The core recovered 90 cm of dark grey mud breccia with soft, centimetric mudstone clasts (Fig. 79). A layer of gas hydrate is present between 20 and 50 cms.

### **Station 15-2 (GC-2)**

The core recovered 87 cm of dark grey mud breccia with soft, centimetric mudstone clasts (Fig. 79). Two millimetric carbonate crusts are present at the top of the core. A layer of gas hydrate is present between 28 and 51 cms.

### **Station 17 (GC-3)**

This gravity core was taken from the 20 m high mound crossed by OFOS line 6, at the centre of the Yalta mud volcano (Fig. 72) and was aimed at recovering gas hydrates, which were sampled from this site during the TTR – 6 cruise. The core recovered 80 cm of grey

to dark grey mud breccia with millimetric to centimetric clasts (mainly mudstones). The mud breccia is matrix supported (Fig. 80). From 35 cm to 45 cm the mud has a higher water content and is very soupy, possibly indicating the former presence of gas hydrates which have dissociated during core recovery (gas hydrates at this depth interval were recovered from this location during the TTR – 6 cruise). The core catcher contains one 'cobble' of massive gas hydrate 6 cm across which was stored in liquid nitrogen.

#### **Station 18 (TGC-1)**

This thermistor gravity core was taken approximately 1.5 km east of the Odessa mud volcano, on OFOS line 1 (Fig. 68) and aimed at obtaining a reference temperature profile in the upper 6 m of sediment. The core recovered 410 cm of grey to dark grey hemipelagic mud (Fig. 79). A 2 cm thick carbonate crust is present at 23 cm depth at a very sharp colour boundary between light grey mud (above crust) and a black sapropel layer which extends from below the crust to 60 cm. Yellowish, bacterial colonies fill sub-millimetric pores on the upper part of the crust and are abundant also in its interior. Another sapropel layer is present between 81 and 83 cm. Gas hydrate is finely dispersed in the mud between 123 and 140 cm and occur in lenses between 260 and 310 cm. In the gas hydrate bearing intervals, the temperature of the sediment measured on board was 6°C. This anomalous low temperature (bottom water temperatures are of roughly 8.5°C) is consistent with the ongoing dissociation of gas hydrates which is an endothermic reaction.

#### **Station 34-1 (TGC-2)**

This thermistor gravity core was taken on the summit of the Dvurechenskii mud volcano, 200 m ESE from its centre (Fig. 74) and aimed at testing for the presence of gas hydrates on the basis of the high methane content found in the sediment of this mud volcano during previous coring investigations (TTR-6 cruise). The core recovered 365 cm of very soupy mousse-like mud breccia with millimetric to centimetric clasts, mainly subrounded, soft, finely bedded mudstones. The mud breccia is matrix supported (Fig. 81). Sub-centimetric gas hydrate is abundant and present throughout the core. Sometimes aggregates of gas hydrate form flat layers less than 1 cm thick and a few centimetres across, parallel to bedding. The top 30 cms of the core give off a strong H<sub>2</sub>S smell.

#### **Station 34-2 (MIC-1)**

This mini corer aimed at obtaining detailed pore-water chemistry data from the eastern part of the summit of the Dvurechenskii mud volcano (Fig. 74). No recovery.

#### **Station 35-1 (MIC-2)**

This mini corer was taken on a mud flow extending south of the Odessa mud volcano (Fig. 68) where mud breccia with gas hydrates had been sampled during the TTR-6 cruise. It is located along OFOS line 1 and aimed at obtaining detailed pore-water chemistry data. All cores recovered over 40 cm of sediment. One core was stored at –20°C for further sedimentological analysis.



**Station 35-2 (GC-4)**

This gravity core was taken on a mud flow extending south of the Odessa mud volcano (Fig. 68) where mud breccia with gas hydrates had been sampled. It is located along OFOS line 1 and aimed at recovering mud breccia with gas hydrate to be freeze-dried in liquid nitrogen in order to perform computer tomography on the whole core. Although a mud breccia section of about 3 m in length was recovered, there was no evidence for the presence of gas hydrates.

**Station 36-1 (TGC-3)**

This thermistor gravity core was taken in the centre of the Dvurechenskii mud volcano (Fig. 74) and aimed at recovering gas hydrates and further investigating the chemical and thermal structure of the core. Extensive bubbling of the sea surface was observed when the core surfaced, indicating a possible dissociation of gas hydrates during core recovery. The section recovered is 280 cm long and consists mostly of mousse-like mud breccia with millimetric to centimetric clasts (Fig. 81). This mud breccia is matrix supported. The interval between 205 and 240 cm, however, is very rich in clasts. Here, clast to clast contacts are very frequent and the sediment is clast supported. Most clasts are soft, subangular to subrounded mudstones although laminated siltstones, marls and a calcareous conglomerates are also present. The sediment gives off an  $\text{H}_2\text{S}$  smell. Nodular subcentimetric gas hydrate crystals are present in the top 70 cm and in the lower meter of the core. A sediment temperature of 7°C was measured from these intervals indicating ongoing gas hydrate dissociation.

**Station 36-2 (MIC-3)**

This mini corer was taken in the centre of the Dvurechenskii mud volcano (Fig. 74) to obtain detailed pore-water chemistry profiles in the same position as core TGC-3 (station 36-1). Four cores containing mud breccia were recovered. Gas hydrate was observed in the mud breccia. Their dissociation is probably the origin of the strong degassing of the sediment observed at the top of the core.

**Station 37 (TGC-4)**

This thermistor gravity core was taken from the north-eastern slope of the Dvurechenskii mud volcano (74) and aimed at recovering gas hydrates and further investigating the chemical and thermal structure of this volcano. The core recovered 580 cm of mousse-like mud breccia with millimetric to centimetric clasts. The sediment is matrix supported. Clasts are mainly mudstones although conglomerates up to 5 centimetres in diameter composed of mm to cm mudstone clasts embedded in a light grey muddy matrix are common. These could be portions of mud breccia which have indurated after mud flow emplacement due to precipitation of carbonatic cements. Subcentimetric gas hydrate crystals are common throughout the core. A level very rich in bivalve shell debris is present at 160 cm depth. The sediment gives off an  $\text{H}_2\text{S}$  smell and its temperature was as low as 2.9°C, indicating ongoing gas hydrate dissociation.

**Station 38 (TGC-5)**

This thermistor gravity core was taken on the summit of the Dvurechenskii mud volcano, 400 m E from its centre (Fig. 74). Extensive bubbling of the sea surface was observed when the core surfaced. The core recovered 390 cm of mousse-like mud breccia with subcentimetric, subrounded mudstone clasts. The sediment is matrix supported. Subcentimetric gas hydrate crystals are common throughout the core. The sediment gives off an H<sub>2</sub>S smell and its temperature was as low as 5.9°C, indicating ongoing gas hydrate dissociation.

**Station 39 (TGC-6)**

This thermistor gravity core was taken on the regional slope 1400 m south of the Dvurechenskii mud volcano (Fig. 8) and was aimed at obtaining the background chemical and thermal structure, unaffected by focused methane seepage, in this area of the Sorokin Trough. The core recovered 310 cm of dark grey, homogeneous hemipelagic mud, with several intervals (90-97, 107-110, 117-118, 136-146, 156-160, 202-206 and 248-250 cm) very rich in bivalve shell debris (Fig. 81). The bivalve shells are often broken and in each layer are well sorted suggesting an emplacement by sediment gravity flow, possibly small turbidites.

**Station 42 (TVG-3)**

This TV-grab was taken on the 60 m high, NNW trending mound crossed by OFOS line 7, at the centre of the Sevastopol collapsed mud volcano (Fig. 72). The aim of this sampling operation was to test the occurrence of gas hydrates and evaluate its potential of this site as a possible target for a 3-D seismic survey. The grab was full and recovered light grey hemipelagic mud (Fig. 80).

**Station 43 (TVG-4)**

This TV-grab was taken on a secondary mound of a bathymetrically negative structure interpreted as a collapsed mud volcano by previous TTR investigations (Fig. 8). It aimed at recovering gas hydrates. The grab recovered mud breccia with millimetric to decimetric clasts. The sediment is matrix supported and its water content is comparably low with respect to the mud breccia sampled in other mud volcanoes during this cruise. Clast lithologies comprise mainly angular laminated sandstones and siltstones which cleave along well-defined parallel plains. Minor constituents are fine grained, micritic carbonate cobbles (Fig. 79).

**Station 48 – 1 (TGC - 7)**

This thermistor gravity core was taken on the southern part of the summit of the Dvurechenskii mud volcano (Fig. 74), in order to complete the investigation of its thermal and chemical structure. The core recovered 500 cm of mousse-like mud breccia with millimetric to centimetric, subrounded to subangular mudstone clasts that cleave along well-defined, parallel planes (Fig. 81). The sediment is matrix supported. Subcentimetric gas hydrate is common throughout the core, but particularly abundant in the top 1.5 m of

the core. The sediment gave off a strong  $\text{H}_2\text{S}$  smell and its temperature was as low as  $6.5^\circ\text{C}$ , indicating ongoing gas hydrate dissociation.

#### **Station 48-2 (MIC-4)**

This mini corer was taken from the southern part of the summit of the Dvurechenskii mud volcano (Fig. 74), in order to provide a detailed pore water chemical profile of the upper 50 cm of sediment, in the same position as core TGC – 7 (station 48-1). The cores were not opened on board. One core was stored at  $-20^\circ\text{C}$  for sedimentological analysis.

#### **Station 49-1 (TGC - 8)**

This thermistor gravity core was taken from the western part of the summit of the Dvurechenskii mud volcano (Fig. 74), in order to complete the investigation of its thermal and chemical structure. The core recovered 480 cm of mousse-like mud breccia with millimetric to centimetric, subrounded to rounded mudstone clasts that cleave along well-defined, parallel planes. Plane-laminated siltstones and sandstones and marls are also present. The sediment is matrix supported. Subcentimetric gas hydrate is common throughout the core, but particularly abundant in its top 1.5 m (Fig. 81). The sediment gave off a smell of  $\text{H}_2\text{S}$  and its temperature was as low as  $-1.1^\circ\text{C}$  in the top metre and between  $3^\circ\text{C}$  and  $5^\circ\text{C}$  in the rest of the core, indicating ongoing gas hydrate dissociation.

#### **Station 49-2 (MIC-5)**

This mini corer was taken from the western part of the summit of the Dvurechenskii mud volcano (Fig. 74), in order to provide a detailed pore water chemical profile of the upper 50 cm of sediment in the same position as TGC – 8 (station 49-1). The four cores recovered dark grey mud giving off a strong  $\text{H}_2\text{S}$  smell. The cores were not opened on board. One core was stored at  $-20^\circ\text{C}$  for further sedimentological analysis.

#### **Station 50-1 (GC-5)**

This gravity core was taken approximately 1.5 km east of the Odessa mud volcano, on OFOS line 1 (Fig. 68) and aimed at recovering gas hydrates based upon their recovery in station 18 (TVG – 1). The whole core was frozen in liquid nitrogen in order to maintain gas hydrates stable for their imaging via computer tomography.

#### **Station 50-2 (MIC-6)**

This mini corer was taken approximately 1.5 km east of the Odessa mud volcano, on OFOS line 1 (Fig. 68) and was planned in order to have a detailed investigation of the pore water chemistry at the same site as core TGC – 1 (station 18). This core recovered 39 cm of dark grey mud, millimetric laminations could be seen through the core liner in the top 4 cms of sediments. The sediment gave off an  $\text{H}_2\text{S}$  smell. One core was stored at  $-20^\circ\text{C}$  for further sedimentological analysis.



**Station 52 (GC-6)**

This core was taken in a small basin in the Sevastopol collapsed mud volcano, between OFOS lines 6 and 7 (Fig. 68) in order to test the occurrence of gas hydrates and evaluate the potential of this site as a possible target for a 3-D seismic survey. The core recovered about 3 m of homogeneous grey hemipelagic mud with occasional submillimetric layers of yellowish brown mud, possibly calcareous nanofossil ooze (Fig. 80).

**Station 53 (GC-7)**

This gravity core was taken on the 60 m high, NNW trending mound on OFOS line 7, at the centre of the Sevastopol collapsed mud volcano (Fig. 72) in order to test the occurrence of gas hydrates at this site and evaluate its potential as a possible target for a 3-D seismic survey. The core recovered about 320 cm of homogeneous grey hemipelagic mud (Fig. 80). Degassing of the mud from 230 cm to the bottom on the core was apparent.

**Station 54 (GC-8)**

This gravity core was taken on the flank of the 60 m high, NNW trending mound on OFOS line 7, at the centre of the Sevastopol mud volcano (Fig. 72) in order to test the occurrence of gas hydrates at this site and evaluate its potential as a possible target for a 3-D seismic survey. The core recovered 402 cm of hemipelagic mud. The top 150 cms are composed of homogeneous grey mud (Fig. 80). At 150 cm a layer of soft light grey carbonaceous nodules and shell debris is present. From 150 cm to the bottom of the core layers of black and olive grey sapropel alternate. A piece of wood bark is present in a sapropel at 250 cm. The sediment degasses vigorously and smells strongly of  $H_2S$ .

**Station 55 (GC-9)**

This gravity core was taken on the flank of the 60 m high, NNW trending mound on OFOS line 7 in the Yalta collapsed mud volcano (Fig. 72) in order to test the occurrence of gas hydrates at this site and evaluate its potential as a possible target for a 3-D seismic survey. The core recovered 165 cm of dark grey, stiff mud devoid of clasts and with a lower water content than the typical mousse-like mud breccia of mud volcanoes (Fig. 80). The mud 'breaks', when disturbed, along irregular surfaces resembling the outlines of soft mud clasts. This could possibly be diapiric material. The sediment smells of  $H_2S$ .

**Station 59 (TVG-5)**

This grab was taken on the central mound of the Yalta collapsed mud volcano (Fig. 72) in an area where metric slabs, possibly carbonate crusts, outcrop in a disordered, disturbed manner. The slabs are covered by a drape of pelagic sediments which hinders the determination of their lithological nature. The grab was empty except for a few 4-5 cm-thick carbonate crusts covered by 2-4 cm of bacterial mats. A carbonate crust composes the lower part of the sampled material and the bacterial mat is on the upper part, in contact with bottom waters. The mats have a gelatinous consistency and are mostly pink to orange in colour (see also Fig. 90), although an additional millimetric black layer separates the mat from the pelagic sediments that drape it. The transition between crust (below) and mat

(above) is continuous, with the lower part of the mats being rich in carbonate precipitate. Centimetric rock clasts were also present in the grab.

### **Station 63, TVG-7**

This grab was taken on the Dvurechenskii mud volcano summit at the crossing of OFOS lines 8 and 9 (Fig. 74) and was aimed at recovering gas hydrates based on the occurrence of seeps seen during the OFOS survey. The seafloor was covered by metric slabs, possibly carbonate crusts, and a 30-40 cm wide white patch. The grab was full of mousse-like mud breccia with scarce centimetric clasts of mudstone, laminated siltstones and sandstones. Lenticular gas hydrate crystals, a few mm thick and several cm wide, are abundant.

### **Discussion of the coring results**

On a lithological basis, the sampled sediments can be divided in two main categories: hemipelagic sediments and mud volcanic deposits (mud breccia). Both types of sediment show indicators of the seepage of CH<sub>4</sub>-rich fluids.

#### **Hemipelagic sediments**

Hemipelagic sediments were recovered both on mud volcanoes (Odessa and Sevastopol) and at a reference station away from them (TGC-6). These are composed of grey to dark grey mud which can show fine alternations with coccolith ooze and sapropels in its upper metre (eg GC-6). Black to dark grey sapropels follow downcore and can be up to 230 cm thick (core GC-8). These observations are consistent with previous descriptions of recent (Holocene) Black Sea hemipelagic sediments. Unusually thick sapropel layers as in core GC-8 are probably due to their dilution by clay as previously described, resulting in very high sedimentation rates of around 80 cm/kyrs which have been recorded previously from this area (Woodside et al., 1997).

The presence of more than 4 m of hemipelagic sediments on the Sevastopol mud volcano and of approximately 80 cm of hemipelagics on the Odessa and mud volcano as well as the absence of mud breccia in cores from these sites attest to a period of inactivity in terms of mud eruptions of these mud volcanoes.

#### **Mud breccia deposits**

Cores containing mud breccia were recovered from the Yalta (Fig. 80) and Dvurechenskii (Fig. 81) mud volcanoes as well as from an unnamed mud volcano (Fig. 79). The lack of hemipelagi sediments in cores from these volcanoes indicates the the emplacement of the cored mud flows is recent. The mud breccia from the Yalta and the unnamed mud volcano show the typical character of the most common type of mud volcanic product where a variable amount of clasts are immersed in a muddy matrix offering support to the sediment. The mud breccia of the Dvurechenskii mud volcano, however, is poorer in clasts, has a very high gas content and is relatively fluid, which are characters typical of the 'mousse-like' mud breccia previously described from mud volcanoes of the eastern Mediterranean and the Black Sea (Woodside et al., 1997). It is interesting to note that such a gas-saturated, fluid-rich mud breccia occurs on a flat topped mud volcano. This morphology is consistent

with the emission of relatively fluid mud volcanic products. Such flat-topped mud volcanoes have already been described from the Barbados accretionary prism (Henry et al., 1966) and have been termed 'mud pies'.

The clasts recovered in the mud breccia cores have been washed and sampled. A preliminary description shows the presence of mudstones, laminated siltstones, sandstones and marls. Mudstones, at least in part, probably originate from the Maikopian formation which is considered the source formation for the material forming the diapiric folds which underly and feed the mud volcanos in the Sorokin Trough (Woodside et al., 1997).

### **Evidence for recent or present methane-emissions from mud volcanoes**

A number of indicators for recent or present methane emission exist in all the explored mud volcanoes. These are present both in the pelagic sediments that drape the relatively dormant Odessa and Sevastopol mud volcanoes, as well as in the mud breccia sediments from the Dvurechenskii, the Yalta and the unnamed mud volcano:

#### *Degassing of sediments*

Degassing of sediments upon opening of the plastic tubing was evident for cores from the Sevastopol, Odessa, Dvurechenskii and the unnamed mud volcano. The high gas content of the sediment corresponds at times to the intervals containing gas hydrates, but can be present also in cores lacking gas hydrates.

#### *Occurrence of gas hydrates*

Gas hydrates were sampled from all mud volcanoes except from the Sevastopol mud volcano. Their presence at very shallow depth (10 cm) in the sediments of the Dvurechenskii mud volcano implies a continuous seepage of methane necessary to keep the gas hydrates below the zone of anaerobic methane oxidation. When existing grains of gas hydrate were too small to be evident, its presence was nicely indicated by the sediment temperature anomaly produced by the endothermic reaction of gas hydrates dissociation.

#### *H<sub>2</sub>S smell stronger in cores from mud volcanoes*

The majority on the cores retrieved from mud volcanoes give off a strong smell of H<sub>2</sub>S, especially in the upper part of the core. This is consistent with the production of H<sub>2</sub>S following anaerobic methane oxidation via sulfate reduction, well documented by the pore water chemical data.

#### *Carbonate crusts*

Authigenic carbonate crusts were recovered in the upper part of the sedimentary succession in the Odessa, Yalta and the unnamed mud volcano. These crusts are formed by cementation of both hemipelagic and mud breccia sediments following the microbially mediated process of anaerobic methane oxidation and attest of the recent or present seepage of CH<sub>4</sub>-rich fluids.

#### *Bacterial mats and colonies*

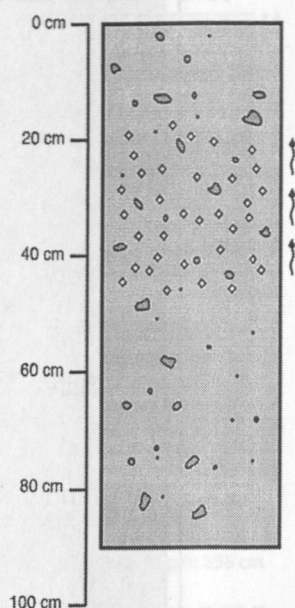
Although the typical chemosynthesis-based cold-seep benthic communities are absent in the Black Sea due to lack of oxygen in the bottom water at this depth, abundant evidence of microbial life most probably associated to the seepage of methane-charged fluids was



## Unnamed Mud Volcano

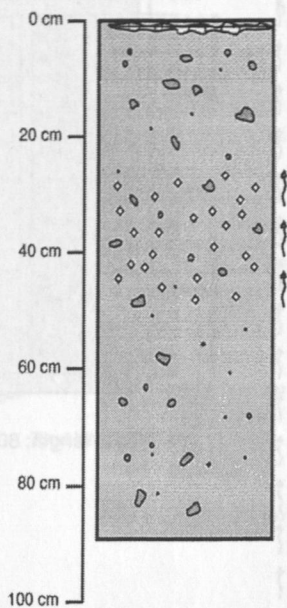
## Odessa Mud Volcano

Station 15-1, GC-1

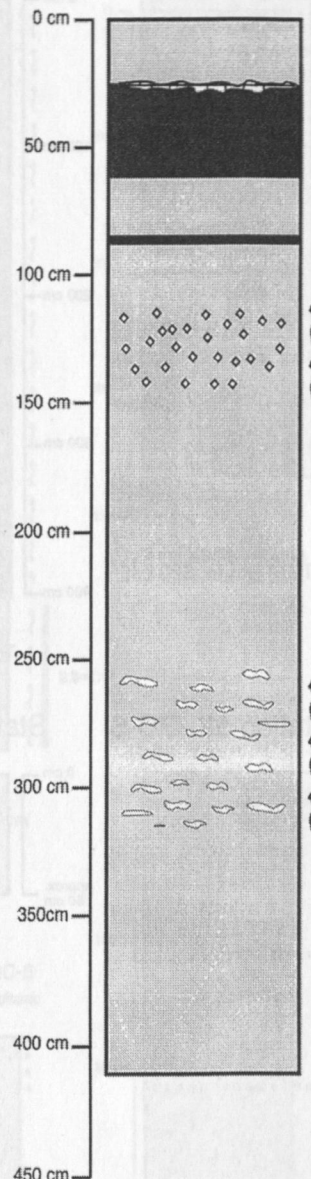


Total length: 90 cm

Station 15-2, GC-2

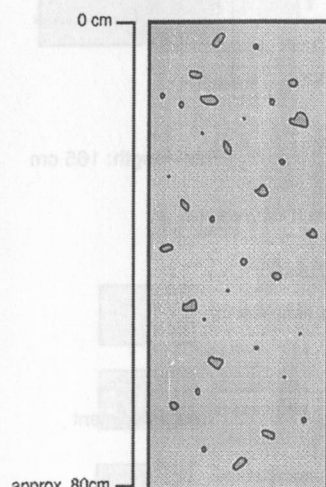


Total length: 87 cm

Station 18, TGC-1  
Slope E of mud volcano

Total length: 410 cm

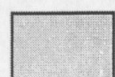
Station 43, TVG-4




Note: approx. stratigraphy

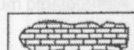
Grab full

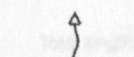
## Legend

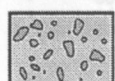
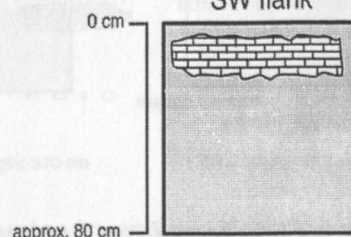
 Homogeneous hemipelagic mud

 Sapropel

 Gas hydrates:  
- dispersed crystals  
- lenses

 Carbonate crust

 Sediment degassing

 Mud breccia
Station 8, TVG-1  
SW flank

Note: approx. stratigraphy

Fig. 79: Schematic core description from Odessa mud volcano and other sites.

## Sevastopol Mud Volcano

## Yalta Mud Volcano

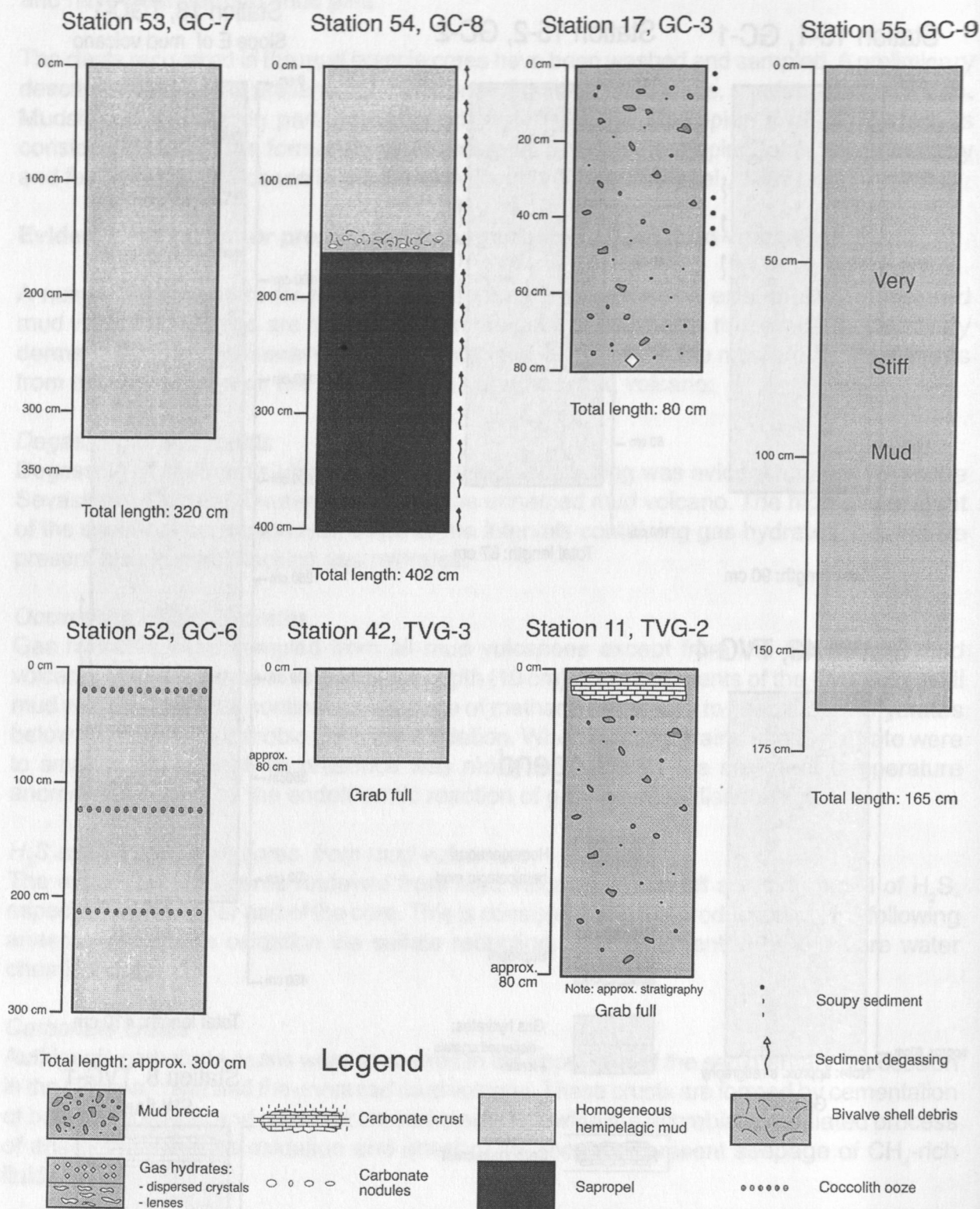


Fig. 80: Core logs from Sevastopol and Yalta mud volcano.

## Dvurechenskii Mud Volcano

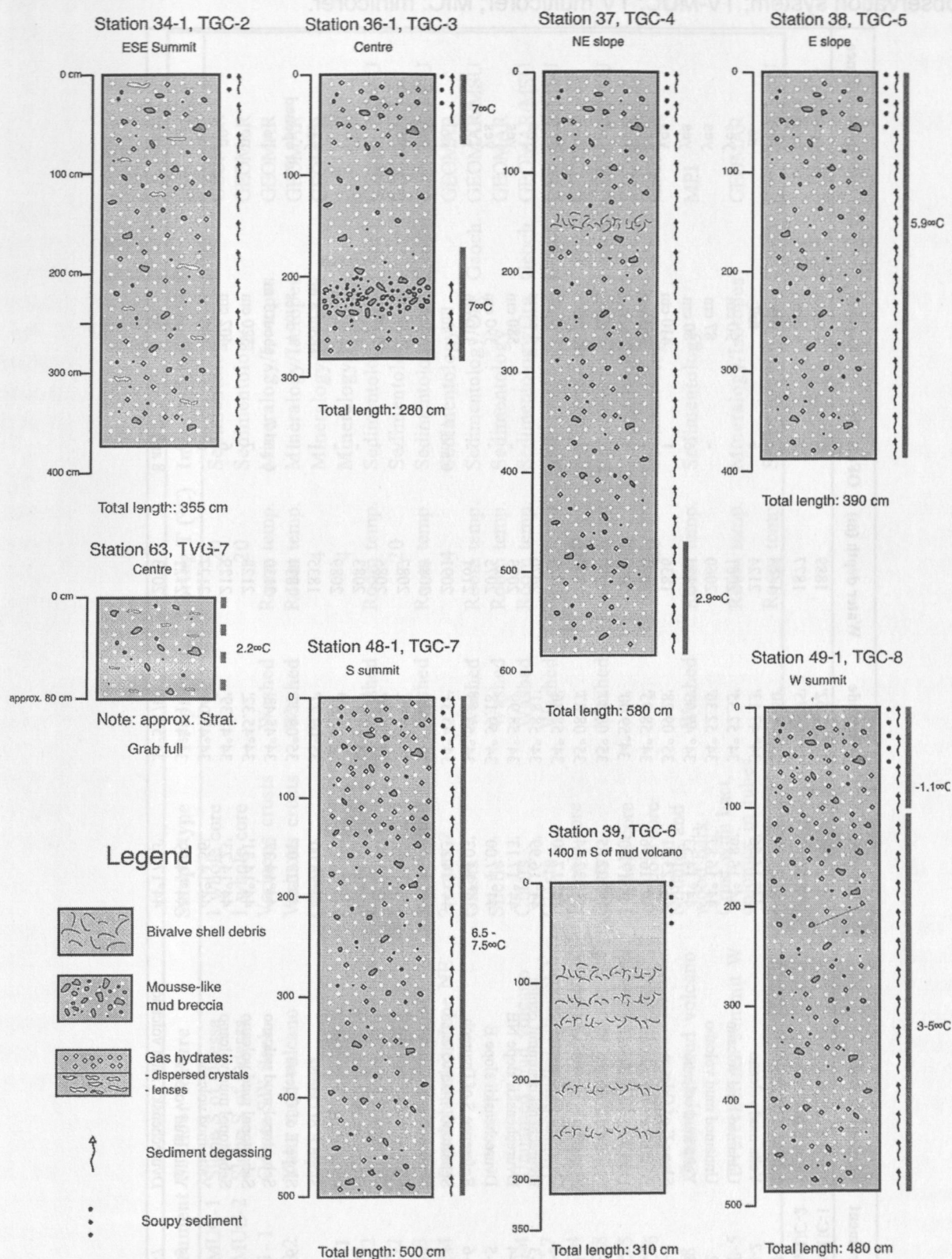


Fig. 81: Schematic core logs from Dvurechenskii mud volcano and a reference site to the south of the mud volcano.



Table 6: Seafloor sampling locations. All locations are within the Sorokin Trough. Sampling devices are abbreviated as follows: TGC: thermistor gravity corer; OFOS: ocean floor observation system; TV-MUC: TV multicorer; MIC: minicorer.

Station	Instrument	Seafloor feature	Latitude	Longitude	Water depth (m)	OFOS line	Recovery	Gas hydrate occurrence
6-1	TV-MUC-1	Slope S of Odessa	44° 22.49'	35° 08.62'	1889	1	7 cores	not opened
6-2	TV-MUC-2	Slope S of Odessa	44° 22.59'	35° 08.75'	1877	1	8 cores	not opened
8	TVG-1	Odessa, SW flank	44° 22.97'	35° 08.50'	1784	2	full	no
11	TVG-2	Yalta mud volcano	44° 14.56'	34° 47.13'	2124	6	full	no
15-1	GC-1	Unnamed mud volcano	44° 16.89'	34° 52.35'	2081	-	90 cm	yes
15-2	GC-2	Unnamed mud volcano	44° 16.87'	34° 52.36'	2060	-	87 cm	yes
17	GC-3	Yalta mud volcano	44° 14.53'	34° 47.03'	2124	6	80 cm	yes
18	TGC-1	Slope E of Odessa	44° 23.01'	35° 09.28'	1836	1	410 cm	yes
34-1	TGC-2	Dvurechenskii summit ESE	44° 16.96'	34° 58.95'	2074	-	365 cm	yes
34-2	MIC-1	Dvurechenskii summit E	44° 17.00'	34° 59.00'	2070	-	no recovery	-
35-1	MIC-2	Slope S of Odessa	44° 22.65'	35° 08.87'	1870	1	4 cores	not opened
35-2	GC-4	Slope S of Odessa	44° 22.64'	35° 08.87'	1870	1	full	no
36-1	TGC-3	Dvurechenskii summit centre	44° 17.00'	34° 58.86'	2071	-	280 cm	yes
36-2	MIC-3	Dvurechenskii summit centre	44° 16.99'	34° 58.81'	2070	-	4 cores	yes
37	TGC-4	Dvurechenskii slope NE	44° 17.13'	34° 58.99'	2073	-	580 cm	yes
38	TGC-5	Dvurechenskii slope E	44° 17.00'	34° 59.18'	2075	-	390 cm	yes
39	TGC-6	Reference S of Dvurech.	44° 14.03'	34° 58.85'	2161	-	310 cm	no
42	TVG-3	Sebastopol mud volcano	44° 14.23'	34° 45.31'	2091	6 and 7	full	no
43	TVG-4	Unnamed mud volcano	44° 16.89'	34° 52.34'	2081	-	full	no
48-1	TGC-7	Dvurechenskii summit S	44° 16.85'	34° 58.80'	2087	-	500 cm	yes
48-2	MIC-4	Dvurechenskii summit S	44° 16.88'	34° 58.80'	2085	-	4 cores	not opened
49-1	TGC-8	Dvurechenskii summit W	44° 16.95'	34° 58.63'	2083	-	480 cm	yes
49-2	MIC-5	Dvurechenskii summit W	44° 16.97'	34° 58.61'	2089	-	50-70 cm	not opened
50-1	GC-5	Slope E of Odessa	44° 23.00'	35° 09.27'	1835	1	about 4 m	yes
50-2	MIC-6	Slope E of Odessa	44° 23.01'	35° 09.27'	1834	1	4 cores	not opened
52	GC-6	Sebastopol mud volcano	44° 14.37'	34° 45.43'	2130	6 and 7	about 3 m	no
53	GC-7	Sebastopol mud volcano	44° 14.31'	34° 45.32'	2128	7	320 cm	no
54	GC-8	Sebastopol mud volcano	44° 14.23'	34° 45.39'	2129	6	402 cm	no
55	GC-9	Yalta mud volcano	44° 14.56'	34° 47.06'	2127	6	160 cm	no
59	TVG-5	Yalta mud volcano	44° 14.59'	34° 47.14'	2121	6	crusts and bacteria	no
63	TVG-7	Dvurechenskii mud volcano	44° 17.03'	34° 58.70'	2073	8 and 9	full	yes

Table 7: Subsamples for shore-based sedimentological and organic geochemical analysis. (MSU: Moscow State University).

Station	Instrument	Seafloor feature	Sample type	Preparation	Storing T (°C)	Investigation	Investigator
6-1	TV-MUC-1	Slope S of Odessa	1 whole core	-	-20	Sedimentology	GEOMAR
6-2	TV-MUC-2	Slope S of Odessa	1 whole core	-	-20	Sedimentology	GEOMAR
8	TVG-1	Odessa SW flank	Various crusts	Washed	Room temp.	Mineralogy/Isotopes	GEOMAR
11	TVG-2	Yalta mud volcano	Various crusts	Washed	Room temp.	Mineralogy/Isotopes	GEOMAR
			Crust	-	4	Mineralogy/Isotopes	GEOMAR
18	TGC-1	Slope E of Odessa	Crust at 20 cm	-	4	Mineralogy/Isotopes	GEOMAR
34-1	TGC-2	Dvurechenskii summit ESE	Clasts	Washed	Room temp.	Sedimentology/Org. Geoch.	GEOMAR/MSU
35-1	MIC-2	Slope S of Odessa	1 whole core	-	-20	Sedimentology	GEOMAR
36-1	TGC-3	Dvurechenskii center	Various clasts	Washed	Room temp.	Sedimentology/Org. Geoch.	GEOMAR/MSU
37	TGC-4	Dvurechenskii slope NE	2 crusts ?	-	4	Sedimentology	GEOMAR
			Clasts	Washed	Room temp.	Sedimentology/Org. Geoch.	GEOMAR/MSU
			Shells	Washed	Room temp.	Sedimentology	GEOMAR
43	TVG-4	Unnamed mud volcano	Clasts	Washed	Room temp.	Sedimentology/Org. Geoch.	GEOMAR/MSU
48-1	TGC-7	Dvurechenskii summit S	Clasts	Washed	Room temp.	Sedimentology/Org. Geoch.	GEOMAR/MSU
48-2	MIC-4	Dvurechenskii summit S	Clasts	Washed	Room temp.	Sedimentology/Org. Geoch.	GEOMAR/MSU
49-1	TGC-8	Dvurechenskii summit W	1 whole core	-	-20	Sedimentology	GEOMAR
49-2	MIC-5	Dvurechenskii summit W	Clasts	Washed	Room temp.	Sedimentology/Org. Geoch.	GEOMAR/MSU
50-2	MIC-6	Slope E of Odessa	1 whole core	-	-20	Sedimentology	GEOMAR
54	GC-8	Sebastopol mud volcano	Nodules and wood bark	Washed	Room temp.	Sedimentology	MPI
59	TVG-5	Dvurechenskii summit W	Crust with bact. colonies in tubes	-	Room temp.	Mineralogy/Isotopes	GEOMAR
			Clasts	-	Room temp.	Sedimentology/Org. Geoch.	GEOMAR/MSU

observed. Microbial mats underlying the authigenic carbonate crusts as well as bacterial colonies inside the authigenic mineral matrix and bacterial mats developed on the upper part of carbonate crusts represent to date one of the best examples of microbe-carbonate mineral associations. It will provide high quality samples to study the role of methane-based microbial activity on the formation of carbonate minerals (see chapter 10.6).

### 10.3 Gas hydrate samples

F. Abegg, G. Aloisi, J. Greinert, J.P. Foucher, V. Blinova, G. Bohrmann

Gas hydrate was recovered with all three sediment sampling devices. Subsamples have been taken from gravity cores and TV grab stations. We got a very impressive sight of gas hydrate destabilization in the mini corer sample 36 MIC-3: when it came on deck, it seemed to be boiling. The stability field, based on measurements of seafloor and water column temperature, ended at a water depth of 700 m. The samples from Dvurechenskii mud volcano, with seafloor temperatures of up to 16°C (see chapter 11 for details of temperature measurements), represent a special case. If the in situ temperature of the seafloor was extrapolated into the water column, the destabilization of gas hydrate would start at a water depth of 1,250 m.

In general the gas hydrates recovered during this cruise can be grouped into three classes. The first group is represented by samples taken at station 15 with both cores GC-1 and GC-2 and station 17 (GC-3). The hydrates have a nodular shape and a size of up to 4x3x2.5 cm. An example is shown in Fig. 82. Because of the small quantities recovered, we did not perform a textural analysis on board.

The second type of gas hydrate has a platy shape. Sizes of up to 10 cm in one direction have been observed. The thickness is limited to a couple of millimeters. In the samples recovered on this cruise, this seems to be the more common variety of gas hydrate. Within the gravity core the orientation of the long axis was parallel to the sedimentary layers. A lot of them have been found in a TV-grab station from Dvurechenskii mud volcano (63 TVG-7) but only a few could be subsampled due to the special heat conditions in this mud volcano (s. above and chapter 11).

The third type consists of very small gas hydrate crystals. They were indicated by constant degassing of the sediment combined with a decrease of sediment temperature. The maximum range was again measured in samples from the Dvurechenskii mud volcano: as mentioned before, the in situ seafloor temperature was around 16°C and the minimum sediment temperature upon core retrieval and after a couple of minutes on deck was less than -1°C. Another indicator for gas hydrate in those cores was the liquid consistency of the mud. Gas hydrate dissociation increases the water content.

A special attempt was made to analyse the depth distribution of the gas hydrates. In preparation of this experiment the liner had been cut into pieces of 55 cm which were fixed together again by tape. The length is determined by the maximum length to be placed in the liquid nitrogen dewars. The pre-cutting responded to the necessity of fast action upon recovery to avoid extended dissociation of the hydrates.



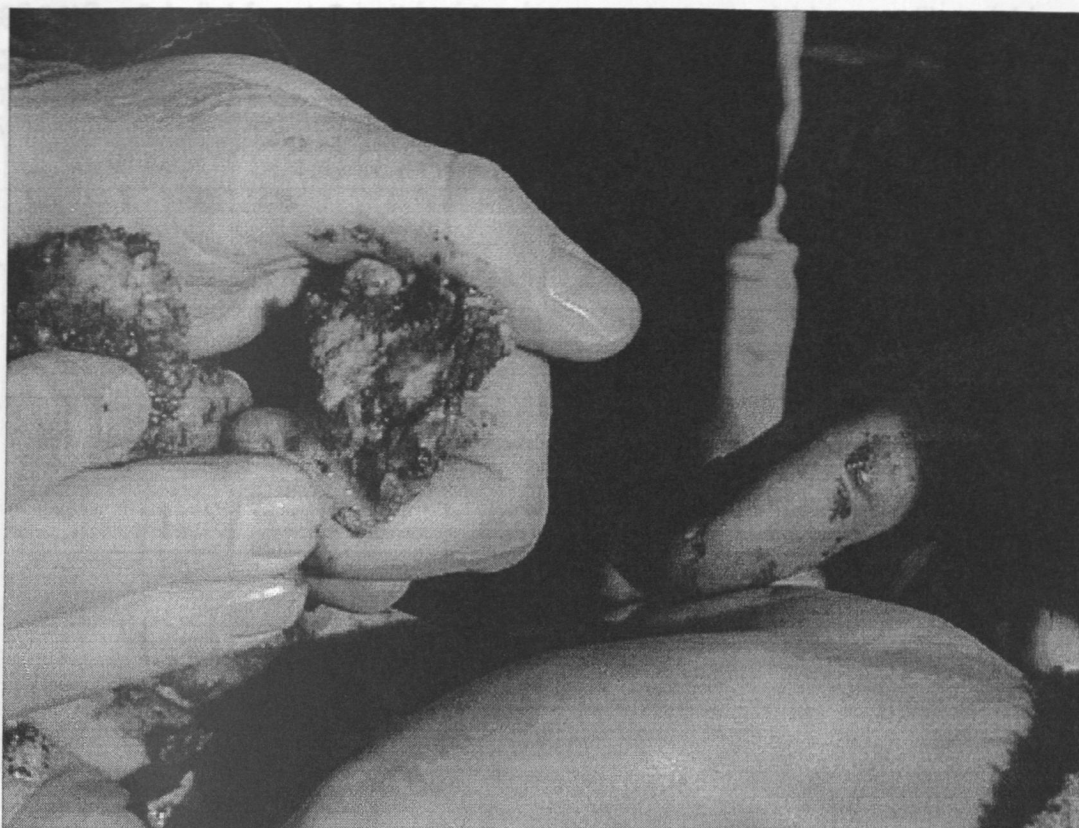


Fig. 82: Nodular gas hydrate specimen from a sediment core of the Sorokin Trough.

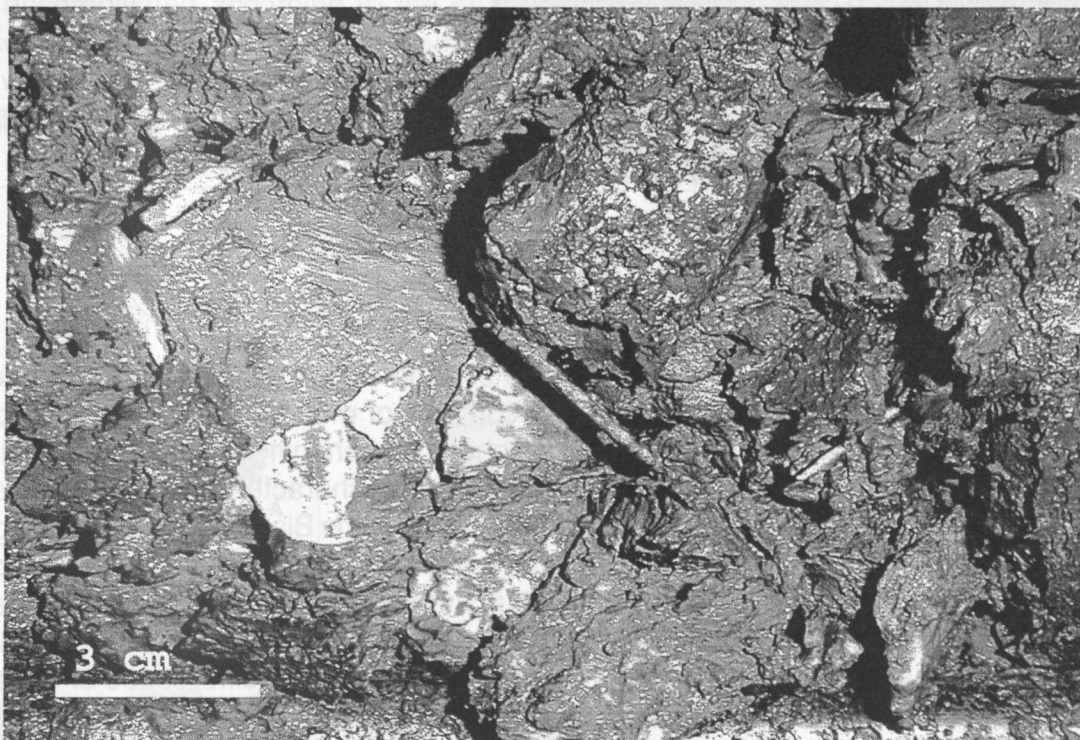


Fig. 83: Gas hydrate plates in sediments from the Sorokin Trough.

The rapid handling could be tested on a core from the Odessa mud flow (35 GC-4). Unfortunately the core did not even show degassing. For this reason it was not frozen to save liquid nitrogen. The second core from the Odessa mud flow (50 GC-5) was frozen within 6 minutes after retrieval. A statement regarding the hydrate content cannot yet be made but the core showed extensive degassing.

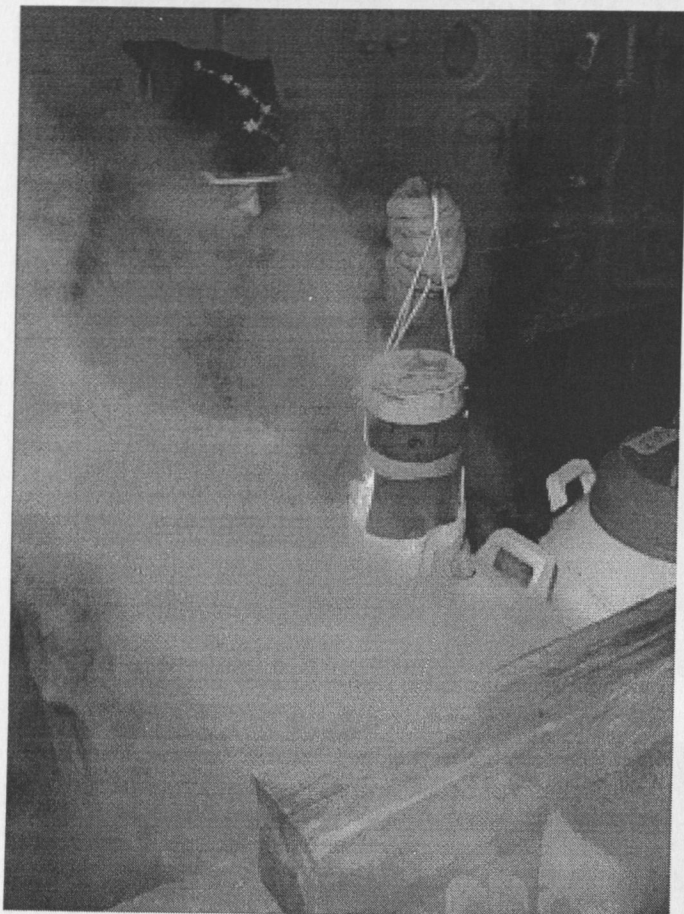


Fig. 84:  
Freezing of a core section in liquid nitrogen for later CT work in the lab.

#### 10.4 Hydrocarbons

V. Blinova, G. Aloisi, F. Abegg, M. Ivanov

The Black Sea is the largest anoxic basin of the world and a very interesting region in particular for geochemical investigations. The complex of mud breccia, hemipelagic and slope sediments indicates an activity of mud volcanoes and ongoing development of diapirs in this region. A lot of subsamples were gas-saturated and characterized by a strong smell of  $H_2S$ . In general, 3 mud volcanoes in the Sorokin Trough of the Black Sea were investigated and more than 50 samples of gas and sediments from the 9 cores were taken for detail geochemical studies (Table 8). The main objective of this study is to determine the composition and concentration of the hydrocarbon gas in sediments and its possible relation to seep fluids. Thus one of the targets of this work is to clarify the differences of the origin of gas from active vents and from background sediments. The intensity of the gas fluxes and ways of their migration from deep sources will be studied.

Routine analyses of the gas in sediments were performed on board. Subsampling of the gas phase was done by bulk methods, using syringe without a tip. Samples were taken



Table 8: Sample list for geochemical analyses.

ID	Station No	Mud volcano	Latitude	Longitude	Sediments	Rock clasts	Gas hydrates	Gas occurrence	Depth (m)	Recovery (cm)
1	M52-1#34 TGC-2	Dvurechenskii	44° 16.96	34° 58.95	Mud breccia	+	+	+	2074	365
2	M52-1#37 TGC-4	Dvurechenskii	44° 17.13	34° 58.99	Mud breccia	+	+	+	2073	580
3	M52-1#38 TGC-5	Dvurechenskii	44° 17.00	34° 59.18	Mud breccia	+	+	+	2075	390
4	M52-1#39 TGC-6	Background	44° 14.03	34° 58.85	Peladgic sed	-	-	-	2161	310
5	M52-1#48 TGC-7	Dvurechenskii	44° 16.85	34° 58.80	Mud breccia	+	+	+	2087	500
6	M52-1#49 TGC-8	Dvurechenskii	44° 16.95	34° 58.63	Mud breccia	+	+	+	2087	480
7	M52-1#53 GC-7	Sevastopol	44° 14.31	34° 45.32	Peladgic sed	-	-	+	2128	320
8	M52-1#54 GC-8	Sevastopol	44° 14.23	34° 45.39	Peladgic sed, sapropel	+	-	+	2129	402
9	M52-1#55 GC-9	Jalta	44° 14.56	34° 47.06	Peladgic sed	-	-	+	2127	165

from the different lithological layers of the core. First, some vials were filled with salt (NaCl) solution (Fig. 85b). Then, before the coring operation, vial 1 was filled with 50ml of distilled water (Fig. 85a). After that the sediment was put into vial 1. After subsampling, the degassing was accomplished according to the head-space analysis, which is based on achieving phase equilibrium conditions between gas and water phases according to Henry's law. Afterwards, the gas phase was transported from the vial 1 into special bottles with salt solution (Fig. 85c). These bottles with gas were stored upside down.

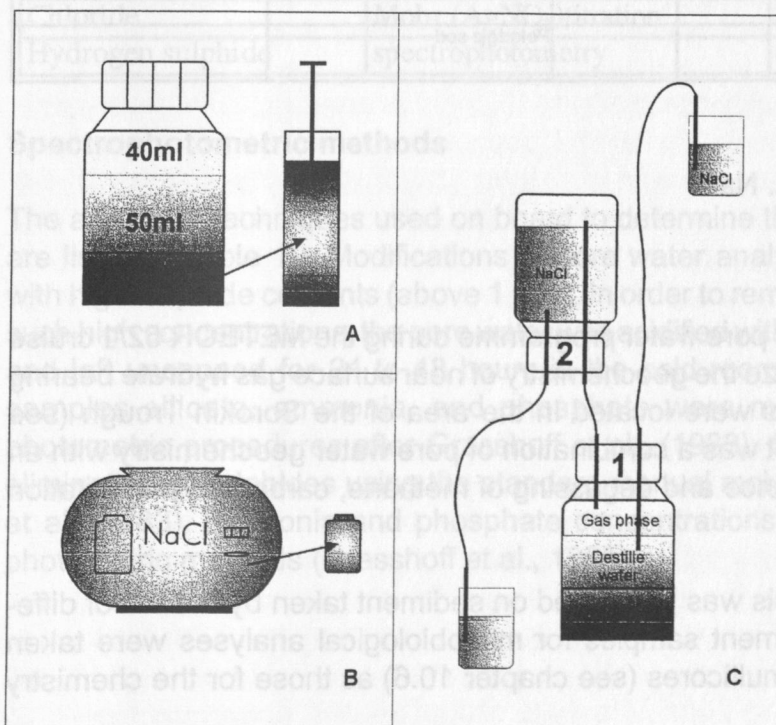


Fig. 85:  
Methodology of gas  
subsampling.



The sediment samples for geochemical analyses of the organic matter were taken at the same intervals as the gas samples. About 50 g of wet sediment were taken for further fluorescent-bitumen analysis. The samples are to be dried at a temperature of about 600°. Bottom sediments will be studied by the following set of methods (Table 9):

- fluorescent analysis,
- determination of total organic carbon (TOC) content and
- chromatography analysis.

The concentration and composition of hydrocarbon gas will be measured using the gas chromatograph at the Moscow State University (MSU) laboratories. The components from C1 to C5 including saturated and unsaturated ones and their isomers are gauged. The isotopic composition of the gas phase will be taken from the most representative samples.

Table 9: Set of geochemical analyses of gas phase and sediments.

ID	Station No	Name of the Mud Volcano	GEOCHEMICAL ANALYSES			
			Gas analyses		Analyses of the Organic Matter	
			Gas from sediments	Gas hydrates	Total Organic Carbon contain (TOC)	Microscopic studies of rock clasts
1	M52-1#34 TGC-2	Dvurechenskii	+	+	Mud breccia	+
2	M52-1#37 TGC-4	Dvurechenskii	+	+	Mud breccia	+
3	M52-1#38 TGC-5	Dvurechenskii	+	+	Mud breccia	+
4	M52-1#39 TGC-6	Background	+		Peladgic sed	-
5	M52-1#48 TGC-7	Dvurechenskii	+	+	Mud breccia	+
6	M52-1#49 TGC-8	Dvurechenskii	+	+	Mud breccia	+
7	M52-1#53 GC-7	Sevastopol	+		Peladgic sed	-
8	M52-1#54 GC-8	Sevastopol	+		Peladgic sed, sapropel	+
9	M52-1#55 GC-9	Jalta	+		Peladgic sed	-

## 10.5 Pore Water Chemistry

M. Drews, B. Domeyer, K. Naß

### 10.5.1 Introduction

The objective of the geochemistry pore water programme during the METEOR 52/1 cruise in the Black Sea was to characterize the geochemistry of near surface gas hydrate bearing sediments. The sampling stations were located in the area of the Sorokin Trough (see chapter 10.2). Of particular interest was a combination of pore water geochemistry with an inspection of gas hydrate occurrence and degassing of methane, carbonate precipitation and microbiological activity.

A geochemical pore water analysis was performed on sediment taken by means of different sampling devices. The sediment samples for microbiological analyses were taken from the same cores or parallel multicores (see chapter 10.6) as those for the chemistry programme.

### 10.5.2 Samples and analytical methods

Sediment samples were taken with the video-guided multicorer (TV-MUC), the standard multicorer (MIC), the video-guided sediment grab (TVG), and the 3 or 6 m long gravity corer (GC, TGC). Undisturbed surface sediment could only be sampled with the multicorer. The laboratory consisted of a vented  $\text{H}_2\text{S}$ -container with cooling system. Using a mechanical polypropylen press pore water was squeezed from the sediment through  $0,2\ \mu\text{m}$  cellulose acetate membrane filters at  $6^\circ\text{C}$  and a maximum pressure of 3 bar using argon gas. Sediment from the multicorer was cut into 1–3 cm slices; gravity core samples were taken in 10–30 cm intervals with a spatula immediately after opening the core.

The types of analyses performed on the pore water are listed in Table 9. The same methods have been applied for analysis of pore water at gas hydrate sites on Hydrate Ridge in the Cascadia convergent margin (Linke and Suess, 2000).

In addition water samples were collected with the CTD rosette sampler. Subsamples were fixated for  $\text{H}_2\text{S}$  analysis almost immediately after opening the Niskin bottles. These samples were used to obtain chloride and calcium background values. The pH, alkalinity, and  $\text{H}_2\text{S}$  concentrations were determined almost immediately after the pore water samples had been collected in order to avoid artifacts from outgassing of  $\text{H}_2\text{S}$  during long-time storage.

Table 10: Techniques used on board for pore water analysis on freshly gained samples.

Constituent	Method	Reference
Alkalinity	Titration	Ivanenkov and Layakhin (1978)
pH value	2-point titration	Dickson (1993)
Ammonium	spectrophotometry	Grasshoff <i>et al.</i> (1983)
Calcium	EDTA titration	Gieskes <i>et al.</i> (1991)
Phosphate	spectrophotometry	Grasshoff <i>et al.</i> (1983)
Silicate	spectrophotometry	Grasshoff <i>et al.</i> (1983)
Chloride	Mohr ( $\text{AgNO}_3$ ) titration	Gieskes <i>et al.</i> (1991)
Hydrogen sulphide	spectrophotometry	Grasshoff <i>et al.</i> (1983)

### Spectrophotometric methods

The analytical techniques used on board to determine the various dissolved components are listed in Table 10. Modifications of pore water analysis were necessary for samples with high sulphide contents (above 1 mM). In order to remove  $\text{H}_2\text{S}$  from samples containing such high concentrations, the pore water was acidified with suprapure HCl ( $10\ \mu\text{l}/\text{ml}$  sample) and left uncapped for 24 to 48 hours in the cold room ( $4^\circ\text{C}$ ). In these then degassed samples silicate, ammonia, and phosphate were measured applying the standard photometric procedures after Grasshoff *et al.*, (1983). Silicate was determined after the elimination of sulphides using the standard manual molybdenum blue method (Grasshoff *et al.*, 1983). Ammonia and phosphate concentrations were measured using standard photometric methods (Grasshoff *et al.*, 1983).

## Titration methods for calcium and chloride

Calcium titrations are almost unaffected by high sulphide concentrations and can be applied as described by Gieskes et al. (1991). Contrasting this, to perform chloride titrations with silver nitrate, samples with  $\text{H}_2\text{S}$  concentrations of more than 1 mM must be pretreated since otherwise measurements are corrupted by the precipitation of  $\text{Ag}_2\text{S}$ . To remove the  $\text{H}_2\text{S}$ , the pore water samples were diluted 1:1 with 0.01 N suprapure  $\text{HNO}_3$  and the samples were degassed overnight in the cold room in open vials.

## Total alkalinity (TA) and pH value

Total Alkalinity measurements were performed by direct titration of 1 ml pore water with 0.02 N HCl in an open cell (Ivanenkov and Lyakhin, 1978). The acid was standardized using a IAPSO seawater solution.

A standard pH electrode was used for the determination of pH in the sediment subsample at 4°C in the cold room. The electrode was calibrated using a buffer prepared in artificial seawater (Dickson, 1993). For calibration BIS and 2-Aminopyridine were used as buffers in the neutral pH range (pH 7 to 9).

## Analysis at the home laboratory

Acidified subsamples of the pore water (10  $\mu\text{l}$  HCl (30 %) / 1 ml sample) were prepared for ICP analysis (atomic emission spectroscopy with inductively coupled plasma) of major cations (Na, K, Mg, Li, Ca, Sr and Mn). Concentrations of sulfate, bromide and DIC will be determined on selected subsamples in the home laboratory. The remaining squeezed sediment will be used for C/N/S analysis with a Carlo Erba Element Analyser. A complete list of pore water samples, water samples and geochemical analyses performed on board is shown in Table 11.

### 10.5.4 Preliminary Results and Discussion

A total of 5 mini-multicores, 2 TV-guided multicores, 10 gravity cores and 3 TV grabs were retrieved from which pore water was analysed for its constituents (Table 7). The results of the CTD water sample analysis are described in chapter 11 of this volume. A summary on the cores with the amount of samples and geochemical analyses performed on board is given in Table 11. Selected depth profiles of chemical constituents in pore waters are given in Figure 86 to 89 and discussed in this section.

## Dvurechenskii mud volcano

The area of the Dvurechenskii mud volcano in the Sorokin Trough was sampled intensively. The central summit of this mud volcano resembles station 36 where a gravity core brought up sediment with a core length of 275 cm and a multicorer obtained adjacent undisturbed sediment surface. The sediment showed heavy degassing of methane, which appeared in the form of soaring bubbles. A combined pore water profile from the multicorer and the gravity core samples is shown in Figure 86. Sulphide is found only up to 15 cm depth with a maximum value just below the surface. At this station we were able to gain a sediment core which enclosed the transition zone of sulfate reduction and anaerobic methane



Table 11: Number of samples taken from cores and analyses performed on board.

Sample	PO <sub>4</sub> [μM]	NH <sub>4</sub> [μM]	H <sub>2</sub> S [μM]	Cl [mM]	TA [mM]	SiO <sub>2</sub> [mM]	Ca [mM]	pH sedi- ment	analyse d depth [cm]	No.* of samples
15-2 GC-2	x	x	x	x	x	x		x	63	5
8 TVG	x	x	x	x	x	x		x	?	2
11 TVG	x	x	x	x	x	x		x	?	4
18-1 TGC-1	x	x	x	x	x	x	x	x	362	21
6-1 TV MUC-1	x	x	x	x	x	x		x	45	20
6-2 TV MUC-2	x	x	x	x	x	x		x	46	20
34-1 TGC-2	x	x	x	x	x	x		x	355	15
35-1 MIC-2	x	x	x	x	x	x		x	37	20
36-1 TGC-3	x	x	x	x	x	x		x	275	14
36-2 MIC-3	x	x	x	x	x	x		x	27	17
37-1 TGC-4	x	x	x	x	x	x		x	304	14
38-1 TGC-5	x	x	x	x	x	x		x	290	11
39-1 TGC-6	x	x	x	x	x	x		x	315	14
43 TVG	x		x	x					?	2
48-1 TGC-7	x	x	x	x	x	x		x	487	18
48-2 MIC-4	x	x	x	x	x	x		x	28	17
49-1 TGC-8	x	x	x	x	x	x		x	484	17
49-2 MIC-5	x	x	x	x	x	x		x	39	21
50-2 MIC-6	x	x	x	x	x	x		x	38	21
54-1 GC-8	x	x	x	x	x	x		x	400	13
									total	286
CTD 15			x	x			x			12
CTD 29			x							12

\*The numbers for TV MUC and MIC samples include one bottom water sample.

oxidation. The core will be further analyzed for sulfate distribution, microbial sulfate reduction and anaerobic methane oxidation activity (see Chapter 10.6).

The depth profiles of chloride in the multicorer sediment at the stations 36-2 MIC (Figure 86) and 48-2 MIC show a remarkable anomaly with lowest values at the surface and higher values at greater depth. The steady increase of chloride concentration with depth indicates a chloride source and brine flux in deeper layers. Gravity cores from the same stations show equally high chloride concentrations (of about 850 mM) at all depths. Similar results were obtained at stations 34-1 (TGC-1), 48 (48-1 TGC, 48-2 MIC) and 49 (49-1 TGC, 49-2 MIC, see Figure 87). Besides ascending brine fluids salt exclusion during gas hydrate formation may be considered as a cause for up to 2.5-fold chloride concentrations in the pore water compared to the free bottom water. Specimens of gas hydrate were found in cores from stations 34-1, 36-2, 37, and 38, (see chapter 10.3), hinting at the original high content of gas hydrate in the sediment which for the most part had decomposed before the samples could be taken on board.

Hydrogen carbonate concentrations and therefore the total alkalinity increase with sediment depth as a consequence of anaerobic methane oxidation. Carbonate precipitation is induced by the production of carbonate alkalinity during anaerobic methane oxidation.

A very remarkable finding at Dvurechenskii mud volcano was the high ammonia concentration with values reaching more than 20 mM (Fig. 86). The depth profile shows about the same shape as the chloride profile which leads to the assumption that the outflowing mud takes with it brine containing ammonia as an anaerobic degradation product of organic matter.

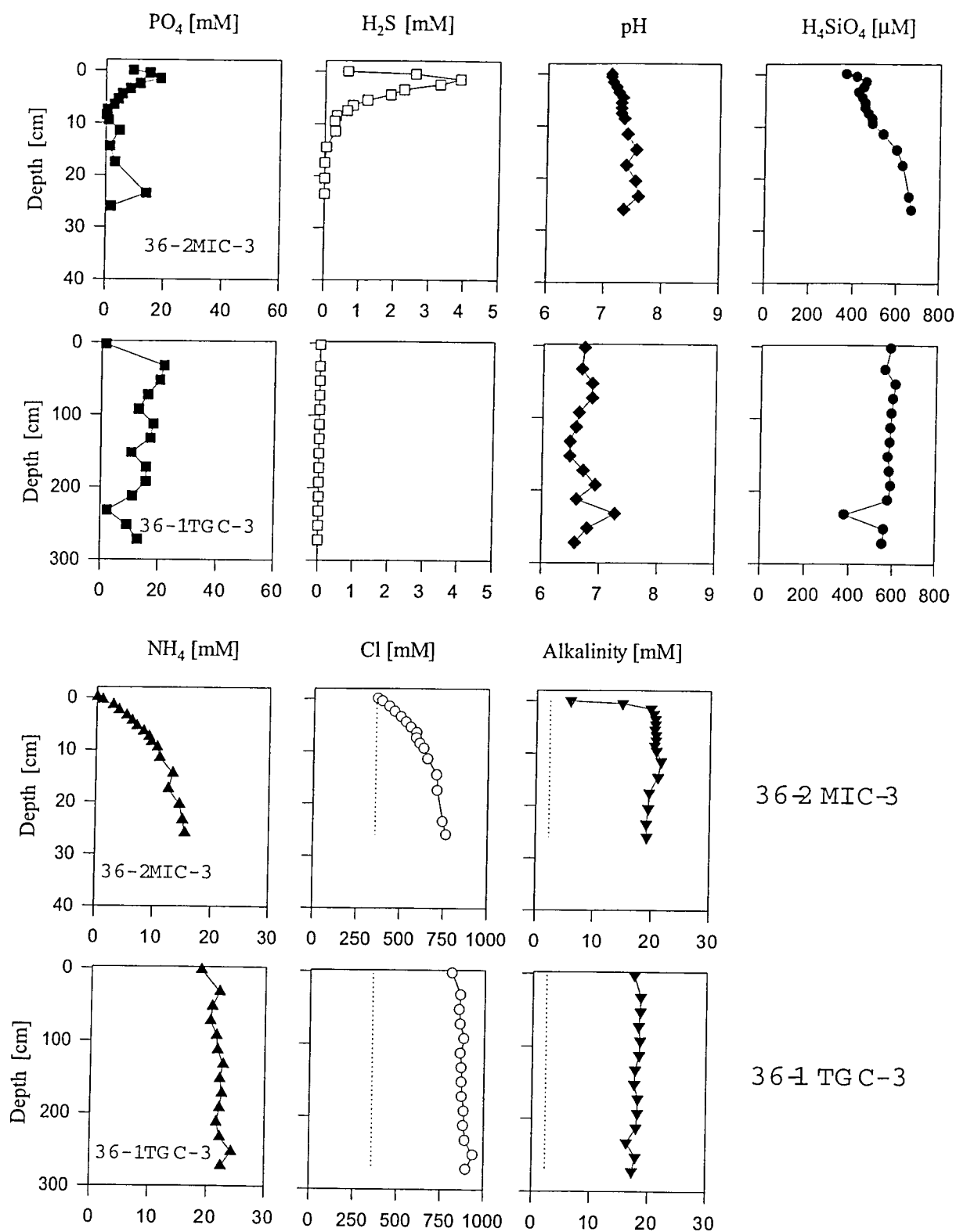


Fig. 86: Pore water chemistry of 36-1 TGC and 36-2 MIC at Dvurechensii mud volcano centre.

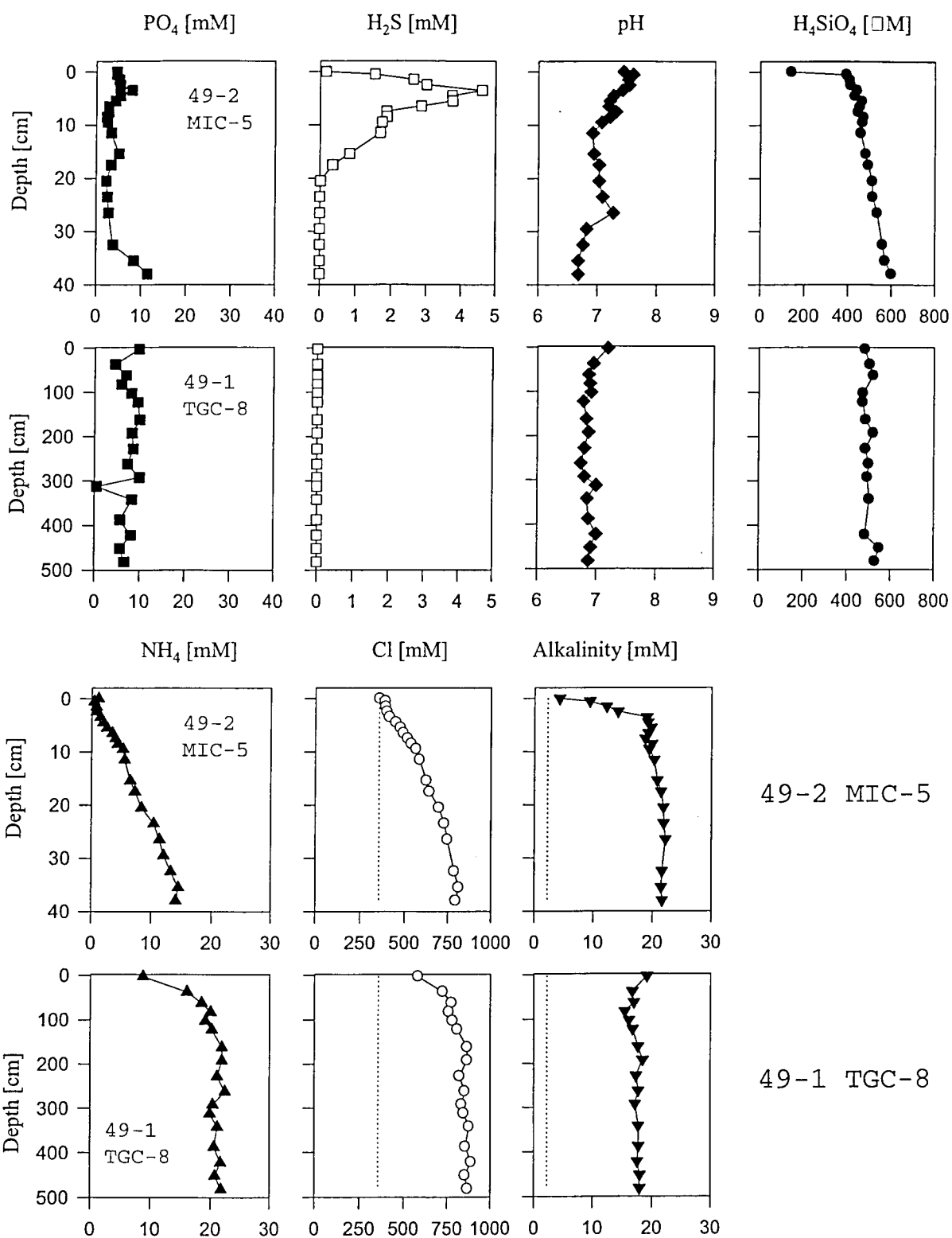


Fig. 87: Pore water chemistry of 49-TGC and 49-2 MIC at Dvurechenskii mud volcano.



## Sites at Odessa mud volcano

The pore water profiles of stations 35-1 MIC, 6-1 and 6-2 TV MUC-1 (Figure 88) in the southern area of Odessa mud volcano do not show a chloride anomaly and hence no brine influence. At these sites the ammonia concentration remained below 200  $\mu\text{M}$ , which is two orders of magnitude lower than at Dvurechenskii mud volcano. Alkalinity reached 6 mM in deeper layers, much less than at Dvurechenskii mud volcano (maximum 22 mM at 49-2 MIC).

Chloride concentrations lower than normal bottom water concentrations—a negative chloride anomaly—were observed in the core from station 18-1 TGC (eastern slope of Odessa mud volcano). Here the probable cause is dissociation of gas hydrates and the release of diluting fresh water into the sediment. A negative chloride anomaly was also found at site 15-2 GC (unnamed mud volcano). In the cores from these two stations 15-2 GC and 18-1 TGC, pieces of gas hydrate a few centimeters thick were found (see chapter 10.3), leading to the assumption of high gas hydrate contents in the sediments.

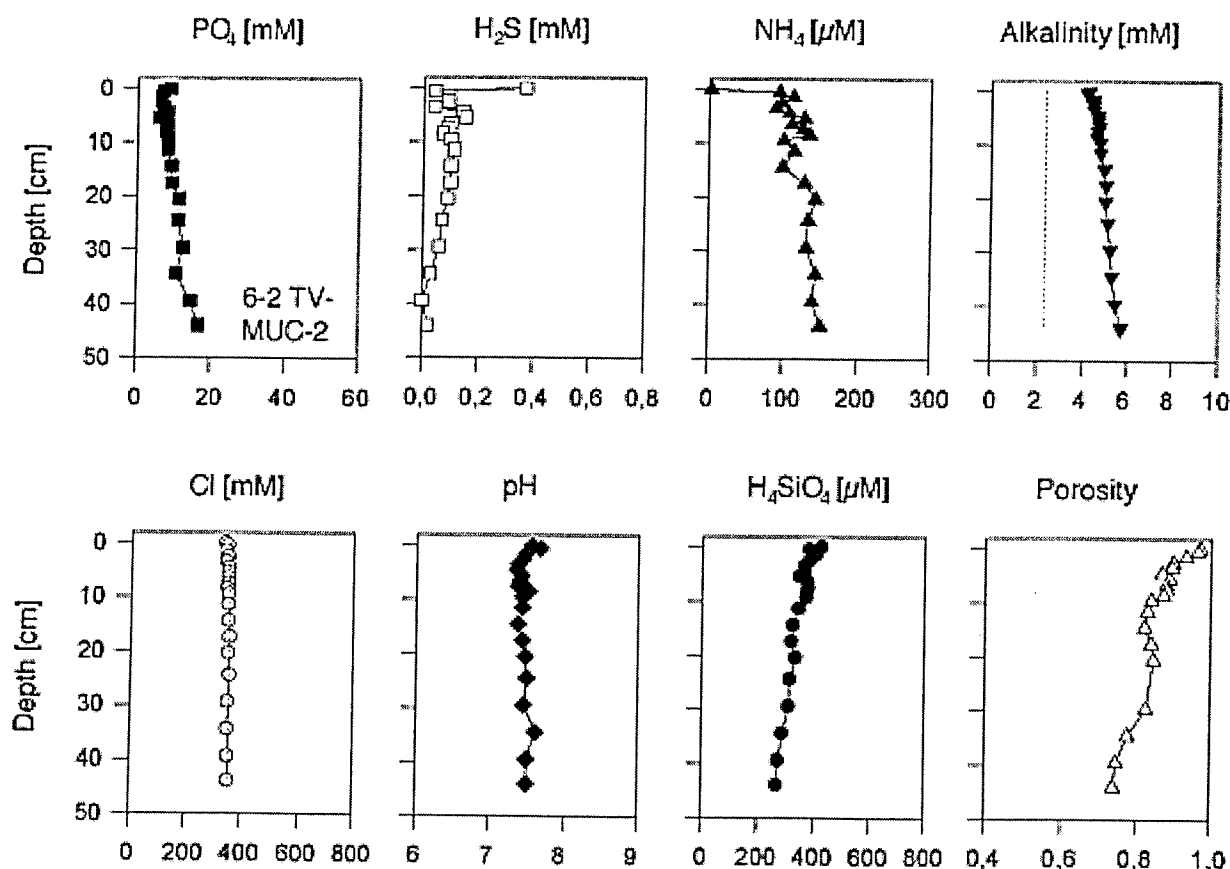


Fig. 88: Pore water chemistry of 6-2 TV-MUC at the southern slope of Odessa mud volcano.

## Reference site south of Dvurechenskii mud volcano

The core from the reference site 39-1 TGC (Figure 89) showed no degassing, but it was the only one of those recovered containing debris including Bivalve shell layers. The chloride concentration profile showed a uniform decrease from sediment surface to depth as the result of diffusion of the now salty bottom water into deeper layers, where limnic sediments

were once deposited. Sulfide occurred to up to 123 cm depth, where a stratum boundary was found. The alkalinity increased from the surface to 15 mM, but below 123 cm it decreased as well as the silicate concentration and pH values.

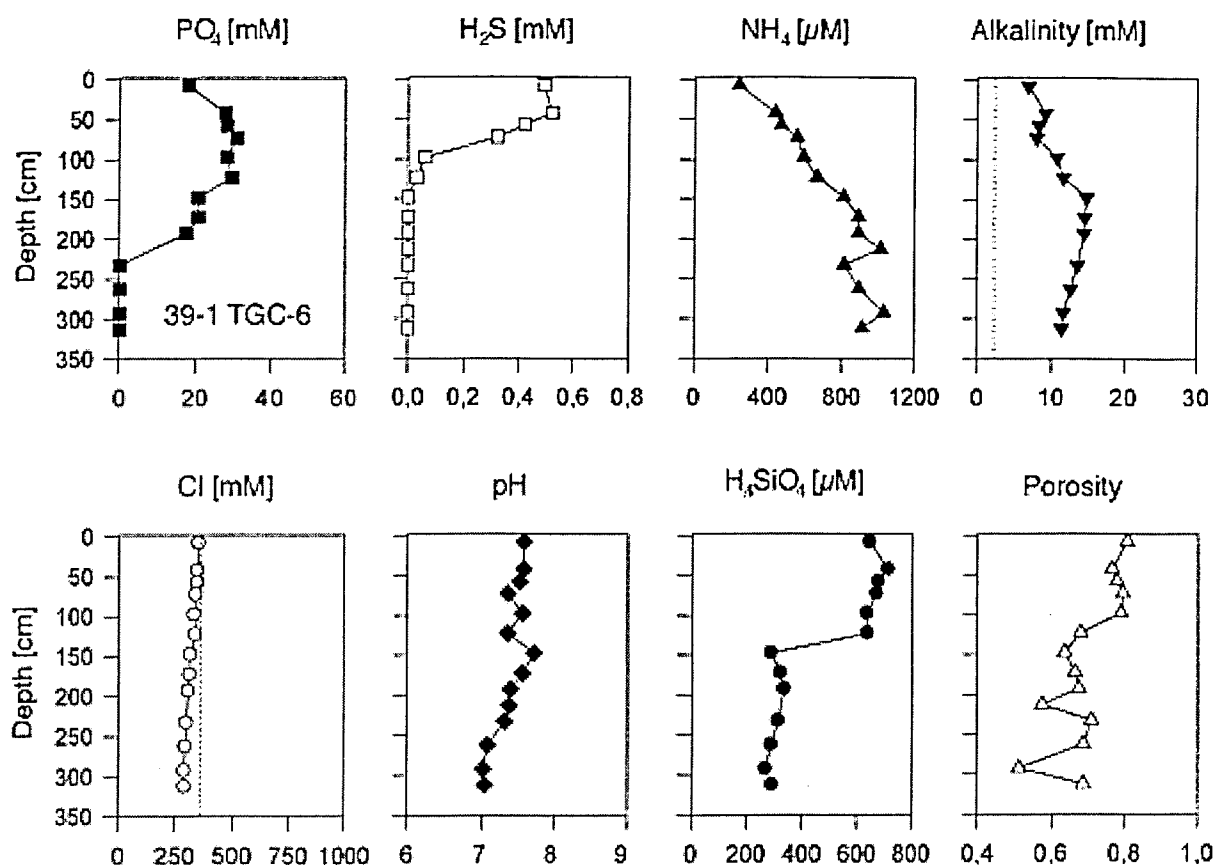


Fig. 89: Pore water chemistry of the reference station 39-1 TGC in the southern area of Odessa mud volcano.

## 10.6 Microbiological investigations at gas hydrate sites

M. Drews, G. Aloisi

### 10.6.1 Introduction

Interest in anaerobic methane oxidation has recently been revived by the identification of methane-consuming archaea at cold seeps in the Eel River basin (Hinrichs et al., 1999) and their direct visualisation in consortium with sulfate reducing bacteria at cold seeps on Hydrate Ridge (Boetius et al., 2000). At these sites, microbially mediated anaerobic methane oxidation occurs at the sulphate-methane transition zone, where methane released from near surface gas hydrates (a few cms to dms deep) meets the sulfate diffusing from bottom waters into the sediment. The resulting rates of bacterial sulfate reduction, and thus of methane oxidation, at the Hydrate Ridge site are the highest ever recorded (Boetius et al., 2000). Microbial anaerobic methane oxidation produces carbonate alkalinity and typically results in the precipitation of authigenic carbonate crusts which are widespread at seafloor cold-seeps worldwide.

In order to investigate quantitatively anaerobic methane oxidation processes in the Black Sea and the role of microorganisms in carbonate diagenesis, a variety of shore-based

microbiological investigations are planned to be carried out parallel to the pore water geochemical investigations. In this section we give a preliminary description of discrete microbial occurrences at the studied sites, introduce the rationale of the sampling and describe the planned investigations.

## 10.6.2 Sampling

The sediments, bacterial mats, and authigenic carbonates for microbiological investigations are listed in Table 12. On the basis of pore water chemical profiles produced on board (see chapter 10.5), sediments from 10 active sites where near-surface gas hydrates occur have been chosen for microbiological sampling in shore-based investigations. Obvious indicators

Table 12: Subsamples for shore-based microbiological and lipid biomarker analysis. Investigators are abbreviated as follows: LPCM - Laboratoire de Physique et Chimie Marines, Paris, France; Bristol - Organic Geochemistry unit, School of Chemistry, Bristol, England; MPI - Max Plank Institute for Marine Microbiology, Bremen, Germany.

Station	Instrument	Seafloor feature	Sample type	Preparation	Storing T (°C)	Investigation	Investigator
6-1	TV-MUC-1	Slope S of Odessa	1 whole core	-	-20	Lipids/Phylog. analysis	LPCM/Bristol/MPI
			Sediment	See text	4	CH <sub>4</sub> oxidation /SO <sub>4</sub> <sup>2-</sup> reduction rates	GEOMAR
6-2	TV-MUC-2	Slope S of Odessa	Sediment	See text	4	CH <sub>4</sub> oxidation /SO <sub>4</sub> <sup>2-</sup> reduction rates	GEOMAR
8	TVG-1	Odessa, SW flank	Sediment	See text	4	CH <sub>4</sub> oxidation /SO <sub>4</sub> <sup>2-</sup> reduction rates	GEOMAR
8	TVG-1	Odessa SW flank	White mat	Fixed	-20	FISH	MPI
			Greenish mat	Fixed	-20	FISH	MPI
			Black fibers	Fixed	-20	FISH	MPI
			White mat	Anoxic	4	Microb. culture work	MPI
			Greenish mat	Anoxic	4	Microb. culture work	MPI
			Black fibers	Anoxic	4	Microb. culture work	MPI
			Mat	Anoxic	4	Microb. culture work	MPI
			White mat	-	-20	Lipids	LPCM/Bristol
			Greenish mat	-	-20	Lipids	LPCM/Bristol
			Black fibers	-	-20	Lipids	LPCM/Bristol
			Crust	-	-20	Lipids	LPCM/Bristol
			Hemp. mud under crust	-	-20	Lipids	LPCM/Bristol
			Indurated hemp. mud under crust	-	-20	Lipids	LPCM/Bristol
			White mat	-	-20	Phylogenetic analysis	MPI
			Greenish mat	-	-20	Phylogenetic analysis	MPI
			Black fibers	-	-20	Phylogenetic analysis	MPI
			Crust with mat	-	-20	Phylogenetic analysis	MPI
			Hemp. mud under crust	-	-20	Lipids	LPCM/Bristol
			Indurated hemp. mud under crust	-	-20	Lipids	LPCM/Bristol
			Crust	-	-20	Lipids	LPCM/Bristol
			Mud breccia	-	-20	Lipids	LPCM/Bristol
			Crust	-	-20	Phylogenetic analysis	MPI
			Mud breccia	-	-20	Phylogenetic analysis	MPI
			Mud breccia	Anoxic	4	Microb. culture work	MPI
15-1	GC-1	Unnamed mud volcano	Sediment	See text	4	CH <sub>4</sub> oxidation /SO <sub>4</sub> <sup>2-</sup> reduction rates	GEOMAR
15-2	GC-2	Unnamed mud volcano	Mud breccia 30 cm	Anoxic	4	Microb. culture work	MPI
			Mud breccia 30 cm	-	-20	Lipids	LPCM/Bristol
			Mud breccia 30 cm	-	-20	Phylogenetic analysis	MPI
			Mud breccia 30 cm	Anoxic	4	Microb. culture work	MPI
18	TGC-1	Slope E of Odessa	Hemipelagic mud 0 cm	-	-20	Lipids/Phylog. analysis	LPCM/Bristol/MPI
			Hemipelagic mud 10 cm	-	-20	Lipids/Phylog. analysis	LPCM/Bristol/MPI
			Hemipelagic mud 20 cm	-	-20	Lipids/Phylog. analysis	LPCM/Bristol/MPI
			Hemipelagic mud 30 cm	-	-20	Lipids/Phylog. analysis	LPCM/Bristol/MPI
			Hemipelagic mud 40 cm	-	-20	Lipids/Phylog. analysis	LPCM/Bristol/MPI
			Crust at 20 cm	-	-20	Phylogenetic analysis	MPI
			Crust at 20 cm	-	-20	Lipids	LPCM/Bristol
			Crust at 20 cm	Anoxic	4	Microb. culture work	MPI
34-1	TGC-2	Dvurechenskii summit ESE	Sediment	See text	4	CH <sub>4</sub> oxidation /SO <sub>4</sub> <sup>2-</sup> reduction rates	GEOMAR
			Mud breccia 0 cm	-	-20	Lipids/Phylog. analysis	LPCM/Bristol/MPI
			Mud breccia 15 cm	-	-20	Lipids/Phylog. analysis	LPCM/Bristol/MPI
			Mud breccia 30 cm	-	-20	Lipids/Phylog. analysis	LPCM/Bristol/MPI
			Mud breccia 45 cm	-	-20	Lipids/Phylog. analysis	LPCM/Bristol/MPI
			Mud breccia 60 cm	-	-20	Lipids/Phylog. analysis	LPCM/Bristol/MPI
			Mud breccia 20 cm	Anoxic	4	Microb. culture work	MPI
35-1	MIC-2	Slope S of Odessa	1 whole core	-	-20	Lipids/Phylog. analysis	LPCM/Bristol/MPI
36-1	TGC-3	Dvurechenskii center	Mud breccia 0-15 cm	Anoxic	4	Microb. culture work	MPI
36-2	MIC-3	Dvurechenskii summit	Sediment	See text	4	CH <sub>4</sub> oxidation /SO <sub>4</sub> <sup>2-</sup> reduction rates	GEOMAR
49-1	TGC-8	Dvurechenskii summit W	Mud breccia 20-25 cm	Anoxic	4	Microb. culture work	MPI
			Mud breccia 20-25 cm	-	-20	Lipids	LPCM/Bristol
			Mud breccia 20-25 cm	-	-20	Phylogenetic analysis	MPI
			Mud breccia 20-25 cm	Fixed	-20	FISH	MPI
49-2	MIC-5	Dvurechenskii summit W	Sediment	See text	4	CH <sub>4</sub> oxidation /SO <sub>4</sub> <sup>2-</sup> reduction rates	GEOMAR
54	GC-8	Sebastopol mud volcano	Hemipelagic mud top 5 cm	Anoxic	4	Microb. culture work	MPI
			Hemipelagic mud top 5 cm	-	-20	Lipids	LPCM/Bristol
			Hemipelagic mud top 5 cm	-	-20	Phylogenetic analysis	MPI
59	TVG-5	Dvurechenskii summit W	3 mats	Fixed	-20	FISH	MPI
			3 mats + crusts	Fixed	-20	FISH	MPI
			2 mats + crusts	Anoxic	4	Microb. culture work	MPI
			Mat pieces	-	-20	Lipids	LPCM/Bristol
			Mat pieces	-	-20	Phylogenetic analysis	MPI
			2 large crusts + mats	-	-20	Lipids	LPCM/Bristol
			Crust with bact. colonies in tubes	Anoxic	4	Microb. culture work	MPI
			Crust with bact. colonies in tubes	-	-20	Lipids/Phylog. analysis	LPCM/Bristol/MPI
			Bacterial mat pore water	-	4	SO <sub>4</sub> <sup>2-</sup> , Cl <sup>-</sup>	GEOMAR
			Bacterial mat pore water	Acidified	4	ICP	GEOMAR
			Sediment	See text	4	CH <sub>4</sub> oxidation /SO <sub>4</sub> <sup>2-</sup> reduction rates	GEOMAR



for zones of anaerobic methane oxidation were high concentrations of sulphide in the upper layer. In sediments from station 18 TVG-1, 36-2 MIC-3 and 49-2 MIC-5, for example, pore water sulphide concentrations decreased from the sediment/water interface to the deeper degassing layers, which indicates that the anaerobic methane oxidation zone is located safely within the recovered sediment cores. Activity measurements will reaffirm this presumption back in the home laboratory. The cores from stations 6-1 and 6-2 TV-MUC were chosen for reference. Here, the sediments showed no degassing and no evidence for gas hydrates. In addition, discrete occurrences of microbial mats, aggregates and colonies associated to authigenic carbonate crusts were also sampled. These occurrences (see below) offer a unique chance to investigate microbe-mineral interactions at cold seeps.

### 10.6.3 On-board description of microbial occurrences

A preliminary examination and description of bacterial mats and colonies was done on board under the binocular (with magnifications of up to 50 times), including photographic documentation. Bacterial mats associated with carbonate crusts or in the sediment were discovered at three stations (8 TVG, 18 TVG-1, 59 TVG 5).

At first sight brownish to yellow slimy homogeneous bacterial mats showed up at surface fractures when station 8 TVG material was retrieved on deck. Below the carbonate crust sediment pieces showed a coating with a stiff mucus-like bacterial mat which was attached to the sediment fracture walls. This gave the idea of filled passages or channels through the sediment which were torn open and released the slimy substance when the grab uncharged.

The carbonate crusts of 8 TVG-1 and 18 TGC-1 were covered with another type of bacterial mat which was also mucus-like, but stiffer and had a spherical colony shape. These 2 to 3 mm thick colonies were of white to pink colour and clearly visible inside the crusts' pores.

The last TV-grab at station 59 TVG-5 yielded impressive 2 to 4 cm thick bacterial mats grown on carbonate crust pieces of up to 30 cm length (Fig. 90). Except for these pieces the grab contained no sediment. The mats were of a yellow to orange or pink color and comprised of a stiff gelatinous fabric.

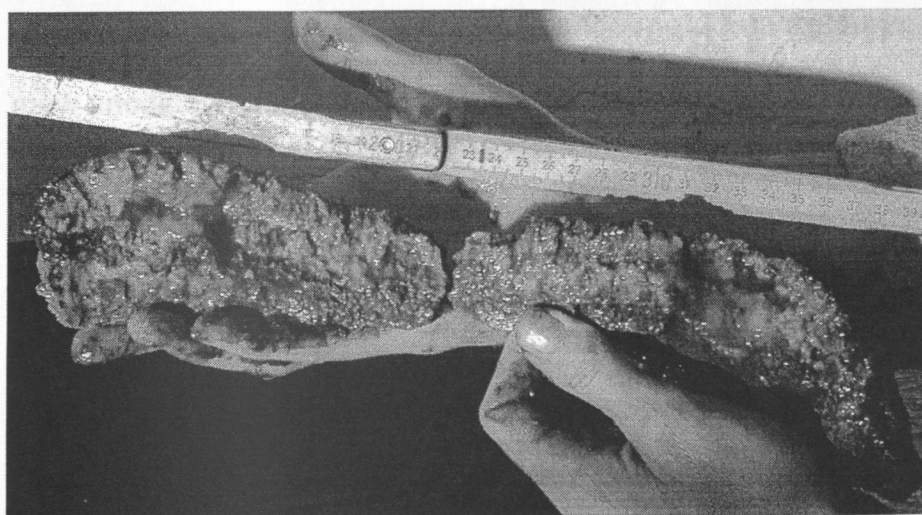


Fig. 90:  
Bacterial mats grown on carbonate crust pieces of up to 30 cm length were recovered at Station 59 TVG-5 (Yalta mud volcano). The 2 to 4 cm thick mats were of a yellow to orange or pink colour and comprised of a stiff gelatinous fabric.

The preparatory TV survey had shown crust structures on the sediment surface with mats mainly appearing as orange to pink homogeneous masses with a number of different colony types like the yellow one described above, but also white grainy forms.

At stations 6-1 and 6-2 MUG a light brown fluffy layer was found which consisted of incompletely degraded organic matter, partly plant fibres. This fluffy substance probably covers wide areas of the highly anoxic sediment bottom in the investigated area. At station 11 TVG mud breccia-like sediment was recovered, with no bacteria colonies visible when scrutinized under the binocular.

#### **10.6.4 Shore-based analysis and sample preparation**

##### **Sulfate reduction and methane oxidation rates**

To determine rates of bacterial sulfate reduction and anaerobic methane oxidation, parallel samples were investigated by adding the radio tracers  $^{35}\text{SO}_4$  and  $^{14}\text{CH}_4$ . The tracers were injected into subsamples obtained in cut off syringes which were plugged with a rubber stopper and sealed with parafilm. These samples were incubated at 6°C in darkness in an argon atmosphere for 24 h. After incubation, the sediment subcores were cut into 1 to 4 cm slices and mixed with zinc acetate (20 % w/w) to stop bacterial sulfate reduction and fix sulphide. To stop methane oxidizing activity the sediment samples were fixed with sodium hydroxide (1 mM).

Almost pure bacterial mat material was incubated in sterile anoxic bottom water and treated likewise. The samples will be analysed in the home laboratory to determine reduction and oxidation rates. Selected subsamples were taken for elemental sulfur concentration and sulfur isotope analysis.

##### **Biomass determination**

At the same sediment depths additional samples were taken for biomass analysis including microorganisms and meiofauna in the home laboratory, using the phospholipide extraction method.

##### **Microbial community structure and biogeochemical investigations**

Bacterial mat, sediment, and crust samples for enrichment cultures and isolations were stored at 4°C without headspace in anoxic Black Sea water, which had been collected during hydrocasts. Similar samples were frozen at -20°C for lipid biomarker analysis and phylogenetic surveys.

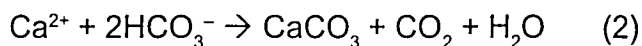
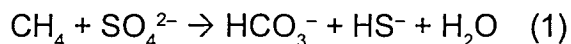
##### **Microscopical investigations**

Samples from bacterial mat substance, crusts, and sediment were fixed in formaline (4 %) for microscopic analysis, in particular Fluorescence In Situ Hybridisation (FISH), and for SEM and TEM observations.

### 10.6.5 Discussion

The bacterial mats discovered during this cruise were probably of the same type Pimenov et al. (1997) described as coral-like structured mats which overgrow aragonite crusts in water depths of 150 to 190 m in the northwestern shelf methane seeping area in the Black Sea. Activity measurements combined with microscopic and radio isotopic investigations revealed anaerobic methane oxidation.

The intimate association of bacterial mats with precipitated carbonate leads to the presumption that these bacteria are those responsible for anaerobic methane oxidation (reaction 1), which results in the production of hydrogen carbonate.



Bicarbonate precipitates as calcium carbonate (reaction 2) in the reaction zone of methane from deeper layers and sulfate from the bottom water. Here, methane feeds the methane oxidating archaea whereas sulfate supplies the reducing partner.



## 11. SEAFLOOR TEMPERATURE MEASUREMENTS

Seafloor temperature measurements were made in conjunction with gravity coring at a total of 8 stations. The collected temperature data are primary information to estimate, at a regional scale, the thickness of the gas hydrate stability zone (GHSZ) in Sorokin Trough. They also point to contrasting thermal regimes of the Odessa and Dvurechenskii mud volcanoes, which probably relates to different stages of eruptive activity and fluid flow regime as well as different occurrences of gas hydrate in the two mud volcanoes.

Station TGC-1 was taken on a mud flow on the eastern flank of Odessa mud volcano. Six measurements, TGC-2 to 5, TGC-7 and TGC-8, were made on Dvurechenskii mud volcano. Station TGC-6 was made in an area of uniform sedimentation approximately 3 miles to the south of Dvurechenskii mud volcano. The latter was intended to provide a reference regional temperature gradient for Sorokin Trough. See Fig. 93 for a general location map of the measurements.

### 11.1 Method

#### 11.1.1 Temperature data acquisition

Four Ifremer/Micrel thermistor temperature sensors were attached to the lower part of a 5.7 m long coring pipe, with a 1 m spacing interval, at distances of 0.45 m, 1.45 m, 2.45 m and 3.45 m from the cutting edge of the corer. The thermistor sensors were mounted on outriggers which held them at a lateral distance of 6 cm away from the outer wall of the core pipe, thus ensuring that frictional heating along the core pipe during the coring procedure did not reach the sensors. The corer was kept in the sediment for a period of 6-10 mn at each station. The tension on the rope was continuously monitored while remaining on station in order to let enough wire out to avoid motion of the corer in the sediment and subsequent disturbances of the temperature records. Lowering the corer to the seafloor was usually stopped at 100-200 m above the seafloor for a short time interval of 2-3 mn to allow comparison of the temperature readings of the four thermistors in the water column and apply intercalibration corrections whenever needed. At each sensor, temperature was measured every 10 s.

#### 11.1.2 Control of verticality of corer

An additional sensor including a tiltmeter and a pressure gauge was attached to the upper part of the coring pipe, about 1 m above the uppermost temperature sensor. The tiltmeter was used to monitor the verticality of the coring pipe during temperature measurement in the sediment. Measurements were taken every 30 s.

#### 11.1.3 Determination of equilibrium temperatures

Equilibrium temperature values in the sediment were extrapolated from the transient temperature curves recorded over the 6-10 min time interval during which the corer was kept in the seafloor. This was achieved using a simple extrapolation law in  $1/t$ , where  $t$  is the time elapsed since penetration. In most cases, equilibrium sediment temperatures could be determined with an accuracy of a few millidegrees. A difficulty arose for stations

taken in the fluid mud in the axial part on top of the Dvurechenskii mud volcano. The temperature curves recorded there did not show a trend towards equilibrium values but instead indicated a continuous increase in temperature. This was interpreted as a consequence of a slow continuous movement of the corer down into the mud after penetration. In this particular case, equilibrium temperatures were simply derived from a visual inspection of the temperature curves.

## 11.2 Temperature data

Good quality data were collected at all stations. Table 13 and Figure 91 summarize the temperature data collected.

Table 13: Summary of seafloor temperature measurements taken during the MARGASCH expedition.

Station N°	Lat N deg°mn	Lon E deg°mn	Water Depth m	Water Temp °C	Penetration* m	Sed Temp °C	Temp Gradient 10-3 °C/m	Comments
<b>Eastern flank of Odessa Mud Volcano</b>								
18-TGC-1	44°23.01	35°9.25	1838	9.04	4.0	9.10-9.23		Non linear temperature profile
<b>Dvurechenskii Mud Volcano</b>								
34-TGC-2	44°16.96	34°58.95	2074	9.07	>6.90	16.35-16.40		Warm mud at constant temperature
36-TGC-3	44°17.00	34°58.86	2071	9.07	>5.30	15.61-16.32		Warm mud at near-constant temperature
37-TGC-4	44°17.13	34°58.99	2073	9.07	4.0	9.42-9.95	177	Linear temperature profile
38-TGC-5	44°17.00	34°59.18	2076	9.07	>5.30	11.32-12.25	310	Warm mud with gradient
48-TGC-7	44°16.85	34°58.80	2087	9.07	>5.30	16.40-16.45		Warm mud at constant temperature
49-TGC-8	44°16.95	34°58.63	2085	9.07	>6.90	11.18-12.19	270	Warm mud with gradient
<b>Sorokin Trough, Reference Station</b>								
39-TGC-6	44°14.03	34°58.86	2161	9.08	4.0	9.09-9.25	29	Linear temperature profile

\* Depth of penetration into the seafloor of the lowermost temperature sensor

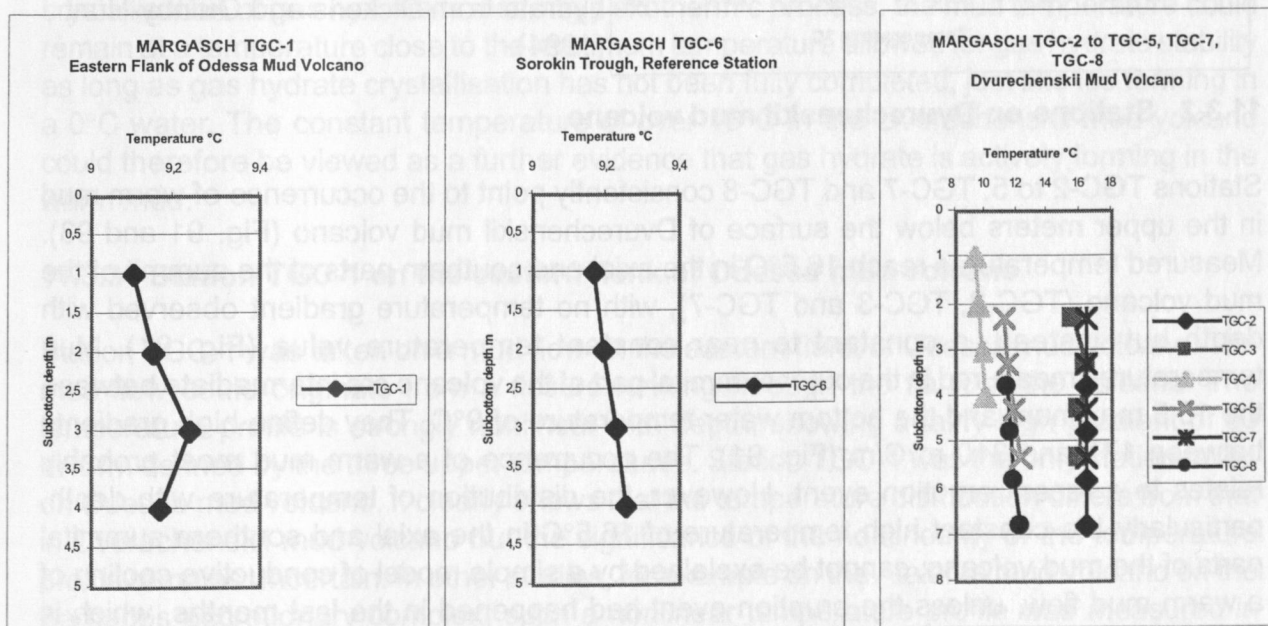


Fig. 91: Seafloor temperature profiles measured during the MARGASCH expedition.

### 11.3 Preliminary analysis

#### 11.3.1 Reference Station TGC-6

Station TGC 6 was taken in an area of smooth topography and laterally uniform sediment cover, about 3 miles south of Dvurechenskii mud volcano. The site was selected from an inspection of Parasound and seismic lines in the area. We measured a mean temperature gradient of  $29^{\circ}\text{C}/\text{km}$  at this station. Taking this value as an estimate of the regional temperature gradient in the study area, we inferred a potential thickness of the methane hydrate bearing sediment layer (GHSZ) of 400 m at a water depth of 2000 m (decreasing to nil at about 700 m water depth, Fig. 92).

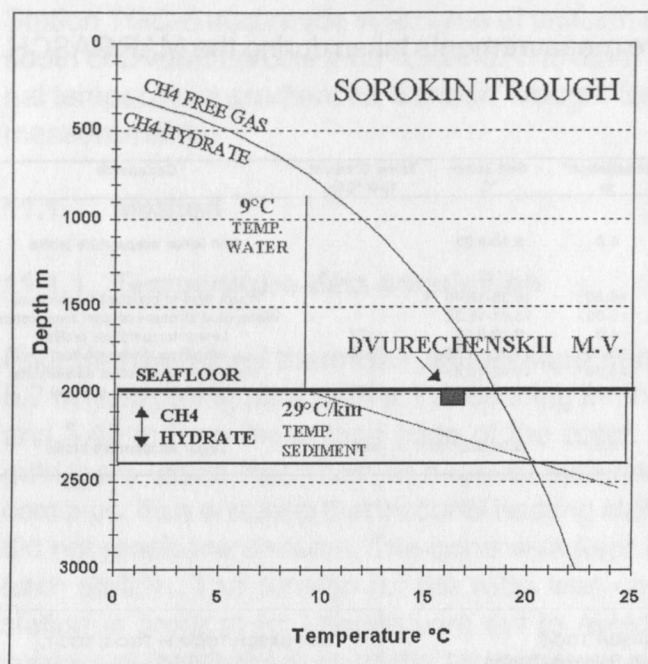


Fig. 92:

Gas hydrate stability zone at 2000 m water depth in Sorokin Trough as graphically inferred from a bottom water temperature of  $9^{\circ}\text{C}$  and a constant temperature gradient in sediment of  $29^{\circ}\text{C}/\text{km}$ . Stability curve for methane hydrate from Dickens and Quinby-Hunt (1994).

#### 11.3.2 Stations on Dvurechenskii mud volcano

Stations TGC-2 to 5, TGC-7 and TGC-8 consistently point to the occurrence of warm mud in the upper meters below the surface of Dvurechenskii mud volcano (Fig. 91 and 93). Measured temperatures reach  $16.5^{\circ}\text{C}$  in the axial and southern parts of the summit of the mud volcano (TGC-2, TGC-3 and TGC-7), with no temperature gradient observed with depth but, instead, a constant to near constant temperature value (Fig. 91). Mud temperatures measured in the outer summital part of the volcano are intermediate between the  $16.5$  maximum and the bottom water temperature of  $9^{\circ}\text{C}$ . They define high gradients between  $177$  and  $310 \text{ m}^{\circ}\text{C}/\text{m}$  (Fig. 91). The occurrence of a warm mud most probably relates to a recent eruption event. However, the distribution of temperature with depth, particularly the constant high temperature of  $16.5^{\circ}\text{C}$  in the axial and southern summital parts of the mud volcano, cannot be explained by a simple model of conductive cooling of a warm mud flow, unless the eruption event had happened in the last months, which is unlikely to be the case because the OFOS video survey showed the presence of a thin hemipelagic sediment cover on top of the erupted mud. Upward advection of warm fluid probably contributes to accounting for the temperature distribution. Evidence for fluid flow comes from OFOS observations of active seeps at the surface of the volcano.



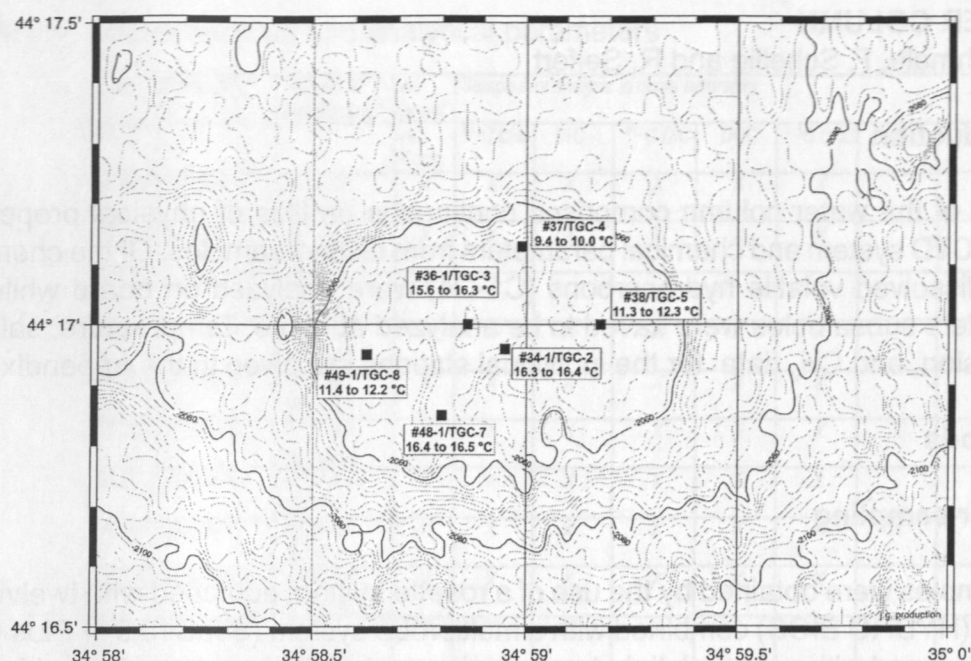


Fig. 93: Location map of seafloor temperature measurements taken on Dvurechenskii mud volcano with recorded mud temperatures.

It is worth noting that the 16.5°C constant high temperature lies close to the maximum temperature of 18°C for methane hydrate stability. This coincidence is probably not fortuitous. It suggests some interaction between the temperature distribution in the mud volcano and the dynamics of the gas hydrate system occurring there. Abundant small pieces of gas hydrate were found disseminated throughout all the cores recovered on Dvurechenskii mud volcano. Gas hydrate crystal growth could be an ongoing process in the mud. Because crystallisation of gas hydrate is a strongly exothermic process, the mud temperature could remain at a temperature close to the maximum temperature allowed for gas hydrate stability as long as gas hydrate crystallisation has not been fully completed, just like ice forming in a 0°C water. The constant temperature of over 16°C in the Dvurechenskii mud volcano could therefore be viewed as a further evidence that gas hydrate is actively forming in the warm mud.

### 11.3.3 Station TGC-1 on the eastern flank of Odessa mud volcano

Station TGC-1 was taken on a mud flow on the eastern flank of Odessa mud volcano. The mud flow could originate from a fissure running through the flank of the volcano. The temperature profile is strongly nonlinear with depth, showing a fairly high gradient of 60 m°C/m defined by the three upper temperatures. Station TGC-1 was the only station taken on Odessa mud volcano. It clearly shows that the temperature distribution differs from that in Dvurechenskii mud volcano but the significance of the nonlinearity of the temperature profile remains uncertain. In other studies, for example on the Atalante mud volcano on the Barbados accretionary complex, such a nonlinear temperature profile was measured in the outer part of the mud volcano and the abnormally low temperature was interpreted to result from gas hydrate dissociation. Odessa and Dvurechenskii mud volcanoes could then illustrate two different stages of the dynamics of gas hydrate systems in mud volcanoes, Dvurechenskii an early stage showing gas hydrate crystallisation and Odessa a late stage, showing gas hydrate dissociation.

## 12. WATER COLUMN

O. Schmale, F. Schellig and R. Seifert

### 12.1 Introduction

Investigations of the water column comprised continuous profiles of physical properties obtained by a CTD system and chemical parameters from distinct samples. Of the chemical parameters, dissolved volatile hydrocarbons (C1-C4) were analyzed on board while for other parameters subsamples were saved to be analyzed at home. Temperature, salinity, light transmission, and CH<sub>4</sub> data for the individual stations are given in the appendix.

### 12.2 Methods

#### 12.2.1 Water sampling

Sea water samples were obtained by the use of a rosette system equipped with twelve 12l Niskin bottles (HYDRO BIOS) combined with a multiprobe system (SeaBird 911 Plus CTD additionally equipped with a WetLab light transmission-meter). The system allowed for on-line observation of recorded data by the SeaBird software. CTD + light transmission profiles were recorded at all stations and a first processing was performed on board. All raw data were saved to be reprocessed at home.

Water samples were taken during the up-casts and sampling depth were chosen with respect to the information obtained during the down-casts. In general, the deepest sample was taken directly above the sediment after bottom contact was notified by a sensor positioned about 3 m below the CTD. Two additional samples were recovered within the water column 100 m above the bottom to record potential seeps. Within the upper part of the water column, samples were obtained from the upper light minimum (about 80 m depth) and close to the surface (2 m below the water surface) in most cases. Subsamples were taken for studies of planktonic organisms. During the cruise, a total number of 16 water stations were performed (Table 14).

136 water samples were analysed on board for concentration of dissolved hydrocarbons (C1–C4). Aliquots of these samples were saved for home-based analysis of the following parameters: Total inorganic carbon (DIC), total dissolved organic carbon (DOC),  $\delta^{13}\text{C}$ -methane,  $\delta^{13}\text{C}$ -DIC,  $\delta^{13}\text{C}$ -DOC. In addition, distinct stations were sampled for concentrations of noble gases ( $^3\text{He}$ ,  $^4\text{He}$ , Ne). At selected locations, high volume water samples were recovered and filtered on board for studies of particulate matter (POM). From the latter, a detailed investigation of biomarkers and their carbon isotope signature is envisaged.

### Dissolved hydrocarbons

Light dissolved hydrocarbons were analysed on board applying a "purge and trap" analytical technique. The analytical apparatus consists of two units, the stripping and trapping system (1) and the analytical and detection system (2).

Table 14: Water stations and analytical parameters

Date	Station No.	Latitude N° Longitude E°	on board	Samples for analysis in home laboratory						
			HC Conc.	$\delta^{13}\text{C CH}_4$	DIC	$\delta^{13}\text{C DIC}$	DOC	$\delta^{13}\text{C DOC}$	HE/NE	POM
2002										
04 Jan.	2-2 CTD-1	44°05.02 35°05.02	X	X	X	X	X	X		
04 Jan.	4 CTD-2	44°23.05 35°08.44	X	X	X	X	X	X		
05 Jan.	6-1 V-MUC	44°22.49 35°08.62	X							
06 Jan.	10 CTD-3	44°14.56 34°46.81	X	X	X	X	X	X		
09 Jan.	16 CTD-4	44°14.53 34°47.00	X	X	X	X	X	X		X
13 Jan.	25 CTD-5	43°31.99 33°06.99	X	X	X	X	X	X	X	
14 Jan.	27 CTD-6	43°31.99 33°07.07	X	X	X	X	X	X		X
14 Jan.	29 CTD-7	43°20.46 33°26.61	X	X	X	X	X	X	X	
17 Jan.	33-2 CTD-8	44°15.03 34°55.96	X	X	X	X	X	X		
18 Jan.	40-2 CTD-9	44°17.01 34°59.00	X	X	X	X	X	X	X	
19 Jan.	45-2 CTD-10	44°14.55 34°46.96	X	X	X	X	X	X		X
21 Jan.	47-2 CTD-11	44°16.96 34°58.62	X	X	X	X	X	X		
21 Jan.	49-2 MIC-5	44°16.97 34°58.61		X						
22 Jan.	51-2 CTD-12	44°14.29 34°47.01								X
27 Jan.	61-1 CTD-13	44°16.94 34°53.25	X	X	X	X	X	X		
27 Jan.	61-3 CTD-14	44°17.05 34°59.12	X	X	X	X	X	X		
28 Jan.	64 CTD-15	44°17.36 35°00.02	X	X	X	X	X	X		
29 Jan.	67-1 CTD-16	44°42.78 35°59.86	X	X	X	X	X	X	X	

(1) In the stripping system up to 200 ml of water sample are transported by pre-cleaned He from the gas tight and head space free sample bottle into a purge vial, where the sample is stripped by He for about 30 min. The analytes in the outflowing gas stream are concentrated in two cooled traps at -85°C. The first trap, filled with  $\text{Al}_2\text{O}_3$ , holds back all hydrocarbons except methane, which is gathered in the second trap, filled with activated charcoal. After the water sample has been degassed, the trapped gases are released by heating the traps to +85°C and carried to unit 2.

(2) A gaschromatograph (CARLO ERBA GC 6000) equipped with a packed (activated  $\text{Al}_2\text{O}_3$ ) stainless steel column and a flame ionisation detector (FID) was used to separate, detect and quantify individual components. The GC temperature was 140°C, carrier gas: He. The results were recorded and calculated using a PC operated integration system (BRUKER Chrom Star).

Analyses were generally done within 12 hrs after sampling. The whole unit is designed as a two channel apparatus for shorter analytical running time and analytical procedures were calibrated daily with commercial gas standards (LINDE).



## **Noble gases**

For onshore measurements of the He and Ne concentrations and isotopic signature, 48 water samples were taken immediately after finishing the respective hydrocast station. The samples were sealed head space free and gastight in copper tubes. Measurements are planned to be performed at the Universität Bremen, Fachbereich 1 by Prof. Dr. Rhein.

## **Carbon isotope signature of dissolved light hydrocarbons**

Samples for determination of the stable carbon isotopic signature of the dissolved light hydrocarbons were obtained by degassing the water samples with a vacuum - ultrasonic technique. The samples were transferred via a septum from the degassing unit into pre-evacuated, gastight glass ampoules until the onshore analysis.

## **Dissolved organic carbon (DOC)**

Subsamples for DOC analysis were taken in precombusted 20mL ampoules and acidified with 50%  $\text{H}_3\text{PO}_4$  (Merck, suprapure) to a  $\text{pH} < 2$ . DOC will be measured by high temperature catalytic (platinum) oxidation to  $\text{CO}_2$ , combined with infrared detection.

## **Dissolved inorganic carbon (DIC)**

250 ml of unfiltered sample were poisoned with  $\text{HgCl}_2$ , sealed airtight and stored for coulometric DIC analysis in the laboratory.

## **Carbon isotope signature of DIC and DOC**

250 ml of unfiltered sample were transferred into glass bottles via gas tight tubes, fixed with 2 ml of 15N NaOH, and the bottles were sealed head space free with Teflon caps.

## **Particulate organic matter (POM)**

High volumes  $>40$  l of water were filtered using glass fibre filters (Whatmann GF/F) and the filters were dried at  $35^\circ\text{C}$ .

## **12.3 Results**

### **Physical properties of the water column**

A total of 16 hydrocasts were performed. Recorded data are presented summarized for the individual working areas (Appendix 5).

### **CENTRAL AREA**

Station 25 CTD-5	MSU mud volcano
Station 27 CTD-6	MSU mud volcano
Station 29 CTD-7	Vassoevitch mud volcano

No considerable differences are observed for the distribution of salinity, temperature and light transmission between the stations. Generally, salinity increases from 18.1 at the surface to 22.34 at the bottom. A relatively steep gradient exists between 30 m (18.2) and 110 m depth (21), while below 800m hardly any increase is observed. Temperature ranges from 6.9°C in the less saline surface water to 9.1°C at depth. Thermoclines are observed at 10–20 m und 30–50 m depth. Low light transmission characterizes the surface layer down to 60 m depth, most probably brought about by an abundance of phytoplankton. No substantial variability occurs in deeper waters.

## SOROKIN TROUGH

Station 2-2	CTD-1	background
Station 4	CTD-2	Odessa mud volcano
Station 10	CTD-3	gas hydrate sampling side, mud volcano
Station 16	CTD-4	gas hydrate sampling side, mud volcano
Station 33-2	CTD-8	background
Station 40-2	CTD-9	Dvurechenskii mud volcano
Station 45-2	CTD-10	gas hydrate sampling side, mud volcano
Station 47-2	CTD-11	Dvurechenskii mud volcano
Station 51-2	CTD-12	gas hydrate sampling side, mud volcano
Station 61-1	CTD-13	Dvurechenskii mud volcano
Station 61-3	CTD-14	Dvurechenskii mud volcano
Station 64	CTD-15	inactive mud volcano, NE of Dvurechenskii mud volcano
Station 67	CTD-16	Gas plume on the shelf

There are similar patterns of salinity at all stations except for some deviations with regard to the surface layer. From about 17.9 at surface it increases below the pycnocline (~30–35 m) to reach 22.34 at the bottom.

Temperatures in the Sorokin Trough are between 6.8°C and 9.1°C, with stations CTD-13 and CTD-14 showing colder temperature minima than other stations. Compared to the central area, distinct temperature minima are present at various depths within the upper 80m of the water column.

The distribution pattern of light transmission at CTD-1 and CTD-2 is similar to that observed for the central area. However, other stations in the Sorokin-Trough reveal zones of diminished light transmission within the depth zone between 90 m and 120 m. These horizons of low transparency presumably coincide with the chemocline, as indicated by methane concentrations (see below).

## Methane

### CENTRAL AREA

Station 25	CTD-5	MSU mud volcano
Station 29	CTD-7	Vassoevitch mud volcano

The two stations investigated in the central area yielded quite similar distribution patterns for dissolved methane. At the surface, concentrations of about 0.04  $\mu\text{mol L}^{-1}$  are found.

representing a strong supersaturation of methane with respect to the atmospheric equilibrium ( $0.002 \mu\text{mol L}^{-1}$ ). At the transition zone from the oxic to the anoxic water body at about 100m depth, methane concentrations increase to  $14 \mu\text{mol L}^{-1}$  at about 500 m depth. Below that depth no strong variations are observed. However, a slight decrease of dissolved methane found close to the bottom might indicate the influence of methane consumption by anaerobic oxidation.

## SOROKIN TROUGH

Station 2-2	CTD-1	background
Station 4	CTD-2	Odessa mud volcano
Station 10	CTD-3	gas hydrate sampling side, mud volcano
Station 33-2	CTD-8	background
Station 40-2	CTD-9	Dvurechenskii mud volcano
Station 47-2	CTD-11	Dvurechenskii mud volcano
Station 61-1	CTD-13	Dvurechenskii mud volcano
Station 61-3	CTD-14	Dvurechenskii mud volcano
Station 64	CTD-15	inactive mud volcano, NE of Dvurechenskii mud volcano
Station 67	CTD-16	Gas plume on the shelf

Methane concentrations of ca.  $0.03 \mu\text{mol L}^{-1}$  found in surface waters of the Sorokin Trough are well above the atmospheric equilibrium. They only slightly increase down to the onset transition zone from the oxic to the anoxic water body. However, position and looks of this zone appear to vary considerably between the investigated locations. Figures 94 and 95 illustrate the methane concentrations and light transmission profiles for selected stations. At Sts. 2-2 and 10, methane concentrations start to increase steeply at about 90 m depth. While this zone is marked by a prominent transmission minimum at St. 10, nothing comparable appears at St. 2-2 (Fig. 94). At both, Sts. 33-2 and 67, the onset of the steep increase of methane concentrations coincides with the lower part of obvious light transmission anomalies (Fig. 95). However, the transmission minimum ceases at 120 m depth at St. 33-2, but occupies the zone from 150 to 180 m depth and is much more pronounced at the shelf (St. 67), imaging the doming of the chemocline. An interesting fact is the relative methane maximum at St. 10 (115 m depth), whereas the sampling was focused on the upper part of the water column. This enrichment of methane, positioned at the upper rim of the anoxic zone might be brought about by microbial methanogenesis in situ. Results of particular interest could be obtained from the currently active Dvurechenskii mud volcano. Fig. 96 reveals the methane distribution in the deep water of two casts located directly above the volcano. In both cases an increase at bottom is observed that hints to a considerable methane flux from the sediment into the water column.



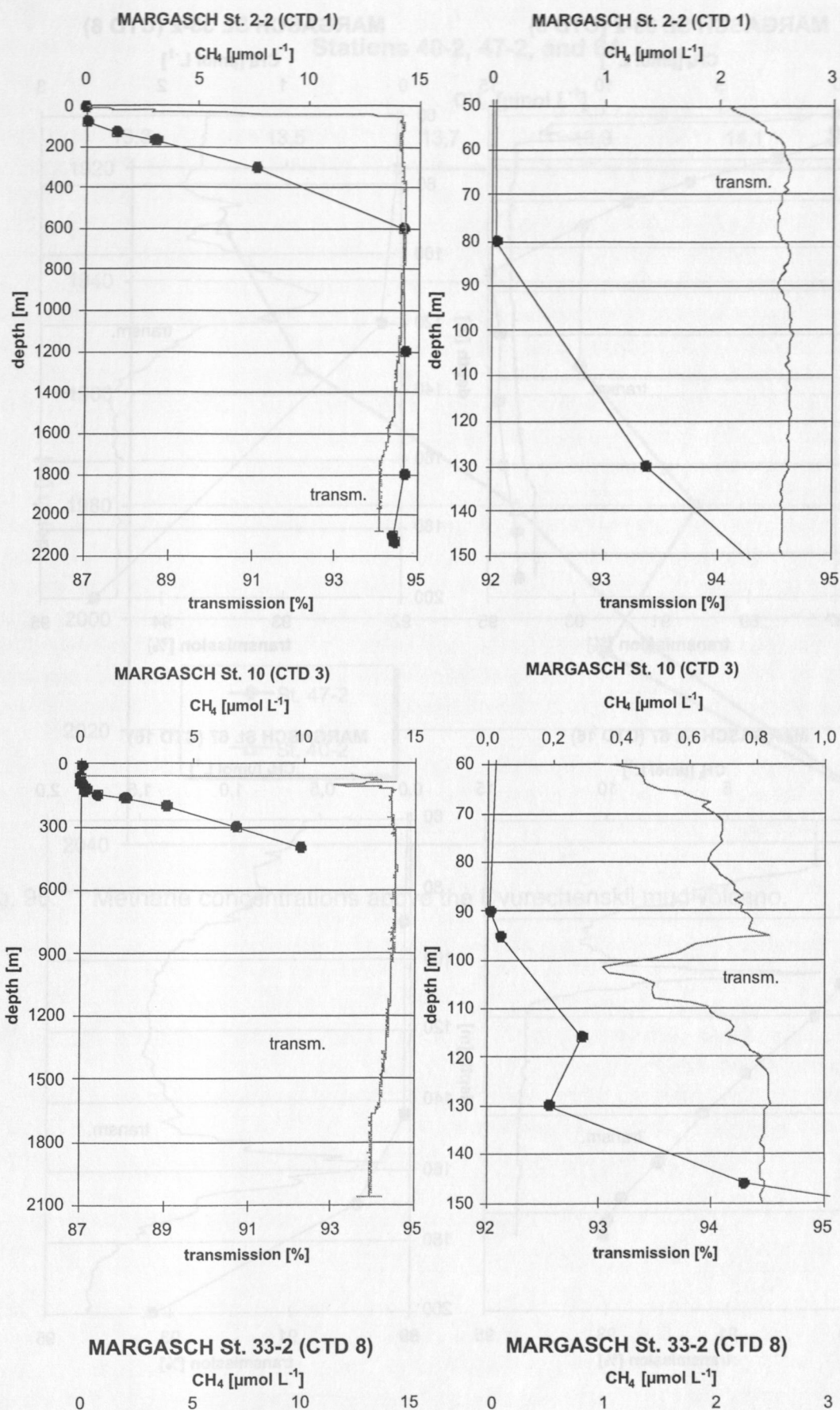


Fig. 94: Methane concentrations and light transmission for selected stations.

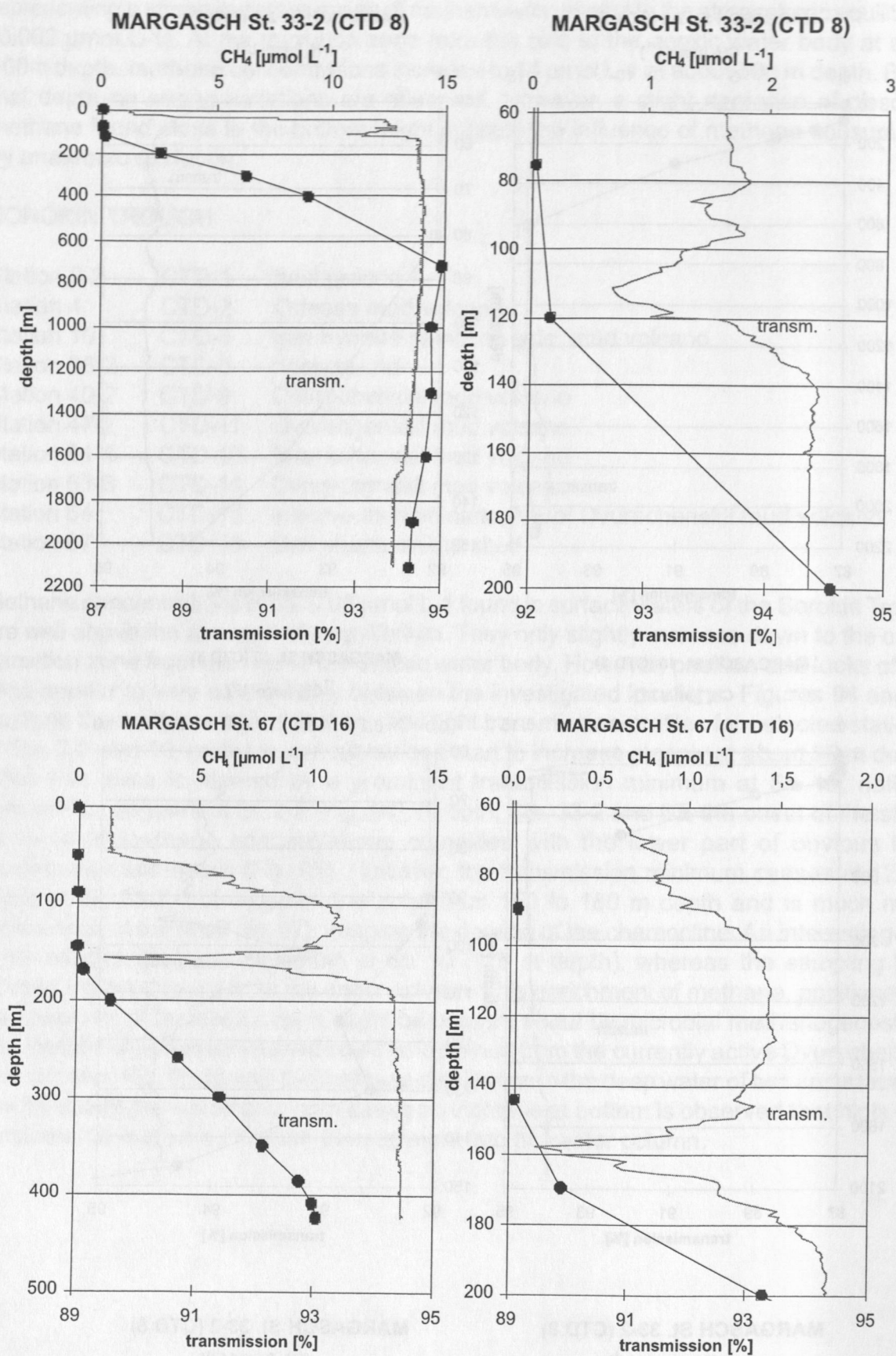


Fig. 95: Methane concentrations and light transmission for selected stations.

Stations 40-2, 47-2, and 64

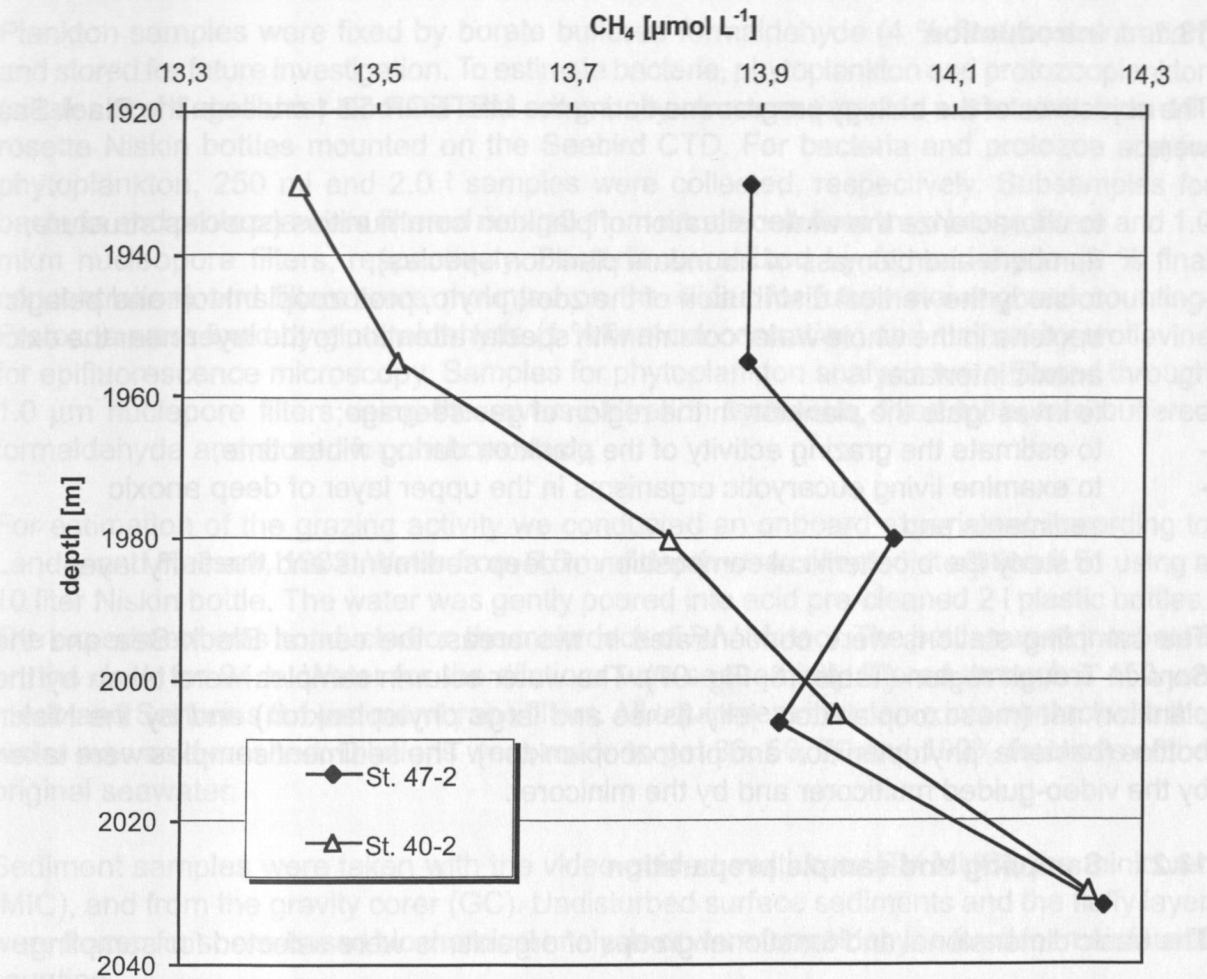


Fig. 96: Methane concentrations above the Dvurechenskii mud volcano.



## 13. BIOLOGY

I. Polikarpov, M. Saburova

### 13.1 Introduction

The objectives of the biology programme during the METEOR 52-1 cruise in the Black Sea were:

- to characterize the winter situation of plankton communities (species structure, numbers and biomass of abundant plankton species);
- to study the vertical distribution of the zoo-, phyto, protozooplankton and pelagic bacteria in the whole water column with special attention to the layer near the oxic-anoxic interface;
- to investigate the plankton in the region of gas seepage;
- to estimate the grazing activity of the plankton during winter time;
- to examine living eucaryotic organisms in the upper layer of deep anoxic sediments and
- to study the biochemical composition of deep sediments and the fluffy layer.

The sampling stations were concentrated in two areas: the central Black Sea and the Sorokin Trough region (Table 16, Fig. 97). The water column samples were taken by the plankton net (mesozooplankton, jelly-fishes and large phytoplankton) and by the Niskin bottles (bacteria, phytoplankton and protozooplankton). The sediment samples were taken by the video-guided multicorer and by the minicorer.

### 13.2 Sampling and sample preparation

The basic dimensional and functional groups of organisms were selected for sampling:

- Bacterioplankton – heterotrophic and autotrophic fraction of nanoplankton with sizes between 0.1-5.0  $\mu\text{m}$ ;
- Phytoplankton – photoautotrophic fraction of microplankton with sizes between 5-200  $\mu\text{m}$ ;
- Protozooplankton – heterotrophic flagellates and ciliates, 20-500  $\mu\text{m}$ ;
- Larval plankton – larval stages of life cycles of the different planktonic and benthic invertebrates, 100-1000  $\mu\text{m}$ ;
- Mezozooplankton – small organisms from different taxonomical groups with predominance of copepods, up to a few mm;
- Macroplankton – large planktonic organisms such as jelly-fish and arrow-worms.

The different sampling and treatment methods were used to determine planktonic organism densities (Table 15).

Samples of mesozooplankton (mainly Copepoda and Chaetognata), jellyfish and large phytoplankton (phytoflagellates and diatom algae) were taken by Juday plankton net with mouth of 37 cm diameter and 150  $\mu\text{m}$  net mesh size. The net was deployed to the depth of the oxic-anoxic interface (16.1 water density) and then upload with speed of 0.5 m/s to the water surface with washing at the surface. In three cases (st. # 47, # 51 and # 61) the net was deployed to three or two depths - to 120 m, 60 m and 25 m at st. #47 and # 51 and to

120 m and 50 m at st. # 61, respectively. In several cases water from Niskin bottles was filtered through a 74  $\mu\text{m}$  plankton net mesh for examination of larval plankton.

Plankton samples were fixed by borate buffered formaldehyde (4 % final concentration) and stored for future investigation. To estimate bacteria, phytoplankton and protozooplankton (ciliates and flagellates) biomass and community structure samples were taken from 10 l rosette Niskin bottles mounted on the Seabird CTD. For bacteria and protozoa and for phytoplankton, 250 ml and 2.0 l samples were collected, respectively. Subsamples for bacteria and protozoa were filtered using 0.1  $\mu\text{m}$  nitrate cellulose membrane filters and 1.0  $\mu\text{m}$  nucleopore filters, respectively. Bacteria were fixed by formaldehyde (2 % final concentration) and filters were mounted on the slides for future staining and counting. Protozoa were fixed by glutaraldehyde (1 % final concentration) and stained by proflavine for epifluorescence microscopy. Samples for phytoplankton analysis were filtered through 1.0  $\mu\text{m}$  nucleopore filters using the reverse filtration technique, fixed by borate buffered formaldehyde and stored for onshore study.

For estimation of the grazing activity we conducted an onboard experiment according to Landry and Hassett, 1982. Water from 0.5 m of depth was collected at station # 51 using a 10 liter Niskin bottle. The water was gently poured into acid pre-cleaned 2 l plastic bottles. The experiment was conducted on the main deck of R/V Meteor. The bottles were incubated on the deck for 24 h. Water for the dilutions was sequentially filtered through a 150  $\mu\text{m}$  mesh and Sartorius 0.1  $\mu\text{m}$  membrane filters. All equipment that came into contact with the water was acid-washed. Dilutions were made to get 30, 50, 70 and 100% fractions of the original seawater.

Sediment samples were taken with the video-guided multicorer (TV MUC), the minicorer (MIC), and from the gravity corer (GC). Undisturbed surface sediments and the fluffy layer were frozen for shore-based biochemical analysis or were formaldehyde fixed for meiofaunal counting.

Table 15: Sampling and sample preparation techniques.

Group of plankton	Sampling method	Sample volume	Method of concentration	Method of conservation	Method of study
Bacterioplankton	Bottle sampling	5 ml	Filtration, 0.1 $\mu\text{m}$ nitrocellulose filters	Fixation, formaldehyde	Razumov's method, light microscopy
			Filtration, 0.1 $\mu\text{m}$ nucleopore filters	Fixation, formaldehyde	Epifluorescent microscopy
Phytoplankton; Larval microplankton	Bottle sampling	2-4 l	Reverse filtration, 1 $\mu\text{m}$ nucleopore filters	Fixation, formaldehyde	Light microscopy
Protozooplankton	Bottle sampling	30 ml	Filtration, 1 $\mu\text{m}$ nucleopore filters	Fixation, glutaraldehyde	Epifluorescent microscopy
Mezozooplankton	Plankton net	0-120 m	Filtration, 150 $\mu\text{m}$ plankton net	Fixation, formaldehyde	Light microscopy
Macroplankton	Plankton net	0-120 m	Filtration, 150 $\mu\text{m}$ plankton net	-	Vital count and weighting

A synopsis of water and sediment samples performed in cruise is shown in Table 16 and the map of sampling is shown in Fig. 97.

Table 16: List of samples.

Date	Number of station	Coordinates	Depth, m	Planktonic group	Water temperature, °C	Air temperature, °C
04.01.02	002	44°05.01'N 35°05.04'E	3	Bacterio-, phyto- and protozooplankton	6.2	-3.0
			80			
			130			
			170	Bacterioplankton		
			300			
			600			
04.01.02	004	44°23.11'N 35°08.36'E	3	Bacterio-, phyto- and protozooplankton	6.4	-2.0
			78			
			254			
			350	Bacterioplankton		
05.01.02	006	44°22.46'N 35°08.61'E	1900	Bottom sediments		
09.01.02	016	44°14.55'N 34°46.97'E	90	Bacterio- and protozooplankton	6.4	-5.2
			146			
13.01.02	024	43°32.00'N 33°06.99'E	100-0	Mezo- and macrozooplankton	6.6	3.2
13.01.02	024	43°32.00'N 33°06.99'E	5	Bacterio-, phyto- and protozooplankton	6.8	4.3
			80			
14.01.02	029	43°20.46'N 33°26.62'E	100-0	Mezo- and macrozooplankton	6.6	4.7
17.01.02	033	44°14.90'N 34°55.90'E	5	Bacterio-, phyto- and protozooplankton	8.2	5.8
			75	Bacterio- and protozooplankton		
17.01.02	033	44°14.90'N 34°55.90'E	120-0	Mezo- and macrozooplankton	8.2	5.8
18.01.02	040	44°16.99'N 34°59.00'E	120-0	Mezo- and macrozooplankton	8.7	5.0
19.01.02	045	44°14.53'N 34°46.92'E	140-0	Mezo- and macrozooplankton	7.6	5.8
			140-0			
21.01.02	047	44°16.96'N 34°58.65'E	120-0	Mezo- and macrozooplankton	8.2	5.8
			60-0			
			25-0			
22.01.02	050	44°23.01'N 35°09.28'E	2140	Bottom sediments		
22.01.02	051	44°14.45'N 34°46.98'E	130-0	Mezo- and macrozooplankton	8.1	5.5
			60-0			
			25-0			
27.01.02	061	44°16.90'N 34°58.98'E	140-0	Mezo- and macrozooplankton	7.7	8.1
			60-0			
			25-0			
28.01.02	061	44°17.01'N 34°59.10'E	5	Bacterio-, phyto-, larval and protozooplankton	7.7	7.9
			15			
			25			
			35			
			45			
			55			
			60			
			70			
			80			
			90			
			94			
			100			



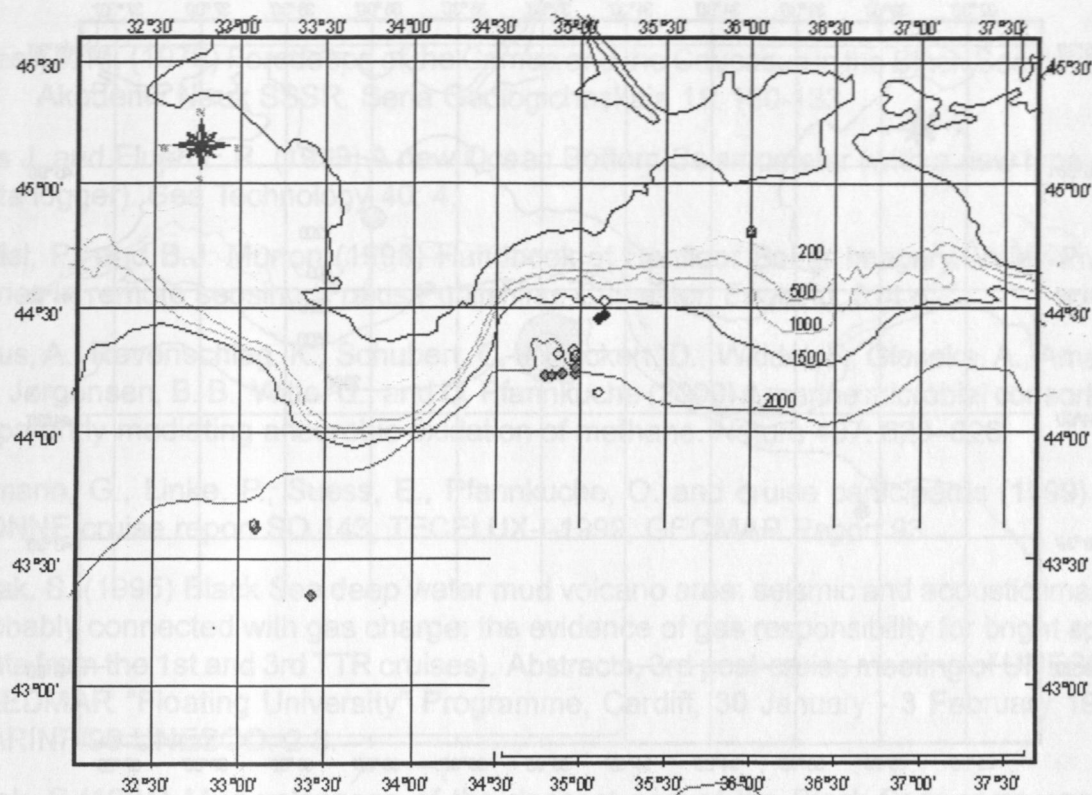


Fig. 97: Map of sampling (empty circles - bottle samples; grey circles - plankton net samples and black circles - multicorer samples).

### 13.3 Preliminary results

Before shore-based detailed quantitative and qualitative analyses of the samples (for taxonomic composition, abundance and biomass estimation) we can only give small results concerning the jelly-fish abundance and biomass (Table 17). Jellyfish were only represented by native Black Sea *Pleurobrachia pileus* and medusae *Aurelia aurita* in all net samples (Fig. 99). Their biomass distribution is shown in Fig. 98. The Atlantic jelly-fish invader *Mnemiopsis leidyi* which intensively eats zooplankton, as well as the new invader *Beroe* sp. were absent from all samples. The biomass of copepods (mezoplankton) in the studied waters was higher than usually during the winter period.

Table 17: Abundance and biomass of jelly-fish *Pleurobrachia pileus* and *Aurelia aurita*.

Station	<i>Pleurobrachia pileus</i>		<i>Aurelia aurita</i>	
	Abundance, ind./m <sup>2</sup>	Biomass, g/m <sup>2</sup>	Abundance, ind./m <sup>2</sup>	Biomass, g/m <sup>2</sup>
024	3,84	2,16	0	0
029	0	0	0	0
033	5,76	2,50	0	0
040	3,84	2,40	0,96	75,30
045	7,20	4,40	0,96	33,25
047	7,68	5,20	0,96	0,60
051	2,90	3,40	0,96	12,30
061	24,00	9,40	5,76	337,92
067	3,84	3,1	0	0

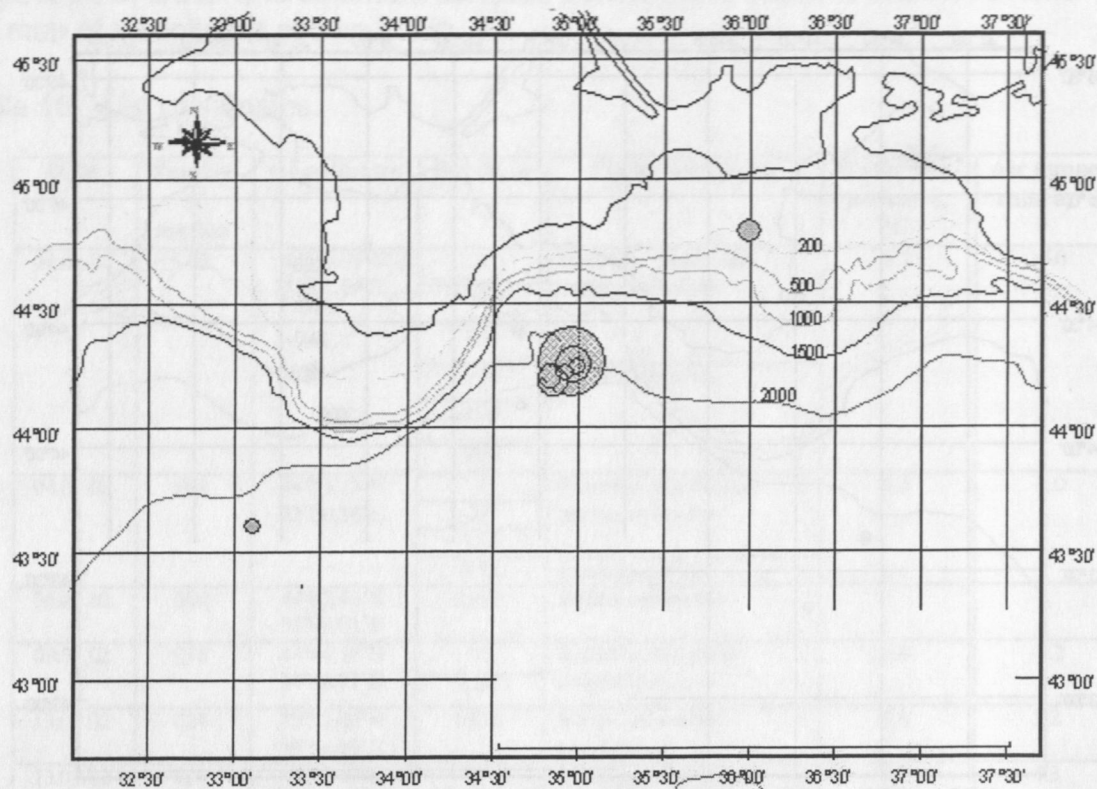


Fig. 98: Distribution of jelly-fish *Pleurobrachia pileus* biomass distribution (wet weight, g/m<sup>2</sup>).

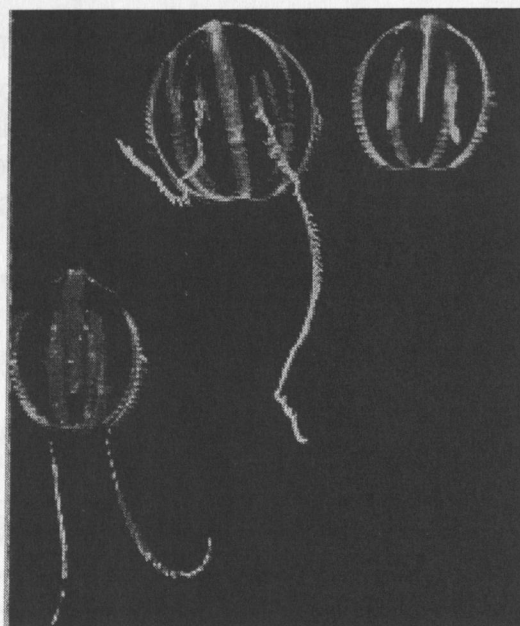


Fig. 99: *Pleurobrachia pileus* living image.

#### 14. REFERENCES

- Andreev, V. M. (1976) Foredeeps of the Crimea and the Caucasus in the Black Sea. *Izvestia Akademii Nauk SSSR. Seria Geologicheskaja* 11: 130-133
- Bialas J. and Flueh E.R. (1999) A new Ocean Bottom Seismometer (with a new type of data logger). *Sea Technology* 40: 4.
- Blondel, P., and B.J. Murton (1998) *Handbook of Seafloor Sonar Imagery*. Wiley-Praxis series in remote sensing, Praxis Publishing, Chicester, England: 314 p.
- Boetius, A., Ravensschlag, K., Schubert, C. J., Rickert, D., Widdel, F., Gieseke, A., Amann, R., Jørgensen, B. B., Witte, U., and O. Pfannkuche (2000) A marine microbial consortium apparently mediating anaerobic oxidation of methane. *Nature* 407: 623-626.
- Bohrmann, G., Linke, P., Suess, E., Pfannkuche, O. and cruise participants (1999) RV SONNE cruise report SO 143, TECFLUX-I-1999, GEOMAR Report 93.
- Bouriak, S. (1995) Black Sea deep water mud volcano area: seismic and acoustic images probably connected with gas charge: the evidence of gas responsibility for bright spots (data from the 1st and 3rd TTR cruises). Abstracts, 3rd post-cruise meeting of UNESCO/TREDMAR "Floating University" Programme, Cardiff, 30 January - 3 February 1995, MARINF/99 UNESCO: 2-3.
- Bouriak, S. (1994) Mud volcanoes of the deepest part of the Black Sea: some special structures connected with mud volcanism of the region. (According to seismic data of the cruises of 1991 and 1993). In: *Recent Marine Geological Research in the Mediterranean and Black Seas through the UNESCO/TREDMAR Programme and its "Floating University" Project*, Abstracts, Free University, Amsterdam, 31 January - 4 February 1994. - MARINF/94, UNESCO, June 1994: 25.
- Caress, D. W. and D. N. Chayes (1996) Improved processing of Hydrosweep DS multibeam data on the R/V Ewing. *Mar. Geophys. Res.* 18: 631-650.
- Dickens, G.R., M.S. Quinby-Hunt (1994) Methane hydrate stability in seawater. *Geophysical Research Letters*, 21 (19): 2115-2118.
- Dickson, A. D. (1993) pH buffers for sea water media based on the total hydrogen ion concentration scale. *Deep-Sea Research I*, 40: 107-118.
- Flueh E.R., and J. Bialas (1996) A digital, high data capacity ocean bottom recorder for marine seismic investigations. *Underwater Systems Design*, 18 (3): 18-20.
- Flueh, E. and R von Huene (1994) KODIAK-SEIS, *Fahrtbericht SO-96*, GEOMAR, Kiel.
- Ivanov, M.K., Limonov, A.F. and J.M. Woodside (1992). Initial results of the "Training-Through-Research" cruise of R/V "Gelendzhik" in the Eastern Mediterranean and Black seas (June-July, 1991). *UNESCO Reports in Marine Sciences* 56: 208 pp.
- Gieskes, J. M., Gamo, T., and H. Brumsack (1991) Chemical methods for interstitial water analysis aboard JOIDES Resolution. *ODP Technical Notes* 15, College Station, TX (Ocean Drilling Program).



- Ginzburg, G.D., Kremlev, A.N., Grigoriev, M.N., Larkin, G.N., Pavlenkin, A.D., and N.A.Saltykova (1990) Filtrigenic gas hydrates in the Black Sea. 21th Cruise of R/V *evpatoria*. *Geologiya i Geofizika* 3: 10-19 (in Russian).
- Grasshoff, K., Ehrhardt, M. and K. Kremling (1983) *Methods of seawater analysis*, 2nd edition, Verlag Chemie, Weinheim: 419 pp.
- Henry, P.H., LePichon, X. et al. (1996) Fluid flow in and around a mud volcano field seaward of the Barbados accretionary wedge: results from Manon cruise. *J. Geophys. Res.* 101:20297-20323.
- Hinrichs, K.-U., Hayes, J. M., Sylva, S. P., Brewer, P. G. and E. F. DeLong (1999) Methane consuming archaeobacteria in marine sediments. *Nature* 398: 802–805.
- Ivanenkov, V.N. and Y.I. Lyakhin (1978) Determination of total alkalinity in seawater. In: Bordovsky, O.K. and V.N. Ivanenkov (eds.): *Methodes of hydrochemical investigations in the ocean*. Nauka Publ. House, Moscow: 110–114 (in Russian).
- Ivanov M.K., Koniukhov A.I., Kulnitskii L.M., and A.A. Musatov (1989) Mud volcanism in the deep Black sea basin. *Vestnik MGU, geologicheskaya seriya*, N3.
- Limonov A. F., Ivanov M.K., Meisner L.B., Glumov I.F., Krylov O.V., and E.V. Kozlova (1997) New data of the sedimentary cover structure of the Sorokin Trough. *Vestnik Moskovskogo Universiteta, Geologiya* 4 (3): 36-43 (in Russian).
- Limonov, A.F., Woodside, J.M. and M.K. Ivanov (1994) Mud volcanism in the Mediterranean and Black Seas and shallow structure of the Eratosthenes Seamount. *UNESCO reports in marine science* 64: 173.
- Linke, P., Suess, E. and cruise participants (2000) RV SONNE cruise report SO 148, TECFLUX-II-2000, GEOMAR Report 98.
- Schreiber, R. and H. W. Schencke (1990) Efficient hydrographic surveying of EEZ with new multibeam echosounder technology for shallow and deep water. *Ocean resources* 1: 73-87.
- Spieß, V. (1993) *Digitale Sedimentechographie - Neue Wege zu einer hochauflösenden Akustostratigraphie*. Berichte, Fachbereich Geowissenschaften, Universität Bremen, 35: 199 pp. (Habilitationsschrift).
- Tugolesov, D. A., Gorshkov, A. S., Meisner L. B., Solov'ev, V.V., and E.M. Khakhalev (1985) *Tectonics of Mezo-Kainozoik deposits of the Black Sea basin*. Moscow, Nedra (in Russian).
- Weinrebe, W. (1997) HIRESBAT, Fahrtbericht SO-112, GEOMAR, Kiel.
- Woodside, J. M., Ivanov, M.K., Limonov, A.F. (1997) Neotectonics and fluid flow through seafloor sediments in the Eastern Mediterranean and Black Seas, Part II: Black Sea, Intergovernmental Oceanographic Commission technical series, UNESCO, 48.

15. APPENDIX

Appendix 1

Appendix 1.1 List of stations

MARGASCH 2002 : RV Meteor M52/1												
Date 2002	Stat No	Instrument	Begin (UTC)	at seafloor max depth	off seafloor	End (UTC)	Duration hh:mm	Latitude N° begin: at sf / end: off sf	Longitude E° begin: at sf / end: off sf	Water depth m	Recovery	Remarks
M52/1												
Sorokin Trough												
03. Jan	1	MCS	13:18			17:12	3:54					
04. Jan	2-1	OBSH	3:57			5:40	1:43	44° 05.04	35° 04.92	2180		Streamer/Airgun Test
	2-2	CTD-1	5:50	6:36		7:23	1:33	44° 05.02	35° 05.02	2181	10 bottles	Releaser Test 1
	2-3	OBSH	7:33			9:02	1:29	44° 05.00	35° 05.04	2190		(4+6 not closed)
	3	HS	9:04			15:17	6:13	44° 05.03 / 44° 29.19	35° 05.07 / 35° 12.55	2180 / 1590		Releaser Test 2
	4	CTD-2	16:10	16:40		17:19	1:09	44° 23.05	35° 08.44	1785	10 bottles	(4+5 not closed)
	5-1	OPOS-1	18:04	18:41	20:45	21:23	3:19	44° 22.46 / 44° 23.27	35° 08.64 / 35° 09.49	1883 / 1803		SE of Odesa MV
05. Jan	5-2	OPOS-2	22:15	22:48	0:28	1:07	2:52	44° 22.87 / 44° 23.28	35° 08.24 / 35° 08.91	1867 / 1804		over Odesa MV
	5-3	OPOS-3	1:38	2:14	4:21	4:47	3:09	44° 23.01 / 44° 23.64	35° 06.22 / 35° 07.49	1887 / 1840		over MV west of Odesa MV
	6-1	TV-MUC-1	6:12	6:56	6:59	7:36	1:24	44° 22.49	35° 08.62	1889	7 cores	without video control
	6-2	TV-MUC-2	8:43	9:22	9:42	10:22	1:39	44° 22.59	35° 08.75	1877	8 cores	sampling of white patches
	7	OBSH	10:28			12:05	1:37	44° 22.94	35° 08.07	1843		Releaser Test 3
	8	TVG-1	12:31	13:03	14:09	14:48	2:17	44° 22.97	35° 08.50	1784	full	carbonate crusts with bacteria
	9-1	MCS-1	17:07			19:52	2:45	44° 20.55 / 44° 16.67	34° 55.64 / 35° 16.40			
	9-2	MCS-2	20:05			20:43	0:38	44° 15.48 / 44° 13.53	35° 15.86 / 35° 10.79			
	9-3	MCS-3	20:59			23:20	2:21	44° 13.94 / 44° 28.01	35° 09.15 / 35° 13.41			
	9-4	MCS-4	23:29			4:48	5:19	44° 28.12 / 44° 09.85	35° 14.67 / 35° 50.16			
06. Jan	9-5	MCS-5	4:58			6:27	1:29	44° 10.13 / 44° 19.66	35° 51.17 / 35° 51.13			
	9-6	MCS-6	6:31			9:18	2:47	44° 20.09 / 44° 34.91	35° 50.85 / 35° 38.45			
	9-7	MCS-7	9:30			12:02	2:32	44° 35.74 / 44° 38.81	35° 37.65 / 35° 00.24			
	9-8	MCS-8	12:15			12:59	0:44	44° 38.17 / 44° 33.47	35° 01.65 / 35° 04.75			
	9-9	MCS-9	13:03			15:50	2:47	44° 33.11 / 44° 23.14	35° 01.38 / 35° 40.61			
	9-10	MCS-10	16:00			18:00	2:00	44° 23.05 / 44° 29.56	35° 39.27 / 35° 23.49			
	9-11	MCS-11	18:11			19:22	1:11	44° 28.96 / 44° 21.35	35° 22.18 / 35° 24.26			
	9-12	MCS-12	19:32			21:37	2:05	44° 20.82 / 44° 25.95	35° 23.27 / 35° 05.61			
	10	CTD-3	23:55	0:20		1:28	1:33	44° 14.56	34° 46.81	2105	12 bottles	
07. Jan	11	TVG-2	1:51	2:30	2:51	3:31	1:40	44° 14.56	34° 47.13	2124	full	carbonates and mud breccia
	12-1	OBS-1	5:32					44° 24.60	35° 05.40	1893		deployment
	12-2	OBS-2	6:09					44° 23.70	35° 06.00	1876		deployment
	12-3	OBS-3	6:43					44° 22.90	35° 06.70	1887		deployment
	12-4	OBS-4	7:07					44° 22.00	35° 07.30	1946		deployment
	12-5	OBS-5	7:39					44° 20.70	35° 08.30	2008		deployment
	12-6	OBS-6	8:06					44° 19.30	35° 09.30	2040		deployment
	12-7	OBS-7	8:24					44° 18.50	35° 09.90	2051		deployment
	12-8	OBS-8	9:35					44° 17.50	35° 10.60	1943		deployment
	12-9	OBS-9	9:57					44° 16.60	35° 11.30	2058		deployment
	12-10	OBS-10	10:20					44° 15.80	35° 11.90	2087		deployment
	12-11	OBS-11	10:49					44° 14.00	35° 13.20	2087		deployment
	12-12	OBS-12	11:40					44° 19.50	35° 15.60	1994		deployment
	12-13	OBS-13	12:02					44° 18.50	35° 13.10	2032		deployment
	12-14	OBS-14	12:35					44° 16.60	35° 08.20	2092		deployment
	12-15	OBS-15	13:03					44° 15.60	35° 05.80	2124		deployment



MARGASCH 2002 : RV Meteor M52/1													
Date 2002	Stat. No	Instrument	Begin (UTC)	at seafloor max. depth	off seafloor	End (UTC)	Duration hh:mm	Latitude N° begin: at sf./end: off sf.	Longitude E° begin: at sf./end: off sf.	Water depth m	Recovery	Remarks	
08. Jan	M52/1												
	13-1	OBSH-P1	16:49			2:18	9:29	44° 13.20 / 44° 27.50	35° 00.00 / 35° 04.20	2157 / 1818			
	13-2	OBSH-P2	2:31			10:37	8:06	44° 27.20 / 43° 59.80	35° 03.60 / 35° 23.50	1834 / 2143			
	14-1	OBSH	12:49			17:46	4:57						
	14-2	OBSH	1:37			7:22	5:45						
	15-1	GC-1	8:47	9:49	9:51	10:27	1:40	44° 16.89	34° 52.35	2081	approx. 90 cm	retrieval of 5 OBSH	
	15-2	GC-2	10:57	11:32	11:34	12:07	1:10	44° 16.87	34° 52.36	2060	87 cm	massive gas hydrates	
	16	CTD-4	12:59	195 m	13:08	13:20	0:21	44° 14.53	34° 47.00	2136	12 bottles	22 cm of gas hydrate layer	
	17	GC-3	13:28	14:06	14:07	14:40	1:12	44° 14.53	34° 47.03	2124	80 cm	6 bottles in 90m and 8 bottles in 147m	
	18	TGC-1	16:33	17:09	17:19	17:50	1:17	44° 23.01	35° 09.28	1836	410 cm	1 piece of gas hydrate in core catcher	
10. Jan	19	OBSH	18:21			22:10	3:49					many gas hydrates in thin layers	
	20-1	MCS-13	23:46			1:19	1:33	44° 20.00 / 44° 15.93	35° 08.19 / 34° 53.60			retrieval of 4 OBSH	
	20-2	MCS-14	1:24			2:24	1:00	44° 16.01 / 44° 18.92	34° 54.87 / 34° 46.83				
	20-3	MCS-15	2:33			3:23	0:50	44° 18.42 / 44° 13.20	34° 46.11 / 34° 48.10				
	20-4	MCS-16	3:29			3:39	0:10	44° 12.77 / 44° 12.25	34° 47.95 / 34° 46.43				
	20-5	MCS-17	3:48			4:39	0:51	44° 12.76 / 44° 18.32	34° 45.52 / 34° 44.50				
	20-6	MCS-18	4:47			5:10	0:23	44° 18.44 / 44° 17.51	34° 43.51 / 34° 40.35				
	20-7	MCS-19	5:18			6:08	0:50	44° 16.73 / 44° 11.87	34° 40.20 / 34° 43.20				
	20-8	MCS-20	6:15			6:43	0:28	44° 11.19 / 44° 09.61	34° 42.85 / 34° 39.20				
	20-9	MCS-21	6:53			7:39	0:46	44° 09.97 / 44° 14.57	34° 38.07 / 34° 35.28				
11. Jan	20-10	MCS-22	7:49			9:19	1:30	44° 15.10 / 44° 14.55	34° 36.06 / 34° 49.24				
	20-11	MCS-23	9:28			10:09	0:41	44° 15.23 / 44° 19.64	34° 49.91 / 34° 49.78				
	20-12	MCS-24	10:29			11:12	0:43	44° 19.51 / 44° 15.04	34° 52.00 / 34° 52.08				
	20-13	MCS-25	11:31			12:05	0:34	44° 15.06 / 44° 18.79	34° 54.07 / 34° 53.88				
	21	DTIS-1	14:12	16:26	19:33	21:13	7:01	44° 19.50 / 44° 17.30	35° 00.10 / 35° 12.60	2054 / 2312			
	22	HS/PS	21:24			2:00	4:36						
	11. Jan	Sewastopol	7:42			8:24	24:42						
	Central Black Sea												
	12. Jan	23-1	MCS-26	15:48			19:42	3:54	43° 47.01 / 43° 42.01	33° 05.06 / 33° 39.30			
		23-2	MCS-27	19:50			20:43	0:53	43° 41.33 / 43° 35.60	33° 39.67 / 33° 37.59			
23-3		MCS-28	20:52			0:41	3:49	43° 35.28 / 43° 41.06	33° 36.54 / 33° 02.80				
23-4		MCS-29	0:52			1:57	1:05	43° 40.40 / 43° 33.26	33° 01.69 / 33° 02.02				
23-5		MCS-30	2:05			5:57	3:52	43° 32.70 / 43° 27.85	33° 02.83 / 33° 36.61				
23-6		MCS-31	6:30			7:10	0:40	43° 24.48 / 43° 20.25	33° 36.16 / 33° 35.00				
23-7		MCS-32	7:18			10:47	3:29	43° 19.96 / 43° 24.01	33° 33.95 / 33° 03.17				
23-8		MCS-33	10:57			12:41	1:44	43° 24.66 / 43° 32.91	33° 03.03 / 33° 14.41				
23-9		MCS-34	12:50			13:28	0:38	43° 33.68 / 43° 34.80	33° 13.61 / 33° 08.22				
23-10		MCS-35	13:37			14:16	0:39	43° 34.19 / 43° 29.88	33° 07.53 / 33° 07.33				
14. Jan	23-11	MCS-36	14:39			15:43	1:04	43° 30.06 / 43° 35.05	33° 05.02 / 33° 11.51				
	24	WS-1	17:00	100m		17:12	0:12	43° 32.01	33° 06.96	2126			
	25	CTD-5	17:22	18:03		18:47	1:25	43° 31.99	33° 06.89	2073	12 bottles		
	26-1	OPOS-4	19:12	19:57	23:51	4:39	4:39	43° 32.34 / 43° 31.52	33° 07.44 / 33° 08.30	2174			
	26-2	OPOS-5	4:05	0:43	4:05	4:49	4:08	43° 31.62 / 43° 31.64	33° 06.24 / 33° 06.49	2167 / 2167			

MARGASCH 2002: RV Meteor M52/1												
Date 2002	Stat. No	Instrument	Begin (UTC)	at seafloor max depth	off seafloor	End (UTC)	Duration hh:mm	Latitude N° begin, at sl / end, off sl	Longitude E° begin, at sl / end, off sl	Water depth m	Recovery	Remarks
M52/1												
	27	CTD-8	5:48	08:25 / 1900		7:01	1:13	43° 31.99	33° 07.07	2129	12 bottles	6 bottles in 300m and 6 bottles in 1900m
	28	WS-2	9:47	9:52		9:56	0:09	43° 20.48	33° 40:26.61	2208		
	29	CTD-7	8:05	8:46		9:30	1:25	43° 20.46	33° 26.61	2145	12 bottles	
	30	DTG-2	13:25	14:13	22:19	0:45	11:20	43° 24:20 / 44° 19:60	33° 02:20 / 33° 39:60	2179 / 2224		
Sorokin Trough												
15 Jan	31-1	MCS-37	6:48			8:08	1:18	44° 03:06 / 44° 10:50	34° 27:79 / 34° 23:57			
	31-2	MCS-38	8:16			10:00	1:44	44° 11:23 / 44° 16:33	34° 24:05 / 34° 37:96			
	31-3	MCS-39	10:00			10:40	0:40	44° 16:32 / 44° 20:19	34° 37:96 / 34° 40:72			
	31-4	MCS-40	10:50			12:20	1:30	44° 19:79 / 44° 10:44	34° 41:67 / 34° 44:76			
	31-5	MCS-41	12:30			14:45	2:15	44° 10:56 / 44° 24:05	34° 45:88 / 34° 53:06			
	31-6	MCS-42	15:10			16:44	1:34	44° 24:02 / 44° 13:94	34° 55:95 / 34° 55:99			
	31-7	MCS-43	16:44			18:51	2:07	44° 14:06 / 44° 25:04	34° 58:87 / 34° 59:16			
	31-8	MCS-44	19:01			20:55	1:54	44° 25:40 / 44° 21:00	34° 00:21 / 34° 16:40			
16 Jan	32-1	DTG-3	22:54	1:15	6:00	7:06	7:06	44° 23:50 / 44° 14:30	35° 18:00 / 34° 53:80	1859 / 2161		
	32-2	DTG-4		11:40	17:17	18:51	5:37	44° 16:30 / 44° 25:10	34° 58:80 / 35° 20:50	2153 / 1751		
	32-3	DTG-5		20:22	2:02	4:58	8:36	44° 24:90 / 44° 15:40	35° 15:50 / 34° 52:80	1793 / 2153		
17 Jan	33-1	WS-3	6:19	06:24 / 100		6:31	0:12	44° 15:02	34° 55:84	2157	12 bottles	
	33-2	CTD-8	6:33	7:19		8:06	1:33	44° 15:03	34° 55:96	2112		
	34-1	TGC-2	8:39	9:18	9:31	10:12	1:33	44° 16:96	34° 58:95	2074	365 cm	gas hydrates
	34-2	MIC-1	10:46	11:38		12:28	1:42	44° 17:00	34° 59:00	2070	empty	
	35-1	MIC-2	13:33	14:19	14:19	15:01	1:28	44° 22:65	35° 08:87	1870	4 cores	
	35-2	GC-4	15:14	15:58		16:22	1:08	44° 22:65	35° 08:92	1870	full	no gas hydrates
	36-1	TGC-3	17:27	18:06	18:15	18:49	1:22	44° 17:00	34° 58:86	2071	280 cm	gas hydrates
	36-2	MIC-3	18:58	20:00		20:45	1:47	44° 16:99	34° 58:81	2070	4 cores	gas hydrates
	37	TGC-4	21:02	21:42	21:49	22:24	1:22	44° 17:13	34° 58:99	2073	580 cm	gas hydrates
	38	TGC-5	23:41	0:17	0:26	0:59	1:18	44° 17:00	34° 59:18	2075	390 cm	gas hydrates
18 Jan	39	TGC-6	1:56	2:39	2:48	3:24	1:28	44° 14:03	34° 58:85	2161	310 cm	no gas hydrates
	40-1	WS-4	5:08	5:12		5:17	0:11	44° 16:99	34° 58:87	2074		
	40-2	CTD-9	5:29	6:07		6:52	1:23	44° 17:01	34° 59:00	2030	12 bottles	
	41-1	OFOS-6	8:35	9:16	12:58	13:37	5:02	44° 14:89 / 44° 14:72	34° 44:91 / 34° 48:09	2097 / 2074		
	41-2	OFOS-7	14:09	14:46	17:10	17:53	3:44	44° 14:89 / 44° 13:94	34° 45:20 / 34° 45:40	2090 / 2114		
	42	TVG-3	18:17	18:57	20:15	20:52	2:35	44° 14:16	34° 45:34	2089	full	grey mud
	43	TVG-4	22:52	23:32	23:36	0:11	1:19	44° 16:89	34° 52:34	2091	full	
19 Jan	44	HSPS	0:13			3:27	3:14					
	45-1	WS-5	3:52	3:57		4:03	0:11	44° 14:49	34° 46:85	2120		
	45-2	CTD-10	4:34	5:14		5:56	1:22	44° 14:55	34° 46:96	2080	12 bottles	
	46-1	DTG-6	8:02	10:33	16:56	17:10	8:54	44° 10:03 / 44° 17:90	34° 38:50 / 35° 11:50	2154 / 2078		
	46-2	DTG-7	23:30	18:28	23:30	23:30	5:02	44° 17:30 / 44° 51:70	34° 57:70 / 34° 33:50	2096 / 2138		
	46-3	DTG-8	2:12	7:23		7:23	5:11	44° 11:40 / 44° 16:60	34° 36:50 / 34° 59:20	2087 / 2068		
	46-4	DTG-9	10:26	14:32		14:32	4:06	44° 18:00 / 44° 11:30	34° 54:80 / 34° 34:00	2078 / 2116		
	46-5	DTG-10	17:34	21:49		21:49	4:15	44° 12:80 / 44° 18:90	34° 36:50 / 34° 55:00	2063 / 2069		
21 Jan	46-6	DTG-11	3:39	0:16	3:39	3:23	3:23	44° 18:80 / 44° 13:00	34° 52:10 / 34° 35:30	2065 / 2085		

MARGASCH 2002 : RV Meteor M52/1												
Date 2002	Stat. No.	Instrument	Begin (UTC)	at seafloor max. depth	off seafloor	End (UTC)	Duration hh:mm	Latitude N° begin at sl / end off sl	Longitude E° begin at sl / end off sl	Water depth m	Recovery	Remarks
M52/1	46-7	DTS-12		6.32	8.27	9.30	9.30	44° 14.20 / 44° 17.00	34° 36.70 / 34° 44.80	2043 / 1990		
	47-1	WS-6	10.59			11.29	0.30	44° 16.95	34° 58.60	2083		
	47-2	CTD-11	12.17	12.59		13.47	1.30	44° 16.96	34° 58.62	2039	12 bottles	
	48-1	TGC-7	14.05	14.45	14.52	15.28	1.23	44° 16.85	34° 58.80	2087	500 cm	gas hydrates
	48-2	MIC-4	15.35	16.24		17.06	1.31	44° 16.88	34° 58.80	2085	4 cores	
	49-1	TGC-8	17.30	18.17	18.24			44° 16.95	34° 58.63	2087	480 cm	gas hydrates
	49-2	MIC-5	19.15	20.06		20.53	1.38	44° 16.97	34° 58.61	2089	4 cores	
	50-1	GC-5	22.16	22.48		23.18	1.02	44° 23.00	35° 09.27	1835	165 cm	gas hydrates
	50-2	MIC-6	23.35	0.19		23.35	1.01	44° 23.01	35° 09.27	1834	4 cores	
	51-1	WS-7	2.54	3.00		3.06	0.12	44° 14.45	34° 47.01	2136		
	51-2	CTD-12	3.31	03.57 / 1300		4.24	0.53	44° 14.29	34° 47.01	2145	12 bottles	
	52	GC-6	4.47	5.27		6.02	1.15	44° 14.37	34° 45.43	2130	300 cm	no gas hydrate
	53	GC-7	6.22	7.06		7.40	1.18	44° 14.31	34° 45.32	2128	320 cm	no gas hydrate
	54	GC-8	7.59	8.36		9.10	1.11	44° 14.23	34° 45.39	2129	402 cm	no gas hydrate
	55	GC-9	9.42	10.19		11.00	1.18	44° 14.55	34° 47.06	2127	165 cm	no gas hydrate
	56-1	OBS-16	11.41					44° 14.16	34° 45.09	2124		
	56-2	OBS-17	11.53					44° 14.21	34° 45.43	2119		
	56-3	OBS-18	12.06					44° 14.28	34° 45.80	2116		
	56-4	OBS-19	12.37					44° 14.49	34° 45.74	2536		
	56-5	OBS-20	12.51					44° 14.43	34° 45.38	2116		
56-6	OBS-21	13.05					44° 14.35	34° 45.01	2113			
56-7	OBS-22	13.17					44° 14.54	34° 44.94	2090			
56-8	OBS-23	13.28					44° 14.61	34° 45.30	2086			
56-9	OBS-24	13.43					44° 14.68	34° 45.63	2070			
56-10	OBS-25	14.03					44° 14.76	34° 45.98	2086	200 m above bottom		
56-11	OBS-26	14.20					44° 14.90	34° 45.55	2086	200 m above bottom		
56-12	OBS-27	14.33					44° 14.83	34° 45.18	2069			
56-13	OBS-28	14.51					44° 14.74	34° 44.84	2074	200 m above bottom		
56-14	OBS-29	15.08					44° 15.04	34° 45.10	2045	200 m above bottom		
57	3D-Seismics, MSC-45 to MCS-163 coordinates in clockwise order indicate box											
27. Jan	58	OBSH	0.30			8.05	7.35	44° 12.49	34° 48.69			retrieval
	59	TVG-5	8.50	9.31	13.13	13.50	5.00	44° 16.16	34° 42.90		approx. 1.5 l	carbonates and bacteria
	60	TVG-6	14.19	14.57	18.17	19.00	4.41	44° 14.19	34° 47.11	2124	empty	because of weak batteries
	61-1	CTD-13	20.22	20.32 / 545		20.58	0.34	44° 16.94	34° 53.25	2079	12 bottles	
	61-2	WS-8	21.07			21.50	0.43	44° 17.01	34° 59.10			
	61-3	CTD-14	22.20	22.23		22.34	0.14	44° 17.05	34° 59.12	2078	12 bottles	
	62-1	OFS-8	23.12	23.47	2.10	2.51	3.39	44° 16.35 / 44° 17.41	34° 57.96 / 34° 59.37	2147 / 2094		
	62-2	OFS-9	3.16	3.55	6.07	6.51	3.35	44° 17.24 / 44° 16.70	34° 57.99 / 34° 59.85	2100 / 2116	full	gas hydrates
	63	TVG-7	7.32	8.11	8.51	9.26	1.54	44° 16.95	34° 58.89	2075		
	64	CTD-15	10.42	11.23		12.10	1.28	44° 17.38	35° 00.02	2101	12 bottles	
28. Jan	65-1	DTS-13	13.17	14.36	18.21		3.04	44° 17.40 / 44° 12.50	34° 58.90 / 34° 57.20	/ 2171		
	65-2	DTS-14		18.49	20.56		2.07	44° 15.10 / 44° 18.50	34° 57.00 / 35° 06.20	2154 / 2058		



MARGASCH 2002: RV Meteor M52/1												
Date 2002	Stat No	Instrument	Begin (UTC)	at seafloor max. depth	off seafloor	End (UTC)	Duration hh:mm	Latitude N° begin: at st / end: off st	Longitude E° begin: at st / end: off st	Water depth m	Recovery	Remarks
M52/1												
29 Jan	55-3	DTS-15		20.56	22.26		1:30	44° 18.50 / 44° 23.30	35° 06.20 / 35° 06.00	2058 / 1878		
	55-4	DTS-16		22.26	0:23		1:57	44° 23.30 / 44° 25.70	35° 06.00 / 35° 14.70	1878 / 1757		
	55-5	DTS-17		0:23	3:10		2:47	44° 25.70 / 44° 23.20	35° 14.70 / 35° 27.30	1757 / 1769		
	55-6	DTS-18		6:11	8:44		2:33	44° 23.00 / 44° 23.30	35° 29.60 / 35° 13.10	1823 / 1752		
	55-7	DTS-19		8:44	11:02		2:18	44° 25.00 / 44° 22.20	35° 13.10 / 35° 04.20	1752 / 1979		
	55-8	DTS-20		12.00	13:41	15:49	3:49	44° 20.80 / 44° 16.60	35° 01.90 / 35° 07.30	2008 / 2093		
	66	HS/PS	17:46			22:22	4:36					
	67-1	CTD-16	23:12	23.22		23:39	0:27	44° 42.78	35° 59.86	424	12 bottles	
Central Black Sea	67-2	WS-9	23:47	23.53		23:58	0:11	44° 42.75	35° 59.90	472		
	68-1	HS/PS	0:05			11:26	11:21					
68-2												
		HS/PS	12.45			16:23						

Appendix 1.2 Use of equipment

FS M E T E O R  
Reise M 52/1  
Kapitän Niels Jakobi

Einsätze von Geräten und Winden  
M 52/1 02.01. - 01.02.02

R F Reedereigemeinschaft  
Forschungsschifffahrt GmbH

Station #	CTD/RO	Argpuns/Streamer	Test Releaser OBS	Aussetzen/Aufln. OBS/OBH	OPOS	TV/MUC	TV-Greifer	Minicorer (MIC)	SL (Schwerlot)	Plankton	Side-Scan-Sonar (DTS)	PN/HS-Vermessungsprofil	sm PN/HS-Profil	W 1 Zeit	W 2 Zeit	W 3 Zeit	W 4 Zeit	W 9 Zeit	W 11 Zeit	W 12 Zeit	W 1 Länge	W 2 Länge	W 3 Länge	W 4 Länge	W 9 Länge	W 11 Länge	W 12 Länge	Bemerkungen		
# 1		1										1	152															Profil Test		
# 2	1		1												1,7						2100									
# 3															1,6						2185									
# 4			1									1	68		1,5						2100									
# 5	1														1,2						1798									
# 6																											1867			
# 7																											1845			
# 8																											1855			
# 9																											1866			
# 10																											1862			
# 11															1,6						1800						1783			
# 12	1		1				1					12	190		1,6						2105							2080	Ausselzen von 15 OBS/OBH ohne Streamer, seism. Profile m. OBS Aufnahme von 11 OBS/OBH	
# 13																														
# 14																														
# 15																														
# 16		1																												
# 17																														
# 18															0,4						205						2081			
# 19																											2067			
# 20																											2099			
# 21																											1804			
# 22																														
# 23		1																												
# 24																														
# 25	1																													
# 26																														
# 27	1																													
# 28																														
# 29	1																													
# 30																														
# 31		1																												
# 32																														
# 33															0,2						30,2	120						6308		

Appendix 2

Sonar.ini file

```
=====
This file contains settings you can use to customize
the sonar data acquisition processor SEE SONAR.TXT for
documentation
;=====

;Honeywell Pitch Roll
[Seria12]
Create=1
Parser=4
Baud=19200
NetworkRaw=1
Port=2
DISK=1
DiskRaw=0

[Seria13]
Create=0
Port=3
Baud=9600

[Seria14]
Create=0
Port=4
Baud=9600

[Seria15]
Create=0
Port=5
Baud=9600

[Seria16]
Create=0
Port=6
Baud=9600

;=====
Main / overall settings.
;=====

[Main]
;Do not change:
DisableDisplay=0
Priority=1
```



```
NetDataIF=1
DspSimulator=0
NCARD=1
NETWORK QUEUE SIZE=1024
DSP QUEUE SIZE=1024
PostProcessing=1
IgnoreMFOverlap=0
;COMMAND PORT=1600
;DATA PORT=1601
CmdXmitSize=60000
CmdRecvSize=60000
DataXmitSize=150000
DataRecvSize=60000
NSUB=3
DSPSyncInterva1=30000
;XmitRate=400000
;XmitBufSize=40000
;New Command Follows
TimeSyncNetwork=0
;PciPollInterva1=10

PostCodes=00001 10001 11001 00012 00022 00032 00042
IgnorePostError=0

;=====
;Options for Subbottom
;=====

[SUB0]
;Do not change:
PulseDirectory=../SBPulse/
NCHAN=1
SystemType=0
;User configurable options:
PING RATE=8000
Ping Select=Default
;PING TRIGGER=3
;TriggerDelay=300000
TriggerSystem=1
TriggerMask=2
Trig-B IN Only
PING TRIGGER=2

TelemetryFormat=0
EnableData=1

;=====
;Subbottom Channel 0 of IO
```

;  
=====

[SUB0IO0]  
;Do not change:  
DACChan=0  
ADCCChan=0  
Data\_Type=1  
ADC ANALOGCARDGAIN=1  
CompressNet=0  
CompressDisk=0

;User configurable options:  
;Note that full power = 1000 on PING\_GAIN  
PING\_GAIN=1000  
ADC\_GAIN=2  
ADC\_AGC=0  
DATA\_NETWORK\_WINDOW=1 1 0 4000 40000  
DATA\_FILE\_WINDOW=1 1 0 4000 40000  
DATA\_FILE=1

;  
=====

;Options for Side Scan Low (2 Channels)

;  
=====

[SUB1]  
;Do not change the following:  
PulseDirectory=../SLPulse/  
NCHAN=3  
SystemType=1  
SystemNumber=20  
USE\_ANALOG\_CARD=8  
;USE\_ANALOG\_CARD=0  
;Some of the user configurable defaults  
PING\_RATE=12000  
PING\_SELECT=Default  
PING\_TRIGGER=0  
;TriggerDelay=1000000  
TriggerMask=200  
;Trig-B OUT Only  
TelemetryFormat=0  
EnableData=I

;  
=====

SSL Channel 0 of IO (Port)

;  
=====

[SUB1IO0]  
;Do not change:

```
DACChan=2 ADCChan=2
PROCESSING_PAKDELAY=-1
Data_Type=0
ADC_GAIN=32000
ADC_ANALOGCARDGAIN=1
ADC_AGC=0
CompressNet=0
CompressDisk=0
;Some user configurable options:
DATA_NETWORK_WINDOW=1 1 0 13021 40000
DATA_FILE_WINDOW=1 1 0 13021 40000
;Note that full power = 1000 on PING_GAIN
PING_GAIN=1000
DATA_FILE=1

;=====
SSL Channel 1 of IO (Starboard)
;=====

[SUB1IO1]
;Do not change:
DACChan=3
ADCChan=3
Data_Type=0
PROCESSING_PAKDELAY=-1
ADC_GAIN=32000
ADC_ANALOGCARDGAIN=1
ADC_AGC=0
CompressNet=0
CompressDisk=0
;Some user configurable options:
DATA_NETWORK_WINDOW=1 1 0 13021 40000
DATA_FILE WINDOW=1 1 0 13021 40000
;Note that full power = 1000 on PING_GAIN
PING_GAIN=1000
DATA_FILE=1

;=====
SSL Channel 2 (Variable Gain Amp)
;=====

[SUB1IO2]
;Do not change:
DACChan=6
ADCChan=-2

;=====
;Options for Side Scan High (2 Channels)
```



;=====

[SUB2]  
;Do not change the folowing:  
PulseDirectory=../SHPulse/  
NCHAN=3  
SystemType=2  
SystemNumber=21  
USE\_ANALOG\_CARD=8

;Some of the user configurable defaults  
PING\_RATE=30000  
Ping\_select=Default  
PING\_TRIGGER=0  
;TriggerDelay=1000000  
TriggerMask=200 ;Trig-B OUT Only  
TriggerSystem=20  
TelemetryFormat=0  
EnableData=I

;=====

SSH Channel 0 of IO (Port)

;=====

[SUB2IO0]  
;Do not change:  
DACChan=4  
ADCChan=4  
Data\_Type=0  
PROCESSING\_PAKDELAY=-1  
ADC\_GAIN=32000  
ADC\_ANALOGCARDGAIN=1  
ADC\_AGC=0  
CompressNet=0  
CompressDisk=0  
;User configurable options:  
DATA\_NETWORK\_WINDOW=1 1 0 58593 40000  
DATA\_FILE\_WINDOW=1 1 0 58593 40000  
Note that full power = 1000 on PING\_GAIN  
PING\_GAIN=1000  
DATA\_FILE=1

;=====

SSH Channel 1 of IO (Starboard)

;=====

```
[SUB2IO1]
;Do not change:
DACChan=5
ADCCChan=5
Data_Type=0
PROCESSING_PAKDELAY=-1
ADC_GAIN=32000
ADC_ANALOGCARDGAIN=1
ADC_AGC=0
CompressNet=0
CompressDisk=0

;User configurable options:
DATA_NETWORK_WINDOW=1 1 0 58593 40000
DATA_FILE_WINDOW=1 1 0 58593 40000
; Note that full power = 1000 on PING_GAIN
PING_GAIN=1000
DATA_FILE=1

;=====
;SSH Variable Gain Amp
;=====

[SUB2IO2]
;Do not change:
DACChan=7
ADCCChan=-2

;=====
;Options for the First (and only) DSP Card
;=====

[DSP0]
;Do not change the following:
BigBuf=1
USE_ANALOG_CARD=0
DspExecutable=.\Sonrfsic.out
FPGAFile=fsic_v6.bit

DIAGNOSTIC_PARAMETERS=2 4000 2000 2000 40000 64000 -
20000 100000 0 0
TemperatureAlertsEnable=1
LowRateIOAlgorithm=4
LOWRATEIO_NETWORK=1

; TimeSyncMask Values: 4=BNC_2, 2=BNC_1, 1=BNC_0
; Uncomment line below to enable 1 pps hardware time
sync;
```

TimeSyncMask=0

;  
;=====

;Pitch Roll Serial Ports

;=====

[xSerial]

Create=2

DMUVersion=1

HeaveTC=50

TIMECONSTANT=50

CALCONSTANT=100

[xSeria13]

Create=2

DMUVersion=1

HeaveTC=50

TIMECONSTANT=50

CALCONSTANT=100

Port=5

[FILE]

BaseName=\\DATA\\DATA

PrimaryDrive=D:

BackupDrive=E:

FileQueueSize=1000

MaxFileSize=



Appendix 3

**Appendix 3.1** Channel assignment and midpoint distances of hydrophone groups from beginning of each active section.

Segment of 25 m length	Hydrophone Group No.	Channel No. In Section	Midpoint Distance
A (0-25 m)	1	1	3.1 m
A	2	3	11.3 m
A	3	2	15.6 m
A	4	4	23.3 m
B (25-50 m)	1	5	28.1 m
B	2	7	36.3 m
B	3	6	40.6 m
B	4	8	48.3 m
C (50-75 m)	1	9	53.1 m
C	2	11	61.3 m
C	3	10	65.6 m
C	4	12	73.3 m
d (75-100 m)	1	13	78.1 m
D	2	15	86.3 m
D	3	14	90.6 m
D	4	16	98.3 m

**Appendix 3.2a** Bird positions along the seismic streamer for profilesGeoB01-017 to GeoB01-029

Bird No.	Position	Distance to Streamer Winch	Bird Type
3	End of Stretch Section No. 2	123 m	MTC-Bird
11	Mid of Active section No. 1	173 m	DigiBird
4	Mid of Active Section No. 2	273 m	MTC-Bird
13	End of Active Section No. 2	323 m	DigiBird
6	End of Active Section No. 3	423 m	MTC-Bird
14	Mid of Active Section No. 4	473 m	DigiBird
5	Mid of Active Section No. 5	573 m	MTC-Bird
2	End of Active Section No. 5	623 m	MTC-Bird
15	End of Active Section No. 6	723 m	DigiBird

**Appendix 3.2b** Bird positions along the seismic streamer for profiles GeoB01-030 to GeoB01-087

Bird No.	Position	Distance to Streamer Winch	Bird Type
3	End of Stretch Section No. 2	123 m	MTC-Bird
11	Mid of Active section No. 1	173 m	DigiBird
12	End of Active Section No. 1	223 m	DigiBird
4	Mid of Active Section No. 2	273 m	MTC-Bird
13	End of Active Section No. 2	323 m	DigiBird
6	End of Active Section No. 3	423 m	MTC-Bird
14	Mid of Active Section No. 4	473 m	DigiBird
5	Mid of Active Section No. 5	573 m	MTC-Bird
2	End of Active Section No. 5	623 m	MTC-Bird
15	End of Active Section No. 6	723 m	DigiBird

**Appendix 3.3 Streamer Channel Assignments for Output Recording Channels.****Appendix 3.3a Streamer channel 1 to 48 assignment to output channel for Jupiter recording system (GI Gun)**

Input Channel	Output Channel	Hydrophone Group	Number of Hydrophones per Group	Hydrophone Group Length [m]	Hydrophone Group distance [m]
1	1	HG1	13	6.25	12.5
2	2	HG3	13	6.25	12.5
5	3	HG1	13	6.25	12.5
6	4	HG3	13	6.25	12.5
9	5	HG1	13	6.25	12.5
10	6	HG3	13	6.25	12.5
13	7	HG1	13	6.25	12.5
14	8	HG3	13	6.25	12.5
17	9	HG1	13	6.25	12.5
18	10	HG3	13	6.25	12.5
21	11	HG1	13	6.25	12.5
22	12	HG3	13	6.25	12.5
25	13	HG1	13	6.25	12.5
26	14	HG3	13	6.25	12.5
29	15	HG1	13	6.25	12.5
30	16	HG3	13	6.25	12.5
33	17	HG1	13	6.25	12.5
34	18	HG3	13	6.25	12.5
37	19	HG1	13	6.25	12.5
38	20	HG3	13	6.25	12.5
41	21	HG1	13	6.25	12.5
42	22	HG3	13	6.25	12.5
45	23	HG1	13	6.25	12.5
46	24	HG3	13	6.25	12.5
49	25	HG1	13	6.25	12.5
50	26	HG3	13	6.25	12.5
53	27	HG1	13	6.25	12.5
54	28	HG3	13	6.25	12.5
57	29	HG1	13	6.25	12.5
58	30	HG3	13	6.25	12.5
61	31	HG1	13	6.25	12.5
62	32	HG3	13	6.25	12.5
65	33	HG1	13	6.25	12.5
66	34	HG3	13	6.25	12.5
69	35	HG1	13	6.25	12.5
70	36	HG3	13	6.25	12.5
73	37	HG1	13	6.25	12.5
74	38	HG3	13	6.25	12.5
77	39	HG1	13	6.25	12.5
78	40	HG3	13	6.25	12.5
81	41	HG1	13	6.25	12.5
82	42	HG3	13	6.25	12.5
85	43	HG1	13	6.25	12.5
86	44	HG3	13	6.25	12.5
89	45	HG1	13	6.25	12.5
90	46	HG3	13	6.25	12.5
93	47	HG1	13	6.25	12.5
94	48	HG3	13	6.25	12.5

**Appendix 3.3b** Streamer channel 49 to 96 assignment to output channel for Spectra recording system (Watergun)

Input Channel	Output Channel	Hydrophone Group	Number of Hydrophones per Group	Hydrophone Group Length [m]	Hydrophone Group distance [m]
3	49	HG2	6	2.2	13
4	50	HG4	9	3.3	12
7	51	HG2	6	2.2	13
8	52	HG4	9	3.3	12
11	53	HG2	6	2.2	13
12	54	HG4	9	3.3	12
15	55	HG2	6	2.2	13
16	56	HG4	9	3.3	12
19	57	HG2	6	2.2	13
20	58	HG4	9	3.3	12
23	59	HG2	6	2.2	13
24	60	HG4	9	3.3	12
27	61	HG2	6	2.2	13
28	62	HG4	9	3.3	12
31	63	HG2	6	2.2	13
32	64	HG4	9	3.3	12
35	65	HG2	6	2.2	13
36	66	HG4	9	3.3	12
39	67	HG2	6	2.2	13
40	68	HG4	9	3.3	12
43	69	HG2	6	2.2	13
44	70	HG4	9	3.3	12
47	71	HG2	6	2.2	13
48	72	HG4	9	3.3	12
51	73	HG2	6	2.2	13
52	74	HG4	9	3.3	12
55	75	HG2	6	2.2	13
56	76	HG4	9	3.3	12
59	77	HG2	6	2.2	13
60	78	HG4	9	3.3	12
63	79	HG2	6	2.2	13
64	80	HG4	9	3.3	12
67	81	HG2	6	2.2	13
68	82	HG4	9	3.3	12
71	83	HG2	6	2.2	13
72	84	HG4	9	3.3	12
75	85	HG2	6	2.2	13
76	86	HG4	9	3.3	12
79	87	HG2	6	2.2	13
80	88	HG4	9	3.3	12
83	89	HG2	6	2.2	13
84	90	HG4	9	3.3	12
87	91	HG2	6	2.2	13
88	92	HG4	9	3.3	12
91	93	HG2	6	2.2	13
92	94	HG4	9	3.3	12
95	95	HG2	6	2.2	13
96	96	HG4	9	3.3	12

Appendix 3.4

Trigger and Delays M52/1

Depth [m]	TWT [ms]	Delay [ms]	Shot Time Watergun [ms]	Shot Time GI Gun [ms]	Recording Time Watergun [ms]	Recording Time GI Gun (BISON-2) [ms]	DigiBird Controller [ms]	MTC- Controller [ms]	EPC Online Recording [ms]	Total Trigger Period [ms]
0	0	0	0	1500	0 - 1500	1500 - 4500	5000	5500	0	9000
375	500	500	0	2000	500 - 2000	2500 - 5500	6000	6500	2500	9000
750	1000	1000	0	2500	1000 - 2500	3500 - 6500	7000	7500	3000	9000
1125	1500	1500	0	3000	1500 - 3000	4500 - 7500	3300	0	4500	9000
1500	2000	2000	0	3500	2000 - 3500	5500 - 8500	0	500	5000	9000
1875	2500	2500	0	4000	2500 - 4000	6500 - 9500	0	500	6500	9500



Appendix 3.5

List of stations

Profile	Start Latitude	Start Longitude	Date	Time (UTC)	End Latitude	End Longitude	Date	Time (UTC)
GeoB 02-045	44 18,06 N	34 52,48 E	22.01.2002	17:30				
WP	44 17,06 N	34 47,16 E	22.01.2002	18:07				
WP	44 16,15 N	34 42,88 E	22.01.2002	18:37				
					44 15,62 N	34 40,15 E	22.01.2002	18:56
GeoB 02-046	44 15,03 N	34 40,63 E	22.01.2002	19:13	44 15,03 N	34 40,63 E	22.01.2002	19:13
WP	44 15,55 N	34 43,23 E	22.01.2002	19:30				
WP	44 16,41 N	34 47,56 E	22.01.2002	20:01				
					44 17,01 N	34 50,54 E	22.01.2002	20:22
GeoB 02-047	44 10,11 N	34 50,48 E	22.01.2002	20:35				
WP	44 15,56 N	34 47,67 E	22.01.2002	20:54				
WP	44 14,70 N	34 43,42 E	22.01.2002	21:24				
					44 14,22 N	34 41,02 E	22.01.2002	21:40
GeoB 02-048	44 13,64 N	34 41,47 E	22.01.2002	21:53				
Sorcus Reset	44 14,02 N	34 43,42	22.01.2002	22:06				
WP	44 14,10 N	34 43,80 E	22.01.2002	22:09				
WP	44 14,95	34 48,06	22.01.2002	22:40				
					44 15,45 N	34 50,66 E	22.01.2002	22:57
GeoB 02-049	44 15,84	34 50,25	22.01.2002	23:08				
WP	44 15,35 N	34 47,81 E	22.01.2002	23:24				
WP	44 14,50 N	34 43,36 E	22.01.2002	23:55				
					44 14,02 N	34 41,11 E	23.01.2002	0:11
GeoB 02-050	44 13,43 N	34 41,55 E	23.01.2002	0:26				
WP	44 13,95 N	34 44,13 E	23.01.2002	0:43				
WP	44 14,79 N	34 48,40 E	23.01.2002	1:14				
					44 15,23 N	34 50,24 E	23.01.2002	1:29
GeoB 02-051	44 15,62 N	34 50,24 E	23.01.2002	1:41				
WP	44 15,16 N	34 47,92 E	23.01.2002	1:57				
WP	44 14,25 N	34 43,36 E	23.01.2002	2:28				
					44 13,83 N	34 41,22 E	23.01.2002	2:43
GeoB 02-052	44 13,27 N	34 41,86 E	23.01.2002	2:58				
WP	44 13,71 N	34 44,06 E	23.01.2002	3:13				
WP	44 14,56 N	34 48,40 E	23.01.2001	3:43				
					44 15,00 N	34 50,53 E	23.01.2002	3:58
GeoB 02-053	44 14,07 N	34 50,31 E	23.01.2002	4:15				
WP	44 13,70 N	34 48,43 E	23.01.2002	4:28				
WP	44 12,83 N	34 44,08 E	23.01.2002	4:58				
					44 12,35 N	34 41,69 E	23.01.2002	5:14
GeoB 02-054	44 11,94 N	34 42,09 E	23.01.2002	5:25 ca. 06:05				
					44 13,63 N	34 50,69 E	23.01.2002	6:24
GeoB 02-055	44 14,48 N	34 50,20 E	23.01.2002	6:39				
WP	44 14,11 N	34 48,29 E	23.01.2002	6:52				
WP	44 13,24 N	34 43,96 E	23.01.2002	7:22				
					44 12,73 N	34 41,44 E	23.01.2002	7:39
GeoB 02-056	44 12,26 N	34 42,01 E	23.01.2002	7:48			23.01.2002	
GeoB 02-057	44 12,30 N	34 46,72 E	23.01.2002	8:24				
WP	44 12,96 N	34 46,46 E	23.01.2002	8:30				
WP	44 16,67 N	34 45,04 E	23.01.2002	9:06				
					44 18,89 N	34 44,19 E	23.01.2002	9:28
GeoB 02-058	44 18,64 N	34 43,68 E	23.01.2002	9:47				
WP	44 16,45 N	34 44,56 E	23.01.2002	10:09				
WP	44 12,64 N	34 46,04 E	23.01.2002	10:45				
					44 11,86 N	34 46,33 E	23.01.2002	10:52
GeoB 02-059	44 12,10 N	34 46,61 E	23.01.2002	11:10 ca. 11:10				
WP	44 15,23 N	34 45,41 E	23.01.2002	11:40				
WP				11:54				
					44 18,84 N	34 44,01 E	23.01.2002	12:15
GeoB 02-060	44 18,49 N	34 43,39 E	23.01.2002	12:34				
WP	44 16,34 N	34 44,23 E	23.01.2002	12:54				
WP	44 12,63 N	34 45,65 E	23.01.2002	13:29				
					44 11,79 N	34 46,00 E	23.01.2002	13:38
GeoB 02-061	44 12,18 N	34 46,35 E	23.01.2002	13:55				
WP	44 13,87 N	34 46,05 E	23.01.2002	14:03				
					44 16,65 N	34 44,65 E	23.01.2002	14:37
GeoB 02-062	44 16,32 N	34 44,05 E	23.01.2002	14:48	44 12,53 N	34 45,49 E	23.01.2002	15:25

GeoB 02-063 44	13,10 N	34 46,80 E	24.01.2006	15:40	44 16,72 N	34 45,42 E	24.01.2006	16:15
GeoB 02-064 44	16,48 N	34 44,68 E	24.01.2006	16:27	44 12,73 N	34 46,11 E	24.01.2006	17:02
GeoB 02-065 44	12,99 N	34 46,78 E	24.01.2006	17:14	44 16,69 N	34 45,34 E	24.01.2006	17:50
GeoB 02-066 44	16,42 N	34 44,60 E	24.01.2006	18:03	44 12,67 N	34 46,06 E	24.01.2006	18:39
GeoB 02-067 44	12,97 N	34 46,71 E	24.01.2006	18:50	44 16,84 N	34 45,22 E	24.01.2006	19:26
GeoB 02-068 44	16,47 N	34 44,51 E	24.01.2006	19:38	44 12,59 N	34 46,02 E	24.01.2006	20:16
GeoB 02-069 44	12,97 N	34 46,61 E	24.01.2006	20:27	44 16,85 N	34 45,12 E	24.01.2006	21:04
GeoB 02-070 44	16,42 N	34 44,43 E	24.01.2006	21:15	44 12,56 N	34 45,97 E	24.01.2006	21:53
GeoB 02-071 44	12,99 N	34 46,52 E	24.01.2006	22:02	44 16,79 N	34 45,12 E	24.01.2006	22:37
GeoB 02-072 44	16,37 N	34 44,30 E	24.01.2006	22:49	44 12,58 N	34 45,79 E	24.01.2006	23:26
GeoB 02-073 44	13,01 N	34 46,45 E	24.01.2006	23:37	44 16,67 N	34 45,04 E	25.01.2006	0:13
GeoB 02-074 44	16,26 N	34 44,28 E	25.01.2006	0:25	44 12,62 N	34 45,69 E	25.01.2006	1:00
GeoB 02-075 44	12,98 N	34 46,40 E	25.01.2006	1:12	44 16,64 N	34 44,98 E	25.01.2006	1:48
GeoB 02-076 44	16,35 N	34 44,17 E	25.01.2006	2:00	44 12,65 N	34 45,60 E	25.01.2006	2:36
GeoB 02-077 44	13,02 N	34 46,30 E	25.01.2006	2:50	44 16,67 N	34 44,89 E	25.01.2006	3:25
GeoB 02-078 44	16,25 N	34 44,13 E	25.01.2006	3:41	44 12,65 N	34 45,53 E	25.01.2006	4:16
GeoB 02-079 44	12,90 N	34 46,26 E	25.01.2006	4:30	44 16,60 N	34 44,84 E	25.01.2006	5:06
GeoB 02-080 44	16,33 N	34 43,94 E	25.01.2006	5:20	44 12,63 N	34 43,38 E	25.01.2006	5:56
GeoB 02-081 44	12,90 N	34 46,18 E	25.01.2006	6:09	44 16,75 N	34 44,69 E	25.01.2006	6:46
GeoB 02-082 44	18,31 N	34 43,89 E	25.01.2006	6:56	44 12,47 N	34 45,40 E	25.01.2006	7:33
GeoB 02-083 44	12,93 N	34 46,21 E	25.01.2006	7:45	44 16,73 N	34 44,74 E	25.01.2006	8:22
GeoB 02-084 44	16,30 N	34 43,86 E	25.01.2006	8:34	44 12,51 N	34 45,34 E	25.01.2006	9:10
GeoB 02-085 44	12,90 N	34 46,16 E	25.01.2006	9:21	44 16,65 N	34 44,70 E	25.01.2006	9:57
GeoB 02-086 44	16,17 N	34 43,88 E	25.01.2006	10:12	44 12,49 N	34 45,31 E	25.01.2006	10:47
GeoB 02-087 44	12,86 N	34 46,08 E	25.01.2006	10:59	44 16,61 N	34 44,64 E	25.01.2006	11:35
GeoB 02-088 44	16,30 N	34 43,79 E	25.01.2006	11:48	44 12,58 N	34 45,24 E	25.01.2006	12:24
GeoB 02-089 44	13,05 N	34 45,95 E	25.01.2006	12:36	44 16,65 N	34 44,53 E	25.01.2006	13:11
GeoB 02-090 44	16,22 N	34 43,79 E	25.01.2006	13:24	44 12,54 N	34 45,22 E	25.01.2006	14:00
GeoB 02-091 44	12,91 N	34 45,90 E	25.01.2006	14:13	44 16,57 N	34 44,49 E	25.01.2006	14:48
GeoB 02-092 44	16,26 N	34 43,73 E	25.01.2006	15:03	44 12,55 N	34 45,18 E	25.01.2006	15:38
GeoB 02-093 44	12,86 N	34 45,85 E	25.01.2006	15:52	44 16,56 N	34 44,42 E	25.01.2006	16:27
GeoB 02-094 44	16,25 N	34 43,71 E	25.01.2006	16:42	44 12,57 N	34 45,13 E	25.01.2006	17:17
GeoB 02-095 44	12,80 N	34 45,81 E	25.01.2006	17:30	44 16,60 N	34 44,33 E	25.01.2006	18:07
GeoB 02-096 44	16,27 N	34 43,57 E	25.01.2006	18:18	44 12,39 N	34 45,08 E	25.01.2006	18:55
GeoB 02-097 44	12,78 N	34 45,73 E	25.01.2006	19:06	44 16,65 N	34 44,24 E	25.01.2006	19:42
GeoB 02-098 44	16,23 N	34 43,44 E	25.01.2006	19:53	44 12,40 N	34 44,92 E	25.01.2006	20:30
GeoB 02-099 44	12,78 N	34 45,64 E	25.01.2006	20:41	44 16,60 N	34 44,18 E	25.01.2006	21:17
GeoB 02-100 44	16,24 N	34 43,21 E	25.01.2006	21:29	44 12,40 N	34 44,69 E	25.01.2006	22:05
GeoB 02-101 44	12,79 N	34 45,51 E	25.01.2006	22:18	44 16,46 N	34 44,06 E	25.01.2006	22:54
GeoB 02-102 44	16,15 N	34 43,11 E	25.01.2006	23:06	44 12,33 N	34 44,46 E	25.01.2006	23:42
GeoB 02-103 44	12,84 N	34 45,38 E	25.01.2006	23:54	44 16,51 N	34 43,97 E	26.01.2006	0:29
GeoB 02-104 44	16,04 N	34 43,03 E	26.01.2006	0:44	44 12,36 N	34 44,47 E	26.01.2006	1:20
GeoB 02-105 44	12,79 N	34 45,34 E	26.01.2006	1:32	44 16,46 N	34 43,90 E	26.01.2006	2:08
GeoB 02-106 44	16,11 N	34 42,94 E	26.01.2006	2:24	44 12,41 N	34 44,37 E	26.01.2006	3:00
GeoB 02-107 44	12,86 N	34 45,74 E	26.01.2006	3:19	44 16,53 N	34 44,33 E	26.01.2006	3:54
GeoB 02-108 44	16,20 N	34 43,33 E	26.01.2006	4:10	44 12,52 N	34 44,76 E	26.01.2006	4:46
GeoB 02-109 44	12,80 N	34 45,86 E	26.01.2006	5:01	44 16,53 N	34 44,42 E	26.01.2006	5:37
GeoB 02-110 44	16,25 N	34 43,50 E	26.01.2006	5:53	44 12,40 N	34 45,02 E	26.01.2006	6:30
GeoB 02-111 44	12,85 N	34 45,93 E	26.01.2006	6:42	44 16,67 N	34 44,44 E	26.01.2006	7:18
GeoB 02-112 44	16,26 N	34 43,68 E	26.01.2006	7:30	44 12,43 N	34 45,18 E	26.01.2006	8:06
GeoB 02-113 44	12,89 N	34 45,96 E	26.01.2006	8:17	44 16,65 N	34 44,47 E	26.01.2006	8:53
GeoB 02-114 44	16,28 N	34 43,75 E	26.01.2006	9:04	44 12,47 N	34 45,25 E	26.01.2006	9:40
GeoB 02-115 44	12,94 N	34 46,01 E	26.01.2006	9:51	44 16,60 N	34 44,58 E	26.01.2006	10:27
GeoB 02-116 44	16,20 N	34 43,85 E	26.01.2006	10:41	44 12,48 N	34 45,33 E	26.01.2006	11:16
GeoB 02-117 44	12,89 N	34 46,07 E	26.01.2006	11:27	44 16,59 N	34 44,67 E	26.01.2006	12:03
GeoB 02-118 44	16,29 N	34 43,87 E	26.01.2006	12:15	44 12,51 N	34 45,37 E	26.01.2006	12:52
GeoB 02-119 44	12,96 N	34 46,15 E	26.01.2006	13:03	44 16,61 N	34 44,72 E	26.01.2006	13:38
GeoB 02-120 44	16,29 N	34 43,93 E	26.01.2006	13:50	44 12,57 N	34 45,43 E	26.01.2006	14:26
GeoB 02-121 44	13,02 N	34 46,23 E	26.01.2006	14:39	44 16,61 N	34 44,82 E	26.01.2006	15:15
GeoB 02-122 44	16,33 N	34 44,04 E	26.01.2006	15:29	44 12,63 N	34 45,47 E	26.01.2006	16:05
GeoB 02-123 44	12,93 N	34 46,31 E	26.01.2006	16:19	44 16,65 N	34 44,87 E	26.01.2006	16:55
GeoB 02-124 44	16,36 N	34 44,11 E	26.01.2006	17:10	44 12,62 N	34 45,54 E	26.01.2006	17:46
GeoB 02-125 44	12,91 N	34 46,37 E	26.01.2006	18:00	44 16,77 N	34 44,89 E	26.01.2006	18:37
GeoB 02-126 44	16,36 N	34 44,17 E	26.01.2006	18:49	44 12,52 N	34 45,68 E	26.01.2006	19:25
GeoB 02-127 44	12,93 N	34 46,44 E	26.01.2006	19:37	44 16,73 N	34 44,98 E	26.01.2006	20:14
GeoB 02-128 44	16,40 N	34 44,21 E	26.01.2006	20:26	44 12,53 N	34 45,73 E	26.01.2006	21:00
GeoB 02-129 44	12,91 N	34 46,44 E	26.01.2006	21:10	44 16,77 N	34 44,96 E	26.01.2006	21:45
GeoB 02-130 44	16,38 N	34 44,23 E	26.01.2006	21:55	44 12,68 N	34 45,65 E	26.01.2006	22:29
GeoB 02-131 44	12,93 N	34 46,37 E	26.01.2006	22:40	44 16,73 N	34 44,90 E	26.01.2006	23:14
GeoB 02-132 44	16,35 N	34 44,14 E	26.01.2006	23:25	44 12,62 N	34 45,60 E	26.01.2006	23:58

GeoB 02-133 44	12,94 N	34 46,34 E	27.01.2006	0:09	44 16,70 N	34 44,90 E	27.01.2006	0:43
GeoB 02-134 44	16,31 N	34 44,01 E	27.01.2006	0:56	44 12,52 N	34 45,47 E	27.01.2006	1:30
GeoB 02-135 44	12,93 N	34 46,27 E	27.01.2006	1:41	44 16,65 N	34 44,84 E	27.01.2006	2:15
GeoB 02-136 44	16,36 N	34 44,06 E	27.01.2006	2:25	44 12,58 N	34 45,33 E	27.01.2006	3:02
GeoB 02-137 44	12,92 N	34 46,21 E	27.01.2006	3:16	44 16,64 N	34 44,77 E	27.01.2006	3:49
GeoB 02-138 44	16,28 N	34 43,94 E	27.01.2006	4:03	44 12,61 N	34 45,37 E	27.01.2006	4:36
GeoB 02-139 44	12,88 N	34 46,14 E	27.01.2006	4:49	44 16,63 N	34 44,69 E	27.01.2006	5:22
GeoB 02-140 44	16,32 N	34 43,85 E	27.01.2006	5:37	44 12,46 N	34 45,33 E	27.01.2006	6:11
GeoB 02-141 44	12,83 N	34 46,08 E	27.01.2006	6:23	44 16,72 N	34 44,58 E	27.01.2006	6:58
GeoB 02-142 44	16,29 N	34 43,78 E	27.01.2006	7:10	44 12,47 N	34 45,26 E	27.01.2006	7:44
GeoB 02-143 44	12,85 N	34 46,00 E	27.01.2006	7:55	44 16,68 N	34 44,51 E	27.01.2006	8:30
GeoB 02-144 44	16,26 N	34 43,73 E	27.01.2006	8:40	44 12,43 N	34 45,21 E	27.01.2006	9:15
GeoB 02-145 44	12,84 N	34 45,88 E	27.01.2006	9:26	44 16,62 N	34 44,41 E	27.01.2006	10:00
GeoB 02-146 44	16,20 N	34 43,67 E	27.01.2006	10:11	44 12,56 N	34 45,09 E	27.01.2006	10:44
GeoB 02-147 44	12,99 N	34 46,44 E	27.01.2006	11:01	44 16,66 N	34 45,02 E	27.01.2006	11:34
GeoB 02-148 44	16,34 N	34 44,28 E	27.01.2006	11:43	44 12,61 N	34 45,75 E	27.01.2006	12:17
GeoB 02-149 44	13,00 N	34 46,50 E	27.01.2006	12:28	44 16,65 N	34 45,08 E	27.01.2006	13:01
GeoB 02-150 44	16,34 N	34 44,34 E	27.01.2006	13:12	44 12,67 N	34 45,77 E	27.01.2006	13:44
GeoB 02-151 44	13,03 N	34 46,55 E	27.01.2006	13:56	44 16,71 N	34 45,14 E	27.01.2006	14:29
GeoB 02-152 44	16,35 N	34 44,36 E	27.01.2006	14:45	44 12,64 N	34 45,82 E	27.01.2006	15:18
GeoB 02-153 44	13,06 N	34 46,62 E	27.01.2006	15:32	44 16,70 N	34 45,23 E	27.01.2006	16:05
GeoB 02-154 44	16,40 N	34 44,38 E	27.01.2006	16:20	44 12,67 N	34 45,83 E	27.01.2006	16:53
GeoB 02-155 44	13,10 N	34 47,22 E	27.01.2006	17:11	44 16,84 N	34 45,79 E	27.01.2006	17:44
GeoB 02-156 44	16,44 N	34 44,42 E	27.01.2006	18:01	44 12,58 N	34 45,92 E	27.01.2006	18:36
GeoB 02-157 44	13,16 N	34 47,44 E	27.01.2006	18:50	44 16,99 N	34 45,96 E	27.01.2006	19:25
GeoB 02-158 44	16,62 N	34 45,35 E	27.01.2006	19:35	44 12,78 N	34 46,83 E	27.01.2006	20:09
GeoB 02-159 44	13,19 N	34 47,55 E	27.01.2006	20:19	44 16,90 N	34 46,12 E	27.01.2006	20:53
GeoB 02-160 44	16,64 N	34 45,42 E	27.01.2006	21:02	44 12,85 N	34 46,89 E	27.01.2006	21:36
GeoB 02-161 44	13,32 N	34 47,63 E	27.01.2006	21:47	44 16,90 N	34 46,24 E	27.01.2006	22:20
GeoB 02-162 44	16,62 N	34 45,65 E	27.01.2006	22:30	44 12,94 N	34 47,09 E	27.01.2006	23:03
GeoB 02-163 44	13,26 N	34 47,75 N	27.01.2006	23:14	44 16,97 N	34 46,32 E	27.01.2006	23:47

Bemerkungen: Es wurden 5 mal eine 0.4 l GI-Gun (Verzögerung Injector: 30 ms) geschossen.

Danach wurde die kleine Gun zusammen mit einer 2x1.7 l GI-Gun im Airgun-Mode geschossen.

Die GI-Guns wurden alle 9.5 sec geschossen. Dazwischen wurde 5.5 s nach der GI-Gun eine Watergun geschossen.

Bei einem Ausfall der Sorcus-Karte oder einem Reset der Sorcus-Karte beginnt das Schießschema immer mit den 5

Bei dem Sorcus-Reset auf Profil 048 wurde die Schußzeit der grossen GI-Gun um 8 ms nach hinten gesetzt,

um die Guns besser zeitgleich zu schießen.

Von Profil Geob 02-048 bis GeoB-054 hat bei der kleinen GI-Gun nur der injector geschossen. Zum Teil wurden die

Appendix 4.1

INSTRUMENT	LAT (S) D:M	LON (W) D:M	DEPTH (m)	RELEASER- CODE	ANT. CH.	RECORDER NUMBER	SKEW (ms)
OBS01	44 :24,653	35 :05,392	1907	C459 (A)	C	991202	0
OBS02	44 :23,780	35 :06,002	1876	C454 (A)	D	000613	0
OBS03	44 :22,895	35 :06,656	1904	6354 (B)	C	980908	10
OBS04	44 :21,999	35 :07,318	1959	4A49 (B)	C	990901	-6
OBS05	44 :20,656	35 :08,309	2022	4A54 (B)	C	990712	-3
OBS06	44 :19,359	35 :09,277	2051	A314 (A)	C	991292	-16
OBS07	44 :18,491	35 :09,915	2060	6339 (B)	D	001005	-23
OBS08	44 :17,504	35 :10,543	1892	B559 (A)	C	001006	0
OBS09	44 :16,679	35 :11,238	2065	3A06 (B)	D	001002	10
OBS10	44 :15,800	35 :11,891	2069	3619 (B)	D	980907	-6
OBH11	44 :14,041	35 :13,166	2087	D654 (A)	D	971201	-3
OBH12	44 :19,447	35 :15,536	1993	C679 (A)	D	980906	-16
OBH13	44 :18,490	35 :13,080	2034	C464 (A)	D	001003	-23
OBH14	44 :16,536	35 :08,156	2091	3679 (B)	D	001001	4
OBH15	44 :15,565	35 :05,727	2121	A324 (A)	D	980905	-8

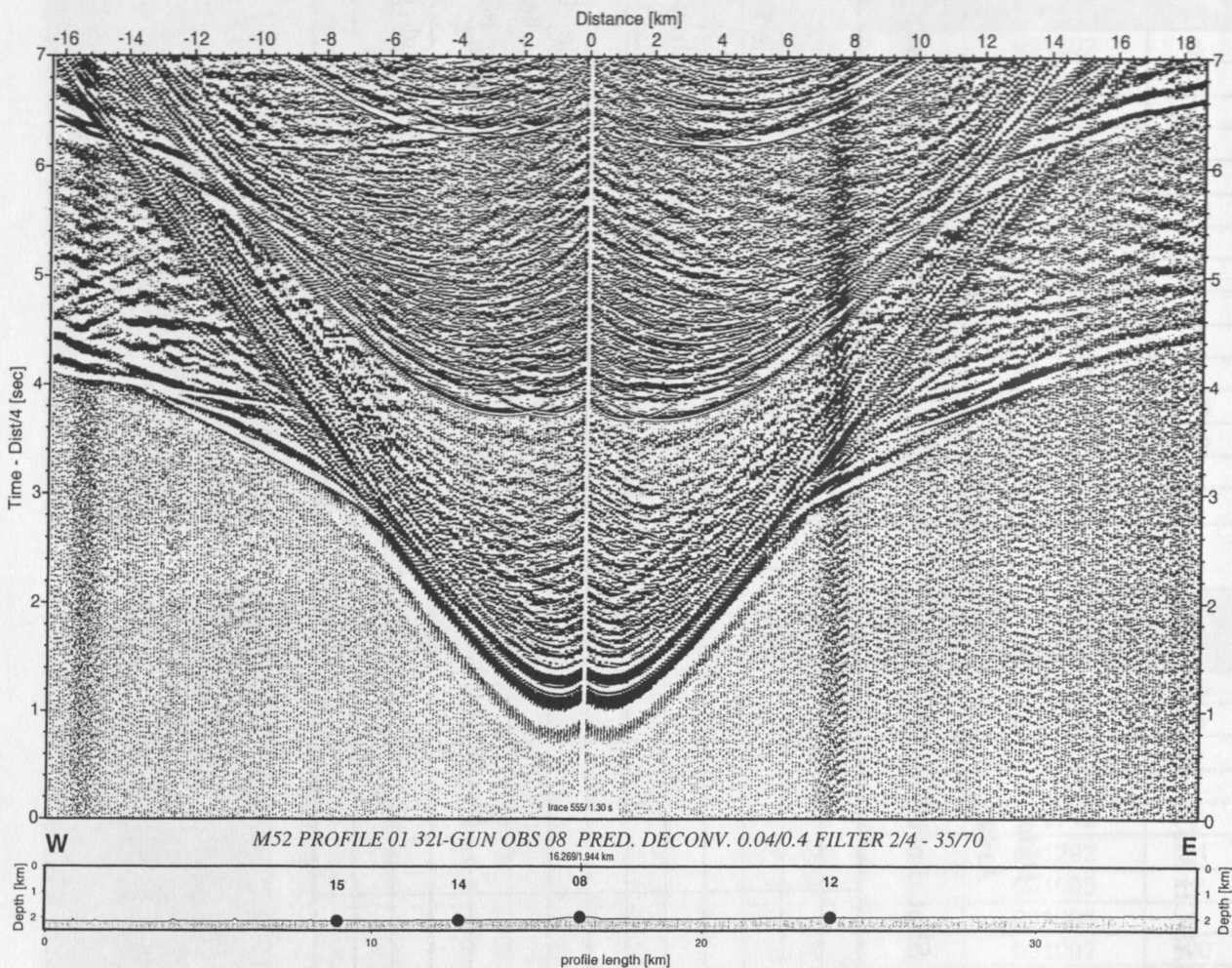
INSTRUMENT	LAT (S) D:M	LON (W) D:M	DEPTH (m)	RELEASER- CODE	ANT. CH.	RECORDER NUMBER	SKEW (ms)
OBS16	44 :14,160	34 :45,090	2124	C459 (A)	D	991202	-19
OBS17	44 :14,210	34 :45,430	2119	C454 (A)	C	000613	86
OBS18	44 :14,280	34 :45,800	2116	6354 (B)	D	980908	5
OBS19	44 :14,490	34 :45,740	2536	4A49 (B)	C	990901	-1
OBS20	44 :14,430	34 :45,380	2116	4A54 (B)	D	990712	-7
OBS21	44 :14,350	34 :45,010	2113	A314 (A)	C	991292	-21
OBS22	44 :14,540	34 :44,940	2090	6339 (B)	D	001005	12
OBS23	44 :14,610	34 :45,300	2096	B559 (A)	C	001006	4
OBS24	44 :14,680	34 :45,630	2641	3A06 (B)	D	001002	190
OBH25	44 :14,760	34 :45,980	2096	A324 (A)	C	911201	-20
OBH26	44 :14,900	34 :45,550	2066	3679 (B)	D	980906	8
OBS27	44 :14,830	34 :45,180	2069	3619 (B)	C	980907	91
OBH28	44 :14,740	34 :44,840	2074	C464 (A)	D	001001	89
OBH29	44 :15,040	34 :45,100	2045	C679 (A)	C	980905	-14

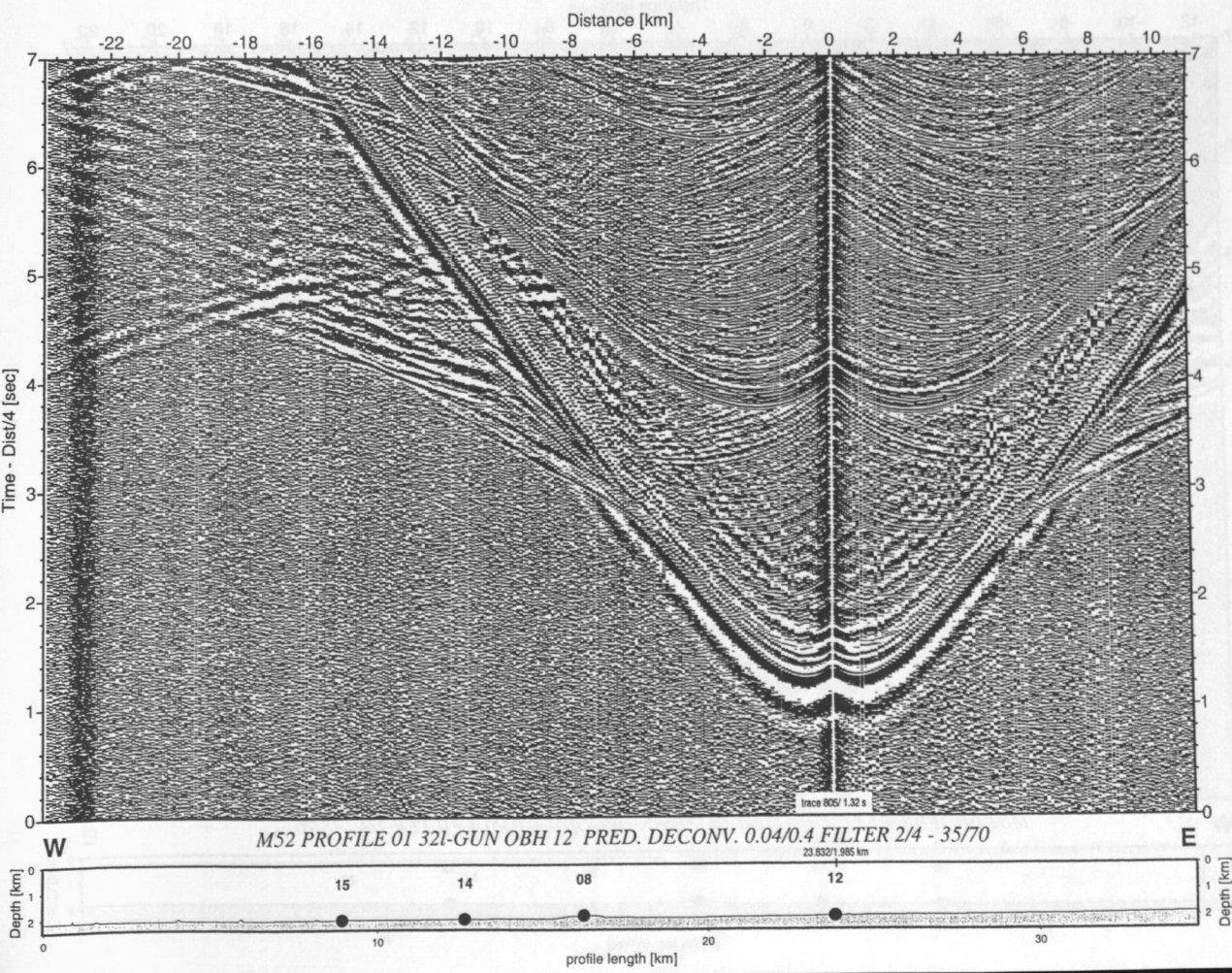
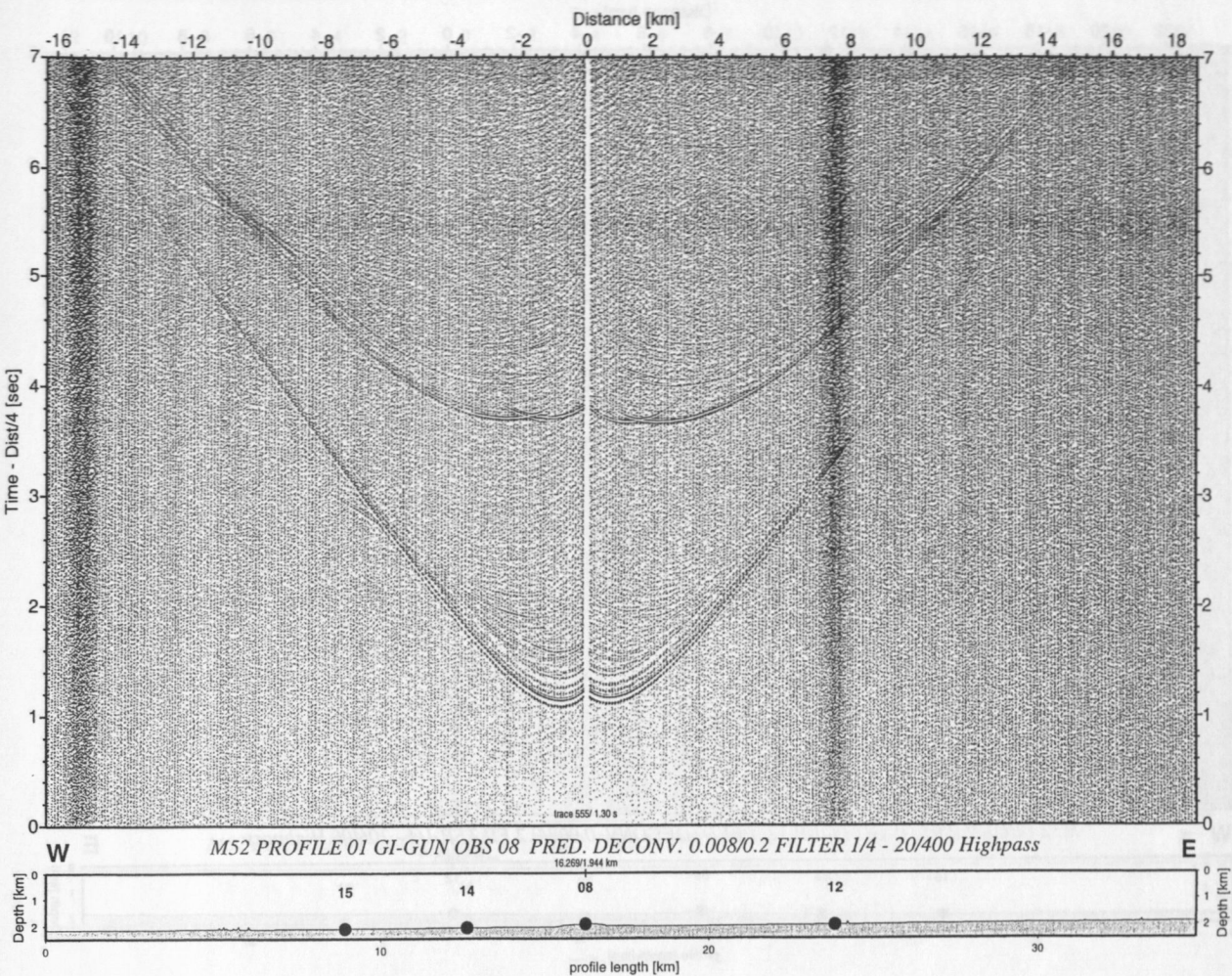


MARGASCH M52 - AIRGUN PROTOCOL

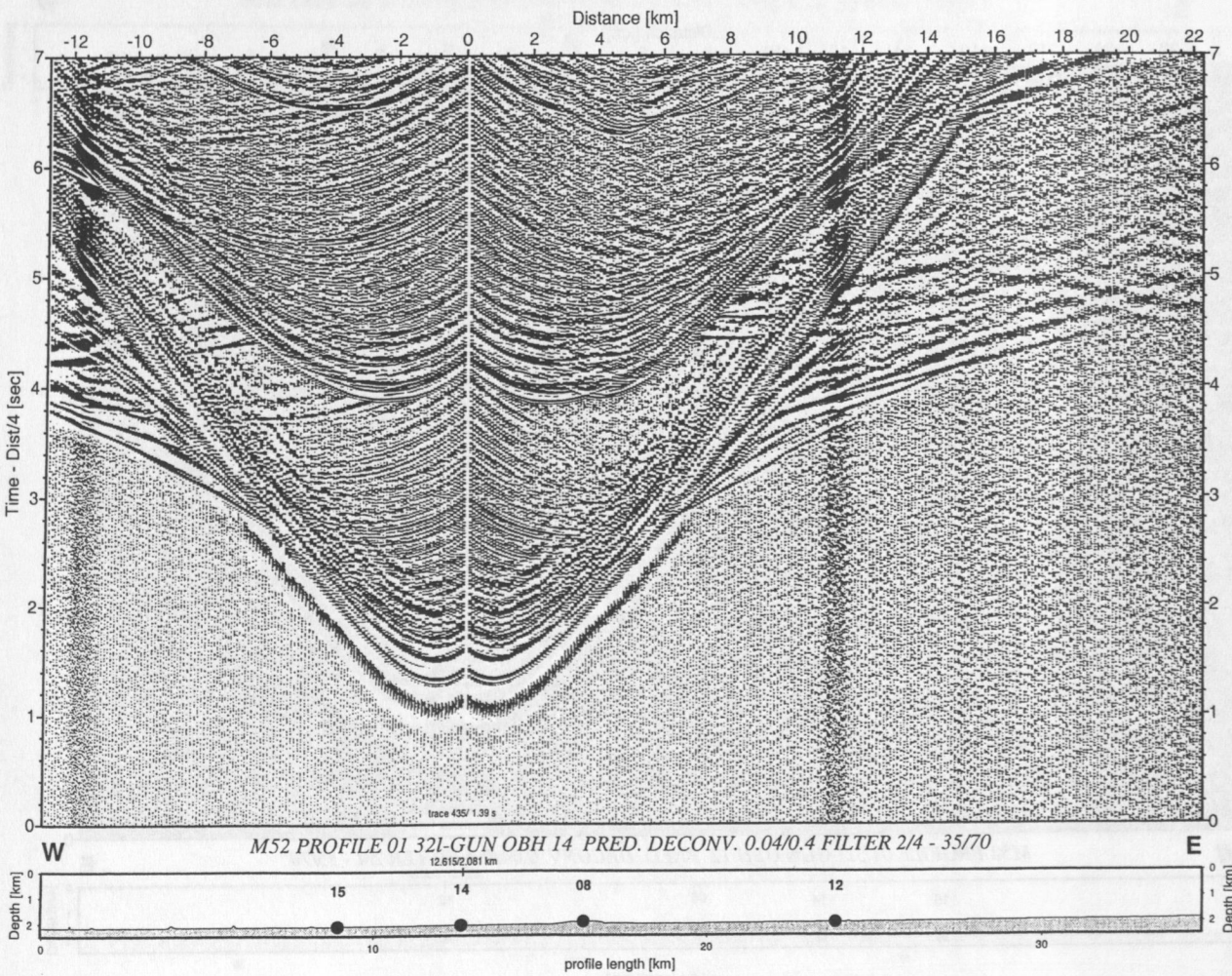
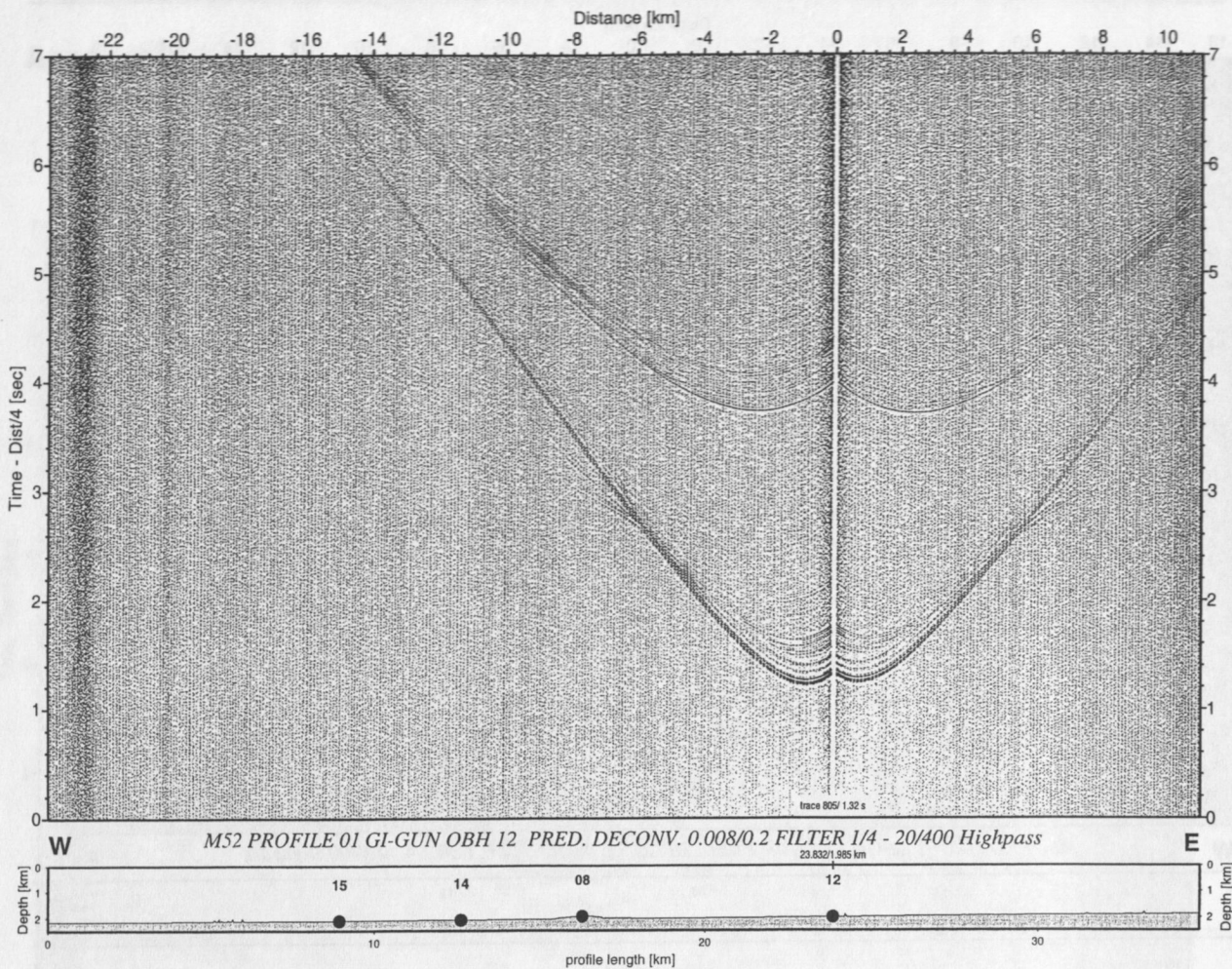
Project:		M52		Date:		07.01.02		
Profile:		P01		Area:		Sorokin		
Coordinates								
Latitude: N	Longitude: E	Time	First Shot	Last Shot	Starbord 35l	Port 35l	Port 0.7l	Remarks
44°12,65	34°54,06	14:57	X		150bar	150bar	150bar	
44°14,97	34°59,41	16:39				150bar	150bar	trigger cable stb gun cut
44°13,00	35°00,00	16:49				150bar	150bar	start profile P01
		17:00				150bar		0.7l gun out
44°13,76	35°01,29	17:20				150bar	150bar	0.7l gun shooting again
44°22,44	35°22,94	23:08				145bar	145bar	end profile P01
08.01.02								
44°27,20	35°03,06	02:31				145bar	145bar	start profile P02
44°10,11	35°16,14	07:38			145bar	145bar	145bar	both 35l guns shooting
43°59,69	35°23,54	10:38		X				end profile P02
								Number of total shots =
								3175

Appendix 4.2

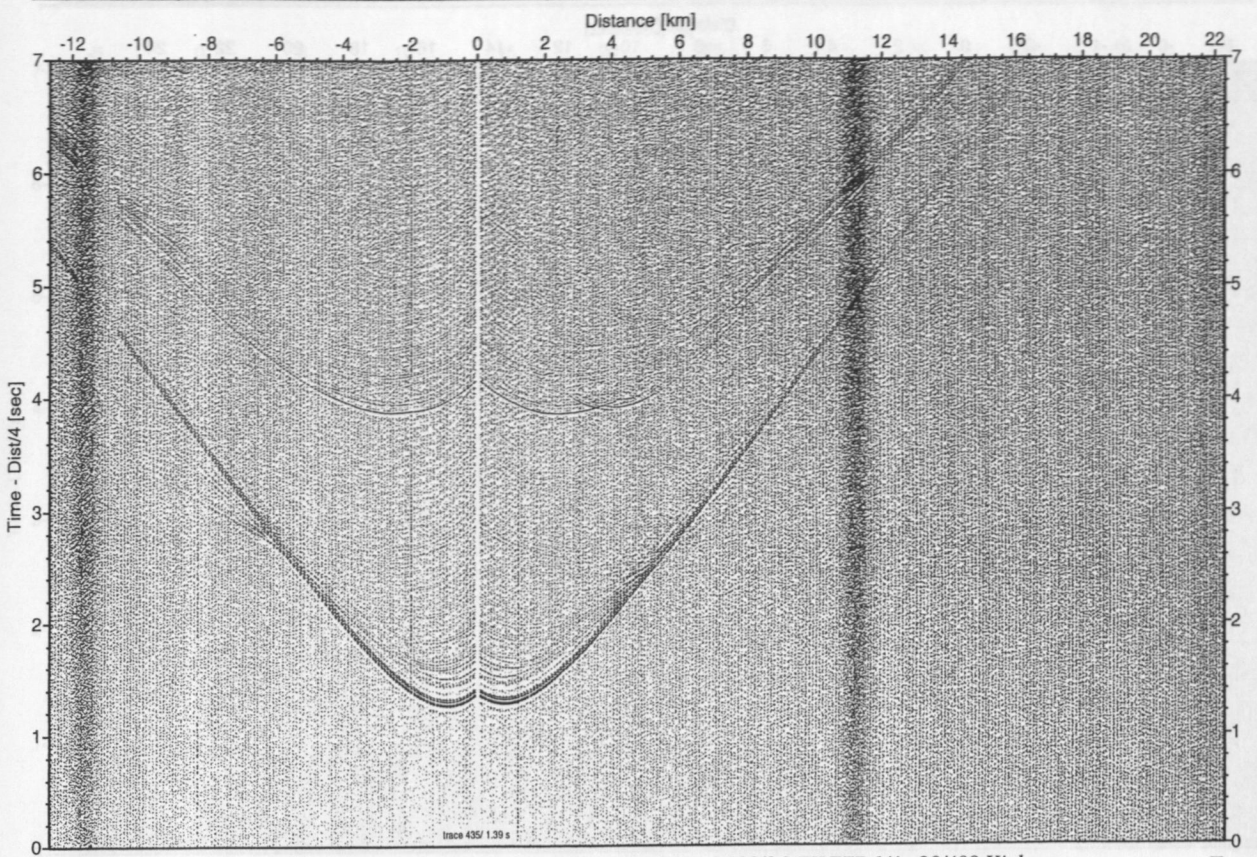




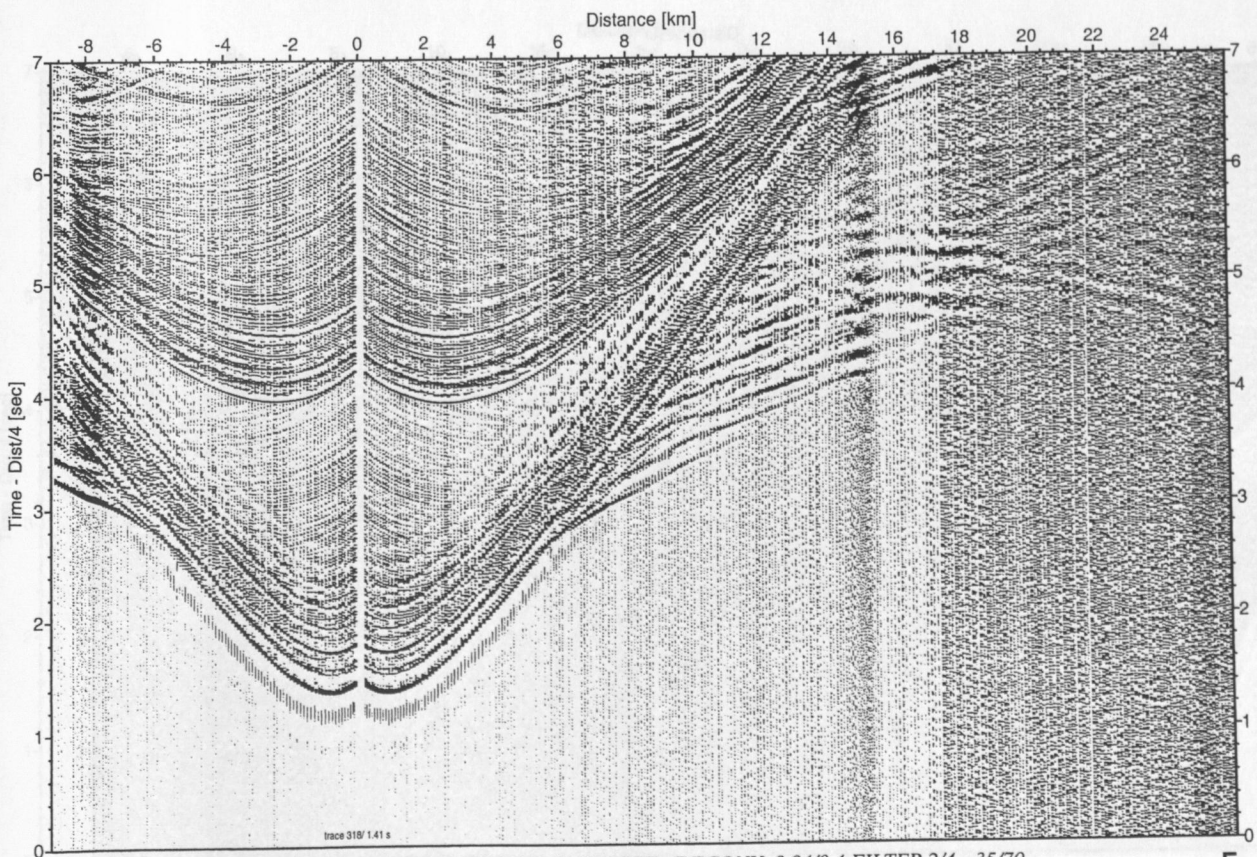
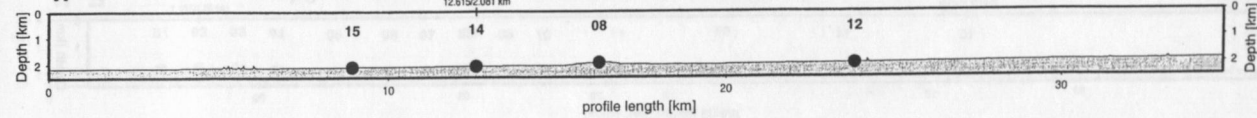




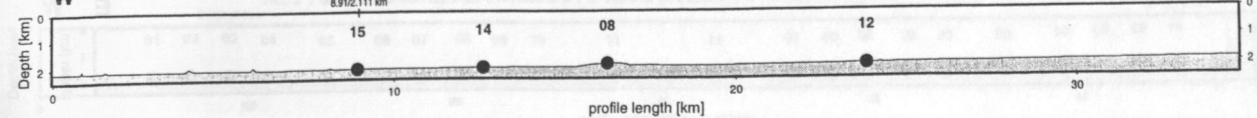


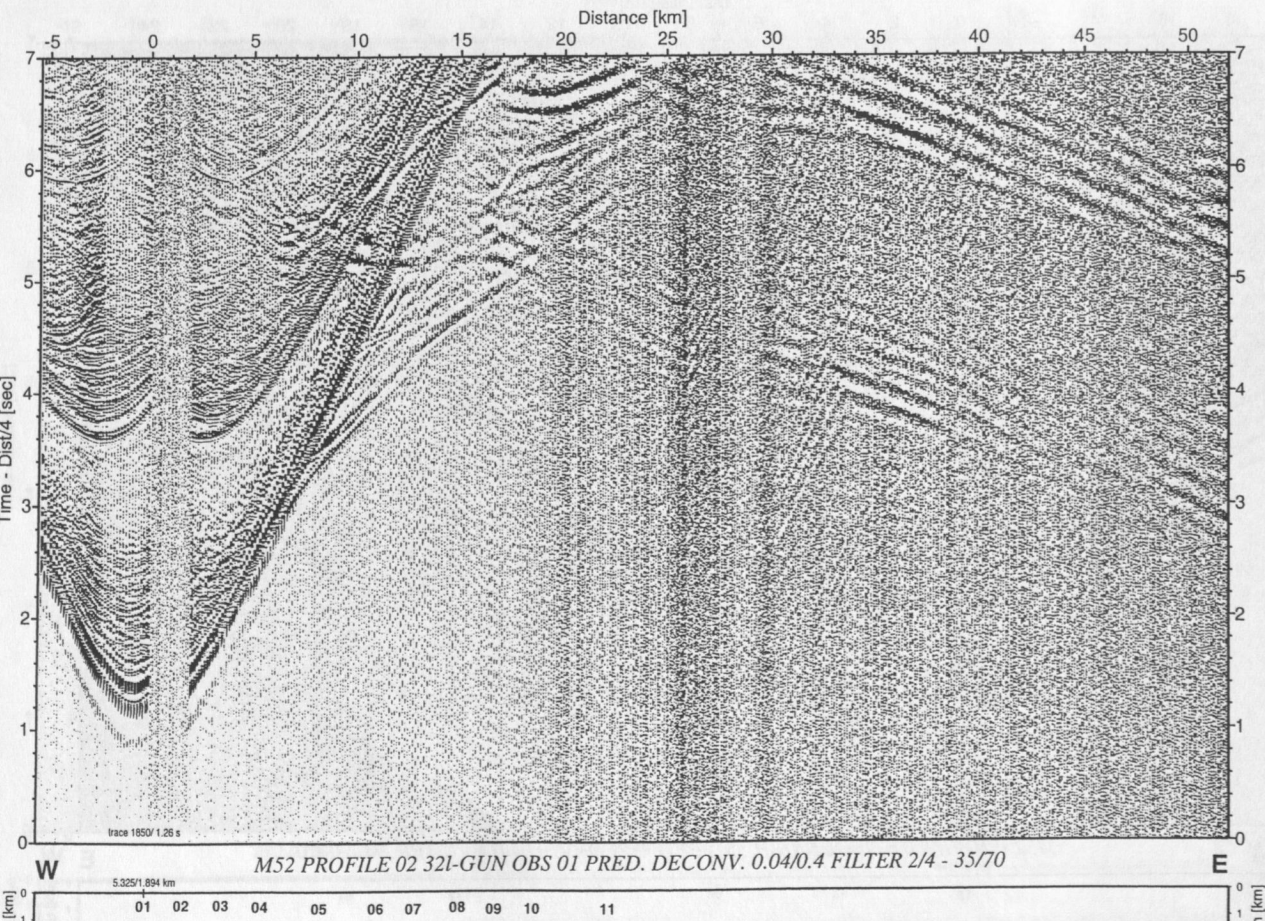
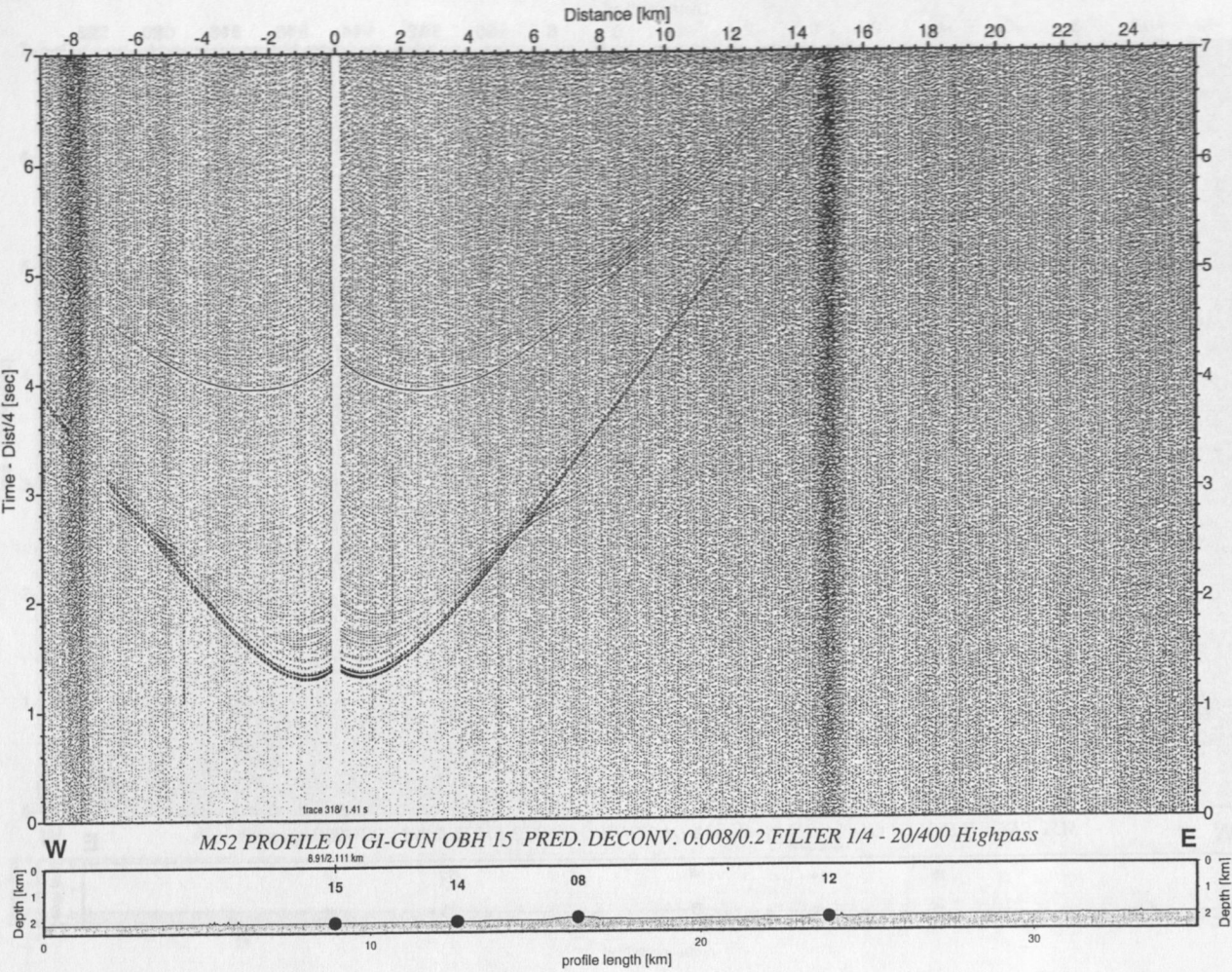


M52 PROFILE 01 GI-GUN OBH 14 PRED. DECONV. 0.008/0.2 FILTER 1/4 - 20/400 Highpass

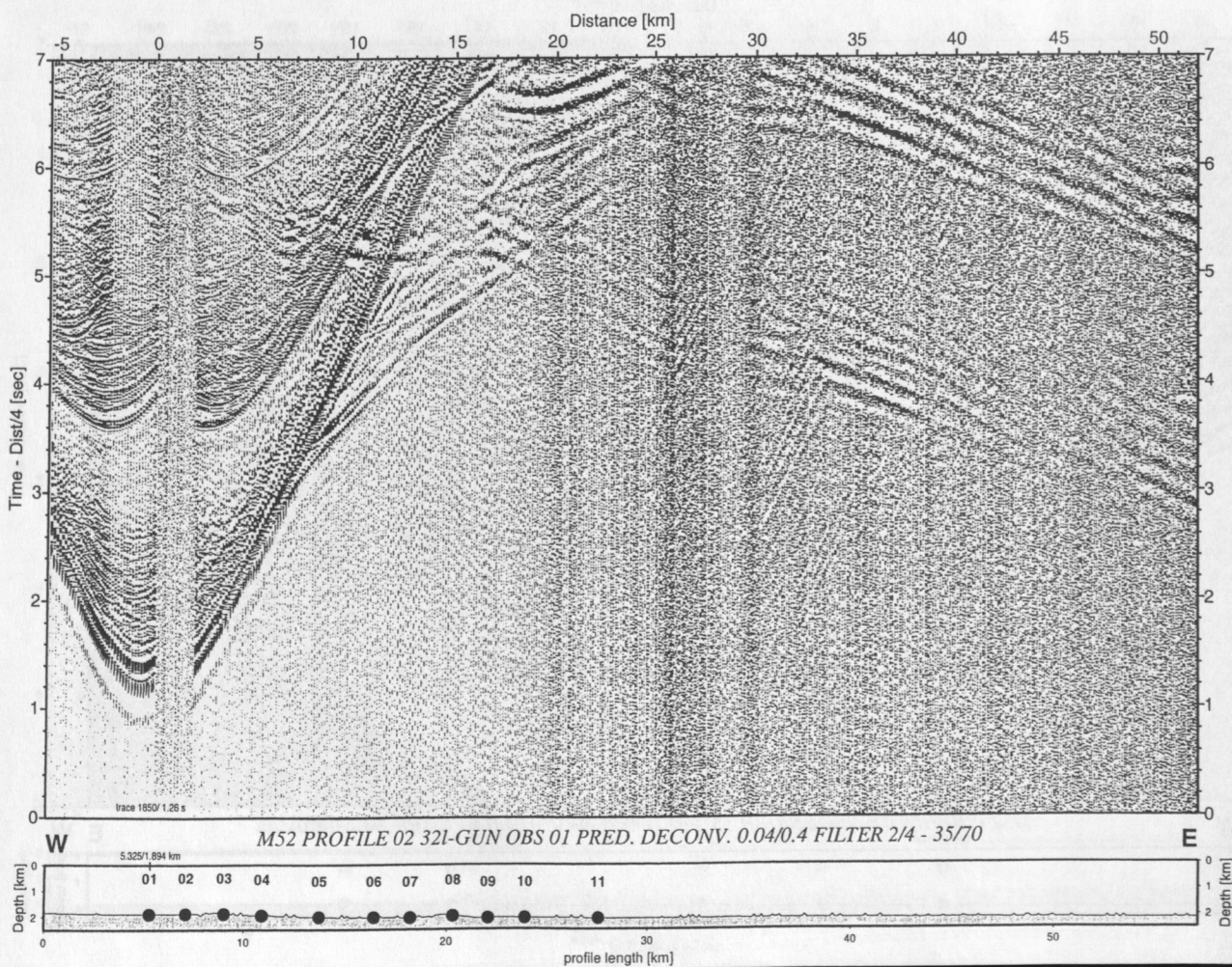
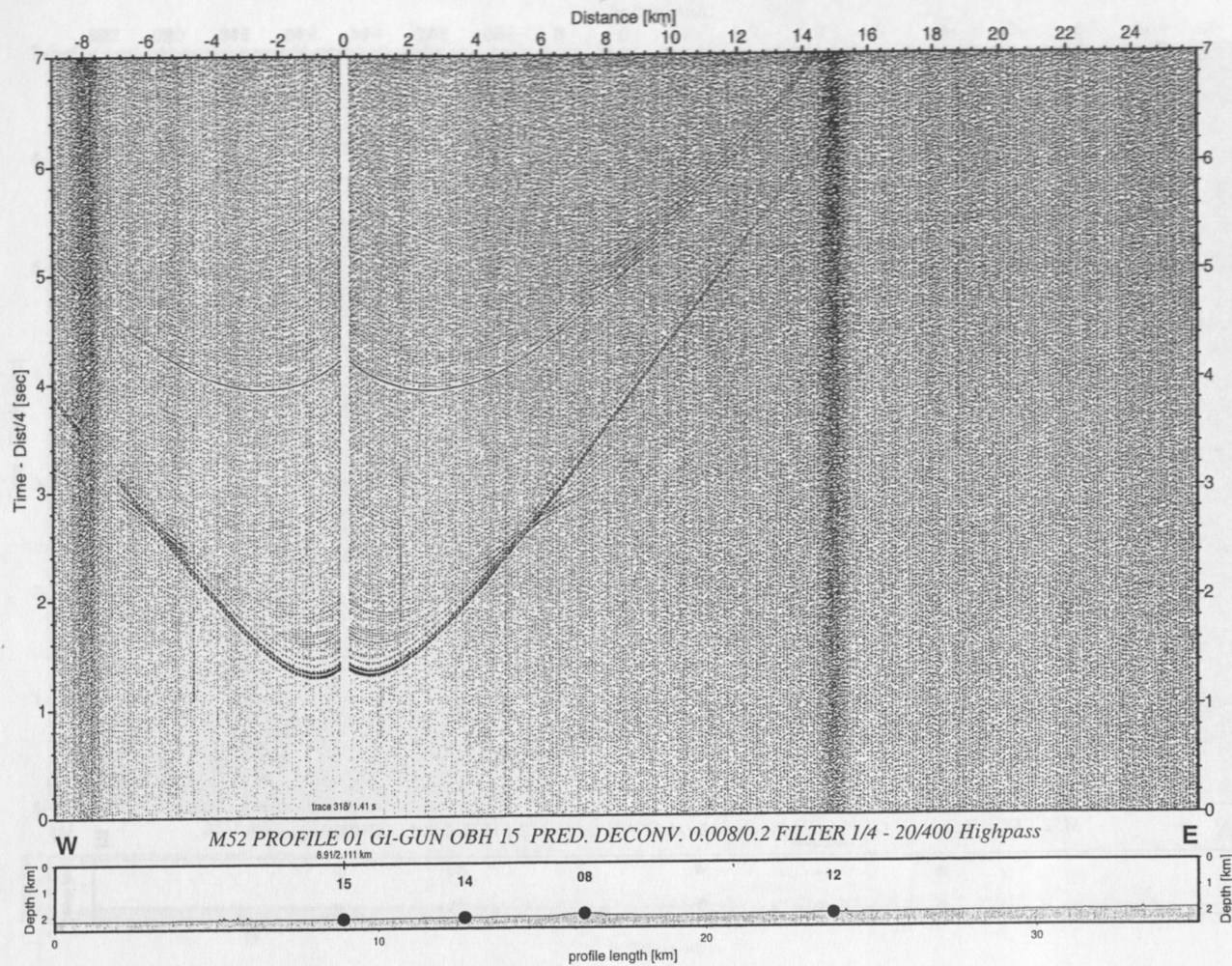


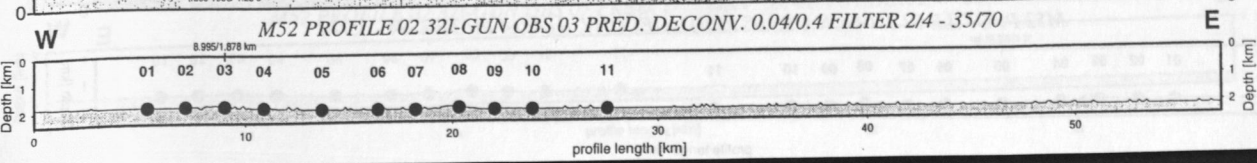
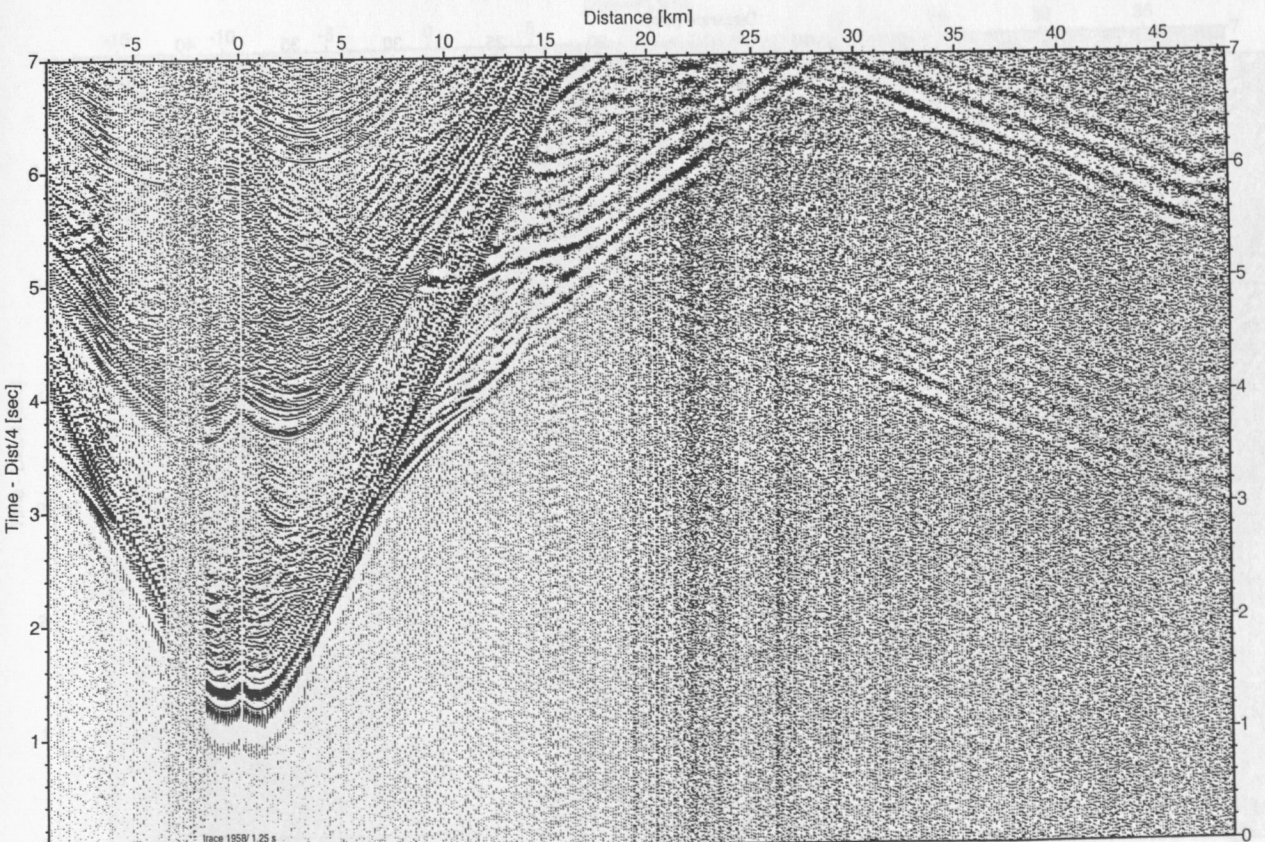
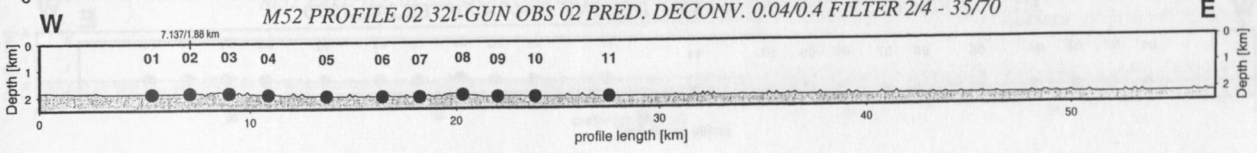
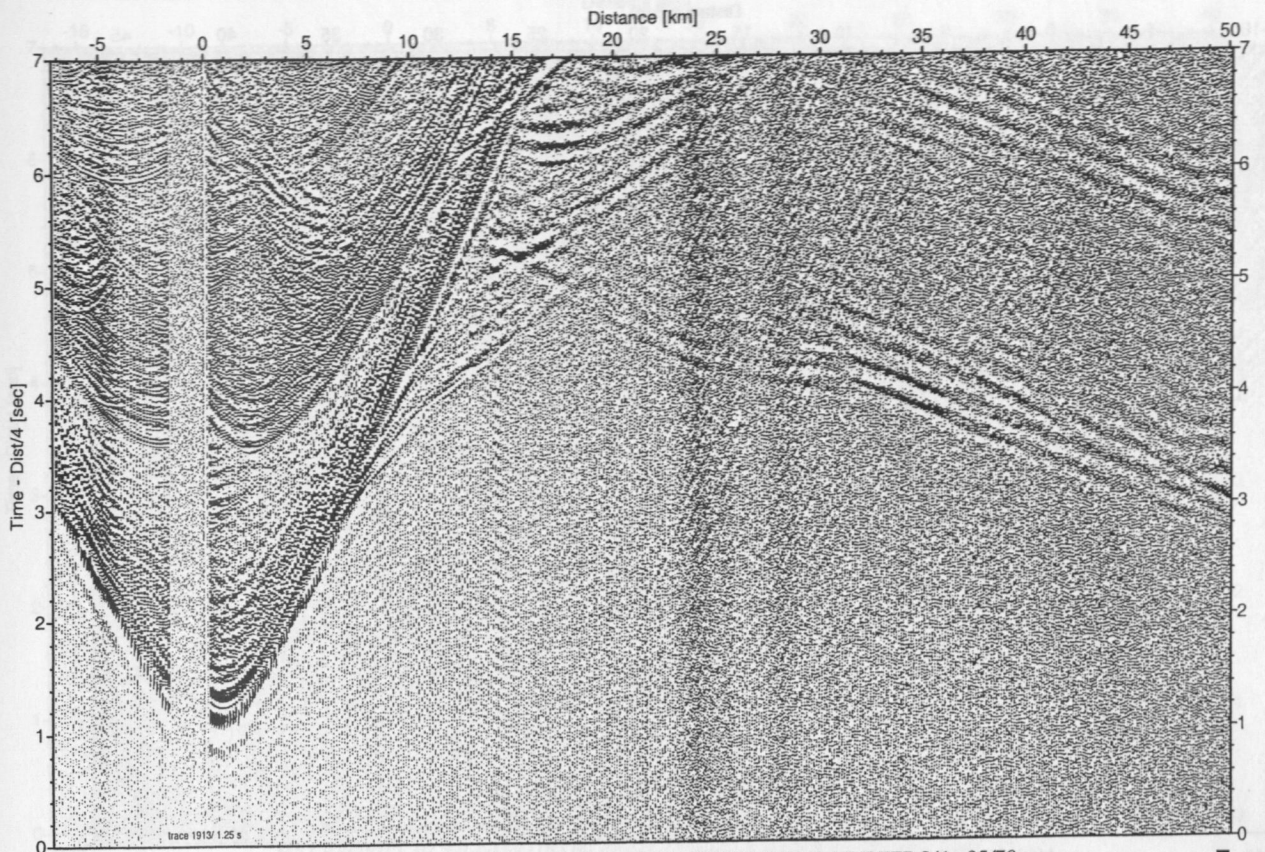
M52 PROFILE 01 32I-GUN OBH 15 PRED. DECONV. 0.04/0.4 FILTER 2/4 - 35/70



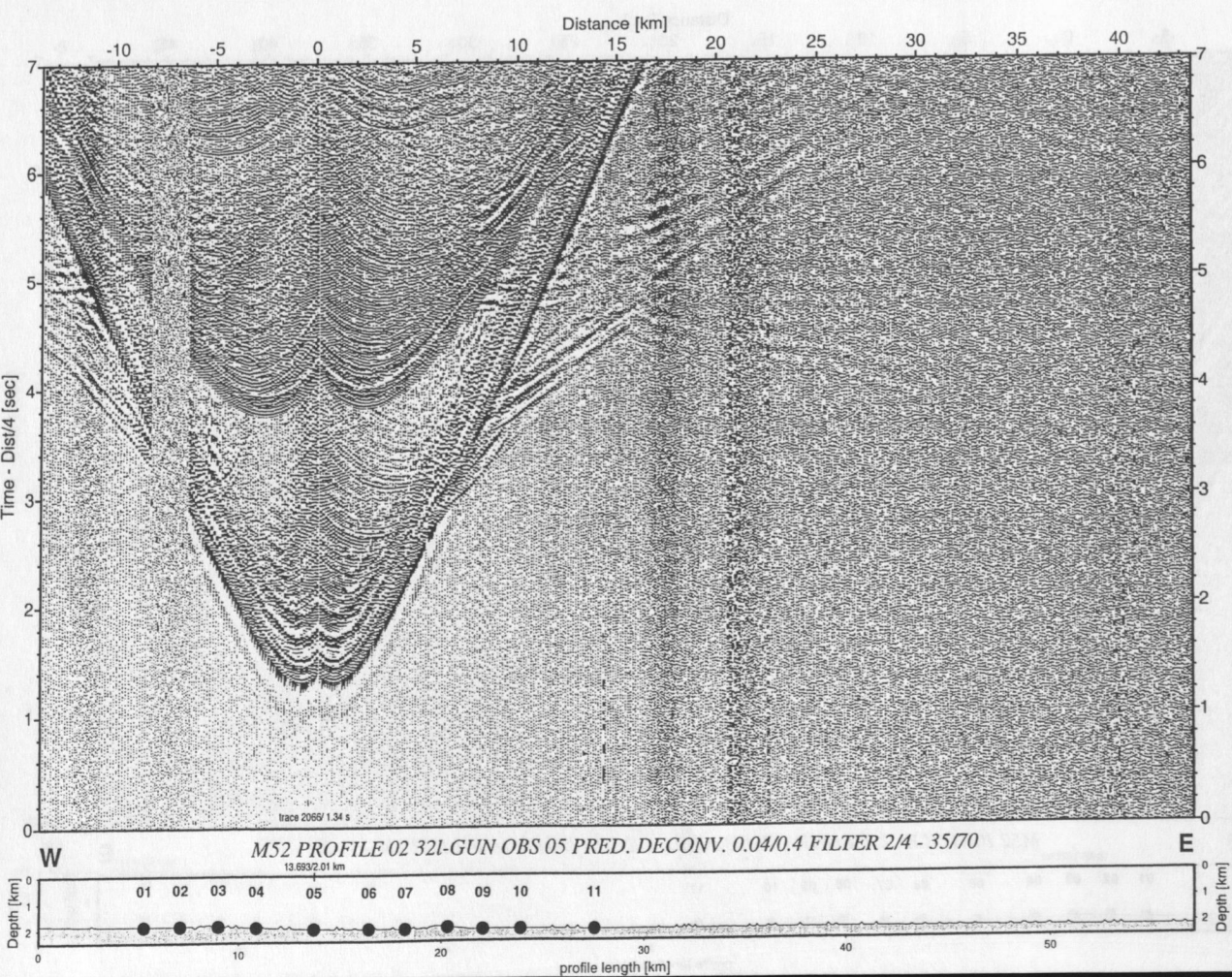
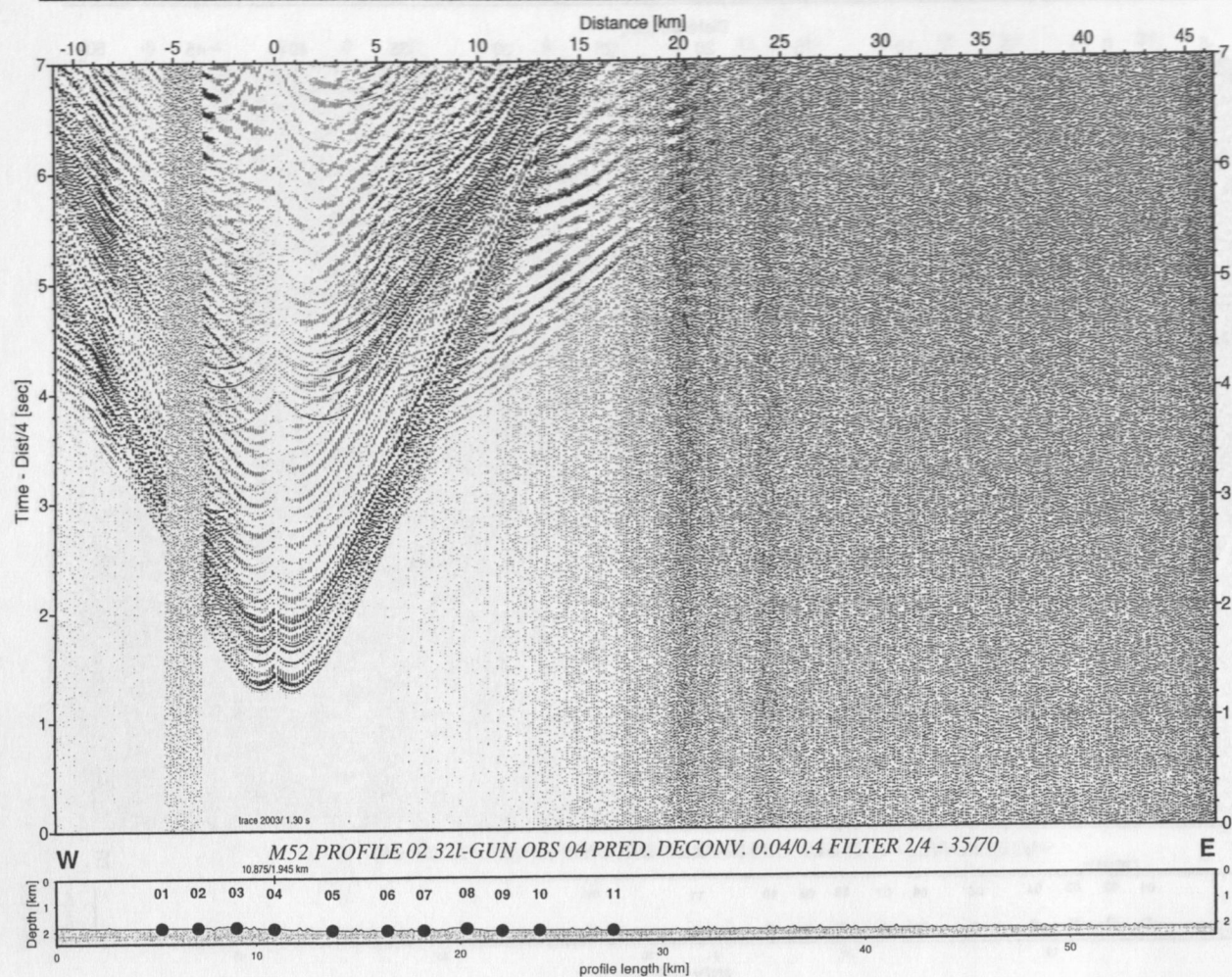


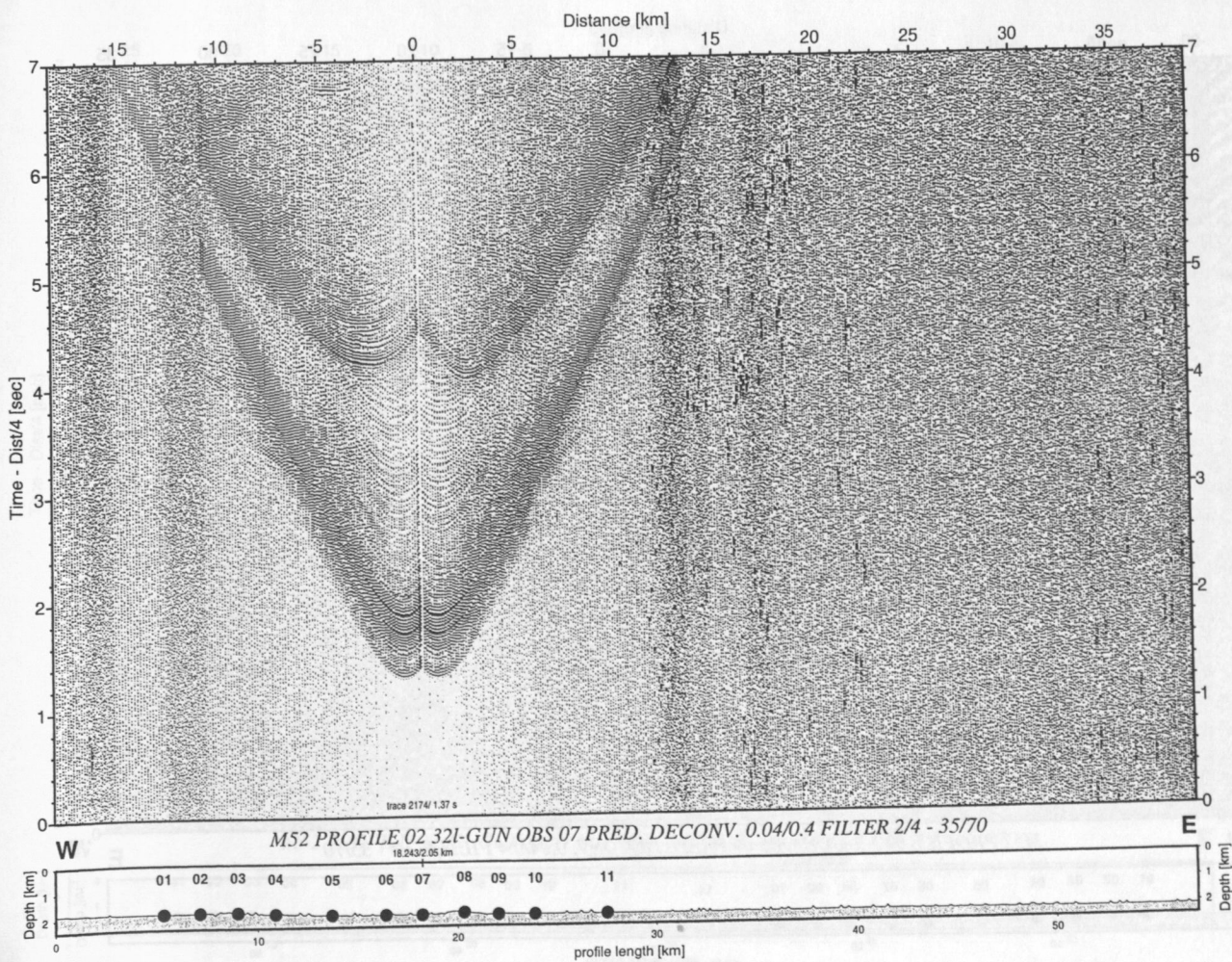
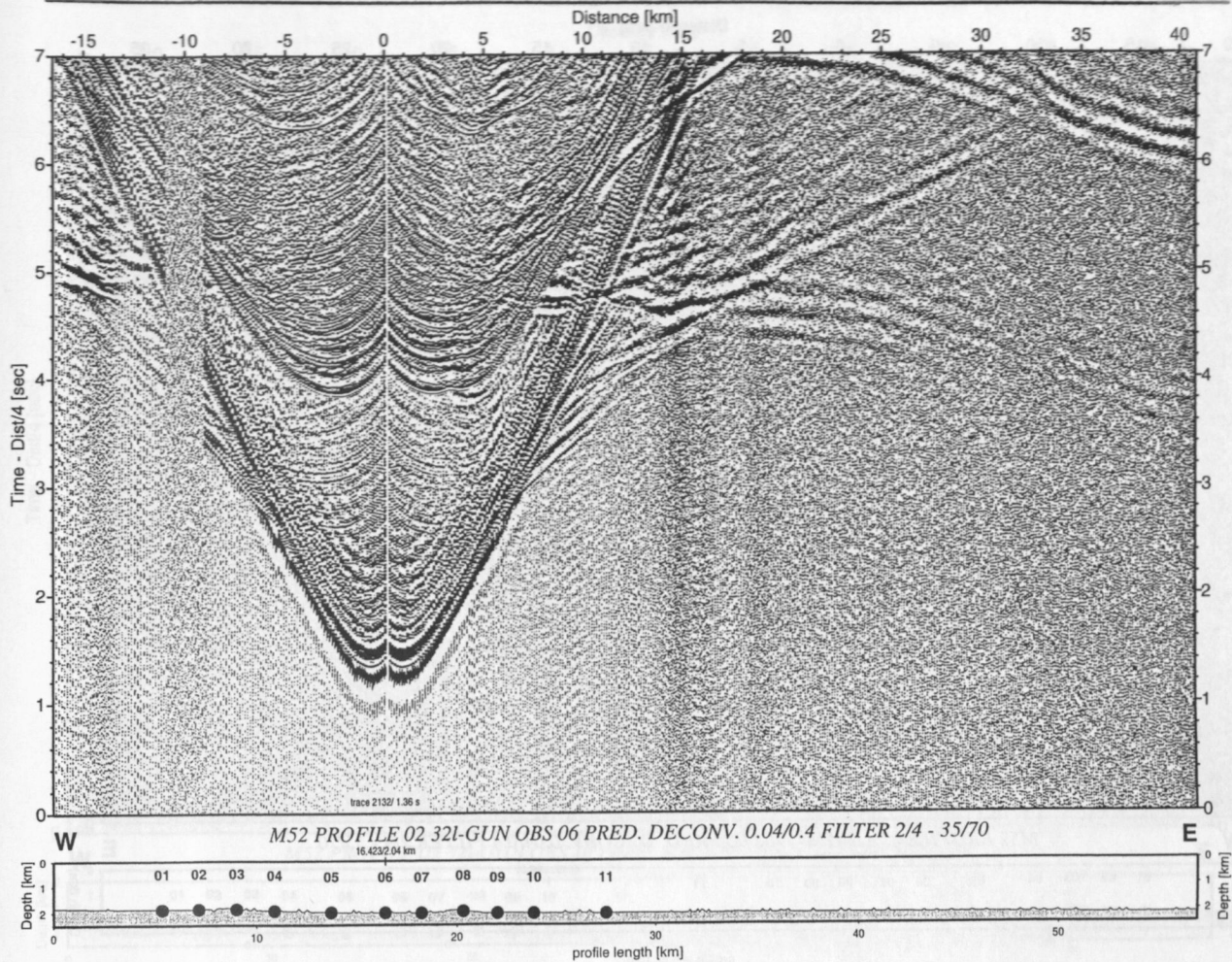




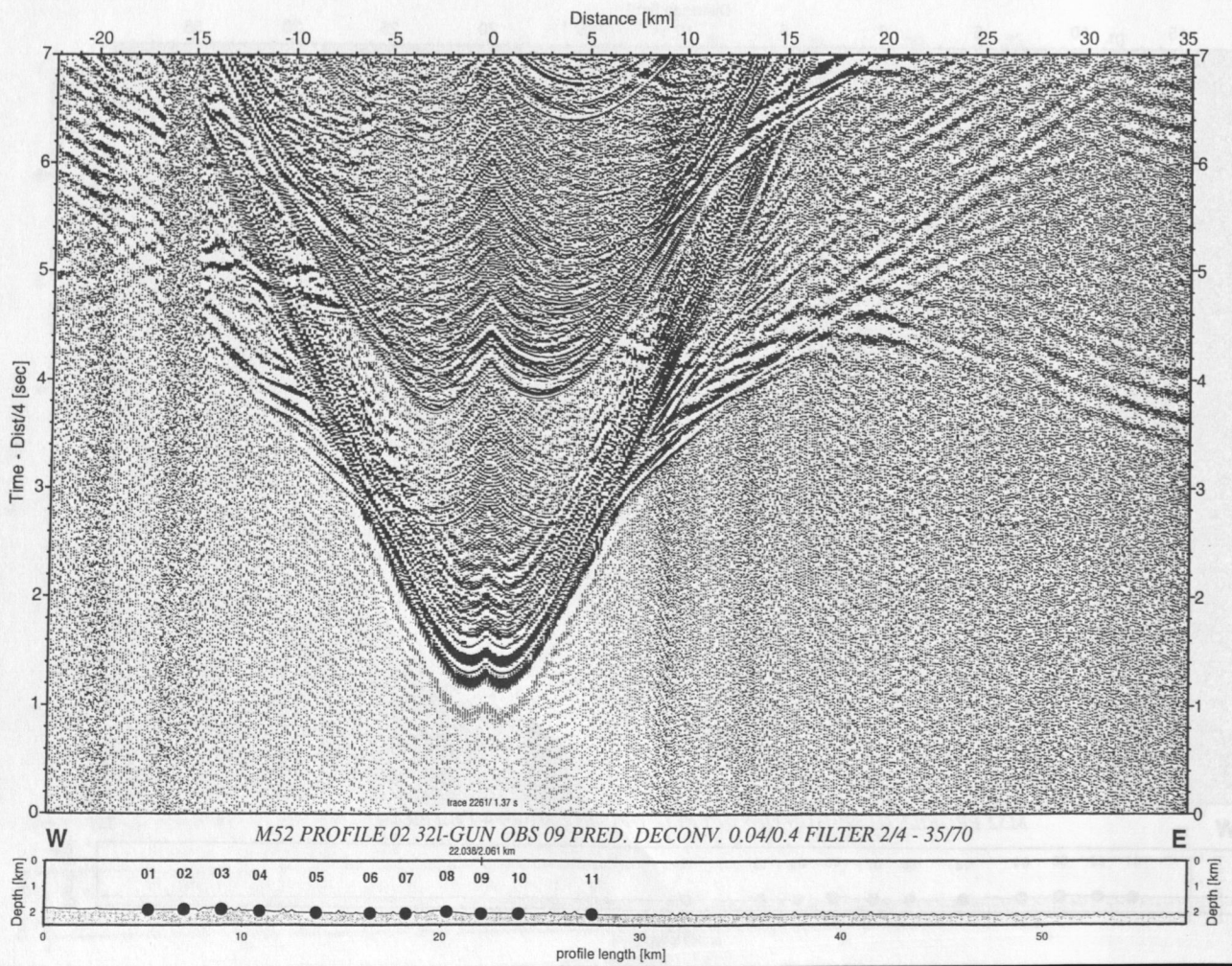
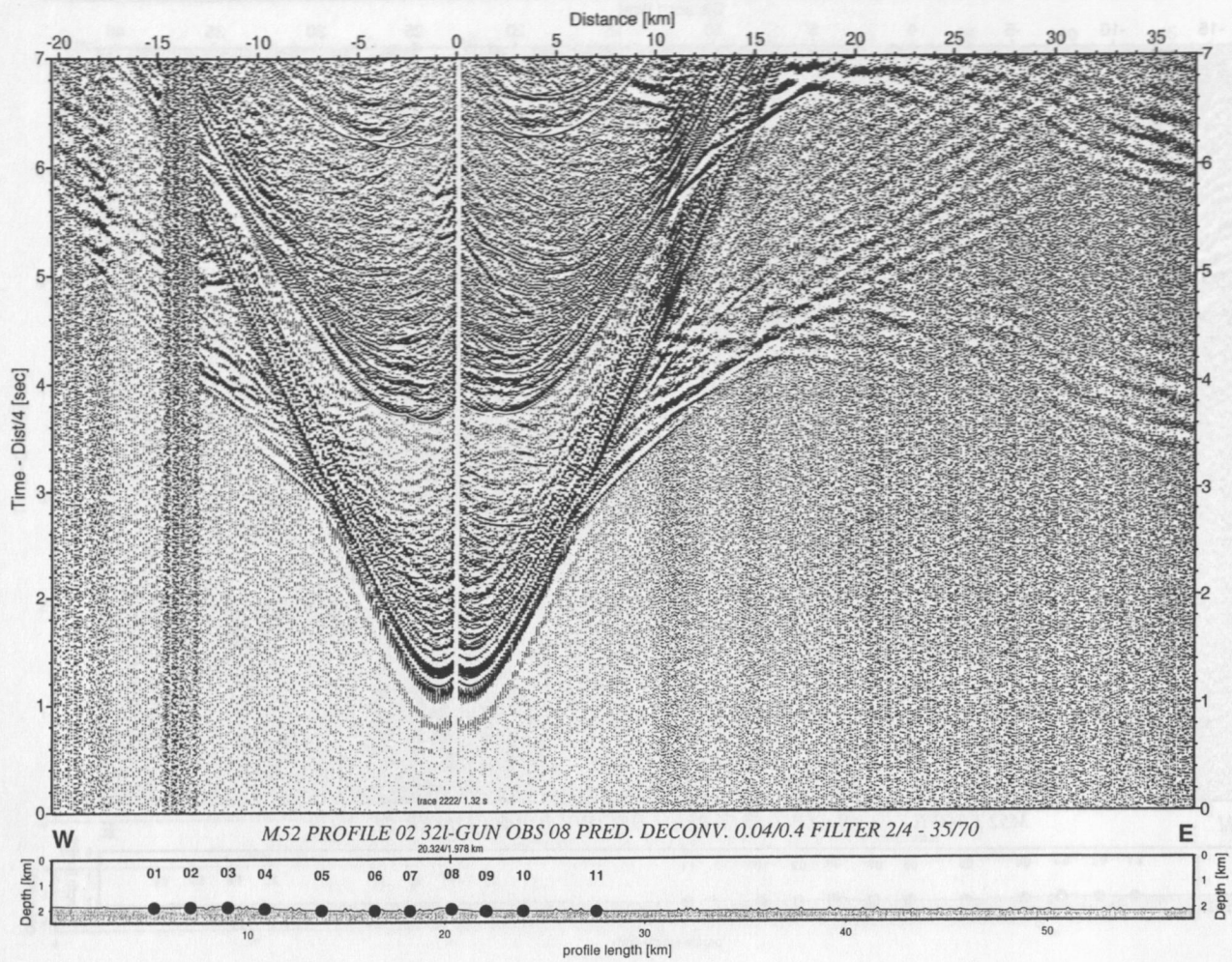


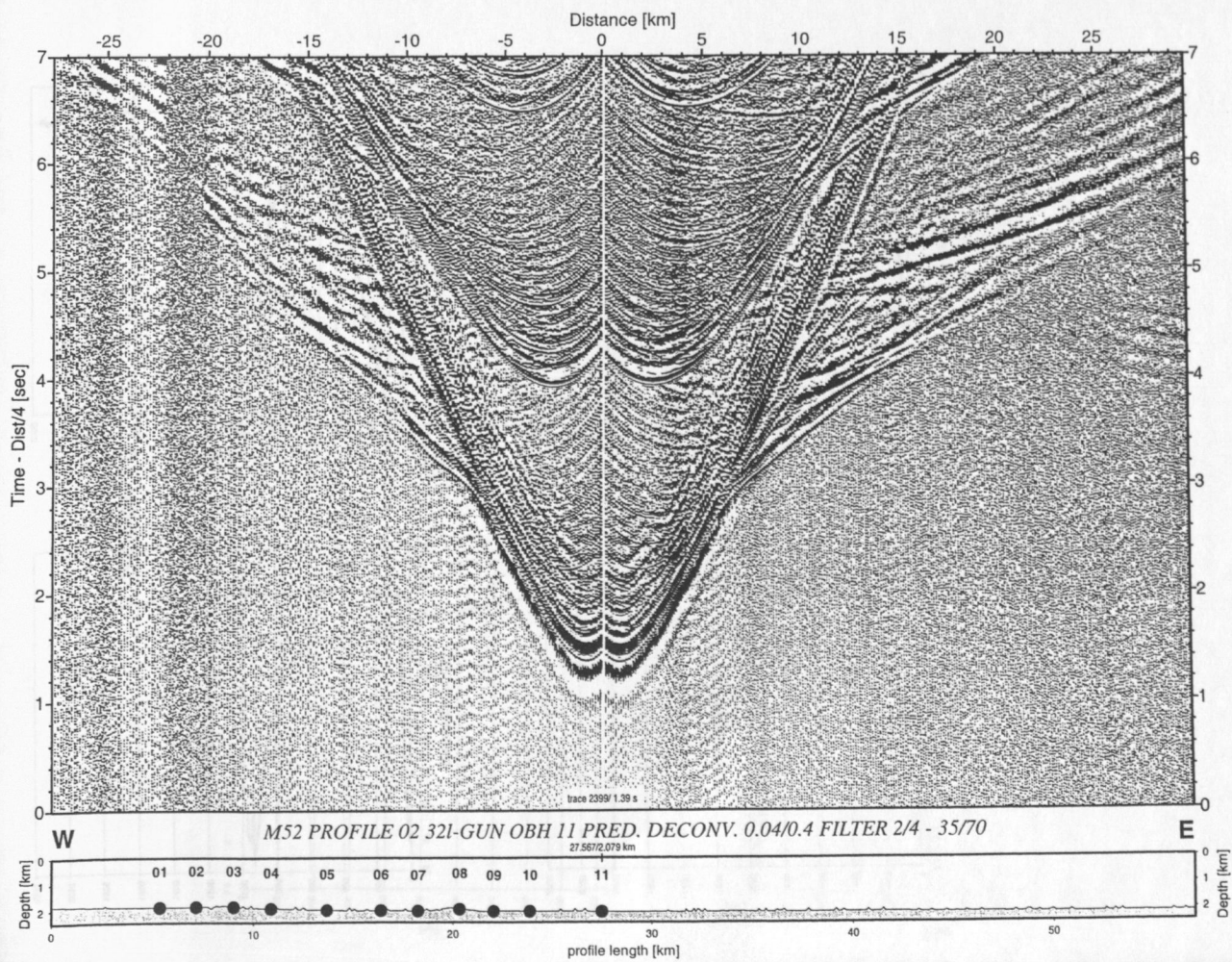
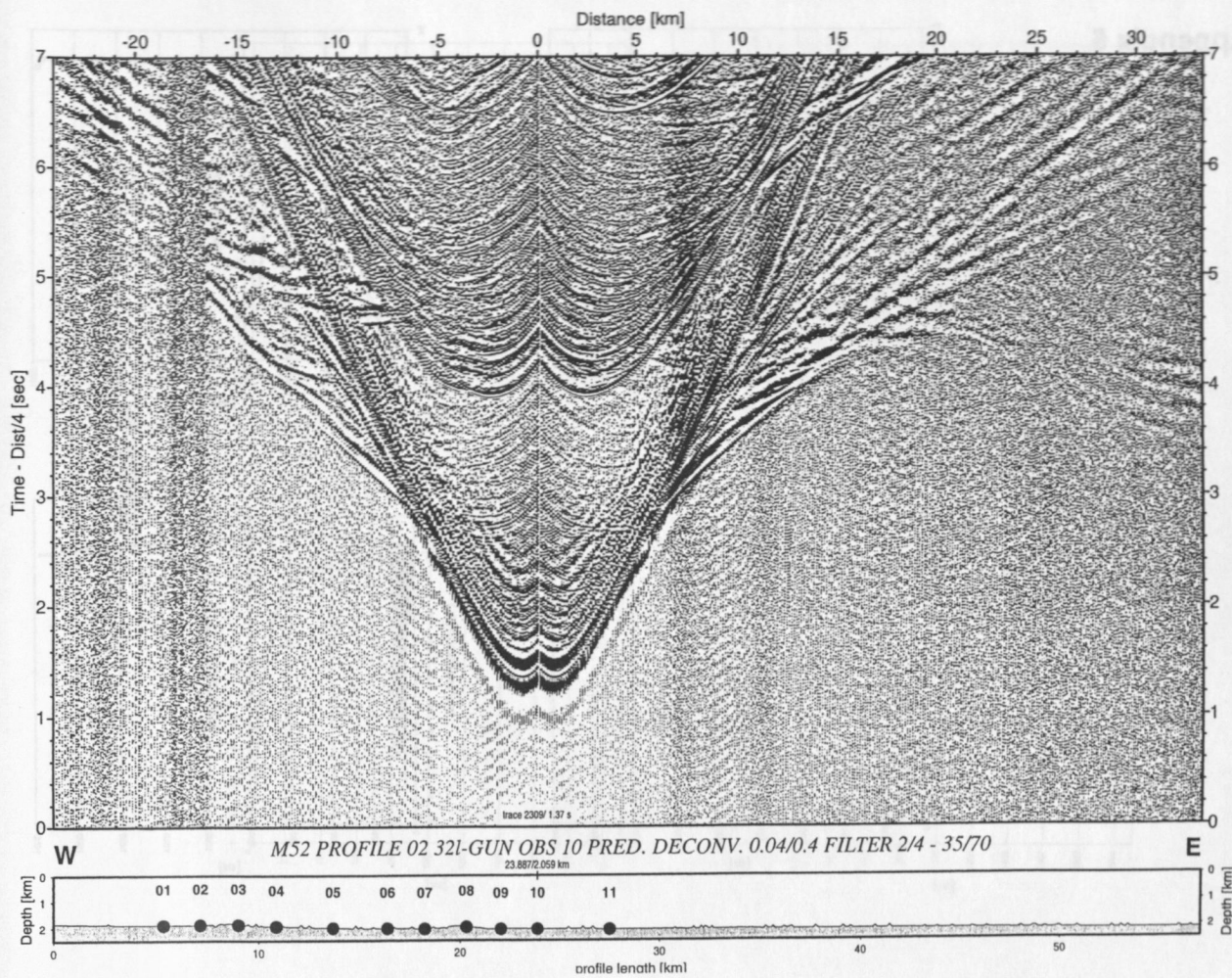








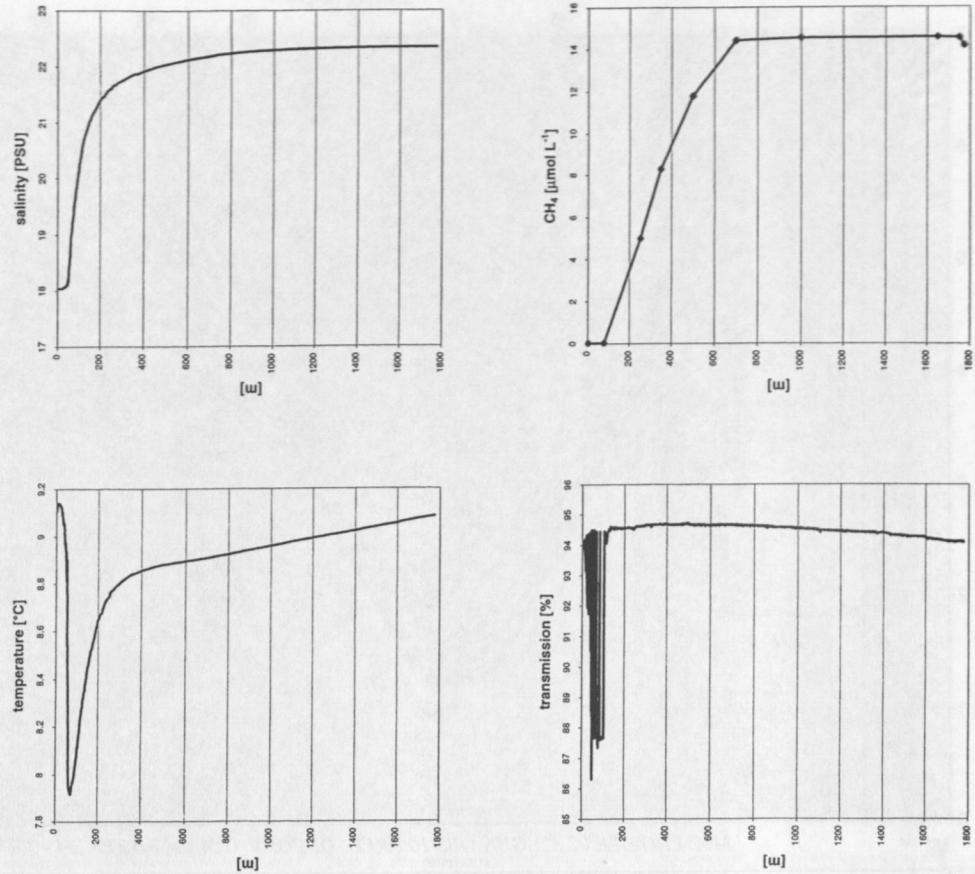




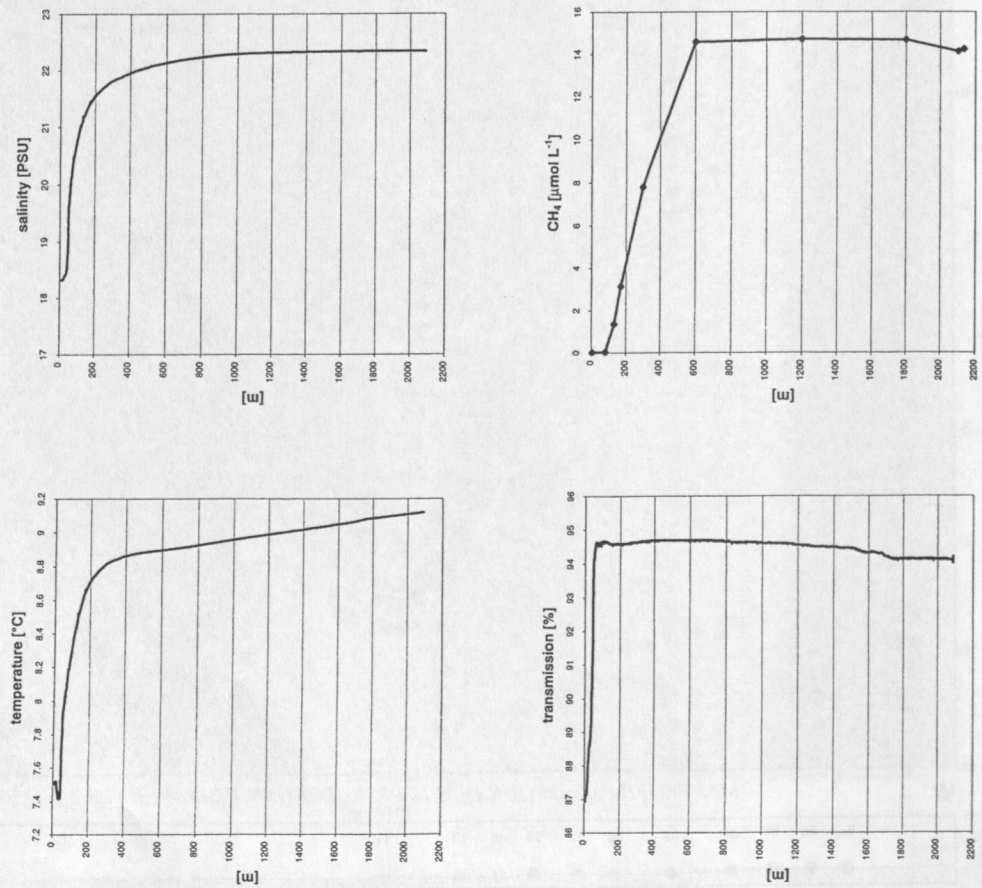


Appendix 5

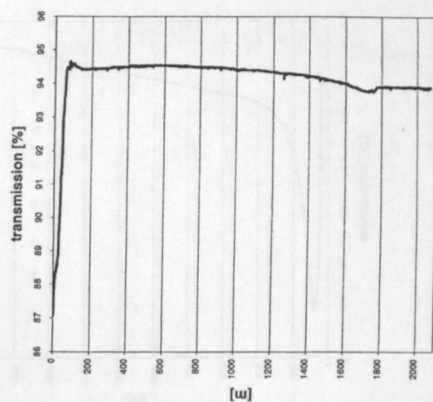
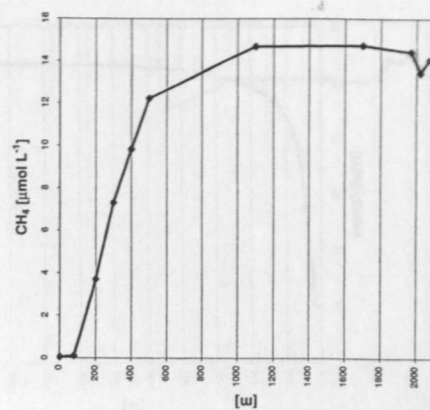
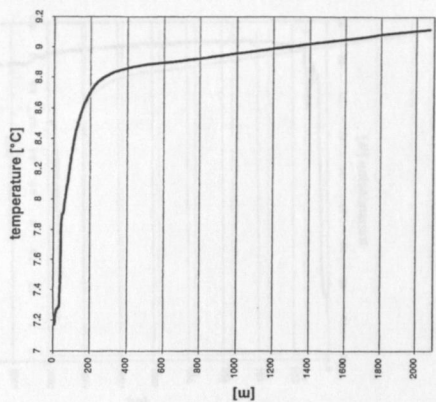
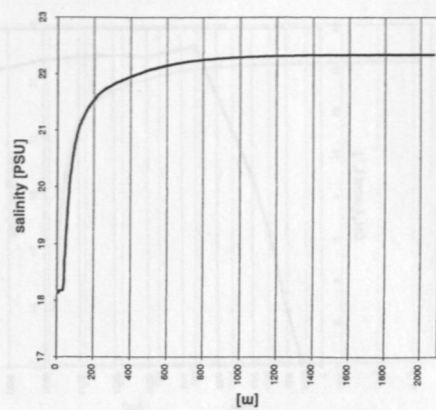
Station 4



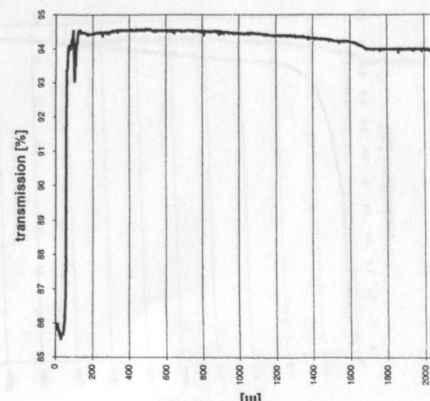
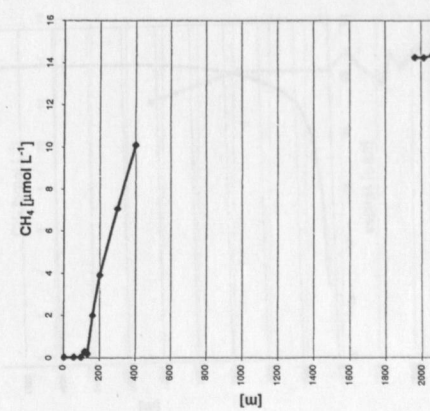
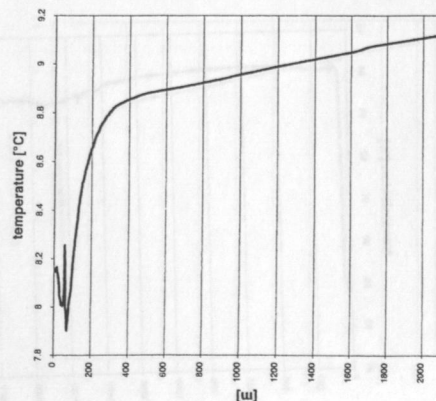
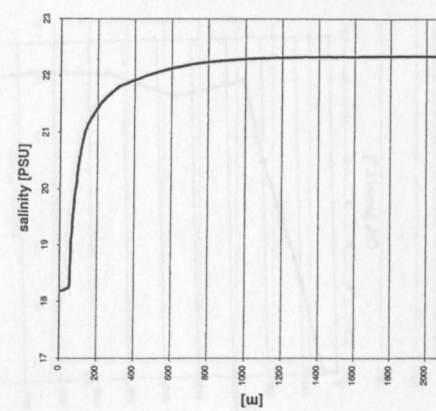
Station 2-2



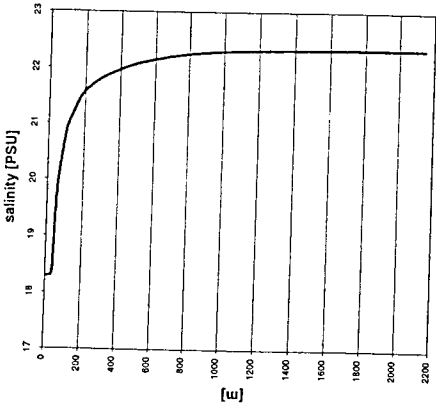
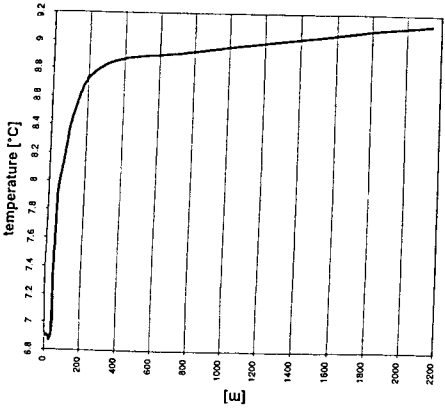
## Station 25



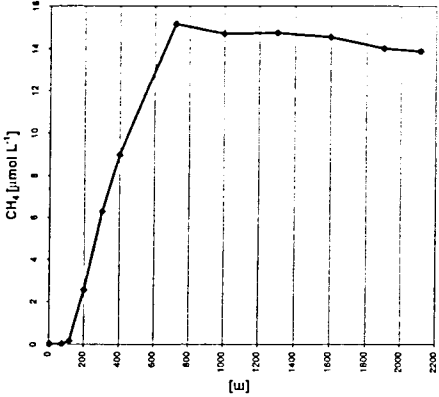
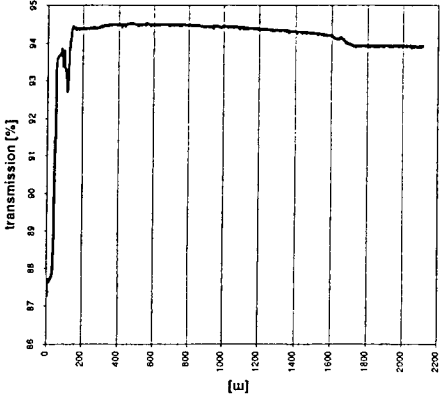
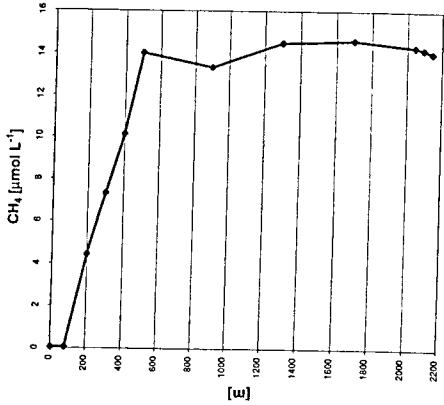
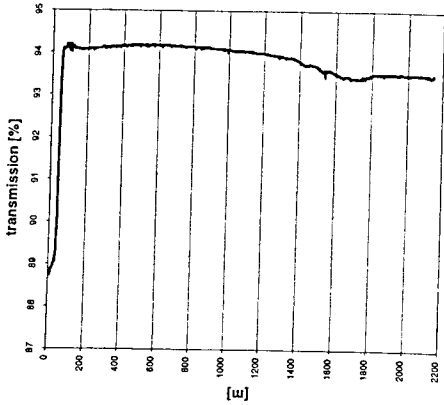
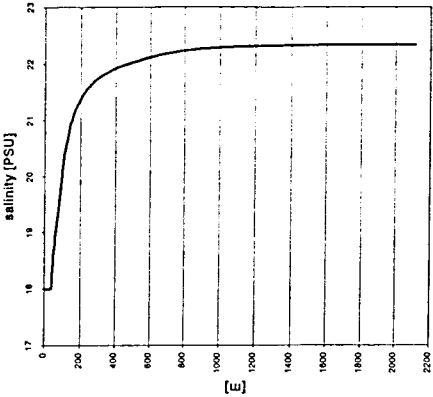
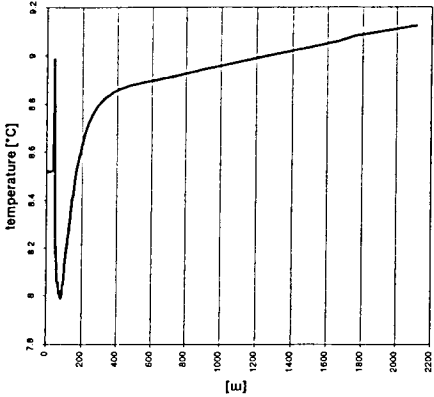
## Station 10



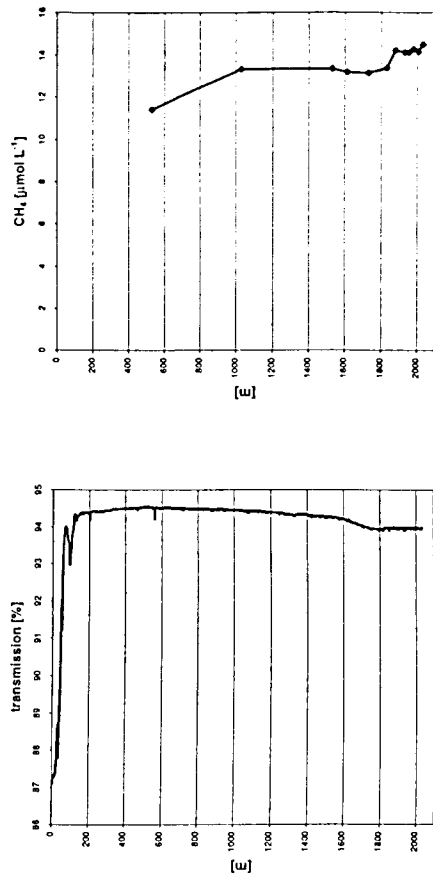
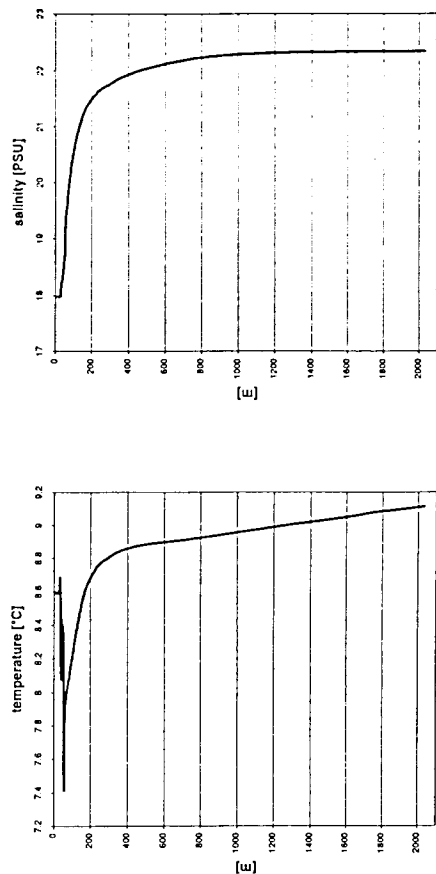
Station 29



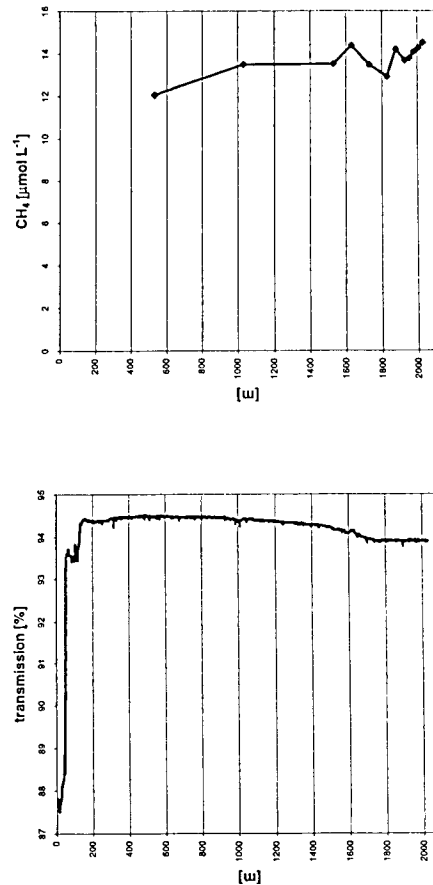
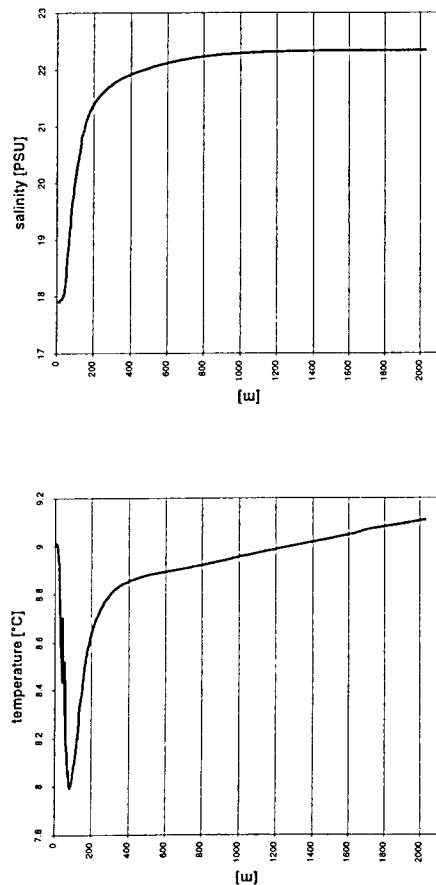
Station 33-2



Station 47-2

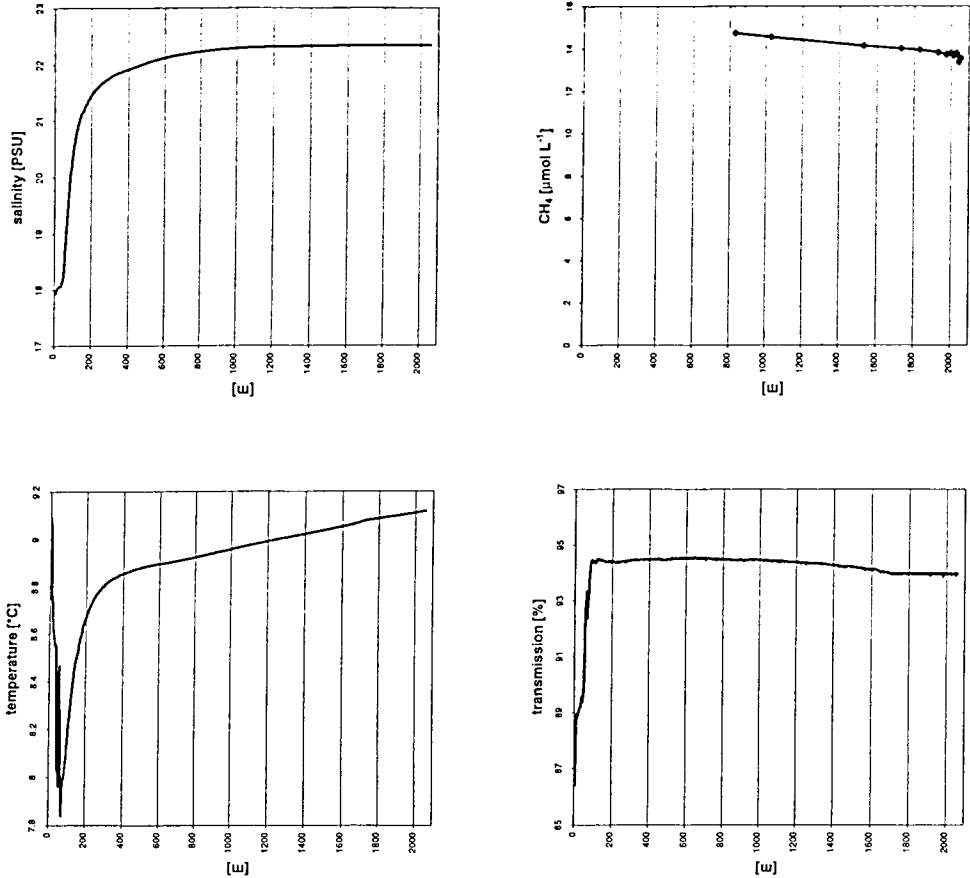


Station 40-2

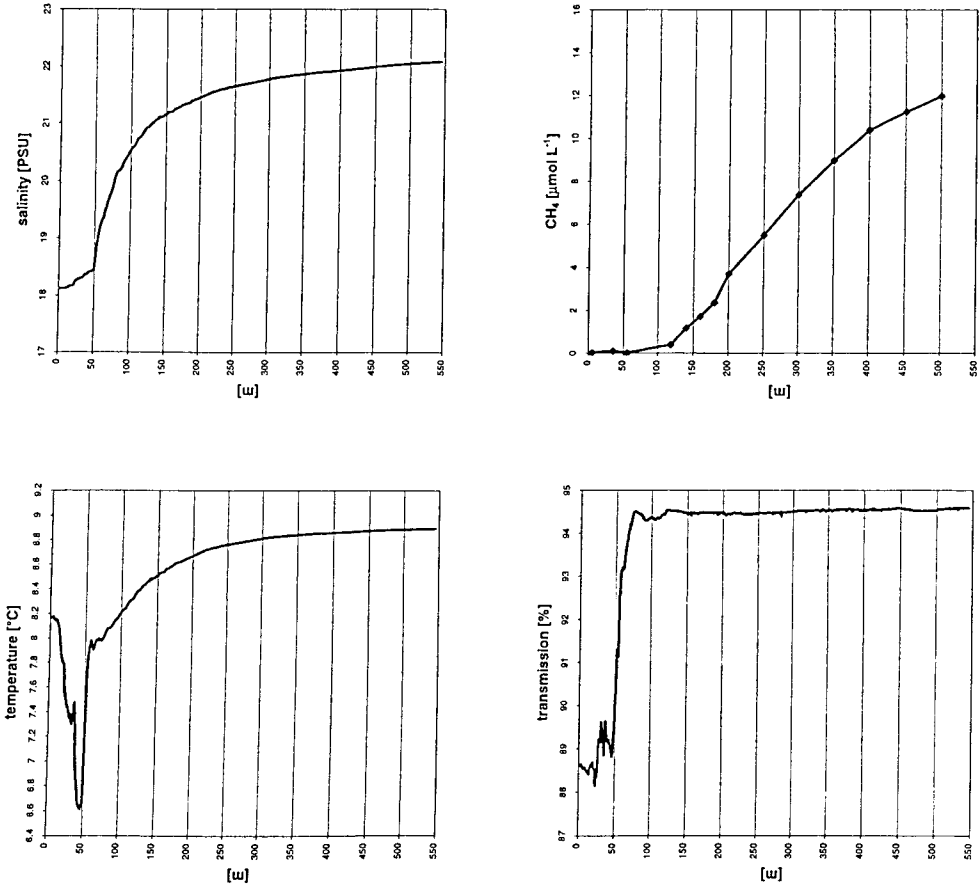




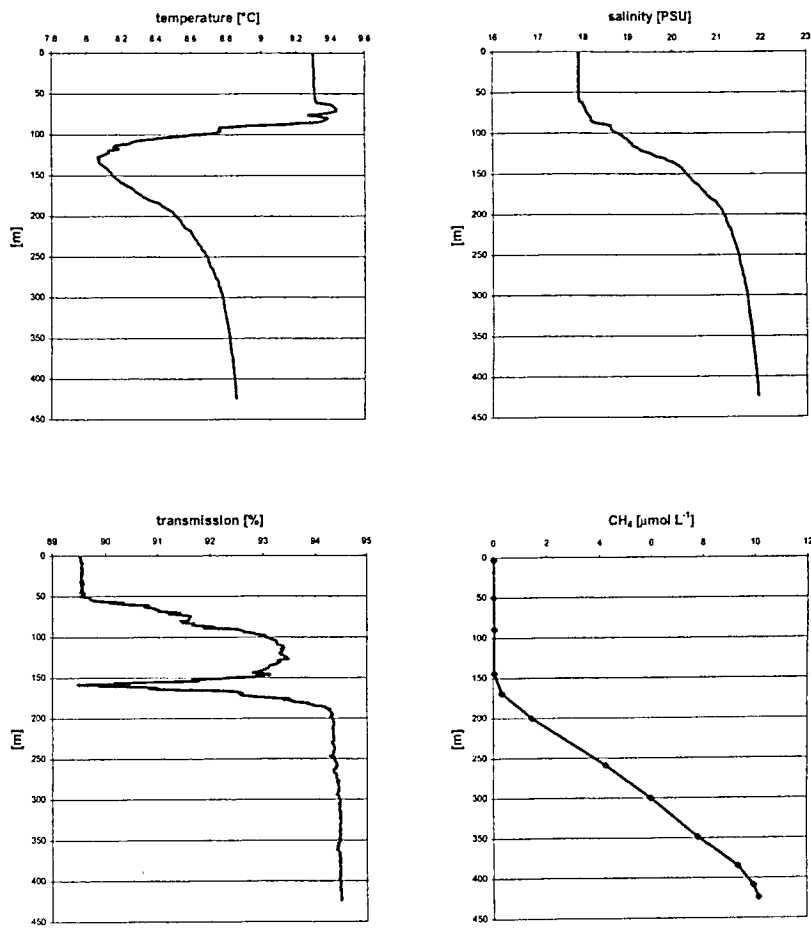
Station 64-1



Station 61-1

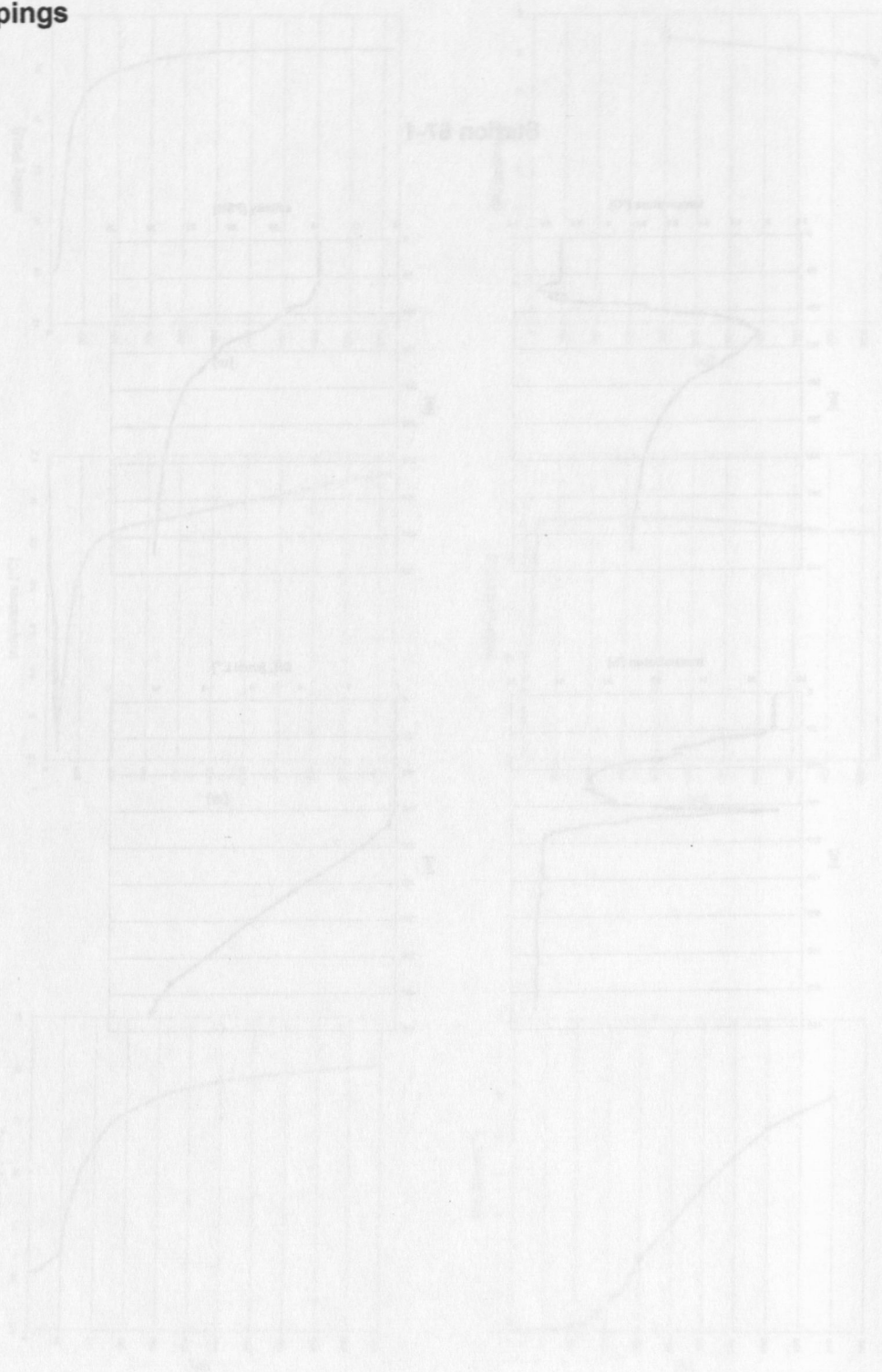


Station 67-1



## Press Clippings

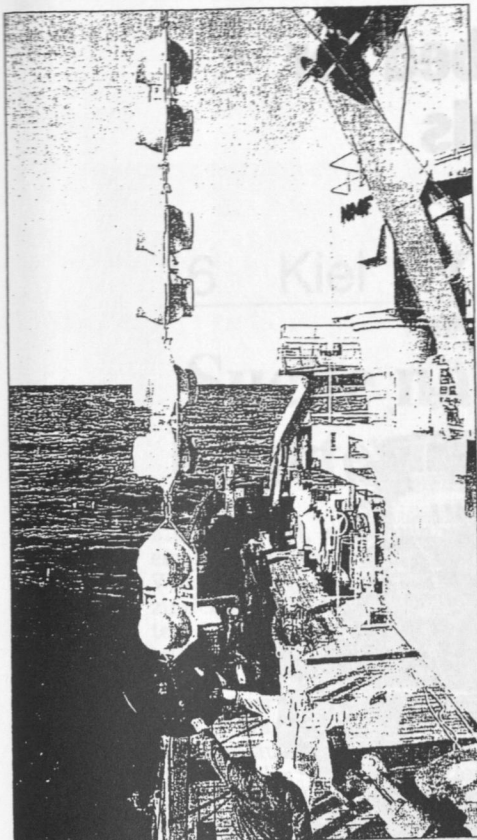
Station 64-1



Station 61-1



Landeszeitung  
Jan 2002



Forschung auf dem Meer ist auch harte Knochenarbeit. Zum Einsatz kommt auch ein neu entwickeltes Radargerät zur Untersuchung des Meeresbodens.

Auf der Jagd nach dem brennenden Eis

# „Meteor“ im Schwarzen Meer

KIEL  
( u m e )

Die weltweit führende Adresse bei der Gashydratforschung, einem möglichen Energieträger der Zukunft, ist das Forschungszentrum für marine Geowissenschaften (Geomar) in Kiel. Seit 2000 forscht das Kieler Zentrum mit zusätzlicher Unterstützung vom Bundesforschungsministerium — drei Jahre lang können die Kieler mit einem Extrat von 15,4 Millionen



Mark Grundlagenforschung betreiben. Neue Arbeitsplätze für Wissenschaftler und Techniker konnten bereits geschaffen werden.

Dass Geomar die Nummer Eins bei der Gashydratforschung ist, wird auch mit der Forschungsfahrt der „Meteor“ in das Schwarze Meer dokumentiert. Seit dem 2. Januar bereits ist die „Meteor“ in diesem Meeresgebiet unterwegs. Sie ist damit das erste deutsche Forschungsschiff im Schwarzen Meer. Drei

deutsche und drei ausländische Institute nehmen an der Fahrt teil. Es sind (GEOMAR, IFBM: Institut für Biogeochemie und Meereschemie, Universität Hamburg, Universität Bremen, UNESCO-MSU Centre for Marine Geosciences, Faculty of Geology, Moscow State University, Russia, IBSS: A.O. Kovalevsky Institute of Biology of the Southern Seas, National Academy of Science of the Ukraine, Ukraine, IFREMER: Institut Français de Recherche pour l'Exploitation de la Mer, France). Im Schwarzen Meer sollen Gashydratvorkommen lokalisiert werden. Gleichzeitig soll herausgefunden werden, was passiert, wenn sich das Methan im Wasser zersetzt und in die Atmosphäre entweicht. Zum Aufspüren der Vorkommen wird auch ein neu entwickeltes Side-Scan-Radar eingesetzt. Dieses Gerät ist gerade erst unter anderem von Geomar mit entwickelt worden.

Das Radar soll den Meeresboden regelrecht abscannen und detaillierte Informationen über die Bodenbeschaffenheit liefern, mit denen

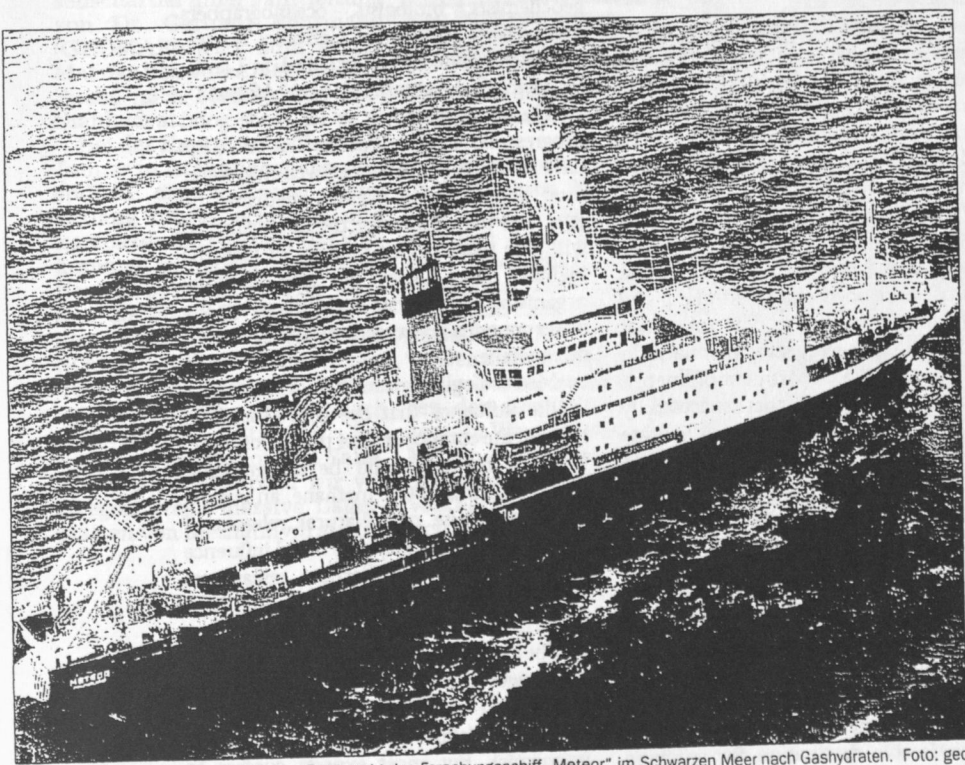
dann Gashydratvorkommen nachgewiesen werden können. Zum Aufspüren der Gashydraten kommt auch ein spezieller Videoschlitten zum Einsatz, der mit einem Greifer ausgerüstet ist und damit Proben an die Oberfläche holen kann.

Neben der reinen Forschungsarbeit an Bord der „Meteor“ wird auch einmal kräftig gefeiert. Am 11. Januar gibt es anlässlich der ersten Fahrt eines deutschen Forschungsschiffes einen Empfang mit dem deutschen Botschafter in Sevastopol.

Die Gashydrate könnten ein wichtiger Energieträger der Zukunft sein, denn nach bisherigen Schätzungen gibt es weltweit davon rund 10000 Giganonnen, während die Vorräte der anderen fossilen Energieträger wie Erdöl, Kohle und Erdgas zusammen auf lediglich rund 5000 Giganonnen geschätzt werden. Schon in wenigen Jahren will etwa Japan mit der Förderung von Gashydraten vom Meeresgrund beginnen, um langfristig von Lieferungen konventioneller Energieträger unabhängig zu werden.

Neben der Verwendung als möglicher Energielieferant — ein Kubikmeter Gasydrat enthält 164 Kubikmeter Methan und 0,8 Kubikmeter Wasser — wird Gashydrat auch als Ursache für Klimaveränderungen für die Forschung immer interessanter. Das Treibhausgas Methan steigt zwar nicht direkt von den riesigen Gashydratfeldern an die Oberfläche und dann in die Atmosphäre auf, jedoch werde es vom Meerwasser aufgenommen und dann vermutlich nach längerer Zeit an die Oberfläche abgegeben. Beobachtet wurde sogar schon der Auftrieb von Gashydratbrocken bis an die Meeresoberfläche. Welch gigantischen Energiereserven in der Tiefe des Meeres schlummern, macht ein Gashydratfeld vor North Carolina deutlich. Mit dem dort gespeicherten Methangas könnten die USA für 50 Jahre ihren gesamten Energiebedarf decken. Ungeklärt ist allerdings noch, wie das bei der Methan-Verbrennung freigesetzte Klimagas CO<sub>2</sub> wieder gebunden werden kann.

Die 25 Forscher suchen auf ihrer Reise auch nach urzeitlichen Mikroorganismen, die Methan ohne Sauerstoff abbauen können. Sie spielen eine wichtige Rolle im Methankreislauf des Meeres. Spuren dieser Organismen seien im Karbonatgestein des Schwarzen Meeres zu finden und könnten möglicherweise eines Tages von Nutzen sein.



Mit 28 Wissenschaftlern an Bord sucht das Forschungsschiff „Meteor“ im Schwarzen Meer nach Gashydraten. Foto: geo



# Expedition trawls sea bed for energy-rich gas crystals



Hot property: the team aboard the *Meteor* hopes to capitalize on the huge energy potential of methane hydrate (inset).

Quirin Schiermeier, Munich

An international team is this month scouring the floor of the Black Sea in an effort to gather more information on energy-rich methane hydrate crystals. Resembling ordinary ice, these structures are stuffed with natural gas and have been cited as a potentially massive source of energy.

Methane hydrate can form only at reasonably high pressures and low temperatures, and so is found mainly in the Arctic permafrost and on the sea bed along the edge of continental shelves. The volume of gas it contains gives it great potential as a fossil fuel — the US Department of Energy, for example, estimates that successfully tapping just 1% of existing methane hydrate could yield more energy than the world's entire reserves of natural gas.

Margasch, as the Black Sea expedition is known, is studying the structure and architecture of methane hydrate in sediments just below the sea bed. It plans to map their distribution and hopes to estimate the total quantity of hydrate available. It is also using video-guided tools to retrieve samples of the crystals.

"Its near-surface deposits make the Black Sea a preferable destination for studying hydrates," says expedition leader Gerhard Bohrmann, a geologist at the GEOMAR research centre in Kiel.

The team, which includes geophysicists,

geochemists, biologists, oceanographers and meteorologists from Germany, France, Ukraine and Russia, left Istanbul on 2 January on the German research vessel *Meteor*.

The expedition has so far made good progress, Bohrmann reports. The scientists have already surveyed an active underwater mud volcano that releases methane, he says, and they hope that the data gathered will help them to test theories of how the hydrates form. They are also studying organisms that flourish at depths where the water contains no oxygen, surviving instead on methane.

Meteorologists, meanwhile, are interested in the influence that the hydrates might have on the composition of the atmosphere. Methane hydrate could be a significant source of atmospheric methane, an important greenhouse gas. Natural releases of the gas into the atmosphere could influence climate change, and German researchers aboard the ship are trying to establish how these releases occur.

The breakdown of the hydrates, triggered by changes in water pressure and temperature, is also thought to be responsible for seafloor landslides and large water waves (tsunamis). But most experts confess to being sceptical of the popular theory that they also sink ships in the foaming waters of the Bermuda Triangle.

www.gashydrate.de/projekte/omega/margasch

## Suche nach Methan: Forscher kehrten von Expedition zurück

Methanhydrat, eine brennbare eisähnliche Verbindung von Wasser und Sumpfgas, gehört zu den Hauptforschungsgebieten des Kieler Forschungszentrums GEOMAR. Die Mengen, die weltweit am Meeresboden lagern oder als Gas aufsteigen, haben einen entscheidenden Einfluss auf den Treibhauseffekt. Kieler Wissenschaftler hatten 1996 riesige Vorkommen vor der Küste Oregons entdeckt. Mit dem Forschungsschiff „Meteor“ erkundeten 28 Kieler, Bremer, russische, französische und ukrainische Wissenschaftler unter Fahrtleitung von Dr. Gerhard Bohrmann (GEOMAR) jetzt zum ersten Mal das Schwarze Meer auf der Suche nach Methan und Methanhydrat.

Bei der Expedition, die am 2. Januar in Istanbul begann und südlich der Halbinsel Krim entlang führte, erfassten und kartierten die Forscher die Vorkommen mit modernsten akustischen Systemen. Fündig wurden die Forscher vor allem in der Nähe der zahlreichen Schlammvulkane, von denen die Expedition bis zu 30 untersuchte und die größten nach ukrainischen Städten benannte: Sewastopol und Yalta. Bohrmann: „Während wir vor Oregon große massive Lagerstätten von Methanhydrat vor-



Zurück aus dem Schwarzen Meer: 28 Forscher trugen auf der „Meteor“ eine einzigartige Datensammlung zusammen. Foto hfr

fanden, sind die Verbindungen im Schwarzen Meer fein verteilt“. Schlamm und Methan scheinen nach Erkenntnissen der Wissenschaftler aus etwa 6000 Meter Tiefe aufzusteigen. Die Austrittsstellen am Meeresboden sind umsäumt mit weißen Bakterienmatten.

Die Datensammlung sei wegen der detailtreuen Messungen – in Wassertiefen bis zu 150 Metern – einzigartig, erklärte der Bremer Geophysiker Prof. Volkhard Spiess. Es handele sich dabei jedoch nur um eine

Momentaufnahme, da sich Druckverhältnisse und Temperaturen im Schwarzen Meer ständig änderten, erläuterte Bohrmann, der als wichtigstes Expeditionsziel angab, mehr über die Rolle von Gashydraten auf das Klima zu erfahren: „Bisher können wir nur spekulieren.“ Finanziert wurde die vierwöchige Expedition von der Deutschen Forschungsgemeinschaft und dem Bundesforschungsministerium mit weit mehr als eine Million Euro. mad



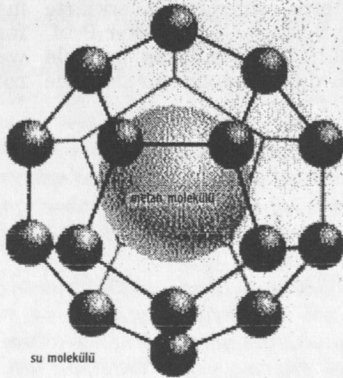
# METANHİDRATLAR

## GELECEĞİN ENERJİ KAYNAĞI

Enerji tüketimimiz son yıllarda hızla artıyor. 1997 yılında dünyanın yıllık petrol tüketiminin günde 73 milyon varil olduğu hesaplanmıştı. 2020 yılında bu miktarın günde 113 milyon varile ulaşacağı tahmin ediliyor. Petrol ve doğalgaz rezervlerinin sınırlı oluşu da göz önüne alınırsa, yakın bir gelecekte insanlığın yeni bir enerji kıtlığıyla karşı karşıya kalacağı açık. Bu nedenle yeni enerji kaynakları arayışına giren petrol ve doğal gaz endüstrisinin hedeflerinden biri, yeni yeni anlaşılmaya başlanan bir madde; metanhidrat. Yapısı, doğalgaz adıyla da bilinen metan ve katı haldeki sudan oluşan metanhidratlar, permafrost bölgelerde ve okyanus tabanlarındaki kıta sahanlıklarının kenarlarında, yüksek basınç ve düşük sıcaklık koşullarında çok yaygın bir biçimde bulunuyor. Örneğin, ABD Enerji Bakanlığı'ndan uzmanların hesaplarına göre, yeryüzündeki metanhidrat yataklarının yalnızca % 1'i bile değerlendirilebilse bu, Dünya'daki doğalgaz rezervlerinin toplamından daha fazla enerji sağlayaca-

cak. Araştırmaların bugün geldiği noktada, yeryüzündeki metanhidrat birikimlerinin hacminin, 3 katrilyon  $m^3$ 'le 30 katrilyon  $m^3$  arasında olduğu tahmin ediliyor. Ancak, gaz hidratlar sanıldığı kadar bol bulunuyor olsa bile, şimdilik bu kaynaklardan ekonomik ve güvenli bir biçimde metan elde etmenin bir yolu yok. Doğal metanhidratlar, küresel ısınmayla bağlantılı

oluşlarıyla da gündemde. Metan, Dünya atmosferinin yapısında bulunan belli başlı gazlardan biri. Bataklık bölgelerde, çöp alanlarında organik maddelerin bozunması ve hayvanlarda sindirim sırasında sürekli metan üretiliyor. Petrol ve doğalgaz üretimi sırasında da atmosfere metan salınıyor. Ancak, bu kaynakların hiçbiri küresel iklimi önemli ölçüde etkileyecek miktarda salıma neden olmuyor. Buna karşılık son araştırmalar, doğal metanhidrat birikiminden açığa çıkabilecek metan gazının küresel iklimi etkileyecek düzeylerde olabileceğini gösteriyor. Metanhidratları konu alan araştırmalar, küresel iklim değişimlerinin de daha iyi anlaşılmasını sağlayacak.



Metanhidratın yapısında, katı haldeki su moleküllerinin içine hapsolmuş bir metan molekülü bulunur.

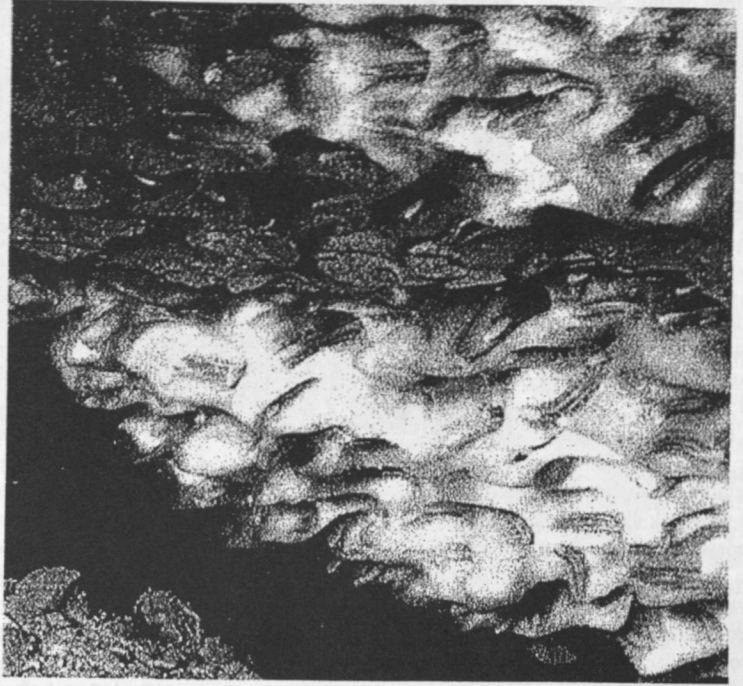
### Geç Kalan Keşif

Günümüzden yalnızca yirmi yıl kadar önce, metanhidratlar pek bilinmiyordu. Hidrat benzeri kimyasal maddeler, 1800'lü yılların başlarında laboratuvar ortamında keşfedilmiş olsa da, bu maddelerin doğada da var olduğu

1960'lı yıllarda anlaşıldı. Doğal metanhidratlar ilk kez 1960'larda Sibirya'daki doğalgaz rezervlerinde gözlemlendi. İlk alan araştırmalarıysa 1970'li yıllarda başladı. Son otuz yıldır kutup bölgelerinde ve okyanus tabanlarında yapılan birçok araştırmada, doğal metanhidratların, uygun basınç ve sıcaklık koşulları varsa büyük miktarlarda bulunabileceği anlaşıldı. Peki, madem metanhidrat doğada böylesine yaygın, neden bu kadar geç keşfedildi? Bunun en önemli nedeni, petrol ve gaz çıkarmak için üreticilerin öncelikle ılıman ya da tropikal iklimlerdeki karalarda bulunan "kolay" kaynaklara yönelmiş olmalarıydı. Denizlerdeyse, daha çok sığ sulardaki rezervler tercih ediliyordu. Metanhidratların en çok rastlandığı permafrost bölgelerde ve derin sulardaki sondajlarsa çok yakın bir zamanda başladı. Son zamanlarda metanhidratlara artan ilgi, yeryüzündeki birikimlerinin, kömür, petrol ve doğalgaz rezervlerinin tümünün toplamından çok daha fazla olmasından kaynaklanıyor. Bugün birçok ülkede, özellikle de Japonya gibi kendi fosil yakıt kaynakları bulunmayan ülkelerde, metanhidratlar üzerine araştırma-geliştirme programları bulunuyor.

Gaz hidratlar, birbirine bağlanarak ağ oluşturmuş katı haldeki "evsahibi" moleküllerle, kimyasal bir bağ olmaksızın bunların içine hapsolmuş uygun büyüklükteki "konuk" moleküllerden oluşur. Metanhidratın yapısında da, katı haldeki su moleküllerinin içine hapsolmuş bir metan molekülü bulunur. Yeryüzündeki metanhidrat birikimlerinin çoğunun kaynağı, okyanus tabanındaki organik maddelerin çürümesi sırasında ortaya çıkan metan gazı. Bu tür hidratlar, çürüyen bu maddelerin fazla ve çökelti oluşumunun hızlı olduğu yerlerde yoğun olarak bulunuyor. Yeryüzündeki metanhidrat birikimlerinin bir bölümü de, yerkabuğundaki kırılmaların manto tabakasından gelen metanın deniz tabanına çıkmasına izin verdiği bölgelerde, uygun basınç ve sıcaklık koşullarına bağlı olarak oluşmuş.

Son yıllarda doğal metanhidrat birikimlerinin hangi koşullarda oluştuğunun, yapılarının ve özelliklerinin anlaşılmasında önemli ilerlemeler kaydedilmiş olsa da, aslında bu alan daha



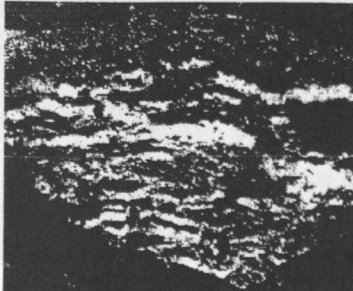
## Metanhidratlarda Yaşam

Doğal metanhidratlar, günümüzün bazı ilginç biyolojik sorularının yanıtlarını da taşıyor. Çok yakın bir zamana kadar, okyanusların derin bölgelerinde deniz tabanına güneş ışığı girmemesi ve oksijensizlik nedeniyle buralarda yaşam olmadığı sanılıyordu. Son yılların en ilginç keşiflerinden biri, yeryüzünün derinliklerinde oksijen ve güneş ışığından yoksun yerlerde yaşayan ve gaz hidratlara uyum sağlamış canlıların bulunması oldu. 1997 yılında, Meksika Körfezi'nin tabanındaki doğal metanhidrat yığınlarında, hidratlardaki metanı besin olarak kullanan or-

ganizmalar bulundu. Metan yiyen ve tüp solucanlarıyla midye gibi canlılarla simbiyotik bir ilişki içinde yaşayan bakteriler bulundu. Bu bakterilerle beslenen canlıların da, burada yaşayan başka canlılara, denizyıldızı ve yengeç gibi zararlılara besin oluşturduğu görüldü. Araştırmacıların en ilginç keşiflerinden biri de, besinlerini metanhidrat birikimlerinden yavaş yavaş salınan metandan sağlayan "buz solucanları"nın bulunması oldu. Metanhidratlar üzerinde çalışan araştırmacıların bir çabası da bu yaşam topluluklarını incelemek ve korumak.

çok yeni sayılır. Metanhidratlardan enerji kaynağı olarak yararlanma aşamasına gelinebilmesi için, öncelikle bu birikimlerin fiziksel ve kimyasal özellikleri konusundaki temel soruların yanıtlanması gerekiyor. Dünyanın birçok bölgesinde doğal metanhidratların varlığı, yalnızca bölgenin jeofiziksel yapısının araştırılması ya da çö-

kelti örneklerinin jeofiziksel incelenmesi gibi dolaylı yollardan anlaşılmış. Ancak, kapsamlı araştırmalar yapılan birçok bölge de var. Metanhidrat araştırmalarının yoğun olarak yürütüldüğü bölgelerden biri, Kuzey Amerika kıtasının kutba yakın bölgeleri. En iyi bilinen ve üzerinde en çok araştırma yapılan metanhidrat birikimlerinden biriyse, yine Kuzey Amerika'nın doğu kıyılarında bulunan Blake Sırtı. Burası, 1970'li yıllardan bu yana düzenli olarak incelendiği için, yeryüzünün başka bölgelerindeki metanhidrat araştırmalarında kullanılacak araçların ve yöntemlerin "ince ayarlarını" yapılması açısından büyük önem taşıyor. Metanhidrat araştırmaları açısından önem taşıyan üçüncü bölge, Meksika Körfezi. Burayı öteki bölgelerden

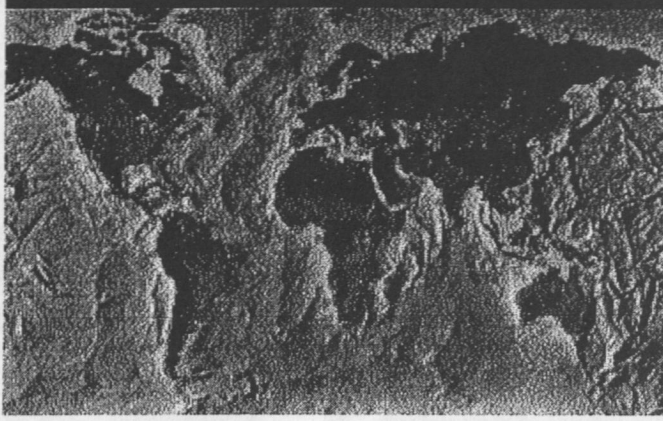




ayırıcı özellik, petrol ve doğal gaz çıkarma çalışmalarının çok yoğun olması. Metanhidrat birikimlerinden çözölen metanın petrol platformları, boru hatları ve öteki araçlar için tehlike oluşturması, buradaki araştırmaların önemini artırıyor. Metanhidratların enerji kaynağı olarak potansiyelini sınamak üzere ilk kez 1999 yılında, Japonya'nın Nankai bölgesinde kazılar yapıldı. Burasının, doğal metanhidratlardan ticari metan üretimi yapılacak ilk yer olması bekleniyor. Sonradan, Pasifik Okyanusu kıyılarında, Nankai bölgesinin özelliklerini taşıyan yeni bir bölge belirlendi. Oregon yakınlarındaki bu bölge, bilimsel araştırmalar açısından Dünya'nın en önemli metanhidrat yatağı olarak kabul ediliyor.

Doğal metanhidratları içeren çökelti okyanus tabanları ve kutuplar gibi yaşam açısından elverişsiz koşullarda bulunduğundan, çıkarılmaları ve laboratuvar araştırmaları için sak-

Doğal Metanhidratların Yeryüzündeki Dağılımı



lanmaları güç. Araştırmacılar, doğal metanhidrat birikimlerini ve özelliklerini belirleyebilmek için, özel olarak geliştirilmiş çeşitli teknolojilerden yararlanıyorlar. Sonar araştırmalarıyla, deniz tabanındaki çökmeler, kaymalar, kabartılar gibi farklı yüzey şekilleri taranarak, deniz tabanının yüzeyine yakın yerlerde metanhidrat bulunup bulunmadığını belirten ilk ipuçları toplanıyor. Araştırmacıların deniz tabanının iç yapısını görüntülemek için başvurdukları yöntemse, sismik incelemeler. Sismik yansıma incelemeleri, okyanusların derinliklerinde

geniş alanların en hızlı ve doğru biçimde değerlendirilmesine yarıyor. Aşağıda gerçekten neler olduğunu anlamak ve sismik çalışmalarını uyumlandırabilmek için bilim adamlarının çökelti örnekleri toplaması da gerekiyor. Hidrat çökeltilerinden örnek toplamak için en çok kullanılan yöntem "piston coring". Bu yöntemde, içi boş özel bir boru deniz

tabanına daldırılarak çökelti örneği alınıyor. Çökelti örneklerinin alınacağı yeri kesin olarak belirlemek için, sualtı araçlarına monte edilmiş özel görüntüleme aygıtlarından da yararlanılıyor. Kimi zaman bu şekilde "sağlam" örnekler elde etmek mümkün oluyor. Ancak genellikle, boru gemiye çekilirken, basınç ve sıcaklık değişimi nedeniyle metanhidrat çözünerek metan ve suya dönüşüyor. Bu nedenle araştırmacılar, ellerinde kalanların jeokimyasal yapısını inceleyerek, aşağıdaki hidrat birikiminin yapısını ve miktarını belirlemeye çalışıyorlar.

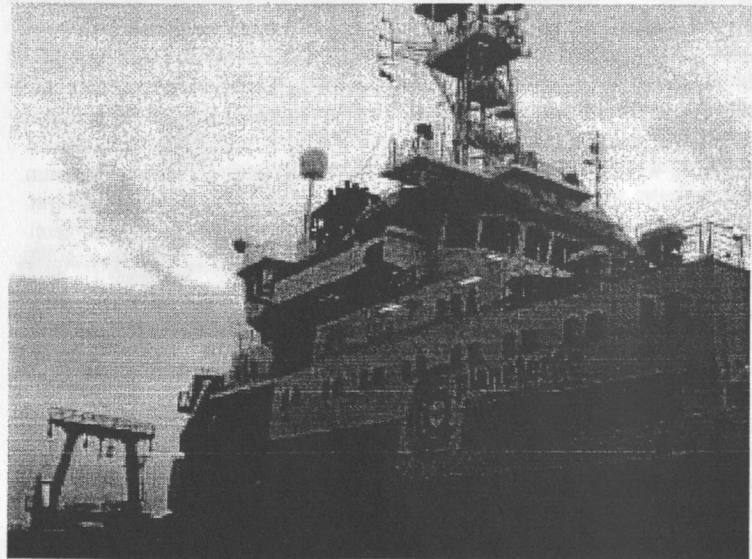
## Meteor Araştırma Gemisi Karadeniz'deydi

Denizlerdeki metanhidrat çökeltileri konusunda çok yönlü bilgi toplamaya yönelik araştırma programları yeni yeni oluşturulmaya başlandı. Bu araştırma programlarının en önemlilerinden biri de, Almanya'nın Kiel kentindeki Christian-Albrecht Üniversitesi'nin Deniz Bilimleri Araştırma Merkezi'nce (GEOMAR) yürütülüyor. GEOMAR araştırmacıları, 2 Ocak - 1 Şubat 2002 tarihleri arasında, deniz tabanındaki metanhidrat çökeltilerini incelemek üzere Meteor araştırma gemisiyle Karadeniz'deydi. MARGASH araştırma gezisinin amacı, Karadeniz'deki metanhidrat çökeltilerini ve bu çökeltilerin dinamiklerini daha iyi anlamaktı.

Son 30 yılda Karadeniz'de Rus bilim adamlarınca düzenlenen birçok araştırma, deniz tabanının yüzeyine yakın yerlerde büyük metanhidrat birikimleri olduğunu ortaya koymuştu. Ayrıca birçok bölgede metan sızmaları olduğu da biliniyordu. Bunların, sürekli değişkenlik gösteren ve tepkimeye oldukça hazır metan depoları olduğu, hatırı sayılır uzaklıklardan bile çevreyi etkiledikleri sanılıyordu. METEOR araştırma gemisiyle Karadeniz'e gelen araştırmacıların bir ay süren incelemeleri de, Karadeniz'deki metanhidrat çökeltilerinin

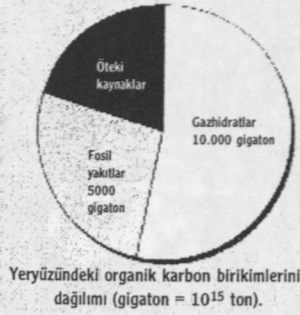
dağılımı, yapısı ve özellikleriyle, bulundukları çevreyle etkileşimlerini konu alıyordu. GEOMAR araştırmacıları, yeryüzünün benzer özel-

likteki öteki bölgelerine bakarak, Karadeniz'de deniz tabanında metanhidrat birikimlerinin çıkarmalar oluşturduğunu tahmin ediyordular.



## Metanhidratlardan Yararlanmak

Doğal metanhidratların yapısında bulunan metanı çıkarmak amacıyla, tek başına ya da birlikte kullanılabilir üç farklı yöntemden yararlanılabileceği tahmin ediliyor. Bu yöntemler temelde, metanhidrat birikimindeki sıcaklık ve basınca müdahale ederek metan gazını serbest bırakacak değişimler yaratmaya dayanıyor. Metanhidrat birikimindeki basıncı azaltmak, kullanılabilir yöntemlerden ilki. Yüksek basınç, gaz hidratlardaki suyun donma noktasını yükseltiyor, yani 0 derecenin üzerinde de var olmalarını sağlıyor. Araştırmacılar, hidrat birikimlerinde yapılacak sondajların, basıncın azalmasına neden olacağı için buzların erimesini ve metanın serbest kalmasını sağlayacağını düşünüyorlar. Metanhidrat birikiminde sıcaklığı artırmaksa kullanılabilir bir başka yöntem. Bunun için, yüzeyden buhar enjeksiyonu yapmak ya da hidratların altına sıcak sıvılar salmak gibi uygulamalar ilk akla gelenler. Başvurulabilir yöntemlerin üçüncüsüyse, metanhidrat birikimine kimyasal maddeler



enjekte etmek. Bilim adamları, tıpkı yollara dökülen tuzun buzu eritmesi gibi kimyasal maddelerle metanhidrat birikimindeki buzları eritmeyi düşünüyorlar. Ancak, hangi yöntem kullanılırsa kullanılsın, metanhidratların yapısındaki buzları eritmenin nasıl bir sonuç vereceğini önceden kestirmek güç. Çalışma yapılan yerin çevresindeki gazın dengesini bozmak, patlamalara ya da toprak kaymalarına neden olabilir.

Öte yandan, doğal metanhidratlardaki gazın çıkarılmasıyla ilgili belki en önemli sorun, bu birikimlerin geniş alanlara yayılmış olmasına karşın, yoğunluğunun az olması. İkinci bir engelse, doğal metanhidrat birikimlerinin bulunduğu çökeltilerin özellikle

rinden kaynaklanıyor. Dünya'daki hidrat kaynaklarının çoğu, 500-700 metreden derin sularda, kıta sahanlıklarının kıyısındaki çökeltilerde bulunuyor. Çökeltiler, çok büyük miktarlarda su ve hidrat içermelerine karşın, ince parçacıklardan oluştukları ve homojen özellikte olduklarından gaz ve sıvıların kaçmasına izin verecek geçirgenlikte olmuyorlar. Permafrost bölgelerde yapılacak kazılarda bu güçlüğü yenmek için yapay yollarla çökeltilerin geçirgenliği artırılabilir. Ancak, yumuşak, deforme olmaya yatkın okyanus tabanlarında bu yöntemi kullanmak mümkün değil. Sonuç olarak, denizlerde hidrat üretimi, büyük bir olasılıkla, en azından ilk başlarda, karalarda ve Japonya'daki Nankai Çukuru ya da Kuzey Amerika'daki Cascadia Sınırı gibi, daha heterojen ve kaba taneli çökeltilerin bulunduğu, tektonik açıdan etkin kıta sahanlıklarında gerçekleştirilecek gibi görünüyor.

## Metanhidratlar ve İklim

Küresel ısınma eğiliminin büyük önem kazandığı günümüzde, enerji kaynakları konusundaki herhangi bir tartışmada fosil yakıt kullanımının kü-

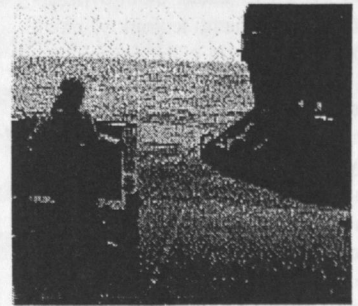
Araştırma ekibinde, Almanya, Fransa, Ukrayna ve Rusya'dan jeofizikçiler, jeokimyacılar, biyologlar, denizbilimciler ve meteorologlar bulunuyor. Karadeniz'deki araştırma gezisi, deniz dibinde oksijensiz ortamda yaşayan canlıların incelenmesini ve metanhidrat çökeltileriyle atmosferdeki metan arasındaki ilişkinin araştırılmasını da kapsıyordu.

Gerhard Bohrmann, Karadeniz'deki metanhidrat çökeltilerinin ve çevreyle ilişkilerinin



Araştırma ekibinin başkanı Gerhard Bohrmann'ın Bilim ve Teknik'e verdiği bilgilere göre, şimdilik Karadeniz'deki metanhidrat birikimlerinin miktarı konusunda bir tahminde bulunabilmek güç. Ancak, Karadeniz'deki metanhidrat birikimlerinin deniz tabanının yüzeyine yakın yerlerde bulunması burayı hidrat araştırmaları açısından ideal kılıyor. Bohrmann, Ka-

radeniz'de inceledikleri çamur yanardağlarının hemen hepsinde, metanhidrat birikimlerine rastladıklarını belirtiyor. Bunların arasında özellikle Dvurechenskii adlı çamur yanardağının çok etken olduğu ve metan saldıığı görülmüş. Araştırmacılar çamur yanardağlarının, metanhidratlar metan salımı arasında önemli bir köprü oluşturduğunu düşünüyorlar.



tam olarak anlaşılabilmesi için, daha pek çok araştırma gezisi düzenlenmesi gerektiğini belirtiyor. GEOMAR araştırmacıları ileride Karadeniz'in Türk sularında kalan bölgelerinde düzenleyecekleri araştırma gezilerinde ülkemizden araştırmacılarla işbirliği yapmayı planlıyorlar.



resel iklime etkilerinin göz ardı edilmesi olanaksız. Peki, gaz hidratlarla, sera gazlarına bağlı küresel ısınma arasında ne gibi bir bağlantı var? Aslında gaz hidratların enerji kaynağı olarak kullanımı, enerji tasarrufuna duyulan gereksinimi ortadan kaldıracaktır. Bir birim elde etmek için yakılan metan, aynı enerjiyi elde etmek için yakılan petrol ve kömüre göre çok daha az karbondioksit çıkarıyor. Öte yandan, karbondioksitin etkisiyle karşılaştırıldığında, metanın sera gazı olarak etkisi çok daha fazla. Yani, gaz hidratlardaki metan gazının kaza sonucu ya da planlanmış olarak salımının, küresel iklim üzerinde önemli etkileri olabilir. Birçokları, derin sulardaki insan etkinlikleri küçük ölçekli ve yerel metan salımlarına neden olsa bile, bunların küresel iklime etkisinin de göz ardı edilebilecek oranda olacağını düşünüyor. Ancak, çöktillerin kimyasal değişimi (bozunma), erozyon, çökme ve deniz tabanının yükselmesi, küresel sıcaklık döngüleri ve deniz seviyelerindeki değişimler gibi, sürüp giden doğal süreçlerin deniz tabanındaki sıcaklık ve basınç özellikleri üzerindeki etkilerini göz ardı etmemek gerekiyor. Küresel sıcaklıklardaki küçük bir artış ya da basınçtaki küçük bir azalma, metanhidratların dengesini bozabilir ve serbest kalacak metan gazı, küresel iklimde önemli değişimlere yol açabilir. Doğal metanhidrat birikimlerindeki metanın, atmosferdeki metan miktarının 3000 katı kadar olduğu hesaplanmış. Ancak, hangi jeolojik ya da atmosferik süreçlerin çöktillerdeki metan dengesini etkileyebileceği ve atmosfere metan salımına neden olacağı konusunda henüz yeterli bilgi bulunmuyor. Örneğin, kıta sahanlıklarında deniz seviyelerindeki düşüşlerin neden olduğu kaymalar sonucu atmosfere metan salınabileceği düşünülüyor. Öte yandan, deniz seviyelerinin yükselmesi nedeniyle kutup bölgelerindeki çöktillerin ısınması da atmosfere metan salımına neden olabilir. Bugün araştırmalar, yeryüzündeki metanhidrat birikintilerinin değişim içinde olduğunu, çevrede sürüp giden doğal değişimlere karşılık olarak metan soğurup saldıgını gösteriyor.



Metan gazının, geçmiş jeolojik zamanlarda iklim özelliklerini belirlemede önemli rol oynadığı biliniyor. Örneğin, günümüzden yaklaşık 65-55 milyon yıl önce, Paleosen dönemde hidratlardan büyük oranda metan açığa çıkmış ve bu gazların birikmesi Geç Paleosen dönemde iklimin ısınmasına neden olmuştu. Bütün bu olayları neyin tetiklediği henüz tam olarak bilinmediğinden, yeniden ortaya çıkıp çıkmayacakları tahmin edilemiyor. Ancak, doğal yollarla gerçekleşen metan salımı, günümüzde de sürüp giden bir süreç. Araştırmalara göre, bu salımın yıllık miktarı konusundaki tahminler,  $10^{11}$ 'le  $10^{14}$  gram arasında değişiyor. Ancak bu tahminler, petrol rezervlerinden kaynaklanan metan salımını bile dikkate almadan, yalnızca bakterilerce salınan metan miktarına dayanıyor. Araştırmacılara göre, metanhidrat çöktillerinin bulunduğu kıta sahanlıklarının kenarlarındaki metan salımı da ölçülebilecek olsa, bu miktar çok daha büyük olacak.

Geçmiş buzul çağlarının kalıntılarıyla gezegenimizin Grönland ve Antarktika'daki buz tabakasına hapsolmuş, eski atmosferine ait örneklerin kimyasal inceleme sonuçları, Dünya'nın küresel ikliminin geçmiş dönemlerden bu yana sürekli olarak büyük değişimler geçirdiğini gösteriyor. Birçok araştırmacıya göre bunlar, Dünya'nın ekseninin yörünge düzlemine olan açısındaki periyodik değişimlerden kaynaklanmıştı. Öte yandan, buzul örneklerinde yapılan incelemeler, bu değişimler sırasında atmosferdeki karbondioksit ve metan oranlarının da değişimlerden geçtiğini gösteriyor. Buzul dönemlerinin baş-

langıcında, atmosferdeki karbondioksit ve metan oranı yavaş yavaş azalıyor ve yaklaşık olarak bu dönemlerin bitişine gelen zamanlarda hızlı bir artış gösteriyordu. Birçok araştırmacıya göre, Dünya atmosferinin geçirdiği bu değişimler, doğal metanhidratlardaki metan gazının salımıyla ilgiliydi.

Doğal metanhidrat çöktillerindeki metan gerçekten 21. yüzyılın enerji kaynağı olacak mı? Metanhidratın yaygın bir biçimde bulunma-

sı, enerji kaynaklarıyla ilgili uluslararası güç dengelerini zorlayacağı ve bugün enerji kaynakları açısından başkalarına bağımlı durumdaki ülkelerin, kendilerine yetecek kaynaklara kavuşmasını sağlayacağı benziyor. Metanhidratların miktarı konusundaki tahminler gerçekten de şaşkınlık verici ölçeklerde. Ancak, en azından yakın bir gelecekte, bu kaynakların rezerv dönüştürülemeyeceği, yani ekonomik açıdan verimli bir biçimde çıkarılamayacağı da ortada. Metanhidratlardan gaz üretimi yapmak için ilk çalışmalar, permafrost bölgelerdeki birikimlerde gerçekleştirilecek. Hidrat birikimlerinin çok küçük bir bölümü bu bölgelerde bulunsa da, bu birikimler hidratların farklı üretim yöntemlerine nasıl tepki vereceğini anlamak açısından önem taşıyor. Aslında, metanhidratlardan gaz elde etmek konusundaki asıl zorluk, kaynakların büyük miktarının, çöktillere yayılmış olması. Petrol ve doğalgaz kaynaklarında olduğu gibi, üretimin ekonomik açıdan verimli olması için, öncelikle yeryüzünde metanhidrat derişiminin yüksek olduğu bölgelerin belirlenmesi gerekiyor. Bunun için de öncelikle gelişmiş sismik ve öteki uzaktan görüntüleme yöntemlerine gereksinim duyuluyor. Araştırmacılar, doğal metanhidratlardan enerji kaynağı olarak yararlanmanın yollarını bulmanın yanı sıra, metanhidratların küresel iklimle bağlantısını da ortaya çıkarmaya çalışıyorlar.

Aslı Zülâil

Kaynaklar:  
<http://www.gashydrate.de/>  
<http://woodshole.er.usgs.gov/>  
<http://www.netl.doe.gov/>

L'accélérateur du savoir

# Science & Vie

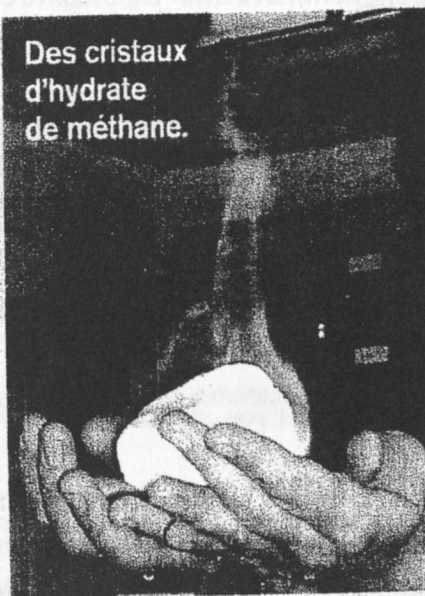
Mensuel n°1015 - avril 2002

## ENERGIE

### DU COMBUSTIBLE GLACÉ

■ A l'occasion de l'expédition scientifique Margasch, le géologiste Gerhard Bohrmann du Centre Geomar de Kiel (Allemagne) et son équipe viennent de collecter dans le sol de la mer Noire des échantillons d'hydrates de méthane. Ces cristaux riches en énergie ressemblent à de la glace ; ils se forment à haute pression et à faible température dans les plateaux continentaux – reliefs sous-marins inclinés prolongeant la côte – et les sols gelés de l'Arctique. Leur teneur en gaz naturel en fait de bons candidats pour les combustibles de demain : selon le Département de l'énergie américain, 1% de ces hydrates existant sur Terre

Des cristaux d'hydrate de méthane.



produiraient plus d'énergie que l'ensemble des réserves de gaz naturel (brut). Encore faut-il les trouver et les exploiter sans polluer. Le méthane est en effet un gaz à effet de serre 21 fois plus puissant que le gaz carbonique.

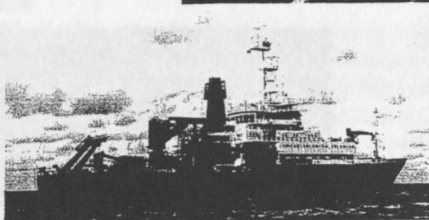
K. B.



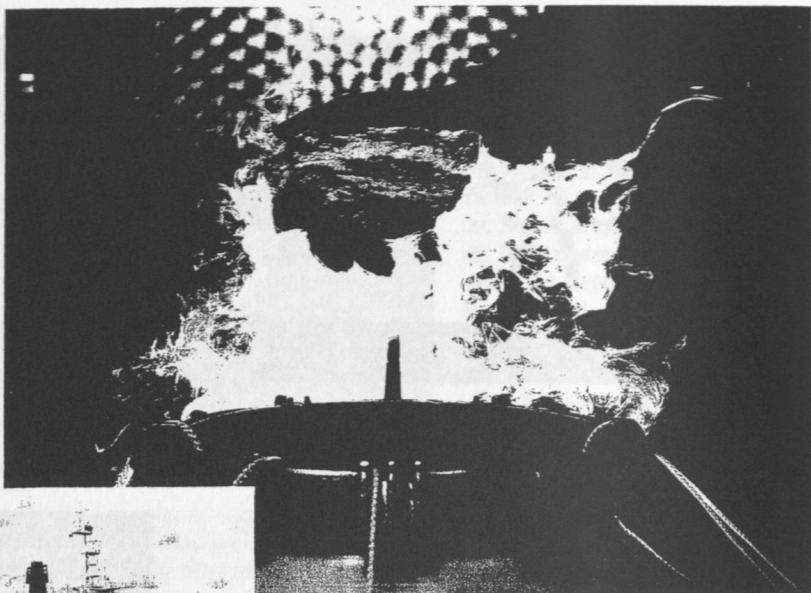
ROHSTOFFE

## Zischende Energie-Reserve

Ein internationales Forscherteam an Bord des deutschen Spezialschiffes „Meteor“ hat Hinweise dafür gefunden, dass auf dem Grund des Schwarzen Meeres ein unerwartet reichhaltiger Methanhydratspeicher schlummert. Das als mögliche Energiequelle der Zukunft geltende Fäulnisgas entsteht bei der Verwesung von Plankton, Algen und Fischen. Bei dem hohen Druck und den niedrigen Temperaturen am Meeresgrund wird das Gas zu Eisschichten verbacken, die sich durch die Sedimente ziehen. In zwei Bohrkernen entdeckten die Wissenschaftler mehrere dünne weiße Methanhydratlagen. Ein dritter, mehr als vier Meter langer Kern war fast auf der ganzen Länge mit vereisten Sumpfgaslagen durchsetzt, die sich beim Öffnen des Bohrkerns an Deck zischend zersetzten. Die Funde deuten nach Ansicht der Forscher auf ein massives Methanhydrat-



DER SPIEGEL 6/2002



Forschungsschiff „Meteor“, Methanhydratklumpen

vorkommen, das zudem überraschend nahe an der Sedimentoberfläche liegt und deshalb leicht zugänglich ist. Die Ausbeutung des eisigen Energieträgers, der in den Ozeanböden, aber auch in den Permafrostböden Sibiriens und Alaskas lagert, könnte dereinst die Bergung gewaltiger Brennstoffmengen ermöglichen.